PIEZOELECTRIC SENSOR ARRAY FOR DETECTING GAS PIPELINE CRACK

KHARUDIN BIN ALI

COLLEGE OF GRADUATE STUDIES
UNIVERSITI TENAGA NASIONAL

2020

PIEZOELECTRIC SENSOR ARRAY FOR DETECTING GAS PIPELINE CRACK

KHARUDIN BIN ALI

A Thesis Submitted to the College of Graduate Studies, Universiti Tenaga Nasional in Fulfilment of the Requirements for the Degree of

Doctor of Philosophy (Engineering)

AUGUST 2020

DECLARATION

I hereby declare that the thesis is my original work except for quotations and citations which have been duly acknowledged. I also declare that it has not been previously, and is not concurrently submitted for any other degree at Universiti Tenaga Nasional or at any other institutions. This thesis may be made available within the university library and may be photocopies and loaned to other libraries for the purpose of consultation.

_____SIGN_____

KHARUDIN BIN ALI

Date: AUGUST 2020

ABSTRACT

Non-destructive testing (NDT) deals with the inspection of an object for determining its properties without destroying its usefulness. The applications include the detection of cracking in steam generator tubing, nuclear power plants, aircraft and etc. In the oil and gas industry, the traditional pipeline maintenance occurs at defined service intervals, so the structural damages like corrosion and crack occurring in between service intervals are not monitored even though it may be detrimental to the instant health of the pipe's structure. Other than the pipeline industry, a single method for detecting or monitoring damage in a pipeline does not exist, currently. Instead, industries typically implement a combination of several different techniques that would normally require the pipeline system to be temporarily taken out of operation. Lastly, most of the temporary techniques used are effective in good weather condition and it does not have the probe covering when raining occurs on the site. Considering the limitations of the conventional ultrasonic transducers, guided Lamb Wave offers new opportunities for cases of effective detection of damage in structures. As a method for NDT, the Piezoelectric with Lamb Wave method testing system (PZ-LW) is also used for crack detection in the pipe or plate due to several factors resulting from positioning, depth and shape of crack including the small angle of pipe joining. In this thesis, the development of (PZ-LW) system and combination of optimization and error compensation of piezoelectric sensor array for detection of cracks on the pipeline is used in measuring the defect positioning and width of defect based on-time response and signal feedback amplitude for actual defect measurement. The main idea can be divided into three parts. Firstly, optimize piezoelectric sensor array by using the Design of Expert (DOE) software for Response Surface Methodology (RSM). Secondly, use SimNDT software to simulate the proposed piezoelectric sensor array. The probe design (2D and 3D) model is integrated with the system design and at the same time, the comparison between simulation and PZ-LW technique is executable. Thirdly, to complement this system, the Mamdani Fuzzy Logic is used as an intelligent technique in PZ-LW for high accuracy results. In system development, the graphical interfacing (GUI) is used for graph display on the computer by using MATLAB software and from here, the value of the width of the defect will be identified based on the graph display. Besides, the comparison between the simulation and the actual devices is used for the validation of measurement in this system. The PZ-LW

system design has higher sensitivity and less noise as compared to the conventional technique. The analysis of the experimental results suggests the PZ-LW system to be more accurate in contrast to the previous researcher's findings by 98.55% of accuracy for the position of defect location. Based on the hole defect, the accuracy achieved to 96.05%. Lastly, the axial defect measurement will exceed 98% of accuracy to identify the shape of the defect. This shows that the merger of the probe and intelligence system which are built will affect the accuracy of the results and it is very useful for the classification of defects apart from the accuracy of the reading displayed. In addition, the comparison of experimental and simulation results in SIMNDT has successfully proven the consistency and accuracy of the proposed PZ-LW system for carbon steel pipe inspection.

.

ACKNOWLEDGMENT

DEDICATION

This thesis is dedicated to my parents for their love, endless support and encouragement.

TABLE OF CONTENTS

LIST OF TABLES

LIST OF FIGURES

LIST OF SYMBOLS

A_0	Fundamental asymmetric Lamb wave mode
c	Speed of sound
c_g	Group velocity
c^E	Elastic stiffness constant matrix
c_l	Longitudinal wave speed
c_p	Phase velocity
c_t	Transverse wave speed
d	Half the thickness of the plate
D	Matrix
D	Electric displacement vector
E	Young's Modulus
E	Electric field strength vector
e	Piezoelectric stress constant matrix
e^t	Transposed matrix
f	Linear frequency
$F(m,n)$	Flexural modes group
k	Wavenumber
$L(m,n)$	Longitudinal mode group
m	Circumferential order of a mode
n	Group order of a mode
S	Strain vector
S_0	Fundamental symmetric Lamb wave mode
T	Stress vector
$T(m,n)$	Torsional mode group
u	Displacement vector
u_q	Displacement in q direction
u_r	Displacement in r direction
u_z	Displacement in z direction

v	Poisson's Ratio of the material
y	Perpendicular to the wave propagation direction
ϕ	Dilatational scale potential
λ	Lam'e constants
μ	Lam'e constants
ρ	Density of the material
$\boldsymbol{\sigma}$	Stress vector
ω	Driving (angular) frequency
χ	Direction of wave propagation
ψ	Vector potential
ε^{S}	Clamping dielectric constant matrix

LIST OF ABBREVIATIONS

AE	Acoustic Emission
ANFIS	Artificial Neural Fuzzy System
AO	Antisymmetric mode
ACU	Air Coupled Ultrasonic
ANN	Artificial Neural Network
BEM	Boundary Element Method
DOE	Design Of Expert
DAQ	Data Acquisitions
DAS	Delay-And-Sum
EMAT	Electromagnetic Acoustic Transducers
FE	Finite Element
FEM	Finite Element Method
HSLA	High-Strength Low-Alloy
HAZ	Heat-Affected Zone
LM	Lamb Wave
LZT	Lead Zirconate Titanate
MFIS	Mamdani Fuzzy Logic Inferences System
MFC	Micro Fiber Composite
MVDR	Minimum Variance Of Less Reaction
NN	Neural Network
NDT	Non Destructed Testing
NDE	Non Destructed Evaluation
PZT	Piezo electric Testing
PTIS	Piezoelectric Testing Inspection System
PZ	Piezoelectric
PZ-LW	Piezo Lamb Wave

PRF	Pulse Repetition Frequency
PL	Pulse Length
PSAW	Piezo Wafer Active Sensor
PSF	Point Spread Function
QP	Quick Pack
QAP	Quality Assurance Procedure
RSM	Response Surface Methodology
SHM	Structure Healthy Monitoring
SH	Shear Horizontal
SO	Symmetrical mode
SAFT	Synthetic Aperture Focusing Technique
SNR	Signal-to-Noise Ratio
ToFD	Time-of-flight diffraction
UT	Ultrasonic Testing

LIST OF PUBLICATIONS

1. Kharudin Ali, Johnny Koh Siaw Paw, Damhuji Rifai, Ahmed N Abda Alla, Moneer A. Faraj, and Chong Kok. Hen.(2020)" Optimization of Ultrasonic Testing for Defect Localization Signal on S55C Carbon Steel Pipe ".*IJESC* vol 10, no 3,

2. D.Rifai, K.Ali, A.Rahim, A.N.Abdalla, M.Faraj. (2019). "Solar Irradiance Measurement Instrumentation and Power Solar Generation Forecasting Based on Artificial Neural Networks (ANN): A Review of Five Years Research Trend". *Science of the Total Environment (Elsevier)*

3. K.Ali, D.Rifai, J.Koh.S.Paw, A.N.Abdalla, C.K.Hen, T.J.Ding, M.Fadzli.M.Sukor, Z.Ismail, T.J.Ding.(2019) "Effect of Crack in Bending Process for S55C carbon Steel with Ultrasonic Testing on Zero Degree Probe". IOP (Journal of Physic) (Scopes).

4. K. Ali, A. N. Abdalla, J. Koh, S. Paw, C. K. Hen, and T. J. Ding,(2018) "Crack identification using piezoelectric testing on carbon steel pipe for transverse, longitudinal and hole defects with low excitation frequency," *International Journal of Engineering Technology(IJET)* , vol. 7, pp. 171–176.

5. K. Ali, J. Koh, S. Paw, M.Aizat, A. N. Abdalla, , C. K. Hen, and T. J. Ding,(2018) "S55C Carbon Steel for Heat Treatment Process with Different Medium in Attenuation Measurement using Ultrasonic Testing", *International Journal of Engineering Technology(IJET)* , 7(4), 527-533.

6. K. Ali, J. K. S. Paw, C. K. Hen, A. N. Abdallah, T. J. Ding, N. A. Ahlam,(2018) "Encircling Probe with Multi-Excitation Frequency Signal For Depth Crack Defect In Eddy Current Testing," *J. Fundam. Appl. Sci., vol. 10, no. 6S(special Issue)*, pp. 1005–1039.

7. K. Ali, A. N. Abdalla, J. K. S. Paw, D. Rifai, and M. A. Faraj,(2018) "A novel eddy current testing error compensation technique based on mamdani-type fuzzy coupled differential and absolute probes," *Sensors Journal MDPI (Switzerland),* vol. 18, no. 7.

8. J. D. Tan, S. P. Koh, S. K. Tiong, K. Ali, and A. Abdalla,(2018) "Fuzzy logic enhanced direct torque control with space vector modulation," *Indones. J. Electr. Eng. Comput. Sci.*, vol. 11, no. 2, pp. 704–710.

CHAPTER 1

INTRODUCTION

1.1   Introduction

The economy of the country is heavily dependent on an extensive network of distribution and transmission pipelines to transport the country's sources of energy. For instance, the single largest source of energy in the United States is petroleum, which includes oil and natural gas. Pipelines play a critical role in delivering the energy resources from producing fields to power communities around. The network of pipelines has advantages over other means of transportation (such as train/truck) because of its high effectiveness in cost. The reliability and integrity of these pipes are reducing due to the deterioration and corrosion or some manmade errors. Due to the rapid degradation of the pipeline systems, regular assessment of their conditions is a critical task. Thus, it is very important to continuously check the conditions of the pipeline regularly (Ghavamian, Mustapha, Baharudin & Yidris, 2018).

Pipeline transport is the transportation of goods or material through a pipe. The latest data, in 2014, gave a total of slightly less than 2,175,000 miles (3,500,000 km) of pipelines in 120 countries across the world. The United States had 65%, Russia had 8%, and Canada had 3%, thus 75% of all these pipelines were in these three countries (Parfomak, 2015).

Pipelines exist for the transportation of crude and refined petroleum, fuels - such as oil, natural gas and biofuels - and other fluids including sewage, slurry, water, and beer. Pipelines are useful for transporting water for drinking or irrigation over long distances when it needs to move over hills, or where canals or channels are poor choices due to considerations of evaporation, pollution, or environmental impact. Pipelines conveying flammable or explosive material, such as natural gas or oil, pose special safety concerns and there have been various accidents.

For instance, the Bellingham explosion of 1999 and the Carlsbad explosion of 2000. The National Transportation Safety Board (NTSB) performed an investigation of each explosion, as it does for all pipeline incidents. Due to the severity of these two accidents, the NTSB released a comprehensive report of each explosion, including a detailed description of the cause of each explosion (Shohe, 2015). According to the NTSB investigation, the cause of each accident was related to typical types of pipeline damage mentioned above. The Bellingham explosion occurred in 1999 in Bellingham, Washington. As a result of a rupture in a (41-cm) diameter pipeline, (897,000-l) of gasoline was released into a creek that flowed through residential and industrial areas in Bellingham, Washington. Approximately 1.5 hours after the rupture, the gasoline in the creek ignited, burning an area (2.4-km) along the creek, as seen in the photograph (see Figure 1.1). The ensuing fire resulted in the death of two ten-year-old boys who suffered first and second-degree burns over 90% of the surface of their bodies. In addition, an eighteen-year-old male teenager fainted as a result of the intense gasoline vapours and drowned in the creek before it ignited.

The estimated total property damage was USD45 million. A photograph of the ruptured pipeline can be seen in Figure 1.1 below.

Figure 1.1   Actual rupture in the pipeline

According to the NTSB, the primary cause of the rupture was the excavation damage to the gasoline pipeline. This damage occurred in 1994 during a nearby modification project which was unrelated to the gasoline pipeline (Shohe, 2015). The secondary cause of the rupture was the inability of the operator to accurately evaluate the results from a magnetic flux inspection, which was performed at regular intervals of every five years for this pipeline. Therefore, the rupture and ensuing explosion could have been prevented if a reliable damage detection system had been implemented with the pipeline in order to continuously monitor its structural integrity.

The second example is the Carlsbad explosion, which occurred on August 19, 2000 near Carlsbad, New Mexico. A rupture in a (76-cm)

diameter natural gas transmission pipeline resulted in the release of natural gas directly into the environment. The ensuing explosion of the released gas burned for 55 minutes, as seen in the photograph in Figure 1.2 below. The estimated total property damage was USD998,000.00.

Figure 1.2   Fire from rupture which lasted approximately 55-min. The support structure of suspension bridge seen in lower left corner of fireball is (26-m) tall (Parfomak, 2015)

Finally, Table 1.1 listed a few recent severe pipeline accidents in a Congressional Research Service Report. The catastrophic incidents have highlighted the necessity of early detection and early warning of defects and imperfections in pipe infrastructures (Parfomak, 2015).

Table 1.1   Severe pipeline accidents

Year	Accidents
1999	A gasoline pipeline explosion in Bellingham, WA, killed 3 people and caused USD45 million in damage to a city water plant and other property.
2000	A natural gas pipeline explosion near Carlsbad, NM, killed 12 campers.
2006	Corroded pipelines on the North Slope of Alaska leaked over 200000 gallons of crude oil in an environmentally sensitive area and temporarily shut down Prudhoe Bay oil production.
2007	An accidental release from a propone pipeline and subsequent fire near Carmichael, MS, killed 2 people, injured several others, destroyed four homes and burned over 70 acres of grassland and woodland.
2010	A pipeline spill in Marshall, MI, released 810900 gallons of crude oil into a tributary of the Kalamazoo River.
2010	A natural gas pipeline explosion in San Bruno, CA, killed 8 people, injured 60 others and destroyed 37 homes.
2011	A natural gas pipeline explosion in Allentown, PA, killed 5 people, damaged 50 buildings and caused 500 people to be evacuated.

In order to continuously check the structural damage of pipeline at the earliest possible stage, several detection methods such as the analysis of images obtained using X-rays, magnetic fields, ultrasounds, eddy-currents and thermal fields have been developed (Doebling, Farrar, & Prime, 1998; Tang, Yao, Wu, & Peng, 2017). These are non-destructive methods hence do not affect the integrity of the structure, but they normally require that the general location of the damage be known before accessing the position of the damage yet this is not always possible. Among the available options for online Structural Health Monitoring (SHM) systems, piezoelectric sensors offer special opportunities for developing sensor arrays for the SHM system. This

is due to several reasons which include their quick response, high linearity, small, inexpensive and easily wired into sensor arrays. A SHM system with built-in piezoelectric sensors or usually called as the smart SHM system which has attracted much attention due to their low cost in the past decade (Ayres & Rogers, 1996; Hickman, Gerardi, & Feng, 1991; Lanza, Sternini, & Nguyen, 2017; Tang et al., 2017; Tzou & Cadre, 1989).

Besides sensors, piezoelectric actuators, which function is to excite diagnostic signals, can also be integrated into the structures to build an active SHM system. Comparing with the conventional passive SHM system (without built-in actuators) which can only tell what happened to the structure i.e. load and strain history, the active SHM system can interrogate the structure and find out "how it feels" i.e. the state of its health. Moreover, a major advantage of the active SHM over a passive one is that the active SHM system is subjected to a prescribed actuation thus increases the possibility of deducing the status of structure from the collected sensor data by choosing suitable monitoring system signals. Implementation of such an active SHM system can replace the schedule-based inspection or maintenance of a structure with the condition-based maintenance instead (Baid, Banerjee, Joshi, & Mal, 2008; Z. Su, Ã, & Lu, 2006).

1.2   Background

Structural health monitoring (SHM) as an essential practice in engineering has been extensively studied in recent years. According to the identification effort level, structural health monitoring can be

classified into four stages, which are as follows – 1) damage detection; 2) location determination; 3) severity quantification; and 4) service life prediction. To date, most researchers primarily focus on stage 1 to stage 3 (Scianna, Jiang, Christenson, & Dewolf, 2012).

Another classification scheme is according to the characteristics of information upon which the detection approach is based. One of these methods is model-based, which utilizes the changes in modal parameters (natural frequencies, mode shapes, and modal damping) to monitor the health condition of the structure. In some situations, the raw data in the form of frequency response functions may also be directly employed to indicate the damage condition on the ground that the resonances shift upon damage occurrence (Y. Zou, 2006).

The noteworthy advantages of the model-based method are easy implementation and global inspection capability (Doebling et al., 1998). However, it suffers from two limitations; firstly, the low detection sensitivity to damage effect and secondly, the usual deficiency of measurement data to uniquely characterize the damage(Shahdin et al., 2018).

The guided wave-based method monitors structural health conditions by utilizing the propagation and reflection pattern difference of transient wave which encountered structural discontinuity to examine the presence of damage. While this method claims high detection sensitivity, it utilizes transient responses thus has difficulty in identifying the exact severity of damage especially for structures with complicated geometry(Zhou, Li, & Yuan, 2014).

In this thesis, the advances in guided wave technologies have demonstrated the feasibility of guided wave SHM. However, there are many challenges for the applications of guided wave SHM, especially for pipeline subjected to multiple damages. Many investigations have been conducted in the field of active smart SHM and these studies could be divided into three major categories:

(i) Integrating Lamb-guided Wave for desired wave propagation and wave reception;

(ii) Optimizing sensor array in pipe structures to analyze complicated dynamic electromechanical behavior; and

(iii) Developing a robust multiple cracks model to extract health status information from the received sensor signals.

1.3 Problem Statement

In the pipeline industry, a single method for detecting or monitoring damage in a pipeline does not exist, currently. Instead, the industries typically implement a combination of several different techniques. For the oil and natural gas pipeline industry, destructive and non-destructive inspection techniques are commonly used together to ensure the integrity of transmission lines. These techniques usually require the pipeline system to be temporarily taken out of operation. The most common destructive technique is a hydrostatic test. For oil pipelines, a hydrostatic test involves pressurizing the pipeline to a point greater than the maximum operating pressure. The pressure is then

observed for several hours to determine if any leaks are present. Because a hydrostatic test could potentially cause a leak or rupture, all the hazardous materials in the pipeline must be replaced with water to prevent environmental damage. Due to service interruptions and water removal difficulties, hydrostatic testing is not used with the natural gas pipelines (Tucker, Kercel, & Varma, 2003).

When the geometry of the pipeline permits, non-destructive techniques are primarily used to ensure the structure's integrity. Such techniques commonly involve sending a magnetic flux or ultrasonic inspection device down on the inside of the pipeline. The size of the device available limits the smallest pipe size which can be tested on and the radius of bends also limits the ability to use a particular device. These devices perform best in oil pipelines because petroleum products act as a good coupling between the instrument and the pipe wall. Accordingly, these techniques do not require oil pipelines to be emptied, contrary to hydrostatic testing. However, natural gas pipelines are more complicated because gases do not provide good coupling for the testing device. Therefore, operators of natural gas pipelines have turned to direct assessment procedures for the determination of the integrity of their systems.

As evidenced by the documented cases of pipeline accidents, the current approaches used in the industry to monitor the structural integrity of pipelines are not proven to be 100% effective. Even though pipelines are one of the safest modes of energy transportation, they are still subject to major improvements. The associated costs of property damage from accidents are quite significant, not to mention the

enormous loss from each and every fatality. Also, the implementation of both destructive and non-destructive inspection techniques requires the pipeline to be taken temporarily out of service, which adds to the costs to an operator. Therefore, the development of a more reliable, cheaper monitoring system would have immense advantages for the pipeline operators.

Hence, innovative monitoring systems and defects diagnosis techniques should be in place to ensure the sustainability of the infrastructure i.e. pipelines and the associated equipment to ensure their integrity and continuity.

Generally, Non-Destructive Testing (NDT) is used by the industry to assess pipeline integrity and reliability. It is a widely accepted practice to detect dangerous defects before risking any potential catastrophic failures or interruptions to the production. The main issue with such a system is that it is performed on a need basis or at regular maintenance intervals and does not provide online monitoring and detection of failures as they happen. The solution proposed in the research of this thesis for a more reliable, economical monitoring system involves a damage detection process known as structural health monitoring.

SHM is a technology to collect data about critical structural components using embedded sensing elements to provide detection and diagnosis when damage occurs. Common forms of structural damage include holes, cracks, notches, corrosion, etc. SHM is also a useful tool for improving the safety and reliability of the structures thereby reduces their operational costs. For example, if the inspected

structure is a pipeline, the abnormalities such as metal loss, holes, or cracks will cause a discontinuity to the transmission of the guided wave along the pipe. Therefore, this emerging research area is worthy of consideration due to its multiple applications.

The guided wave system consists of mainly one or a group of transducers that are placed on the structure to detect the existence of a defect. As a result, some portions of the wave energy are reflected back. The reflected wave then can be analyzed to determine the location, type, and extent of the damage. The main drawbacks of the conventional ultrasonic inspection techniques are that they are point-wise inspection methods, labor-intensive, requiring highly trained operators, and are nearly impossible to use for in-situ high-temperature. There is a need to develop effective techniques for SHM so that the safety and integrity of the structures can be improved.

Traditional pipeline maintenance occurs at defined service intervals, so the structural damages like corrosion and crack occurring between service intervals are not monitored even though such damages may be detrimental to the instant health of the pipe's structure. Furthermore, with no structural data being documented in between service intervals, maintenance specialists and workers may only make experienced predictions or rely on the past data to decide the areas on the pipeline to focus for a defect detection during the routine traditional service intervals. Thus, significant structural changes related to the damage may be missed during the inspection process.

Many researchers have studied the defect detection methods by using guided waves (Sheng, D. G., Jun, W. Y., Yuan, Y. F., & Zhao Qing, 1998; Wei-Can, Shi, & Hou, 2017). These studies have solved the issue of a harmonic wave propagating in an infinite length hollow cylinder by the elastic theory, thus successfully explained the frequency dispersion and multi-mode phenomena of the guided wave, which is a start sign of the guided wave propagation research (Yücel et al., 2016).

Considering the limitations of conventional ultrasonic transducers, guided Lamb waves offer new opportunities for cost-effective detection of damage in structures. The use of Lamb Waves to detect the defects in steel pipe structures employs the pulse-echo method. Therefore, there is a need to further study the position and damage level of multiple cracks. This study will focus on the detection of multiple cracks and holes of steel pipelines using Lamb guided waves or the monitoring of critical pipeline systems utilizing embedded piezoelectric guided waves. Hence, innovative monitoring systems and defects diagnosis techniques should be in place to ensure the sustainability of the infrastructure i.e. pipelines and the associated equipment to ensure their integrity and continuity.

According to the previous problem which occurred in this research field, the problem statement can be listed as below:

(i) The simulation of Piezoelectric should be made applicable for use and also easily accessed with regards to the changes in the material properties. This should also enable the comparison between experimental and simulation to be made. From here,

the proper design of piezoelectric probe for its use on pipeline requires the positioning of the piezo sensor actuator and receiver with certain gaps in order to be able to function and for the controller module to control the excitation and feedback signal.

(ii) The quantity of piezoelectric used should be optimized to ensure the result obtained are accurate and at the same time reduces the redundancy of data received during the inspection process thus also enable the process of inspection to be conducted continuously.

(iii) The percentage of error should be reduced to ensure the result of feedback signal to be more accurate and at the same time the width of defect can be clearly identified.

(iv) The comparison between experimental and simulation should be established for data validation purposes and to also confirm the positioning and width of defect at the pipeline.

1.4 Research Objective

The goal of this research is to integrate a robust and reliable Piezoelectric Array sensor with the Guided Wave Technology for crack positioning and width of crack based on three basic cracks within the pipe, namely the axial crack, hole crack and angle crack defect. From here the three objectives are as follows:

(i) To simulate the three types of basic crack based on sensor array in order to acquire a preliminary understanding of the guided waves in the pipeline.

(ii) To design steel pipeline inspection system using Piezoelectric Sensor array based on optimisation method for best excitation frequency selection and sensor gap distance between two couples of piezoelectric sensor based on basic cracks in pipeline.

(iii) To develop error compensation technique using Mamdani Fuzzy Inference System (MFIS) to accurately obtain the amplitude signal feedback in identifying the actual width of defect on pipeline system.

(iv) To validate the effect of signal time response and signal amplitude for PZ-LW techniques by comparing between experimental and simulation through the use of fuzzy compensation scheme.

1.5   Scope of Research

The scope of this thesis includes:

(i) SimNDT software used to simulate the testing pipeline under different operating conditions.

(ii) The signal developer devices used for excitation signal and a pair of piezoelectric with max frequency 3.2Mhz used in signal receiving.

(iii) Implement error compensation using Mamdani fuzzy logic in ensuring the accuracy of signal amplitude responses which represent the width of defect.

(iv) The carbon steel pipe material (S55C) (outer diameter 60cm), (0.5 cm thickness) is used as a test sample and measuring the changes in position, depth and shape of crack.

(v) Types of defects are including (axial, hole and angle/ gradient).

1.6   Thesis Outline

The rest of the thesis is organized as follows:

Chapter 2, a review of system development in Piezoelectric and Ultrasonic Testing and their respective techniques and methods which were used for defect classification and such characterizations are explained. Henceforth, criticism of the methods used is made following the considerations in the studies conducted previously. It is followed by the description of relation of Piezoelectric and Ultrasonic Testing. Here, the review is based on the conditioning of medium inspection including both solid and fluid mediums. For piezoelectric

testing probe, the enforcement is based on the types of transducer and optimization method used during the inspection. In optimization of acoustic excitation and Phased Array on Defect Detecting in NDT by using ultrasonic testing and piezoelectric testing. Finally, a comprehensive review of previous studies on Acoustic Impedance and Signal for the identification of defect and crack is discussed.

Chapter 3 introduces a general description of the proposed Piezoelectric Lamb Wave (PZ-LW) technique including the detail of proposed system design, principle and model using Lamb Wave method, piezo array, fabrication, optimization based on (Response Surface Methodology (RSM), intelligent fuzzy logic design, and Simulink block development design. The detailed description of the probe selection, design, and instrumentation of the error compensation of piezoelectric with Lamb Wave testing (PZ-LW) along with piezoelectric probe relevant to the present research work are presented. The PZ-LW simulation and hardware design are proposed by using the SIMNDT, and Fuzzy Logic technique for the development of new methodology. Finally, more details on the hardware development, the probe development, and the connection between input, controller and output are explained. The calibration block and testing plate are also explained in the process of inspection for PZ-LW.

Chapter 4 presents the results and discussion including the simulation by using RSM for design optimization, conventional technique with a few types of defect including hole and axial defect, sensor array, error compensated by using MATLAB/Simulink, as well as SIMNDT on the simulation. In addition, the experimental results of comparison with

the conventional technique of UT and PZ-LW which was developed were also presented.

Chapter 5 elaborates on the conclusion and summary of research which are presented with a recommendation for future study.

CHAPTER 2

LITERATURE REVIEW

2.1   Introduction

In this chapter, the state-of-the-art achievement of ultrasonic techniques in defects detection and classification were reviewed. The review would help to get a clear understanding on the factors that affected the defect detections in the conductive and non-conductive materials. The recent enhancement methods that have been used to optimise the Piezoelectric probe parameters and to compensate the thickness in the pipeline were reviewed. Moreover, the impact of various factors such as frequency, the conductivity of test material, types of excitation wave, and medium of testing in inspection were discussed. Finally, the research gaps that would be considered in this study were also described.

This chapter is divided into six main sections and thirteen sub sections. The first section talked about the introduction of Ultrasonic Testing (UT) and its relationship with Piezoelectric, while the second section explained the Ultrasonic and Piezoelectric waves in a solid medium with varying reviews according to the types, including Lamb Waves, Rayleigh Waves and Shear Horizontal (SH). The third section highlighted the fundamentals and theories of the Ultrasonic Waves in a fluid medium which were reviewed by types including the thickness of Shear Waves and Acoustic Wave propagations. The fourth section covered the literature of the application and implementation of a transducer in Ultrasonic Testing, followed by five sections of field

research. The focus on optimisation of acoustic excitation and Phased Array on Defect Detecting in NDT by using Ultrasonic Testing and Piezoelectric Testing was presented in the fifth section, respectively. Finally, a comprehensive review of previous studies on Acoustic Impedance and Signal for identification of defect in the form of crack is discussed in this chapter.

2.2   NDT Technique Implement in Industrial

Non-Destructive Testing (NDT) is a quality control tool that is extremely important in heavy engineering sectors such as the petroleum and gas industry. It is the last test before any components, systems or processes are deemed safe to run. In the petroleum industry, non-destructive testing is widely used to detect the defects in the storage tanks and pipes that deliver oil and gas. Failure to detect and provide accurate information about the status of quality of the components, systems or processes may result in an accident that ends with the destruction of property and loss of life. Table 2.1 shows an overview of the major non-destructive testing techniques that are widely used in the oil and gas industry. With the existing conventional NDT, it is impossible to conduct inspections through the hundreds of kilometres of pipeline system used in the oil and gas industry. Thus, a simple and quick method to inspect the defects in large pipe systems is necessary.

Table 2.1   Major NDT Methods- A Comprehensive Overview

Method	Principles	Application	Advantages	Limitation
Visual Testing (VT)	Uses reflected or transmitted light from test object that is imaged with the human eye or other light sensing device.	Many applications in many industries ranging from raw material to finished products and in service inspection.	Can be inexpensive and simple with minimal training required. Broad scope of uses and benefits.	Only surface conditions can be evaluated. Effective source of illumination required. Access is necessary. Depth inspect 2.4mm-127mm
Penetrant Testing (PT)	A liquid containing visible or fluorescent dye is applied to surface and enters discontinuities by capillary action.	Virtually any solid non-absorbent material having uncoated surfaces that are not contaminated.	Relatively easy and materials are inexpensive. Extremely sensitive, very versatile. Minimal training required.	Discontinuities open to the surface only. Surface condition must be relatively smooth and free of contaminants. Minimum width defect 0.08mm
Magnetic Particle Testing (MT)	Test part is magnetised and fine ferromagnetic particle is applied to surface, aligning at discontinuity.	All ferromagnetic materials, for surface and slightly subsurface of discontinuities; large and small parts.	Relatively easy to use. Equipment/material usually inexpensive. Highly sensitive and fast as compared to PT.	Only surface and a few subsurface discontinuities can be detected. Ferromagnetic materials only. Detection should perpendicular with defect.
Radiographic Testing (RT)	Radiographic film is exposed when radiation passes through the test object. Discontinuities affect exposure.	Most materials, shapes, and structures. Examples include welds, castings, composites, etc. As manufactured or in service.	Provides a permanent record and high sensitivity. Most widely used and accepted volumetric examination.	Limited thickness based on material. Density and orientation of planar of discontinuities are critical. Radiation hazard. Max area detection 35cmx91cm
Ultrasonic Testing	High frequency sound pulses from a transducer propagate through the test material, reflecting at interfaces.	Most materials can be examined if sound transmission and surface finish are good and shape is not complex.	Provides precise, high sensitivity results quickly. Thickness information, depth and type of flaw can be obtained from one side of component.	No permanent record (usually). Material attenuation, surface finish and contour. Required couplant. Max range detection 20cm

2.3 Ultrasonic Background

Ultrasonic waves are well known and widely used in medicine. For example, ultrasound is used in detecting masses in the human body and detecting movement of blood courses in the cardiovascular investigation (Carino, 2001). The application of Ultrasonic Testing (UT) waves in metal identification was studied in detail by Sokolov in 1929 and 1935. In the year 1931, Mulhausner developed ultrasonic testing using the pulse-echo technique for the purpose of detecting the flaws in solid (Tian et al., 2019). After the World War II, Japanese researchers continued to explore the use of ultrasound in the medical field. Unfortunately, their works remained unknown until the 1950s, in the US and Europe where the instrumentation began to develop with continuous technology advancement up to the present time. Moreover, the handling and capability of the instruments have become more advanced with the presence of computers from 1980 until today (Aryan, Sampath, & Sohn, 2018). Furthermore, it should be noted that ultrasound wave on a surface transducer is produced when an electrical field is applied to piezoelectric crystal arrays. More importantly, the electrical pulse generators will create the UT waves or pulses, while a number of parameters are used to describe the vibrations of the UT waves which include Pulse Repetition Frequency (PRF), frequency, Pulse Length (PL), and amplitude (Y. Zou, 2006).

Recently, a considerable amount of research which investigated the conversion of mechanical to electrical energy revealed that piezoelectric materials are excellent in transmuting energy (Kamas, Giurgiutiu, & Lin, n.d.; Kim, Lee, Hwang, & Kang, 2015; Yu & Giurgiutiu, 2008).

Moreover, there are several types of Piezoelectric elements which include monolithic Piezoceramic materials, Quick Pack (QP), Micro-Fibre Composite (MFC), and Lead Zirconate Titanate (PZT) (Abbas & Shafiee, 2018; Lamb, 1917). Apart from that, it is crucial to understand that these substances comprise of numerous engineering utilisation, especially in manufacturing sensors and actuators (Sause, 2016). Furthermore, it should be noted that these materials are robust, adaptable, and inexpensive which have led to its usage in various applications. As a result, most piezoelectric actuators are widely used as sensors (Victor, 2010). On another note, vibration-based damage assessment is one of the most widely used techniques in Structure Health Monitoring (SHM) (Strantza, Aggelis, de Baere, Guillaume, & van Hemelrijck, 2015). In this case, the model-based methods and vibration-based processes are the main classes of the signal. However, this technique is computationally expensive and often includes a large number of parameters. Nevertheless, the transmission wave technique was the first practical application of ultrasonic NDT technique for material assessment. (Y. Zou, 2006) showed that the vibration-based model-dependent methods provide a local-global information about the structure health conditions and they are cost-effective. In a different study, the authors developed a neural network-based method to detect the damage in structures (J. J. Lee, Lee, Yi, Yun, & Jung, 2005). (J. Li & Hao, 2016) have used the mode shape differences or the mode shape ratios between damage states as an input for the neural networks (NN) to reduce the finite element (FE) modelling errors as investigated in the steel truss bridges for joint conditions of using the sensor for relative displacement. Moreover, the previous researchers were focusing more on the application of the Piezoelectric sensor in SHM for defect

identification based on the method, technique, intelligent and integrated system which were applied on SHM. Then, the review on the overall Piezoelectric applications used during inspection especially for Non-Destructed Technique (NDT) post Ultrasonic application or Acoustic Emission (AE) for defect and crack identification. However, the focus of this review is more on the obstruction of the carbon steel material and non-steel material.

2.4   Ultrasonic Testing Transducer

The high-frequency sound waves used for flaw detection and thickness gauging in ultrasonic non-destructive testing applications are generated and received by small probes called ultrasonic transducers. Transducers are the starting point for any ultrasonic test setup, and they come in a wide variety of frequencies, sizes, and case styles to meet inspection needs ranging from flaw detection in enormous multi-ton steel forgings to thickness measurement of paper-thin coatings. In ultrasonic NDT, transducers convert a pulse of electrical energy from the test instrument into mechanical energy in the form of sound waves that travel through the test piece. Sound waves reflecting from the test piece are, in turn, converted by the transducer into a pulse of electrical energy that can be processed and displayed by the test instrument. In effect, the transducer acts as an ultrasonic speaker and microphone, generating and receiving pulses of sound waves at frequencies much higher than the range of human hearing.

Typically, the active element of a NDT transducer is a thin disk, square or rectangle in shape, made up of Piezoelectric ceramic or composite that

converts electrical energy into mechanical energy, and vice versa. This element is sometimes informally called the crystal because, in the early days of ultrasonic NDT, elements were made from quartz crystals; however, ceramics such as lead metaniobate and lead zirconium titanate have long been used in most transducers. Recent years have seen increasing use of composite elements in which the traditional solid ceramic disk or plate is replaced by a micro-machined element in which tiny cylinders of piezoelectric ceramic are embedded in an epoxy matrix. Composite elements can provide increased bandwidth and improved sensitivity in many flaw detection applications.

When it is excited by an electrical pulse, this Piezoelectric element generates sound waves, and when it is vibrated by the returning echoes, voltage is then generated. The active element is protected from damage by a wear plate or acoustic lens and backed by a block of damping material that quiets the transducer after the sound pulse has been generated. This ultrasonic subassembly is mounted in a case with appropriate electrical connections. All common contact, angle beam, delay line, and immersion transducers utilise this basic design. The Phased Array probes used in imaging applications simply combine a number of individual transducer elements in a single assembly. Dual element transducers, commonly used in corrosion survey applications, differ in a way that they have separate transmitting and receiving elements separated by a sound barrier, no backing, and an integral delay line to steer and couple the sound energy rather than a wear plate or lens. Figure 2.1 illustrates the typical transducer construction.

While the basic concept is simple, transducers are precision devices that require great care in design, material selection, and manufacturing to help ensure optimum and consistent performance. The transducers commonly used in conventional ultrasonic NDT fall into five general categories based on their design and intended use. Based on design the crack defect only can detect when the piezoelectric sensor probe is perpendicular with the crack point on plate / pipe.
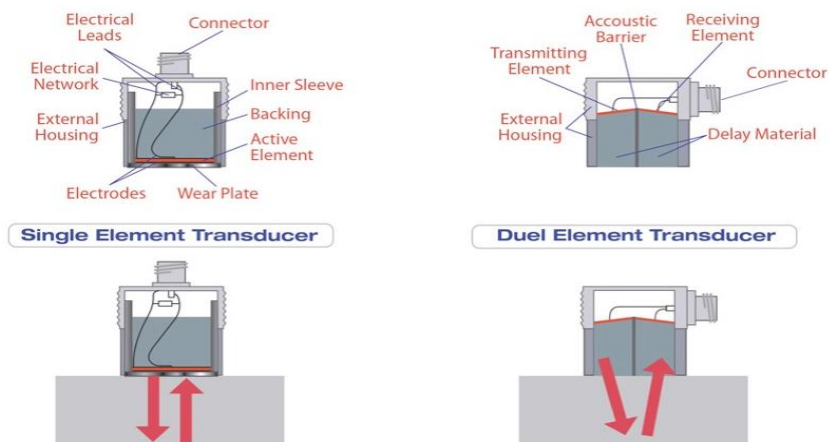
Figure 2.1   Typical single element and dual element transducer construction

2.4.1 Synthetic Aperture Focusing Technique for Heavy Rotor Transducer

Point Spread Function (PSF) simulation needs to be validated, therefore scatters infinitesimally small which should have been inspected by using Ultrasonic Testing for wavelength. The side-drilled holes and flat bottom holes are used as reference reflectors to facilitate access in NDT inspection. However, there is a slight difference between the ideal point

target, and actual penetration marks as shown in Figure 2.2, comparing between PSF and relative radial position 0.2 based on 1mm diameter flat hole. Proportional locations are desirable since it allows to instantly compare the effects of both, slightly differently sized specimen. Since the accepted considerations - far area condition and no attenuation - the final position causes no direct determination on the results (Fendt, Mooshofer, Rupitsch, Lerch, & Ermert, 2013).

(a)

(b)

(c)
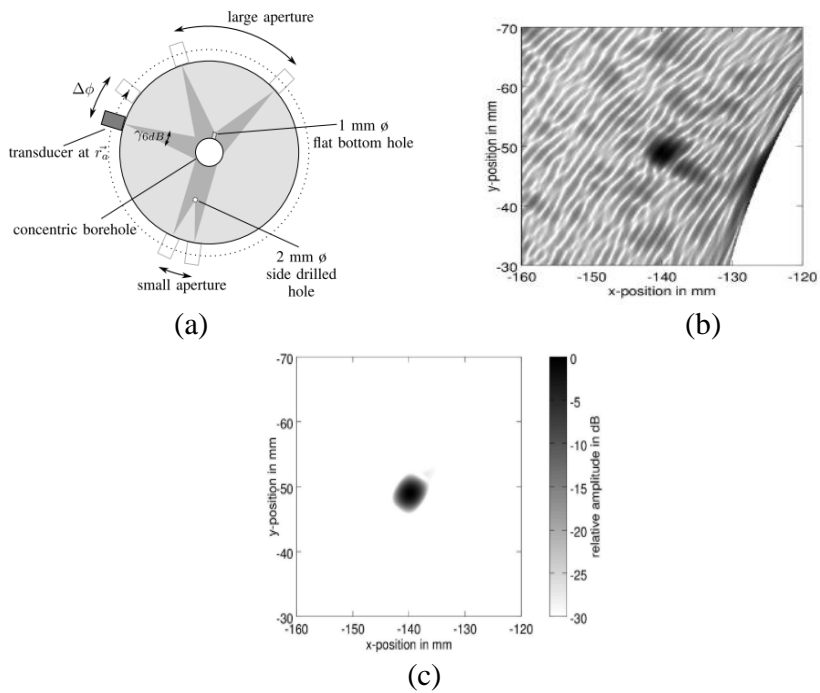
Figure 2.2   (a) Illustration of effective synthetic aperture measurement (b) Gaussian weighted reconstruction image SAFT (c) simulated point spread function.

2.4.2   Automated Non-Contact NDT Transducer

Air-coupled for non-contact techniques is used in synthesising Non-Destructive Tests for characterisation between surface defects and surface structures for scanning purpose using automatic Ultrasonic Testing. One of issues noted was the relationship between the parts examined during the measurement to not occur at all. Therefore, the study of scanners based on several examples include the detection of old railways to identify defects as well as in the concrete walls using the reverse analysis. While the amplitude decomposition for surface wave distributes in a homogenous material encountered signal A(x) which is primarily regulated along coefficient 1/x*0.5 and (ref. Equation. (2.1)) for attenuation. Whenever there is a surface fault, the diversified energy will be reflected due to the obstruction, and consequently, low quantity of diversified energy will infiltrate. Figure 2.3 shows the system and sensing of artificial surface crack in a steel slab of 4 mm's depth and 60 mm's length, as demonstrated in Figure 2.3(a) and (b) in which the Fc=350 kHz, as a transmitting transducer for central frequency was utilised. Figure 2.3(c) shows a decrease in the signal across the defect with the amplitude of A(x). For profile two that is far from the defect, the signal between amplitudes is monotonic to the distance according to Equation 2.1 (Q. Liu, Piwakowski, Lafhaj, & Agred, 2014):

$$S(\omega, x) = S_o(\omega)\frac{1}{\sqrt{x}}e^{-\alpha(\omega)x} - e^{-fk(\omega)x} = A(x).e^{-fk(\omega)x} \qquad (2.1)$$

Where $S_o(\omega)$ the radiated signal spectrum where k and ω are respectively wave number and angular frequency, and the phase velocity ratio $\omega/_k = V_{ph}$ defines.

(a)   (b)

(c)
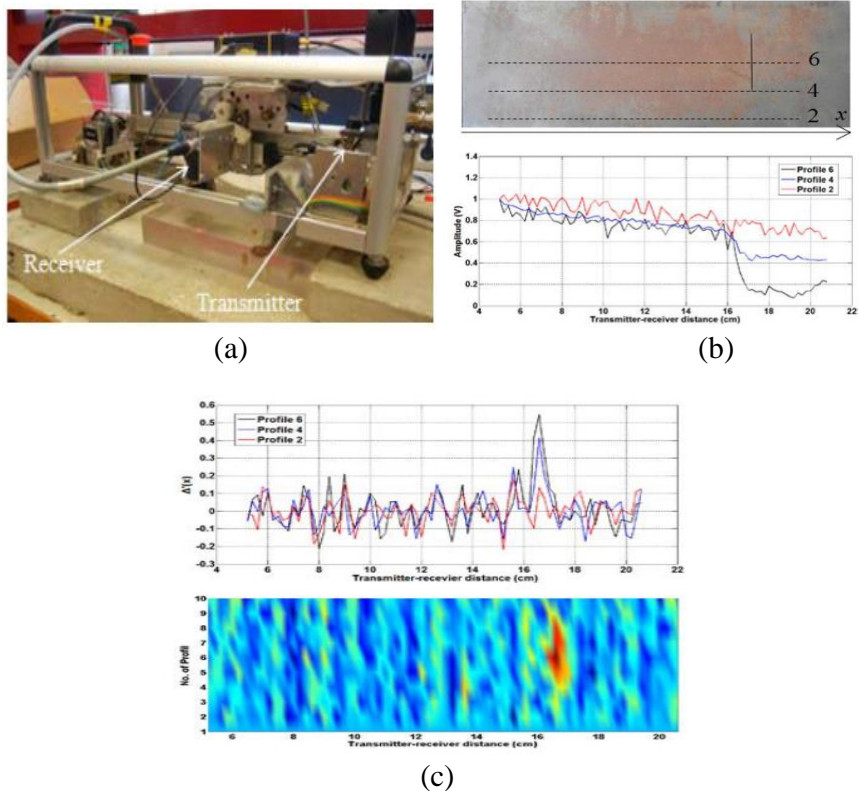
Figure 2.3   (a) System of Emission and acquisition geometry (b)Artificial surface defect in steel slab at the 2, 4 and 6 positions; (b) Normalized amplitude A(x) for each defect; (c) $\Delta'(x)$ parameter for defect; (c) B-scan showing $\Delta'(x)$ parameter for defect.

Figure 2.4(a) shows the speed limit problem, a special sliding probe with belt carrier which was developed, which can achieve a higher inspection speed up to100km/h. Belt wheel carrier is a combination of the wheel

probe carrier and sliding probe carrier (X. Gao, Peng, Wang, & Li, 2016). Figure 2.4(b) shows the C(x) measurements in which C(x) gets maximum values at two major defects. Notice that the fluctuation C(x) shows several smaller defects of the rail surface (Q. Liu et al., 2014).
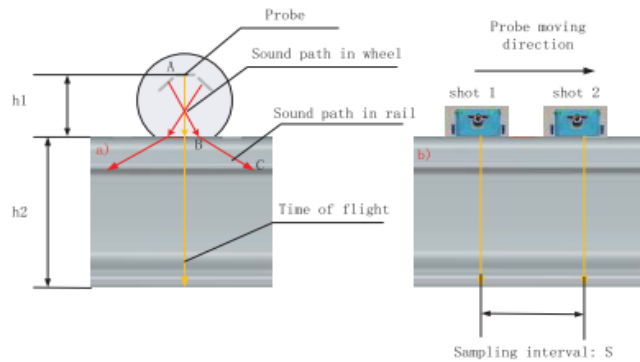
(a)
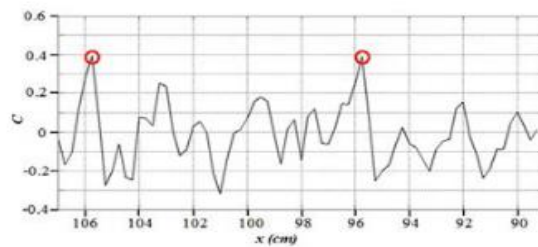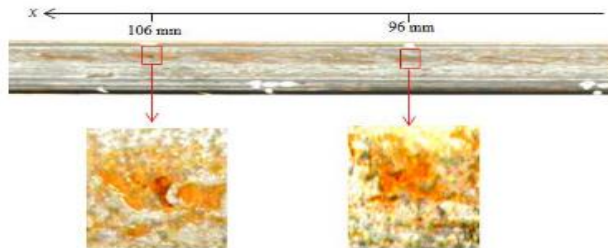
(b)

Figure 2.4   (a) Design of inspection speed (b) Railway rail in the top view for visually for observation two main defects and positions defects C(x).

In porous materials, the introduced velocity gradient is used for rapid inspection. The selection of frequency range and measurement of the levels of surface inhomogeneity can be estimated based on this analysis. Besides, information regarding the depth and irreverence sample can be obtained by inverse analysis based on its characteristics (Q. Liu et al., 2014).

2.4.3   Air-Coupled Ultrasound Transducer

Optimisation of an Air-Coupled Ultrasound (ACU) involves geometric configuration of ultrasound systems for the inspection of a single side of the concrete/asphalt road pavements on the presence of subsurface delamination. The findings can be used as specification baseline for a guideline in system setup of ACU system development under TIE PIE DAQ module as seen in Figure 2.5(a). The geometry model used in the actual dimensions is shown in Figure 2.5(b). The components involved are signal conditioning, sound absorbing shield, air domain, two Piezoelectric transducers (transceiver), sound absorbing shield, concrete/asphalt test slab consisting of surface as well as sound absorbing shield (Bernieri, Ferrigno, Laracca, Rasile, & Ricci, 2017; Uus, Liatsis, Nardoni, & Rahman, 2015).
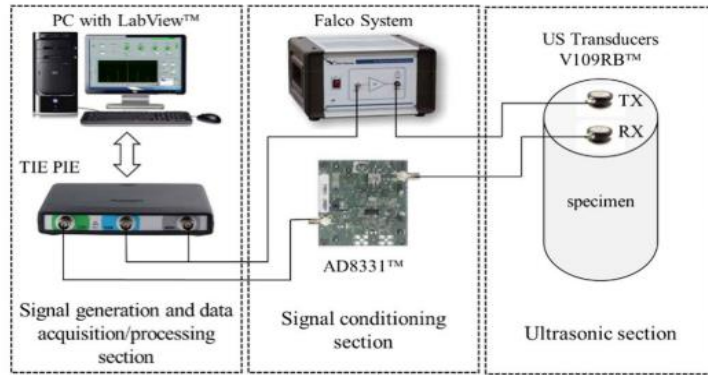
(a)
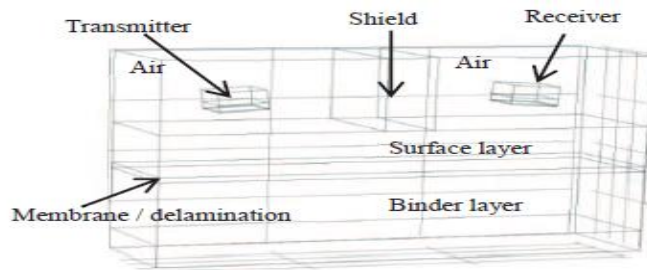
(b)

Figure 2.5   (a) The system measurement set-up (b)3D geometry

setup: ACU transducers and concrete test slab

The instrumentation which was used is shown in Figure 2.6(a). An
arbitrary function generator delivered the excitation signal to an ENI
240L power amplifier wherein the output was sent to the transducer ring;
the individual transducers in the ring being connected in parallel. This
can be seen in the parametric study conducted in a series of FEM
simulation aimed at identifying the optimum rate for the configuration
of the geometric system(Lowe, Alleyne, & Cawley, 1998). The method
used was cross-yielding ultrasound qualitatively and quantitatively
(acoustic pressure level) based on impulse response and test slab (Vpp)
on receipt of Piezoelectric transducers. Referring to Figure 2.6, namely
(a) the level of acoustic pressure is measured as dB for cases without and

(b) thinning 2mm filled the air. Loss of signal pressure can be seen through the different layers of distortion and a binder or a surface reaction than the reception transducer against high pressure (Gaunaurd, 1989)..
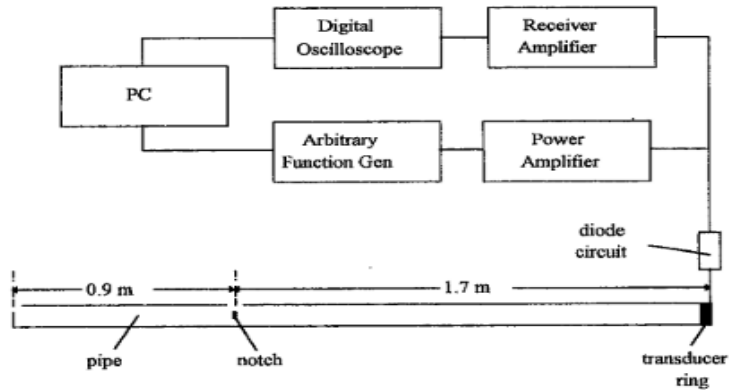
(a)
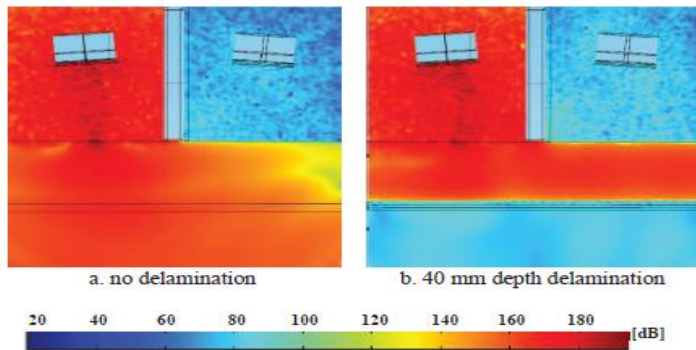
(b)

Figure 2.6   (a) Schematic diagram (b)Simulation results: computed acoustic pressure fields

2.4.4   Piezoelectric Plate Ultrasonic Transducer

Piezoelectric plate is generally used as a conventional ultrasonic transducer where it functions through vibration on its thickness mode.

From the Figure 2.7(a), the vibration produces two ultrasonic waves; firstly, the useful acoustic energy (traveling forward) which used in making the ultrasonic beam and secondly, the wave moving backward which is the unnecessary echoes, could later come back in this direction thus needed to be attenuated. The reason is that it can affect the diagnostics of the forward wave propagation. The Piezoelectric plate vibration affects the ultrasonic projection in the production of two ultrasonic waveforms. Figure 2.7(b) manifests the use of ultrasonic beams on both waves like a set of mirrors that show the same direction for both waves.
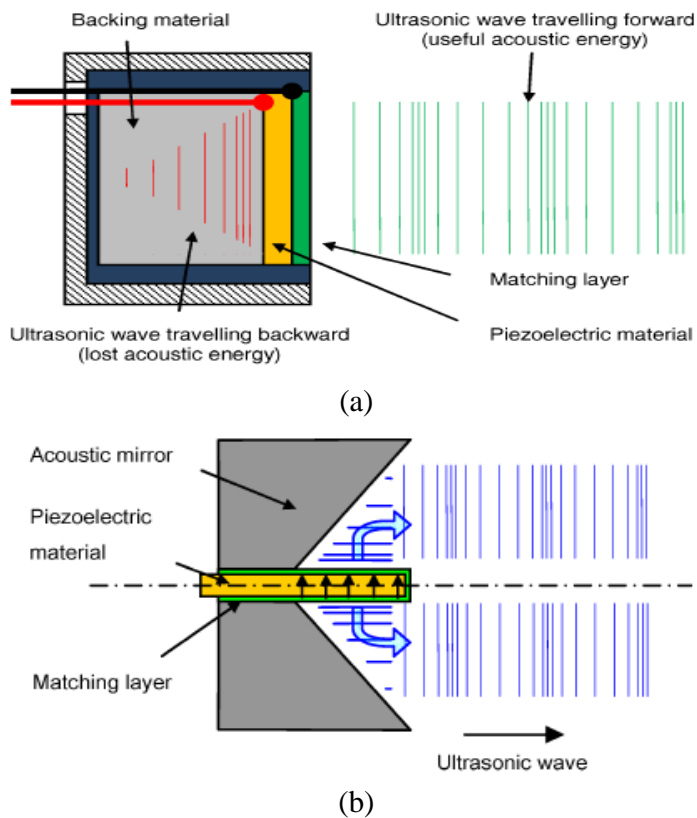
Figure 2.7   (a) Conventional ultrasonic transducer principle,
(b)Ultrasonic Piezoelectric plate principle

2.4.5   Composite Ultrasonic Transducer

Figure 2.8 demonstrates the ultrasonic setup and reactions by every cycle at 600°C of CBT/PZT transducer. On the titanium, substrate had the reflected echoes from the bottom surface found in Signal to Noise Ratio (SNR) which is sensible for clearness. The dependence of the sensitivity of CBT/PZT is shown in Figure 2.8(a) with the three thermal cycles and temperature. The CBT/PZT's sensibility comprised of reduced noise on the first thermal cycle, primarily referring to the permanent deployment of the sol-gel phase PZT. There involved no visible difference between the second cycle and the third cycles (Kibe, Kimoto, & Kobayashi, 2016).

(a)   (b)

(c)   (d)
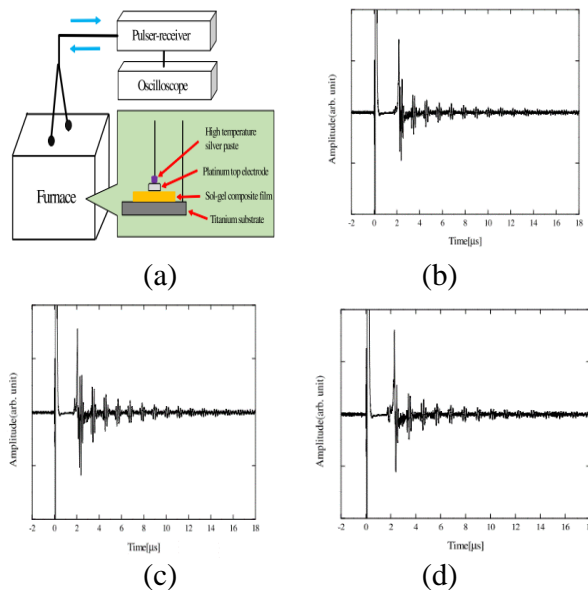
Figure 2.8   (a)Measurement set up, (b)1st cycle of ultrasonic response at 600 °C in CBT/PZT transducer, (c)Ultrasonic response of CBT/PZT transducer at 600 °C in 2nd cycle, (d)3rd cycle of ultrasonic response at 600 °C in CBT/PZT transducer.

The application of Piezoelectric as the transducer in this section gives high impact on crack identification. However, this research is only focusing on the crack with under layer either for plate or pipe. The positioning of probe is perpendicular with crack positioning, in other words, the excitation signal is given in vertically and it will be limiting the crack detection distance at pipe line or plate. At the same time, it is only applicable for short range detection in Piezoelectric sensor inspection method.

2.5   Ultrasonic and Piezoelectric Transducer Waves Form

This section presents a review of Ultrasonic and Shear Horizontal (SH) methods based on elastic waves propagation. The brief detail of understanding the propagation of basic principles of wave generation that lay at the foundation of this process comes from the viewpoint of the fracture mechanics (Nazarchuk, 2017).

2.5.1   The Principle and Model of Lamb Wave

Lamb discovered that an infinite number of different modes can exist within plates. The displacement pattern for these modes can be classified according to the displacement symmetry. Figure 2.9 shows the through wall displacement pattern for the two fundamental Lamb modes for each classification: 'Asymmetric' (A0) and 'Symmetric' (S0). The line of symmetry here is shown as the dotted centre line of the plate. The particle displacements for Lamb waves are similar to the elliptical motion observed in Rayleigh waves. The propagation characteristics of

Lamb waves depend on the excitation frequency as through wall displacement depends upon wavelength. Excitation parameters for this class of wave mode are sometimes expressed in terms of the frequency thickness product. An increase in excitation frequency or thickness results in the presence of more wave modes. It is beneficial to work towards wave mode purity in order to keep the received test data comprehensive and to contain a low level of coherent noise. The nomenclature for sorting Lamb wave modes is as follows; for the symmetric modes, the fundamental mode is S0 and higher order modes increase by n in the form of S1, S2, S3...Sn, while for the asymmetric modes, this becomes A0, A1, A2, A3...An.
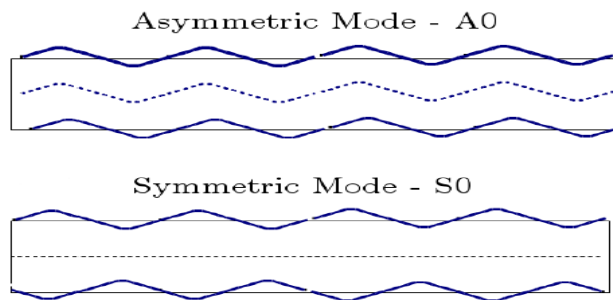
Figure 2.9   A graphical representation of the displacement pattern of Lamb waves

The Lamb Wave method emphasises that an infinite number of different wave modes is able to exist within a sampled test plate. In particular, the displacement pattern for these wave modes can be classified according to the displacement symmetry of the wave. More importantly, Lamb Waves can be considered as the superposition of longitudinal, while shear modes are defined based on Equations 2.2 until Equation 2.5 which

are related to each other. Accordingly, each class of Lamb Wave mode can be described using the wave vectors p and q based on the characteristic Equations as follows;

$$.p^2 = \left(\frac{\omega}{cl}\right)^2 - k^2 \tag{2.2}$$

and

$$q^2 = \left(\frac{\omega}{c_s}\right)^2 - k^2 \tag{2.3}$$

Where ω is angular frequency and k is wave number. The characteristic equations are shown below:

$$\frac{tan(qh)}{tan(ph)} = -\frac{4k^2pq}{(q^2-k^2)^2} \tag{2.4}$$

For symmetric modes

$$\frac{tan(qh)}{tan(ph)} = -\frac{(q^2-k^2)^2}{4k^2pq} \tag{2.5}$$

for asymmetric modes where h represents half of the plate thickness, followed by k which is the wavenumber $(2\pi/\lambda)$.

On another note, waves propagating within an elastic medium can be subjected to a phenomenon known as dispersion. Nevertheless, the causes of dispersion have not been fully understood; however, the effect manifested itself as a distortion of the propagating pulse. Accordingly, it was found that the distortion is caused by the frequency-dependent phase as well as the group velocity of a given wave mode propagating within the medium. A pulse or pulse train contains a number of frequency components within; hence, it will pose a range of group and phase

velocity values if propagated in a dispersive medium. In addition, this range of velocity values will result in some frequency components that overtake others during the propagation through the dispersive medium. Moreover, the change in phase and group information for the pulse tend to cause distortion. As presented in Figure 2.10, all guided wave modes exhibit this effect to a given degree with the two fundamental shear-based modes (T (0; 1) and SH0). However, it is an exception to this rule because they do not exhibit frequency dependent velocities during propagation.
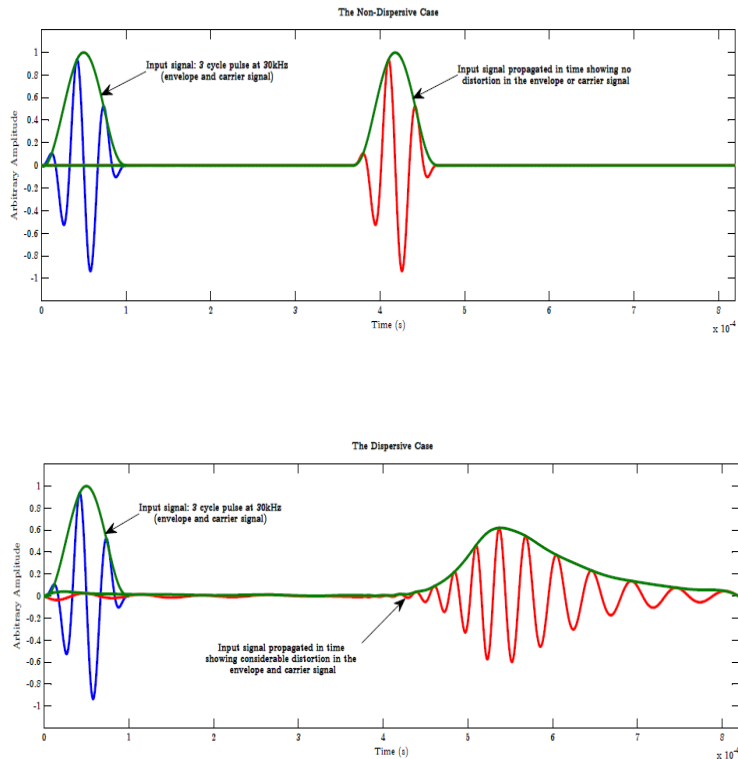
Figure 2.10   The distortion of a 3 cycle, 30kHz pulse when propagated in a dispersive medium.

2.5.2 Lamb Waves

The application of Lamb waves include the ultrasonic waves that guided lower plate and upper surfaces and between two parallel surfaces. The Lamb Waves can exist as symmetrical and antisymmetric types. Figure 2.11(a) shows the particle motion of symmetric and antisymmetric Lamb waves (Kamas et al., 2015). The Lamb Wave motion has asymptotic behaviour at low frequency and high frequency. At low frequency, the symmetric mode resembles axial waves, while the antisymmetric mode resembles flexural waves (Yu & Giurgiutiu, 2008). At high frequency, a combined symmetric and antisymmetric waves approach Rayleigh waves, due to the particle motion which is stronger at the surfaces and decays rapidly across the thickness. The axial and bending waves are according to their nature, at a low frequency of Lamb Waves. The plate structure cannot sustain pure axial and flexural motion at large frequency-thickness product values (Abbas & Shafiee, 2018; Lamb, 1917; Sause, 2016; Victor, 2010). The derivation finally reaches the Rayleigh-Lamb Equation 2.6

$$\frac{\tan \eta_s d}{\tan \eta_p d} = \left[\frac{-4\eta_p \eta_s \xi^2}{(\xi^2 - \eta_s^2)^2}\right]^{\pm 1} \tag{2.6}$$

Where:
d is the half plate thickness ± 1:
(-1) represent antisymmetric Lamb wave modes
(+1) symmetric Lamb wave modes.
The frequency dependent on the wave number ξ is, as η_s and η_p are given in Equation 2.7.

$$\eta_p^2 = \frac{\omega^2}{c_p^2} - \xi^2; \; \eta_s^2 = \frac{\omega^2}{c_s^2} - \xi^2; \; c_p = \sqrt{\frac{\lambda+2\mu}{\rho}}; \; c_s = \sqrt{\frac{\mu}{\rho}}; \qquad (2.7)$$

Where:

ρ is density

λ and μ are constants of the material Lame.

Figure 2.11(b) represents the system PSAW and curves of dispersion for aluminium plates and was calculated based on the Rayleigh-Lamb equations. Simultaneously, there are two wave modes that exist which are the symmetrical mode, S0 and antisymmetric mode, A0 (Shen, 2014). Beyond the corresponding cut-off frequencies, higher Lamb modes will participate in the propagation. At small frequency-thickness product values, the A0 mode is more dispersive than S0 mode, and all the Lamb Wave modes converge to non-dispersive Rayleigh waves at large frequency-thickness product values. The dispersive and nature of Lamb Waves with multi-mode added complexity in both Lamb Wave propagation modelling and SHM application (Shahdin et al., 2018; Victor, 2010). However this method (Pitch Catch) have the disadvantage because of positioning of Piezo actuator and Piezo receiver with different place and the possibility for signal lost is high.

(a)

Wave speed dispersion curve

Wavenumber dispersion curve
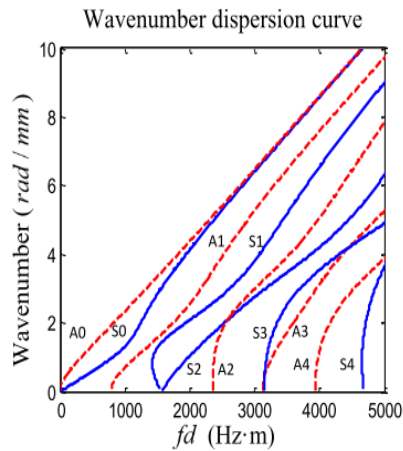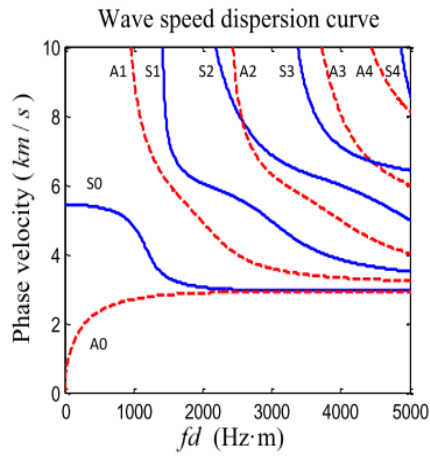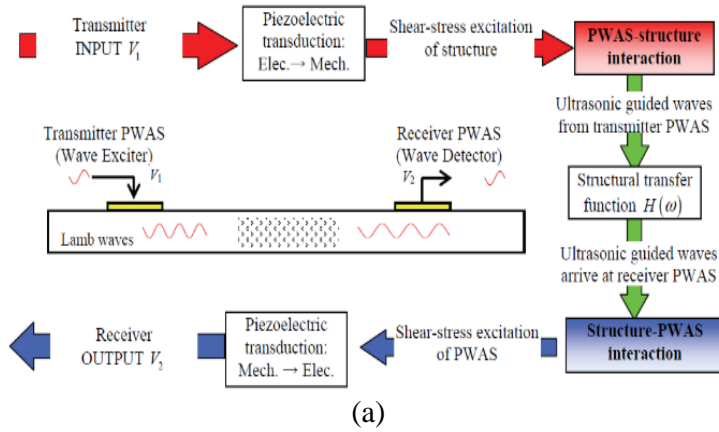
(b)   (c)

Figure 2.11   (a) PWAS system transmitter, (b) Wave speed

dispersion curve, (c) wavenumber dispersion curve.

2.5.3 Rayleigh Waves

Surface waves or Rayleigh Waves spread near the surface of the body and have a rapidly decreasing motion based on the depth of the amplitude. This can be seen based on the polarisation of the plane perpendicular to the surface of the Rayleigh Waves. In addition, the wavelength effect will indicate the effective penetration depth. One of the benefits of using Rayleigh waves for Structural Health Monitoring is the feedback signal will not be scattered on Rayleigh waves; thus, the wave is fixed. A common approximation of the wave speed of Rayleigh Wave c_R is given as Equation 2.8.

$$c_R(v) = c_S \left(\frac{0.87 + 1.12v}{1+v} \right) \qquad (2.8)$$

Where v is the Poisson ratio and c_S .is the shear wave speed. The acceleration of Rayleigh wave acquired measures approximately under the shear wave speed based on the basic Poisson ratio evaluated (Yu, Santoni-Bottai, Xu, Liu, & Giurgiutiu, 2008). The particle motion or the mode shape of the Rayleigh Waves across the thickness direction, y, is given in Equation 2.9 and 2.10.

$$u'_x(y) = Ai \left(\xi e^{-\alpha y} - \frac{\beta^2 + \xi^2}{2\xi} e^{-\beta y} \right) \qquad (2.9)$$

$$u'_y(y) = A \left(-\alpha e^{-\alpha y} + \frac{\beta^2 + \xi^2}{2\beta} e^{-\beta y} \right) \qquad (2.10)$$

Figure 2.12 shows the semi-infinite medium for Rayleigh Waves and circuit transducers (Shen, 2014; Shen & Giurgiutiu, 2014); where A is the wave amplitude factor, $\xi = \omega/c_R$ is the wavenumber of Rayleigh surface waves, α and β are coefficients given in Equation 2.11.

$$\alpha^2 = \xi^2 \left(1 - \frac{c^2}{c_P^2}\right); \ \beta^2 = \ \xi^2 \left(1 - \frac{c^2}{c_S^2}\right) \hspace{2cm} (2.11)$$

(a)   (b)
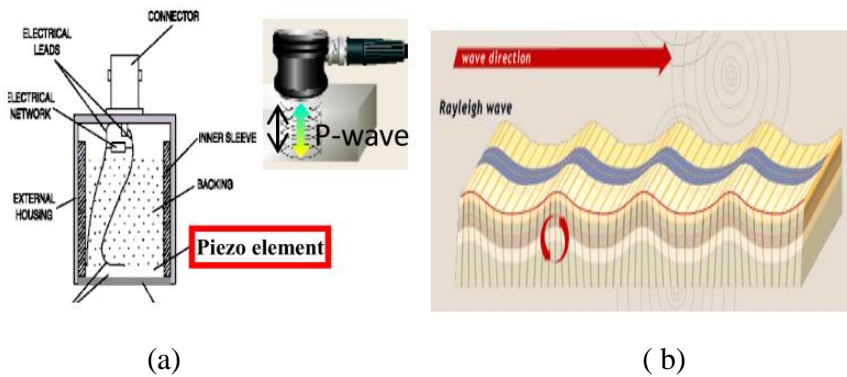
Figure 2.12   (a) The ultrasonic circuit transducer, (b) Rayleigh wave
propagation in a semi-infinite medium

2.5.4   Shear Horizontal Plate Waves

There is a movement in the horizontal plane shear against the wave-particle type horizontal plate (HP). The movement of particles towards the plate SH wave can be designated based on the definition of coordinates in Figure 2.13(a). This can be seen based on the movement of particles along the z-axis while the spread of the wave occurs along the x-axis and it is defined as SH wave coordinates. Figure 2.13(b) shows the hardware setup for SH in which x0z horizontal plane being the only key component of this movement. The second movement of waves with

different modes include Rayleigh waves which are scattered SH and nondispersive (Song, Li, Wang, & Du, 2015; Yu & Giurgiutiu, 2008). The SH wave calculation demonstrated by the phase velocity dispersion curves is presented in Equation 2.12.

$$c(\omega) = \frac{c_S}{\sqrt{1-(nd)^2\left(\frac{c_S}{\omega d}\right)^2}}$$

(2.12)

Where η is given in Equation 2.13 and d is the half plate thickness.

$$\eta^2 = \frac{\omega^2}{c_S^2} - \frac{\omega^2}{c^2}$$

(2.13)
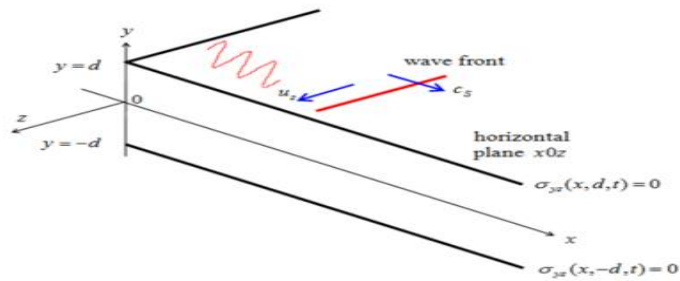
(a)
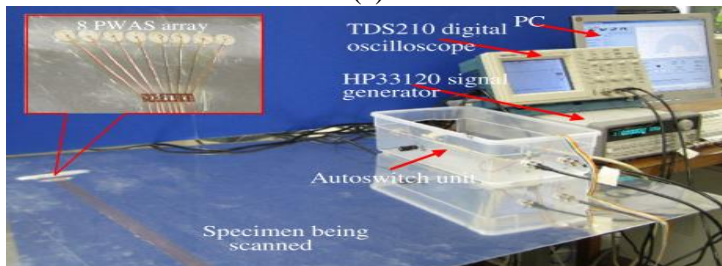
(b)

Figure 2.13   (a) Circuit and hardware setup, (b) Coordinate definition and particle motion of SH plate waves.

Higher wave modes only appear beyond the corresponding cut-off frequencies, showing dispersive characteristics, i.e., their phase velocity changes with frequency. For dispersive waves, the group velocity is usually used to evaluate the propagation of wave packets. The definition of group velocity is given in Equation 2.14.

$$c_g = \frac{d\omega}{d\xi} \tag{2.14}$$

Figure 2.14 shows the wave-speed dispersion curve of SH plate waves and the mode shapes; whereas Figure 2.14(a) indicates a system development for SH plate (Yu et al., 2008). Recently, considerable amount of research has been carried out on the transmission and reception of the SH plate wave for SHM (Kamal & Giurgiutiu, 2014; Zhou et al., 2014).

(a)   (b)
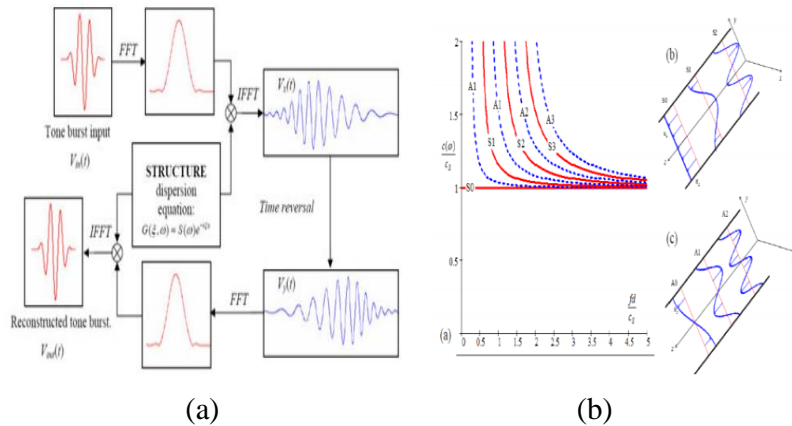
Figure 2.14   (a) System development (b)SH plate wave-speed dispersion curve for symmetric mode shapes and antisymmetric mode shapes.

Table 2.2   Application of Piezoelectric transducer in Ultrasonic
Testing

Method / Technique	Transducer and Material	Benefit
Acoustoelasticity in Polymer Bonded Explosive's Stress (Y. Xu, Yang, Zhou, & Zhang, 2016)	Ultrasonic Waves (Plate)	The velocity of longitudinal waves in a timely and efficient manner.
GaN-based High Energy Delivery in Ultrasound Pulse Generator (H. Peng, Sabate, & Wall, 2017)	Ultrasound and Piezoelectric (Design Transformer Push -Pull Pulse Generator)	High frequencies, high bandwidth transformers are needed to handle broad frequencies, amplitude range, which are easily achieved using EMIS
Ultrasonic Method Residual Stresses in Welded Elements (Kleiman & Kudryavtsev, 2015)	Ultrasonic (The Wide Range of Materials)	Ultrasonic Computerised Complex (UCC) for NDT measurements of residual and applied stresses that was developed in large-welded specimens and high tensile stress pressure structures.
Surface Wave Technology for EMAT-Generated (H. Gao, Lopez, Minguez, & Chen, 2015)	Piezoelectric (Thick-wall)	Electromagnetic acoustic transducers (EMATs) to generate surface acoustic waves.
A Migration Approach (Braconnier, 2016)	Ultrasonic (Simulation)	Migration approach is tailored to the layered objects while standard techniques can customise complex geometries.
Ultrasonic NDT in 3D SAFT for Sparse Deconvolution (Kirchhof et al., 2016)	Ultrasonic (Simulation)	Real-time processing is activated since deconvolution steps rarely work in hardware/software setup ultrasonic.
POD Train Axles for Laser Ultrasonic NDT (Malik, 2016)	Laser Ultrasonic (Train Axles)	Non-contact inspection methods for surface axle inspections of train axles for their lifespan.
Ultrasonic Coda Waves on Deficient Restressed Concrete Bridge T-beam (Xie, Zhuang, Jiang, Fan, & Ren, 2016)	Ultrasonic (T-beams Plate)	T-beams of pre-stressed concrete bridge shortages in elastic coefficient-acoustic wave interferometry.
Twin-robot in Calibration Method using Ultrasonic Testing (S. Liu, Hao, Lu, Zhang, & Zhao, 2016)	Ultrasonic (Plate)	The precision of the calibration method is relatively high.

Table 2.2   Continued

Method / Technique	Transducer and Material	Benefit
Bragg Grating Sensors in Laser-Based Ultrasonic for Adaptive Fibre (Y. Zhao et al., 2016)	Laser-Based Ultrasonic (Fibre Adaptive)	SHM applications, particularly in the detection of infrastructure damage.
NDT for In-situ Concrete Structures (Noufid & Belattar, 2016)	Piezoelectric (Concrete Structures)	Present in quality assurance procedures (QAP) to assess the strength of concrete structures.
Ultrasonic Imaging with Decomposition Time Reversal Operator and Walsh-Hadamard Codes (Lopez Villaverde, Robert, & Prada, 2017)	Ultrasonic (Polyethylene Pipe)	To improve image quality, time reversal operator decomposition method of transmitting.
Evolution of Crack Detection for Railway Track (Lad & Pawar, 2017)	Ultrasonic (Railway Track)	Disabled prone size depends on the Ultrasonic Wavelength.
Two-Dimensional Compressed Pulse Analysis in Discrimination Ultrasonic Coded (Malo, Fateri, Livadas, Mares, & Gan, 2017)	Ultrasonic (Simulation)	Combines the use of pulse compression and dispensing compensation to improve signal-to-noise ratio.
Reconstruction of Shadowed Flaws using Ultrasonic Detection (Kirchhof et al., 2017)	Ultrasonic (Simulation)	The intensity of acoustics due to a protective effect based on geometric considerations.
Electromagnetic Resonant for Pipeline using Ultrasonic Sensor (G. Zhong, Tian, Meng, & Gao, 2017)	Ultrasonic Sensor (Pipelines)	It provides a new design small voltage, high current, high-efficiency excitation power for pipelines.
Time-Varying Wiener Deconvolution in Time Corrected Gain UT (Pipa, Guarneri, & Moura, 2017)	Ultrasonic Testing (Wiener filter)	TCG adjustment is able to handle noise and space attenuation correction.
Non-destructive Line-focused Transducer in Additive Manufacture Metal Alloy (Ji & Wang, 2017)	Ultrasonic (Metal Alloy)	Surface wave velocity and Young modulus have a negative correlation with corrosion level.
Phased-Array C-Scans for Complex Shape 3D Ultrasonic (Mineo, Summan, Riise, Macleod, & Pierce, 2017)	Ultrasonic (Tessellated Surfaces)	3D imaging by multiple levels of ultrasonic using TFM based slice has a high-resolution advantage

The widely used Piezoelectric application in Ultrasonic Testing can be seen from Table 2.2. From here, the Piezoelectric application was not only focusing on steel plate or pipe, but it was also used in concrete structure, polyethylene and also in Wiener filter for the conditioning of materials.

In this section, there are three types of waves form which have been used by the previous researcher including Lamb Waves, Rayleigh Waves and Shear Horizontal Waves. Each wave has the function and advantage in the process of identifying the location of the crack. The crack location identification depends on the feedback signal which is resulting from the excitation wave that is given based on shape and frequency wave, and it will affect the reflection wave. From here, the selection of wave type and frequency should being focusing on ensuring the feedback signal received to accurate in the crack identification.

2.6 Optimization of acoustic excitation in ultrasonic testing

2.6.1 Defects Detection Optimizing

Fatigue cracks visible on about two-thirds of the damage, which classified as the cause of the axle damage(Carino, 2001). The factors that cause the cracks are such as fret corrosion over time, waste tensile stresses and pressure concentrations during acoustic pressure(Kim et al., 2015). Finite element analysis using ultrasonic testing is used to detect the distribution of stresses of the press-acute section(Kazys, Vilpisauskas, & Sestoke, 2018). Ultrasonic use trials for detecting defects between axles with the press and empty axes completed. In

reference to Figure 2.15(a), (b), (c) and (d) is after filtration. The grey represents a disturbance waveform with pressure while the red dot is a region with cracking defects. Finally, algorithmically adaptive filtering is optimized for B data for the repair of disability and noise ratio (C. Y. Peng et al., 2016).

(a)
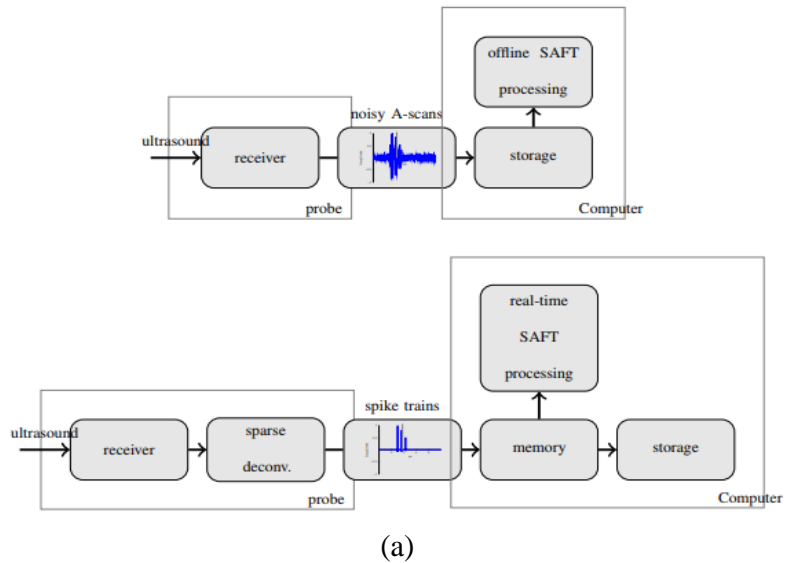
Figure 2.15   (a) Architectures of post-processing Ultrasonic (b)B-scan strong interface (c)Weak interface (d) Interface wave before and after Filtering
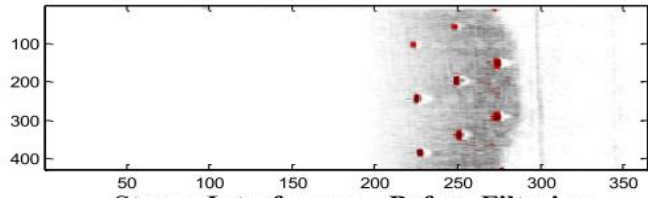
Strong Interference - Before Filtering
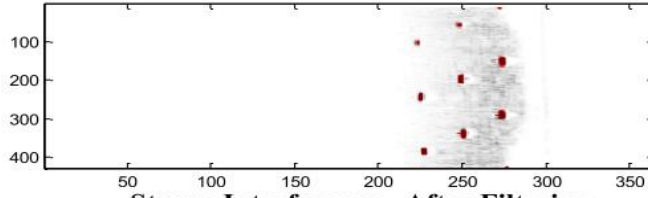
Strong Interference - After Filtering

(b)
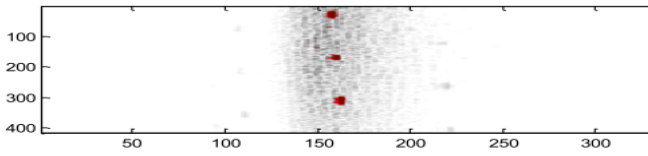
Weak Interference - Before Filtering
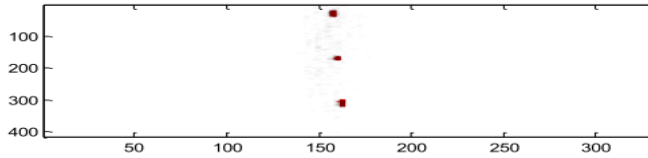
Weak Interference - After Filtering

(c)
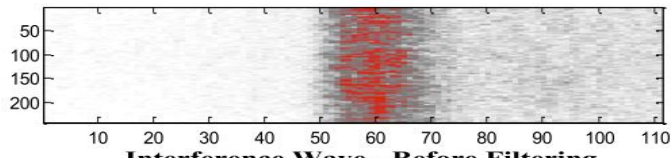
Interference Wave - Before Filtering
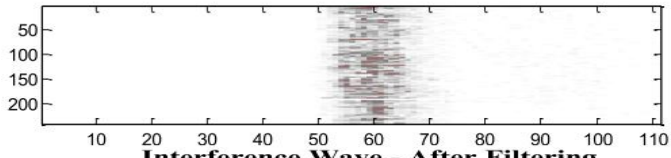
Interference Wave - After Filtering

(d)

Figure 2.15   Continued

2.6.2 Evaluation Of F-K Migration Optimization

The process involved in the formation of a Synthetic Aperture Focusing Technique (SAFT) image is represented schematically in Figure 2.16(a), assuming that Report of Inspection (ROI) is located on the xz plane. Since the length of the transducer in the x-direction is comparable with the wavelength, the wavefront can be approximated as omnidirectional Plane Wave Imaging (PWI) which has recently been talked about for multi-mode imaging in solid (Iriarte, Cosarinsky, & Brizuela, 2016). A new kind of algorithm has been developed in solving this problem where image counting occurs in the F-K frequency domain. The rules were first introduced in seismic migration and synthetic aperture radar. In both frequency domain methods, they are evaluated in the 2D image compared with the method of Lu, and Plane Wave Imaging (PWI) was evaluated in 3D to image small porosity distribution in the steel block. As shown in Figure 2.16(b), the Lu method exhibits better resolution than PWI, the second resolution worsens deeper by using zero rejection factor of 2.5 in time and 3 in both dimensions of space. Overall, for the 100×100×800 vowel image size, Lu reconstruction took 300s to 25 angles while PWI took the same time for each individual angle. The domain frequency method enables shorter calculation time while delivering comparable results and better than PWI-domain time (Merabet, Robert, Prada, & Langevin, 2016; Moallemi, Member, Shahbazpanahi, & Member, 2014).

(a)

z=4mm
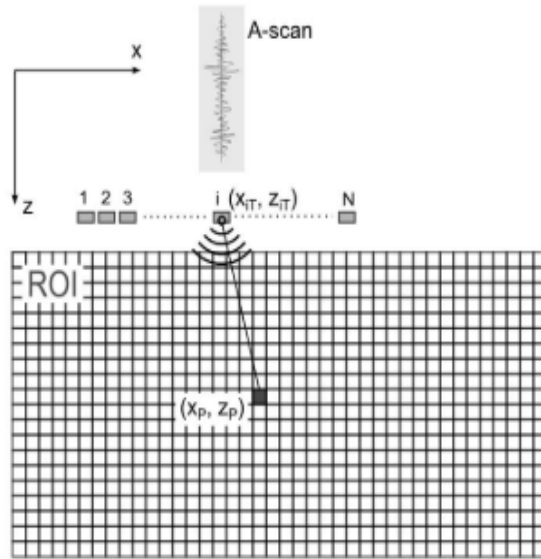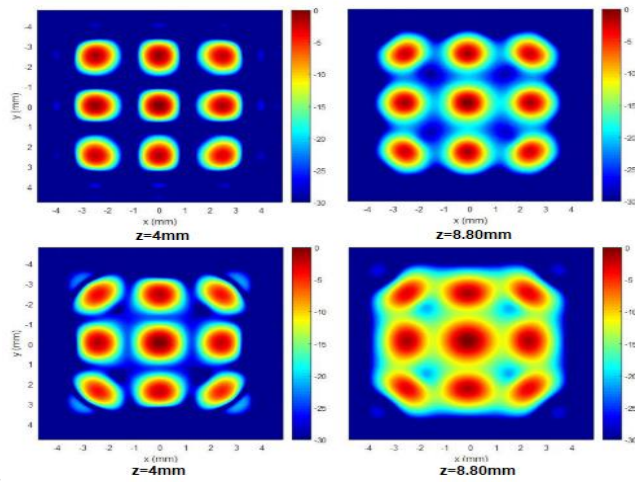
z=8.80mm

z=4mm

z=8.80mm

(b)

Figure 2.16   (a) SAFT image procedure for reconstructing the ROI

(b)3D images of Horizontal slices at z = 4 mm and z = 8.80 mm

2.6.3   Wave Mode Beamforming

An Ultrasound Wave is generated when an electric field is applied to an array of Piezoelectric crystals located on the transducer surface, which usually contains 128-256 arrays of element. To achieve similar current rating, two silicon switches are used in parallel Figure 2.17(a) (H. Peng et al., 2017). Distortion of Minimum Variance of Less Reaction (MVDR) has been used for some imaging areas, including from underwater acoustics for detection of active damage in the structure (Lanza et al., 2017). Weight adjustment MVDR minimises the output array, except in the "viewing direction" scanning. However, MVDR is acquired under noise and the ideal interference noise and it can be harmful when the wave model is inaccurate and/or in the case of Signal-to-Noise Ratio (SNR) (Lanza, Sternini, & Nguyen, 2016). Compound wave mode can be done either inconsistently or coherently, in analogy with the incorporation frequency or double shooting (Lowe et al., 1998)(Moallemi et al., 2014). The amplitude distribution of the measured wave across the array with the expected amplitude distribution from the "true" focus based on the dispersion wave physics, especially the expected distribution of the displacements of the plane across the diagram (Lanza et al., 2016). Relative performance compared coherent explanation should not be dependent on the level of SNR case at hand, the simulation considered here clearly benefit from the term "cross" extras provided by compounding coherent. In conclusion, both in Figure 2.17(b) of the DAS algorithm and MVDR algorithm, the compound wave mode, implemented with a particular adaptive weight of the mode, appear to generate a huge array of profits without increasing the physical size of the arrays. Again, this behaviour is conceptually similar to the

compounding of multiple receiving frequencies or multiple depictions as routinely performed in other imaging applications (Lanza et al., 2017).
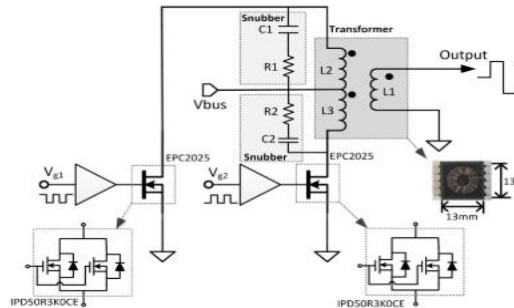
(a)
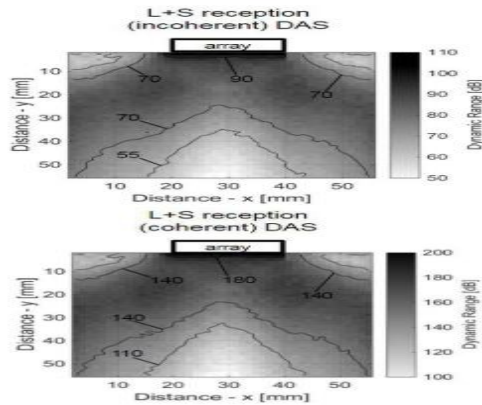
(b)

Figure 2.17   (a)Schematic circuit UT pulse generator (b)Contour plots of dynamic range incoherently and coherently.

From to this section, the optimisation could be shown through the images which are recorded based on optimising method. It also improves the quality of image material and at the same time interpret the defect material image and good condition material images during inspection. Table 2.3 shows the summary of algorithm and optimisation used in Ultrasonic Testing.

Table 2.3   Summary of Image and Algorithms in UT Signal
Optimization

Method / Technique	Transducer and Material	Remark (Benefit)
Axle Press-fit Defects (C. Y. Peng et al., 2016)	Array ultrasonic (Wheels)	Experiment earlier detection of defects between the axle and axle with press-fit have been equipped with ultrasonic multi-level.
Aperture Ultrasound Imaging using GPUs (Iriarte et al., 2016)	Ultrasound Imaging (Austenitic Steel Nuclear Block)	SNR is better, and the lobes reduced scarring and increased the probability of detection of cracks regardless of their orientation.
Evaluation of *f-k* Migration (Merabet et al., 2016)	Ultrasonic Imaging (Steel Block)	Adapt from 2D to 3D imaging more than 30 times faster than the PWI in 2D, about 25 times faster in 3D and provides better lateral resolution in depth.
Wave Mode Beamforming (Lanza et al., 2017)	Ultrasonic Imaging (Aluminium Square)	Improvements that can be obtained by wave adaptive structure compared with either static weight in the conventional delay and some focusing on geometrical spreading.
4S Image Correlation (Cr, Joseph, Samson, Jose, & Subramanian, 2013)	Ultrasonic (Ceramic Products)	Fast 4S to FD block matched with the ability to investigate material which are relatively thick.
Single Ultrasonic Rangefinder (Mahmod, Pauzi, & Bakar, 2013)	Ultrasonic (Composite Laminates)	The proportion between the maximum and minimum image processing and ultrasonic signal.
Real-time Autofocusing Hardware (Cruza, Medina-valdes, & Fritsch, 2015)	Ultrasonic Imaging (Aluminium Part)	Hardware architecture that provides rapid response to performing auto-focus in real time.

Table 2.3   Continued

Method / Technique	Transducer and Material	Remark (Benefit)
Ultrasonic Synthetic Focused Signal Distortion (Ye, Luo, Gao, Jiang, & Yue, 2015)	Ultrasonic Synthetic Focused (Steel Plate)	Improve the quality of the image that is focused and get more useful information on material defects.
Synthesis for Complex Geometry Objects (Tatarnikov, Tsapko, & Pochivalov, 2015)	Ultrasonic System (Object Geometric)	The implementation of new algorithms allowed to realize the possibility of not damaging the test object with an irregular geometry.
Algorithms of Various Defects (Cui et al., 2016)	Ultrasonic Propagation (Thick-wall Pipes)	Prediction on the offset distance to the pipe diameter, defect detection, counting time with good dispersion and detection methods.
CFRP based on Finite Element Modelling (H. Su, Luo, Cao, Zhou, & Lin, 2016)	Ultrasonic Testing (Carbon Fibre Reinforced Plastic)	Designed based on the finite element modelling with consideration of the laminar structure and elastic anisotropy.
Echo Detection using Neural Network (Wang & Saniie, 2017)	Ultrasonic (Steel Block)	Zynq SoC FPGA fabric used to accelerate algorithms and processors.

According on the optimisation section, the inspection is focusing more on the image optimisation generated by using a few methods including Synthetic Aperture Focusing Technique, F-K frequency domain, Plane Wave Imaging, Minimum Variance of Distortion Reaction algorithm, Signal-to-Noise Ratio and Delay-and-Sum algorithm. Following these methods, the image of crack defect will be clear by filtering the noise during the inspection process. The image of the crack will be shown in two or three-dimension image. The critical crack defect is shown by the

colour tone, wherein red indicates a critical point and blue is a normal condition point. Unfortunately, there is no explanation of Piezoelectric sensor array quantity for optimisation that should be applied to ensure the result of image or signal crack to be shown clearly on pipe/plate inspection. From here, the research about Optimisation on Piezoelectric sensor array should be continued to ensure the result of signal crack defect can be identified as a whole, at pipe/plate surface during the Piezoelectric inspection.

2.7   Application of Piezoelectric Transducer in Ultrasonic Testing

Piezoelectric transducer and liquid domain interaction have been commonly investigated through theoretical analysis of resonance spectra in a frequency domain using certain types of standing wave modes; thickness Shear Waves and Shear Horizontal Waves by using different techniques as discussed in the following sections. Table 2.4 below shows the emphasis on method and technique for the image algorithm which were used in defect classification either for 2D or 3D defect during the inspection. Meanwhile, the signal and acoustic impedance section focused more on the feedback signal received from the Piezoelectric sensor and Ultrasonic sensor based on the shape and amplitude. The rest is concentrated on Phase Array, transducer, data acquisition and theory in Piezoelectric and Ultrasonic Testing.

Table 2.4   Summary of UT and Piezoelectric application in Inspection of NDT

Method / Technique **Acoustic Impedance / Signal**	Transducer & Material	Method / Technique **Phased Array**	Transducer & Material	Method / Technique **Testing**	Transducer & Material
Inductively Coupled(C. H. Zhong, Croxford, & Wilcox, 2013)	Ultrasonic (aluminum block)	Complex Curved Surface(F. Liu et al., 2016)	Ultrasonic (aeronautic engine blade)	CIVA Simulation(Bourdais, Baqué, Baronian, & Reverdy, 2013)	Ultrasonic Inspection (Sodium Cooled Reactors)
Conformal Map Theory for NDT(Ramadas, Jackson, Dziewierz, Leary, & Gachagan, 2014)	Ultrasonic(steel)	Axle Defect Detecting(X. Gao, Peng, Zhang, Peng, & Tan, 2013)	Ultrasonic (wheel)	Long Range Inspection (Parthipan, Jackson, Chong, Legg, & Mohimi, 2014)	Ultrasonic (Aircraft Wiring)
Dynamic Characteristic(Kwak, Cho, & Park, 2016)	Ultrasonic (Ultra-thin Coating)	Recursive Feedback (Charutz et al., 2013)	ultrasonic wave (thin plates and pipes)	Weld Central Line in Austenitic (Madhumitha, Ramkishore, Srikanth, & Palanichamy, 2014)	ultrasonic testing (Stainless Steel Weld Joints)
Peniel Method for the automation(José, España, William, & Bedoya, 2013)	Ultrasonic (aluminum, acrylic, and glass)	Reflector Localization (Moallemi et al., 2014)	Ultrasonic (Plate)	Phase Aberration(Yue, Luo, & Gao, 2014)	Ultrasonic Synthetic (nonuniform)
Orthogonal Excitations(Caporale, Callegari, Riccit, & Burrascanot, 2013)	Ultrasound Testing (Simulation)	Detection of Defects in Compound Material (Luo, Lu, Wang, & Wang, 2014)	Ultrasonic (Compound material)	Welch Frequency (Lin, Xu, Yan, Zhou, & Yang, 2014)	ultrasonic (stainless steel and ceramics)
waveforms for air-coupled(Ricci, Laureti, Hutchins, & Davis, 2013)	ultrasonic inspection(The micromachined backplate)	Immersion Non-Destructive Testing (Moallemi & Shahbazpanahi, 2014)	Ultrasonic (solid test sample)	Kinematic Analysis (X. Li, Zhao, Hao, Lu, & Huang, 2014)	Ultrasonic (complex shapes)
Low-Frequency NDT(Thomas, Emadi, Mijares-chan, & Buchanan, 2014)	Ultrasound(Power Cable Insulation)	complex geometries delivered (Mineo, MacLeod, Morozov, & Pierce, 2016)	Ultrasonic (carbon fiber)	rapid volumetric examination (L. Zhao & Rudlin, 2014)	Ultrasonic (aluminothermic rail welds)

Table 2.4   Continued

Method / Technique	Transducer & Material	Method / Technique	Transducer & Material	Method / Technique	Transducer & Material
magnetic flux leakage(Cristina, Blanco, Alvarez, & Dobmann, 2014)	ultrasonic (pipe bends)	High Speed Phased(X. Gao et al., 2016)	Ultrasonic (Railway)	power spectral density (Maia, Schneider, Maia, Neves, & Penteado, 2014)	Ultrasonic (Wood)
Iterative Time-of-Flight Extraction(Yücel et al., 2015)	Ultrasonic Guided Waves (aluminum rod)	Guided Waves (L. Zhang, 2014)	piezoelectric (long distance pipelines)	Active Microwave Thermography (Foudazi, Member, Ghasr, Member, & Donnell, 2014)	Thermography (carbon fiber reinforced polymer)
Acoustoelastic Lamb wave(Pei & Bond, 2015)	Ultrasonic (thin plates)	Effect Of Joint Geometry Parameters (Z. Xu, Yu, & Wang, 2015)	Ultrasonic (Thick Steel Plates)	Flaw Pattern Recognition (Sudheera et al., 2014)	Ultra Sonic Signals (thickly walled weldments)
Guided Wave Response (Yücel et al., 2016)	Ultrasonic (aluminum rod)	Generator Retaining Rings (Savenkov, Turner, Peralta-gorisse, & Services, 2015)	ultrasonic and eddy current (generator rotor)	EMAT Technology (Xin, Yang, & Li, 2014)	Electromagnetic ultrasonic (long straight pipe)
guided wave excitation mode(Fu, Zhou, Li, Xu, & Pan, 2016)	comb transducer (aluminum plate)	CNG Gas Well Detection (Xiaodan et al., 2015)	Ultrasound (pipe)	wavelet denoising technique(Lu, 2014)	Ultrasonic echo Signal (Steel plate)
Butt Fusion Join(Wei-Can et al., 2017)	Ultrasonic Technique (Polyethylene Pipe)	In-service Wheelset (Y. Zhang et al., 2016)	Ultrasonic (Wheelset)	Mathematical Modeling (Singh, Singh, & Sudheera, 2015)	Ultrasonic Signal (welding carbonized steel and stainless steel)
Synthetic Aperture Focusing (Fendt et al., 2013)	ultrasonic inspection (rotor shafts and turbine discs)	Forged Bars (Bernieri et al., 2017)	Ultrasonic (Aluminium)	Signal Compressive Sampling (Song et al., 2015)	Ultrasonic (Pipeline)
Non-Contact Ultrasonic Inspection (Farinas, Alvarez-Arenas, Aguado, & Merino, 2013)	Ultrasonic (Teflon)			low-energy impacted (Wu, Zhou, Wang, Zhang, & Zheng, 2015)	Ultrasonic (carbon fiber composite)

Method / Technique	Transducer & Material	Method / Technique	Transducer & Material	Method / Technique	Transducer & Material
Pulse-Echo System (Khan, Taube, Yogeswaran, Heidari, & Dahiya, 2015)	Piezo-Electric (Simulation)				
air-coupled (Uus et al., 2015)	ultrasound inspection (concrete/asphalt structures)				

According to Table 2.4, the focus of the study done by previous researcher was more on the method and technique in getting the best results of defect identification on pipeline, plate and concrete. Based on the methods and techniques shown in Table 2.4, there is no intelligent method which has been implemented to reducing the error of signal for to obtain the accuracy of signal data. From here, the research on this should be considered and implemented in the industrial inspection especially to identify the critical point and area. At the same time, the result of crack condition in pipeline is accurately obtained within the amplitude signal and time response for feedback signal.

2.8   Different Types of Pipeline Cracks

Damage detection of pipelines is of great significance in terms of safety in the oil and gas industry. Currently, lead zirconate titanates (PZTs) are the most popular Piezoceramic materials as they show great potential in the applications of Structural Health Monitoring. In this paper, the

authors present a feasibility study on the crack detection and severity monitoring of pipelines using PZT transducers. Due to their electromechanical properties, the Piezoceramic transducers can either be an actuator or a sensor to generate or detect the stress wave. Figure 2.18 shows the different defect on welding join (weldment) that occurs at the welding point.

Crater cracks occur when a crater is not filled before the arc is broken. This causes the outer edges of the crater to cool more quickly than the crater, which creates sufficient stresses to form a crack. Longitudinal, transverse and/or multiple radial cracks may also form. Hat cracks get their name from the shape of the cross-section of the weld, because the weld flares out at the face of the weld. The crack starts at the fusion line and extends up through the weld. They are usually caused by too much voltage or not enough speed. Longitudinal cracks run along the length of a weld bead. There are three types, namely, check cracks, root cracks, and full centreline cracks. Check cracks are visible from the surface and extend partially into the weld. They are usually caused by high shrinkage stresses, especially on final passes, or by a hot cracking mechanism. Meanwhile, root cracks start at the root and extend part way into the weld. They are the most common type of longitudinal crack because of the small size of the first weld bead. If this type of crack is not addressed, then it will usually propagate into subsequent weld passes, which is how full cracks (a crack from the root to the surface) usually form (Omar, 2012).

Hot cracking, also known as solidification cracking, can occur with all metals, and happens in the fusion zone of a weld. To diminish the

probability of this type of cracking, excess material restraint should be avoided, and a proper filler material should be utilised (Park, Kang, & Rhee, 2009). Other causes include too high welding current, poor joint design that does not diffuse heat, impurities (such as sulfur and phosphorus), preheating, speed which is too fast, and long arcs (Lippold, Varol, & Baeslack, 1989).

An under bead crack, also known as a Heat-Affected Zone (HAZ) crack is a crack that forms a short distance away from the fusion line; it occurs in low alloy and high alloy steel. The exact causes of this type of crack are not completely understood, but it is known that dissolved hydrogen must be present. The other factor that affects this type of crack is internal stresses resulting from; unequal contraction between the base metal and the weld metal, restraint of the base metal, stresses from the formation of martensite, and stresses from the precipitation of hydrogen out of the metal (Tiyasri & Poopat, 2013).

Reheat cracking is a type of cracking that occurs in High-Strength Low-Alloy (HSLA) steels, particularly chromium, molybdenum and vanadium steels, during post heating. The phenomenon has also been observed in austenitic stainless steels. It is caused by the poor creep ductility of the heat affected zone. Any existing defects or notches aggravate crack formation. Things that help prevent reheat cracking include heat treating, first with a low temperature soak and then with a rapid heating to high temperatures, grinding or peening the weld toes, and using a two layer welding technique to refine the HAZ grain structure (Vinckier & Dhooge, 1979).

A root crack is the crack formed by the short bead at the root (of edge preparation), during the beginning stage of the welding, low current at the beginning and due to improper filler material used for welding. Major reason for these types of cracks to happen is the hydrogen embrittlement. These types of defects can be eliminated using high current at the starting point and proper filler material. Toe crack occurs due to moisture content present in the welded area, as it is a part of the surface crack which can be easily detected. Preheating and proper joint formation are a must to eliminate these types of cracks.

Transverse cracks are perpendicular to the direction of the weld. These are generally the result of longitudinal shrinkage stresses acting on weld metal of low ductility. Crater cracks occur in the crater when the welding arc is terminated prematurely. Crater cracks are normally shallow, hot cracks usually forming single or star cracks. These cracks usually start at a crater pipe and extend longitudinally in the crater. However, they may propagate into longitudinal weld cracks in the rest of the weld.
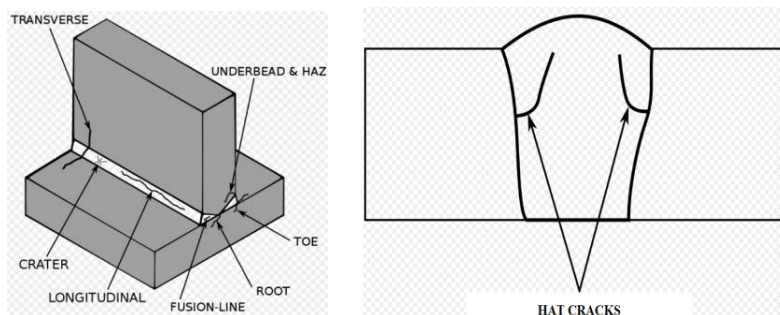
Figure 2.18   Weldment Types of Crack

With reference to the cracks shown, the name of cracks are based on its positioning at the welding points position. The basic crack is coming from four types of crack within; horizontal (transverse), vertical (longitudinal), angle/ gradient and lastly hole cracks. From here horizontal and vertical being categorised as axial crack defect.

2.9   Probe Design Characteristic

The probe design is based on the application of probe for inspection. There have a few design with different application is used of previous researchers.   In ultrasonic wave-based structural health monitoring embedded instrument (Aranguren, Monje, Cokonaj, Barrera, & Ruiz, 2013), the design is more for flat material. This system is design for Phased Array Monitoring in Structural Health Monitoring (SHM). According on this design the 12 piezoelectric is used for inspection and represent the width of plate is around 12cm. Figure 2.19 show the Piezoelectric module for SHM.

Figure 2.19   Design of SHM Piezoelectric module

It follows Piezoelectric inspection in which the metallic plate is used as the subject of inspection. From here, this research is more on knowing the effect of fatigue crack growth in riveted fuselage joints and a cracked metallic plate repaired with a bonded composite patch (Ihn & Chang, 2004). The limitation of this design is it only serves the purpose of flat surface for welding joints. The method used in this inspection is pitch-catch method wherein the Piezo actuator and Piezo receiver are separated and been put in between of plate join. Figure2.20 shows the built-in Piezoelectric sensor/actuator network.
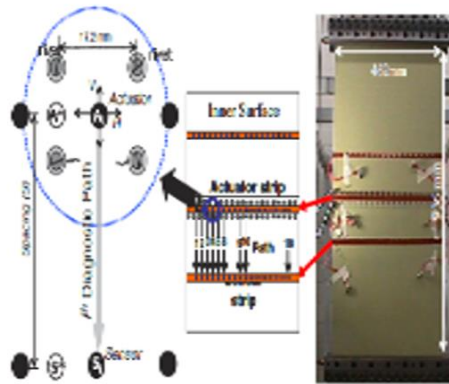
Figure 2.20   Built-in piezoelectric sensor/actuator network

Figure 2.21 shows the system development for detection of pipeline multiple cracks using Piezoceramic transducers. This probe does not have an actual design and the sensor is placed on the surface of the pipe and tested for crack identification. The feasibility of detecting pipeline multi-cracks damage through this system using Piezoceramic transducers includes the electromechanical impedance method and the stress wave based active sensing method were used respectively to

perform the damage detection of pipeline with multi-cracks. The result shows the localisation analysis on the pipeline multi-cracks damage which can be achieved by stress wave method based on sensor arrays (Du, Huo, Kong, & Song, 2016).
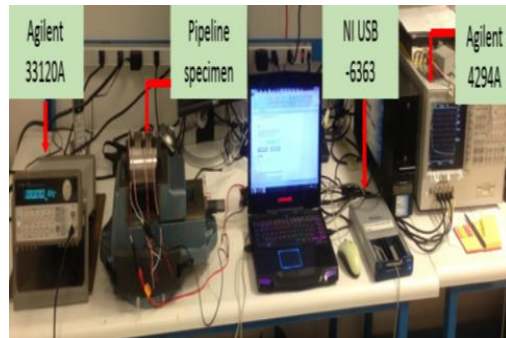
Figure 2.21   Detection of pipeline multiple cracks using
Piezoceramic transducers

In Piezoelectric inspection, most methods refer to the guided wave technique. The advantage of this technique is it provides more information about the presence of damage and severity than previously tested methods (frequency response techniques), and also enables the possibility of determining the damage location due to their local response nature (Kessler, Spearing, & Soutis, 2002) and also sensors can detect both Lamb and SH waves, which have different polarisations, and resolve the received modes into independent modal amplitudes (Baiyang Ren, 2017). Figure 2.22 shows the design of Piezoelectric for guide wave method that is applicable on plate surface for defect inspection.

Figure 2.22   Piezoelectric for guide wave design

To date, the proper design of probe that used for Piezoelectric inspection especially on pipe line inspection is yet to be established. Most of the previous designs focused on the system development and the techniques which are used in Piezoelectric inspection. Based on this problem, the proper design for Piezoelectric inspection should also be made available for pipe line inspection to ensure the process of monitoring of pipeline to be done continuously with less guidance. Table 2.5 shows the summary of Piezoelectric design for plate and pipe system.

Table 2.5   Summary of probe design based on advantage and disadvantage for piezoelectric system

Reference, Author & Year	Content	Advantage	Disadvantage
Ultrasonic wave-based Structural Health Monitoring embedded instrument. G. Aranguren, P. M. Monje, Valerijan Cokonaj, Eduardo Barrera, and Mariano Ruiz (2013)	An all-in-one system for Structural Health Monitoring (SHM) based on Ultrasonic waves is presented, called Phased Array Monitoring for Enhanced Life Assessment.	Generates excitation signals that are sent through Piezoelectric actuators, acquires the received signals in the Piezoelectric sensors, and carry out signal processing to check the health of structures.	The signal received would not be processed nor show the actual depth of defect.
Qualitative identification of cracks using 3D transient elastodynamic topological derivative: Formulation and FE implementation Cédric Bellis, Marc Bonnet (2013)	Emphasises the implementation and exploitation of topological derivative (TD) fields using the standard displacement-based FEM, a straightforward exploitation of the relevant sensitivity formulation established.	Several numerical experiments on 3D elastodynamic and acoustic configurations are reported and discussed, allowing the assessment and highlight many features of the proposed TD-based fast qualitative crack identification, including its ability to identify multiple cracks and its robustness against data noise.	This paper focuses more on simulation for proving crack according to the equation but the comparison with an actual hardware was not done.
Neural-Fuzzy model based steel pipeline multiple cracks classification Hatem Mostafa Elwalwal, Shahruddin Bin Hj. Mahzan, Ahmed N Abdalla (2017)	Carry on the numerical simulation and experimental study, aiming at finding an effective way to detect and localise the crack and hole defects in the main body of pipeline.	The technique used in this research is a guided Lamb Wave based Structural Health Monitoring method whereas Piezoelectric transducers will be used as exciting and receiving sensors by Pitch-Catch method. Implementation of simple learning mechanism has been developed specially for the ANN for fuzzy the system.	This paper explains more about the simulation by using ANSYS software for crack defining and not in its actuality.
Guided wave-based identification of multiple cracks in beams using a Bayesian approach Shuai He, Ching-Tai Ng (2017)	The Transitional Markov Chain Monte Carlo (TMCMC) method is implemented in the Bayesian approach in which the sensitivity of different guided wave modes and effect of different levels of measurement noise in identifying different numbers of cracks.	That the proposed method is able to accurately identify the number, locations and sizes of the cracks, and also quantify the associated uncertainties. In addition, the proposed method is robust under measurement noise and different situations of the cracks.	The research is more about finding the number of crack by using the TMCMC in Bayesian approach but the depth of crack was not considered in this experiment.

Table 2.5 Continued

Reference, Author & Year	Content	Advantage	Disadvantage
Detection and monitoring of hidden fatigue crack growth using a built-in Piezoelectric sensor/actuator network: II. Validation using riveted joints and repair patches Jeong-Beom Ihn, Fu-Kuo Chang (2004)	Proposed diagnostic technique was applied to monitor fatigue crack growth in riveted fuselage joints and a cracked metallic plate repaired with a bonded composite patch.	The damage index successfully detected both crack growth and unbinding damage for the structures considered.	Embedded Pitch Catch Method is used in this system and according to this method, the actuator (transmitter) and receiver should be in parallel and it takes a lot of space and is not appropriate for small space plate inspection.
Damage detection of pipeline multiple cracks using Piezoceramic transducers Guofeng Du, Linsheng Huo, Qingzhao Kong, Gangbing Song (2016)	The feasibility of detecting pipeline multi-cracks damage using Piezoceramic transducers, the electromechanical impedance method and the stress wave based active sensing method were used respectively to perform the damage detection of pipeline with multi-cracks.	Quantitative analysis of pipeline crack damage can be realised by electromechanical impedance method, and localisation analysis on the pipeline multi-cracks damage can be achieved by stress wave method based on sensor arrays.	The experiment discusses more about finding the multiple cracks at materials but the depth of crack was not explained in this research.
Damage detection in composite materials using Lamb Wave methods Seth S Kessler, S Mark Spearing and Constantinos Soutis (2002)	Experimental and analytical survey of candidate methods for in situ damage detection of composite materials.	Lamb Wave techniques provide more information about damage presence and severity than previously tested methods (frequency response techniques), and provide the possibility of determining damage location due to their local response nature.	The study and analysis elaborated on wave form response without much details on pattern of crack defect.

Table 2.1   Continued

Reference, Author & Year	Content	Advantage	Disadvantage
Detecting damage size and shape in a plate structure using PZT transducer array Guangtao Lu, Yourong Li, Mingle Zhou, Qian Feng4, and Gangbing Song (2018)	An algorithm to detect damage size and shape using a lead zirconate titanate (PZT) transducer array for a plate structure is developed in this paper.	The reflection point can be obtained by finding a special point on the ellipse, and this point has the shortest distance to the centre of the curvature of the damage boundary curve. As a result, the damage boundary curve can be determined by finding various reflection points, and the envelope of the identified reflection points is employed to represent the shape of the damage.	The method used is Lamb Wave but according to the research, the arrangement of Piezoelectric is in random and inconsistent. It is also difficult to know the location of defect accurately when using artificial defect plate from the industry.
Active sensing and damage detection using Piezoelectric zinc oxide-based nanocomposites Frederick N Meyers, Kenneth J Loh, John S Dodds and Arturo Baltazar (2013)	Investigated the design and performance of Piezoelectric nanocomposite-based interdigitated transducers (IDTs) for active sensing and damage detection.	This study demonstrated that ZnO/PVDF–TrFE nanocomposite transducers are viable for damage detection and SHM and the prototype sensor/actuator, when combined with this damage index method, was able to quantify the severity of damage.	Not any intelligent technique is used in signal processing especially to finding the error compensated for accuracy.
A guided wave sensor enabling simultaneous wavenumber-frequency analysis for both Lamb and Shear-Horizontal Waves Baiyang Ren , Hwanjeong Cho and Cliff J. Lissenden (2017)	Demonstrated that polyvinylidene difluoride (PVDF) film provides the basis for a multi-element array sensor that detects both Lamb and SH waves and also measures their modal content, i.e., the wavenumber-frequency spectrum	Sensors can detect both Lamb and SH waves, which have different polarisations, and resolve the received modes into independent modal amplitudes.	The analysis based on the signal is obtained from experimental and from here, only the positioning defect can be found other than the analysis especially for depth and shape of defect.

2.10   Summary

This literature review clearly shows the continuous improvement and ongoing emphasis on the Ultrasound method to obtain clarity of cracks and damage in material. At the same time, this approach is suggested to be developed further with regards to UT and Piezoelectric fields. These include the methods of using superimposed, thermography and power spectral either by simulation or against via specific materials such as steel, ceramic, wood, concrete and others. In addition, data acquisition and cracking image damage are also focusing on the emphasis of algorithms such as synthetic focus, complex geometry, phase arrays, and neural networks. Besides, the Ultrasonic and Piezoelectric application has a weakness in the area of the inspection, especially when involving pipe distribution in the industry. As an alternative, the research of Piezoelectric (PZT) as an actuator is currently growing in order to replace the UT technique. This can be seen on various methods of PZT applications, namely, acoustic impedance, Recursive Feedback, an array sensor, Lamb wave, comb transducer and more. According to the previous researcher, the crack position and width of crack on the material can be identified based on the response time analysis, signal amplitude and reached signal inspection in area that was largely covered. Other than that, the overall signal of crack should be considered during the inspection based on Piezoelectric sensor array and at the same time, the optimisation of Piezoelectric sensor gap should be considered to ensure the total signal on inspection process can also be analysed generally. In addition, the study on PZT can be reinforced further with various theories and formulae for accuracy especially on the position of cracks at the material inspection stage. Furthermore, the emphasis on these

fields should be increased and be made a priority especially in identifying the size of defect, the shape of defect and depth of defect based on signal feedback analysis as well as increasing the data accuracy by implementing the intelligent technique for error compensation. Hence, the time for inspection can be reduced and the continuous monitoring could be realised in identifying the condition of the industrial pipeline.

CHAPTER 3

MATERIALS AND METHODOLOGY

3.1   Introduction

This chapter discusses the major steps to accomplish the objectives of this research. This chapter is divided with nine sections including the introduction. The second section explains about general explanation for Piezoelectric test including the research flow chart in Figure 3.1. The third section provides the details on proposed of Piezoelectric system by using Lamb Wave method (PZ-LW). Here, the details of probe design are explained and shown in 2D and 3D picture dimension. Other than that, the optimisation also explains in forth section that includes the simulation software used and the RSM software used for optimisation as well. The Fuzzy Logic for error compensation is illustrated in section five that encompasses the design and rule used in Fuzzy development. The process of data collection is explained in section six by including the circuit design and system development. Next, the pipes with the defect are also included in seventh section. Lastly, the commercial probe and tester are also being explained for validation with PZ-LW probe design.

3.2   Block Diagram

The process of data collection was based on three main steps within; input used, signal process, and output display. Figure 3.1 shows the block diagram for PZ-LW system was employed in this research. For

input, it included the Piezo Actuator and excitation signal. The excitation signal was followed in Gaussian Sine Pulse signal with 5 cycles. Then, the excitation signal would send to Piezo Actuator for generation micro vibration to identify the crack position and crack width. Next, the Gaussian Sine Pulse signal was developed based on this equation $E(t) = \sqrt{A_{t\,e^{-ln2\left(\frac{2t}{\Delta t}\right)^2}e^{-1(\omega 0 t + \theta(t))} + c.c.}}$ where carrier frequency, ω0, pulse duration, Δt, and phase, θ(t), c.c. denoted the complex conjugate. In this expression, At was the amplitude of the pulse, ω0 determined the colour of the pulse, Δt determined the minimum pulse duration and consequently, the bandwidth of the pulse, and θ(t) determined the temporal relationship among the frequency components contained within the bandwidth of the pulse. θ(t) played an important role in altering the pulse duration. It was the term that was responsible for pulse broadening in dispersive media and could be thought of as adding a complex width to the Gaussian envelope. After that, the Piezo Receiver would receive the feedback signal if the crack occurred at gas pipe. From here, the signal would process at Data Acquisition (DT9816) for filtering. In data acquisition the filter type chosen was Chebyshev with BandPass category in Filter order 2. The data from DAQ would be sent to MATLAB Simulink for Fuzzy Logic Error Compensation. The output of Fuzzy could be followed according the equation $Out(fuzzy) = \frac{(W1*NL+W2*NS+W3*PS+W4*NS+W5*ZE+W6*PS+W7*NS+W8*PS+W9*PL)}{\sum_{i=1}^{9}(W_i)}$

where the Wn was rule firing strength used in this Fuzzy development, NL was Fuzzy set with lower negative value in Fuzzy development, NS Fuzzy set with standard negative value, ZE was zero value for Fuzzy set, PS was standard positive value for Fuzzy set and lastly PL was high positive Fuzzy set value. All signal that received the form of DAQ would

be sent directly to Fuzzy Logic system and the error compensated would automatically calculate. Lastly, the signal would show by graph based on voltage was produced from feedback signal by following this equation $Vout(t) = -\frac{q}{C_f} = -\frac{1}{C_f}\iint_{l\ w}(d31E11\varepsilon11 + d32E22\varepsilon22)dxdy.$ From here, the dx was shear stress, $\varepsilon0 =$ was the permittivity of free space and q was dielectric displacement. The detail of this equation was explained in section 3.3. From here, the data received would go through the Fuzzy system for signal amplitude accuracy. It was important to identify the width of defect based on the signal received. The amplitude signal was based on the voltage amplitude received and from here when the amplitude signal was higher than the width of crack low. Otherwise, the width of defect was high.
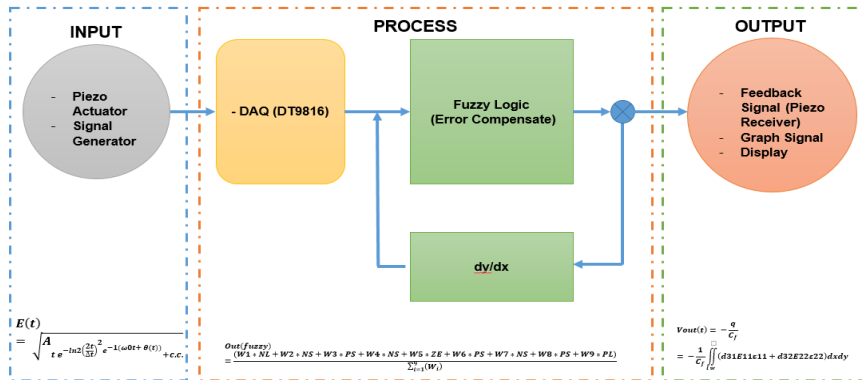
Figure 3.1   Block Diagram

3.3   The Proposed PZ-LW (Piezo Lamb Wave) System

For piezoelectric sensor, in the absence of external electric field, the electric charge generated by stretching its sensing element can be expressed as,

$$\begin{Bmatrix} D1 \\ D2 \\ D3 \end{Bmatrix} = \begin{bmatrix} 0 & 0 & 0 & 0 & d15 & 0 \\ 0 & 0 & 0 & d24 & 0 & 0 \\ d31 & d32 & d33 & 0 & 0 & 0 \end{bmatrix} \{\sigma 1 \ \sigma 2 \ \sigma 3 \ \sigma 4 \ \sigma 5 \ \sigma 6 \ \}^T \quad (3.1)$$

Where $\{\sigma 1 \ \sigma 2 \ \sigma 3 \ \sigma 4 \ \sigma 5 \ \sigma 6 \ \}^T$ = $\{\sigma 11 \ \sigma 12 \ \sigma 13 \ \sigma 14 \ \sigma 15 \ \sigma 16 \ \}^T$; $\sigma 1, \sigma 2,$ and $\sigma 3$ were tensile stress; $\sigma 4, \sigma 5,$ and $\sigma 6$ were shear stress; $d31, d32, d33, d34,$ and $d35$ were Piezoelectric constants; $D1$, $D2,$ and D3 were the electric charge displacements. If shear stress was negligible and considering the fact that Piezoelectric Sensor was placed (meaning $\sigma 33$ equal zero), Equation (3.1) was simplified as;

$$D3 = d31\sigma 1 + d32\sigma 2 + d33\sigma 3 = d31E11\varepsilon 11 + \ d32E22\varepsilon 22 \quad (3.2)$$

If the Piezoelectric Sensing Material was homogeneous and the sensor sensitivity in both directions 1 and 2 were the same, the resulting charge could be written as $D3 = d31E11(\varepsilon 11 + \ \varepsilon 22)$. This was different from Piezoelectric Displacement Sensor which measured the displacement in a single direction (usually direction 3). Assuming the dimension of the sensor was $l \ x \ w \ x \ t$ where $l, w, and \ t$ were sensing elements of length, width, and thickness respectively, as a result, the generated electric charge was related to the dielectric displacement $D3$ by the following relationship;

$$q = \iint D3 dA = \iint D3 dA = \iint (d31E11\varepsilon 11 + d32E22\varepsilon 22)dxdy = \iint_{l \ w} (d31E11\varepsilon 11 + d32E22\varepsilon 22)dxdy \quad (3.3)$$

It could be shown that Piezoelectric AE Sensor could be configured as either strain sensor or strain rate sensor because of the mechanical coupling property of Piezoelectric Materials (Sirohi & Chopra, 2000).

Elamvazhudi and Gopalakannan (2018) summarized the two types of signal conditioning circuit. In summary, if a current amplifier was used as the signal conditioning circuit, the output voltage from the sensor was linear proportional to the total strain change rate and could be expressed as;

$$Vout(t) = -R_f \dot{q} = -R_f \iint_{l\,w} (d31E11\dot{\varepsilon}11 + d32E22\dot{\varepsilon}22)dxdy \quad (3.4)$$

If a charge amplifier was utilised as the signal conditioning circuit, the output voltage from the sensor was linear proportional to the average strain with the sensor area and could be expressed as;

$$Vout(t) = -\frac{q}{C_f} = -\frac{1}{C_f} \iint_{l\,w} (d31E11\varepsilon11 + d32E22\varepsilon22)dxdy \quad (3.5)$$

In this study, piezoelectric AE sensors were mainly used as a strain sensor and it used to identify the location and width of defect based on *Vout* produces based on time.

In methodology, the Piezoelectric sensor proposed design was a significant part of system development in PZ-LW system design. Piezoelectric paint typically comprised tiny piezoelectric particles mixed within polymer matrix and therefore belonged to the "0-3" piezoelectric composite. The "0-3" implied that the ceramic particles were randomly dispersed in a polymer matrix. As compared with other connectivity types, "0-3" had the advantage of ease of fabrication into complex shapes and might conform to any curved surface. The piezoelectric paint offered the unique blending of the high piezoelectric properties of

ferroelectric ceramics (e.g., PZT) and the mechanical compliance and conformability of polymers (e.g., PVDF). It carried out a series of studies on piezoelectric paint sensors for different volume fractions of PZT particles and experimentally characterised the material properties. The material properties of piezoelectric paint and other piezoelectric materials are listed in Table 3.1. It could be concluded from d31 values that the piezoelectric paint had a sensitivity comparable to PVDF but was much lower (about 1/30) than PZT.

Table 3.1   Specification Piezoelectric Material Properties

	PZT-5A[a]	PVDF	Piezoelectric Paint (PZT% by volume)			
			40%	50%	60%	70%
d_{33} [pC/N]	390	-22.1	6.1	13.7	27.1	48.1
-d_{31} [pC/N]	175	-6.2	2.1	4.4	8.6	15.0
k^p	0.63	0.03	0.02	0.06	0.10	0.19
g_{31} [10^{-3}Vm/N]	12.4	-70.8	18.4	24.0	29.1	30.7
k_{31}	0.36	0.03	0.02	0.04	0.7	0.13
$\varepsilon/\varepsilon_0$[b]	1800	9.9	12.9	20.7	33.4	55.2
Z [MRayl]	30	2	4.9	6.0	7.3	9.2
Tc Curie Point [°C]	350	150 (melt)	Degradation temperature of resin >200			

$\varepsilon 0 = 8.85 \times 10^{-12}$ F/m, is the permittivity of free space (vacuum)

The architecture design is shown in Figure 3.2 where it is divided into four parts. First part was about the source supply. From here, the AC source supply was being converted to DC supply and used for circuit controller. The second part was excitation signal generator. From here,

the Gaussian Sine Pulse Wave Excitation signals were used for input device (Piezoelectric). The Gaussian sine pulse would be sent to the Piezoelectric array by switching technique. At one time, only one Piezoelectric would receive that excitation signal. The original probe used in this thesis has been termed as the PZ-LW probe which consisted of two main parts; the excitation devices to induce the Gaussian sine pulse waveform on the test object and the Piezoelectric array sensor to measure the time response feedback and also receive the types of waveform signal from the test object and feed this information to measurement instrument. The third part was about controlling or processing devices. In here, the Data Acquisition System (DAQ) was used as data receiving and filtering devices and the devices were connected to PC for Fuzzification process. The fourth part was material inspected (pipe / plate). From here, the PC was applied to process the data from the DAQ devices and showing in graph. Besides that, the PC was used to simulate the virtual signal from MATLAB/Simulink application, processing in FIS block, and showing the resulting graph.
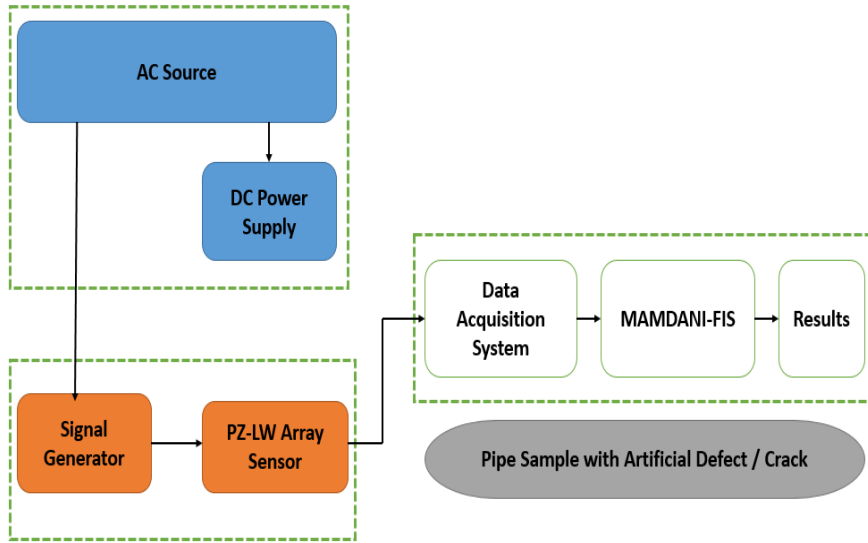
Figure 3.2   Piezoelectric Lamb Wave Inspection System

Based on Piezoelectric Lamb Wave Inspection System, it could be detailed as the main system on this research. This system was operated with 240VAC for signal generator for producing 5Vpp amplitude voltage for excitation frequency. The frequency ranges ~~are~~ set in this excitation frequency were 1Mhz and 1.5Mhz while 2Mhz for optimisation. The excitation frequency effected on the reflection signal that received. From here, the Gaussian Sine Pulse wave selected by 5 cycles were set. The excitation signal form signal generator activated the Piezo actuator for producing the vibration. The connection of between signal generator and piezo actuator was parallel. From here, the Piezoelectric was arranged at pipe surface by parallel and coupled between Piezo actuator and Piezo receiver. The gap between a pair of Piezoelectric was 2.5mm based on the optimisation result retrieved through Response Surface Methodology (RSM) process. In activating the DAQ, the 5VDC was used and DAQ was connected with PC through

USB port for data transfer. The analogue pin was used and connected to positive polarity of Piezo receiver. The negative Piezo receiver was connected to ground analogue. In this system, 10 pairs of Piezoelectrics were used in this process because of consideration on the diameter pipe and gap between pair of piezoelectric sensor. In the process of data analysis, when the crack was identified at pipe, then the feedback signal would receive at Piezo receiver and the signal would process and then sent to PC. From here, two types of software were used to display and analyse the signal that were QuickDAQ and MATLAB Simulink for error compensated. From QuickDAQ software, the raw data would display by graph, value, and also record for further or off-line analysis. To ensure the data being analysed in identifying the right width of crack, the data would be sent to MATLAB Simulink for error compensation. From here, the Fuzzy Logic was used in error compensation. The Fuzzy Logic system would show the actual amplitude voltage of signal from DAQ and percentage of error based on the graph displayed. The amplitude of signal was tuned to the right amplitude because of the amplitude signal that represented width of defect. From here, the user knew the types of crack based on the amplitude receiving and also from sensor array that placed at pipe surface. From here, the amplitude of signal was very vital in identifying the width of crack and at the same time the pattern of could identify based on sensor array.

3.3.1 Piezo Array Sensors

Sensor array was one of mostly used methods in inspection. This method has always been applied in automotive industrial either for aircraft or also in train (railway rail inspection). The effect of this method provided

the actual positioning of defect based on time response and according to the time responses for all sensors, it was tabled and from here the shape of defect was identified. From here, the shape of defect and long of defect was drawn after signal has plotted by base on time respond. Figure 3.3 shows array of the sensor on the FPZ-LW system. Specifically, this array used 10 pairs of Piezoelectric Sensors with a diameter of 10 mm each. The selection of 10 pairs of Piezoelectrics were based on the size of gas pipe used in industrial (diameter 60mm and 5mm thickness). According to the RSM for optimisation, the gaps of between sensors contributed to the total pairs of Piezoelectric Sensor within the max gaps was 2.5mm. The operating frequency of the sensor supported up to 4 MHz with a thickness of 1 mm. Meanwhile, it should be noted that the switching technique was used as the activation technique of the sensor whereby only one pair of Piezoelectric Sensors was activated at a time. Moreover, the activation method was controlled based on the programming for the multiplexer. The reflected signal was received through the DAQ module and then displayed on the PC through QuickDAQ software. The received signal was analysed using the Simulink feature of the MATLAB software for error compensation using Fuzzy Logic method
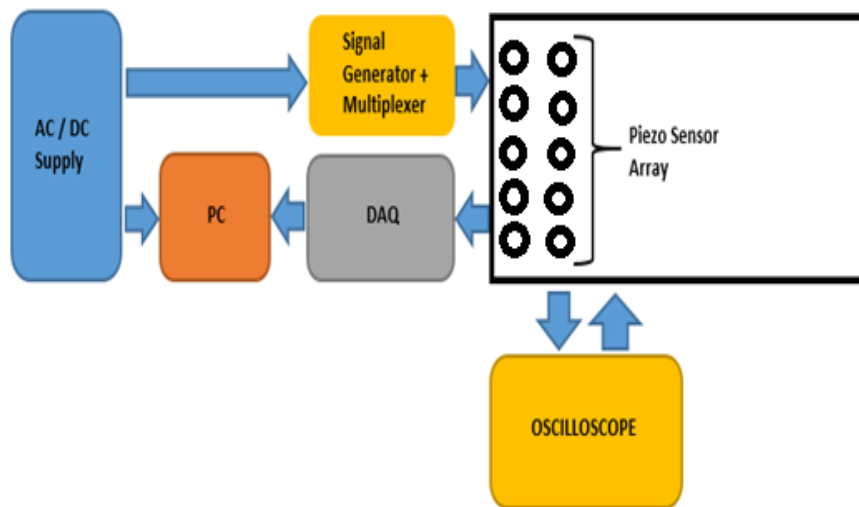
Figure 3.3   Piezo Sensor Array with For PZ-LW System
Architecture

3.3.2   PZ-LW System Setup

In PZ-LW fully system devices development, it consisted of six main
parts. The first main part was Fuzzy Logic Interfacing System. In this
part, the system of Fuzzy Logic was developed by using MATLAB
Simulink software. After the first part finished, the second part for
interface was being developed. From here, the Data Translation DAQ
(DT9816) was used as a controller device in data input processing and
output display. The third part was an input device. In here, the
Piezoelectric was being used as a sensor and actuator for measuring the
defect. To fix it on pipe surface, the grease/epoxy/couplant was used as
a solution to avoid the air gap between Piezoelectric and pipe surface.
This solution was very important in experiment to ensure the
Piezoelectric was fully attached to the pipe surface and at the same time

the excitation and feedback signal transmitted and received properly. In here, the width of defect displayed based on amplitude and time response from sensor, the percentage of error, and Fuzzy output value displayed on Scope in Simulink software. The function of signal generator was used as the gausses sine pulse excitation signal for Piezoelectric Probe Sensor and lastly the test was done by using the calibration block to ensure the depth of defect displayed was correct. Figure 3.4 shows the PZ-LW system device setup for inspection testing.
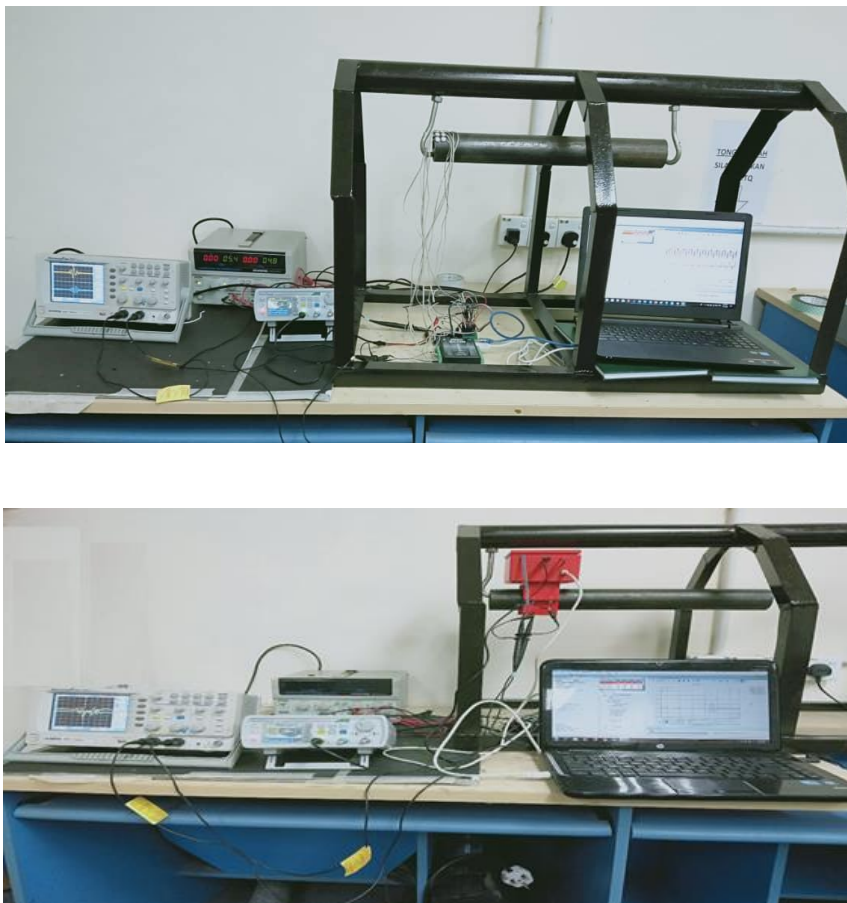
Figure 3.4   Piezo Lamb Wave testing inspection system (PZ-LW)

In the experiment, the sixth section was being setup to ensure that the data received were clear and could be transferred to PC. Figure 3.5 shows the six items in experimental setup section: (a) Oscilloscope, (b) Signal Generator, (c) DC Power supply, (d) Piezo electric actuator and receiver (e) Controller and (f) PC for data analysis which includes Simulink Interfacing software.
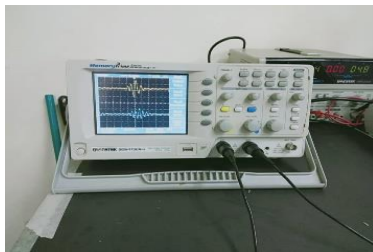
(a)	(b)

(c)	(d)
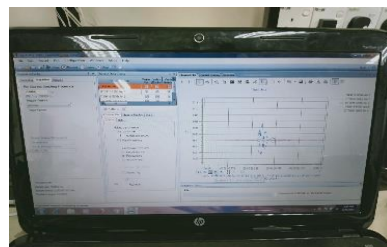
(e)	(f)

Figure 3.5   Part of Experimental Setup (a) Oscilloscope, (b) Signal Generator, (c) DC Power Supply, (d) Piezoelectric array, (e) Controller and (f) PC

From experiment, the oscilloscope (a) was used to display the excitation signal and feedback signal waveform especially to identify the high of amplitude signal and how many amplitude reducing based on the crack positioning and width of crack on pipe line. From here, the equation was generated based on rate of crack distance changes and amplitude of signal by considering the width of crack was consistent. From Figure (b), the signal generator was used in generating the Gaussian Sine Wave type in this experiment. Based on experiment of the 5Vpp for amplitude, 5 cycle wave was setup at signal generator. This was because of Piezoelectric limitation until 5Vpp and 5 cycle was used to ensure actual feedback signal received correctly and could be interpreted between noise and actual feedback signal. The supply used to activate the DAQ module was 5VDC. From here, the DC power supply was placed in this experiment for 5VDC supply. To ensure in each Piezoelectric actuator and receiver functioned very well, the piezoelectric sensor was arrayed by series between Piezo actuator and Piezo receiver (by pairing). The gap between a pair piezoelectric and another piezo electric was set at 2.5mm based on Response Surface Methodology (RSM) analysis in chapter 4. The quantity of piezoelectric was according to the diameter pipe and gaps between piezoelectric used in experimental. From here, 10 pairs of Piezos were used in analysis. All feedback data signal was processed by DAQ module (DT9816). DAQ module (e) have Analog I/O and Digital I/O and it could process the data in high frequency 0Hz until 2Mhz and also appropriate used in this experiment. The data from DAQ processed and sent to PC through the USB port. From here, the data analysed in Simulink software for error compensation (f) in accuracy signal and at the same time, the signal form was showed in

scope of Simulink software for time response analysis and amplitude analysis.

3.3.3 Schematic PZ-LW System

In the schematic circuit, it consisted of six important parts that should have in ensuring the system was properly functioning. The first part was oscilloscope (a) that functioned to display the waveform from excitation signal and Piezoelectric Receiver. The comparison between Excitation Signal Amplitude and Piezoelectric Receiver Amplitude could be done based on crack position. Thus, the amplitude showed in voltage value and at the same time the frequency of signal was displayed here. The second part (b) was signal generator. The signal generator was used to generate the Gaussian Sine Wave as Excitation Signal for Piezo Actuator and from here the Piezo Actuator generated the vibration based on the excitation signal was given. The excitation signal was given in sequence based on time delay. In here, the signal generator was used according to the frequency, amplitude, and type of waveform selection and setting. It continued with the third part (c) was DC supplies that functioned to supply the DC voltage for signal generator and converting to Gaussian Sine Wave while DC supply (5VDC) also used in DAQ module for activation. The type of probe used was Piezoelectric Sensor (d). The concept probe was vibration probe sensor that generated the vibration when the Gaussian Sine Wave was through it. Each defect especially the crack on the pipe occurred that was identified through the signal response from Piezoelectric Sensor. From here, the time response and amplitude signal was analysed in distinguishing the positioning crack at pipe line and at the same time the width of crack was identified. The

second last part was controller devices. In this system, the DAQ (DT9816) was used as a controller to control, filter, and switch the signal through the multiplexer before going to Piezoelectric Receiver probe used. The processing speed for the controller was 32-bit and it was appropriate in this system to receive the signal with high frequency (1Mhz-2Mhz). The last part was Personal Computer (PC) interface. From here, the PC was used to receive the signal response from pipeline inspection and being analysed on MATLAB 2015 as a signal analysis and intelligent application in this project. From here, the Fuzzy Logic application and output waveform of each defect were shown on the monitor from scope in Simulink software. The connection between PC and DAQ was used by serial communication interfacing with 9600 baud rate data transfer. Figure 3.6 shows the design of driver circuit for probes connection, microcontroller, and PC interface.
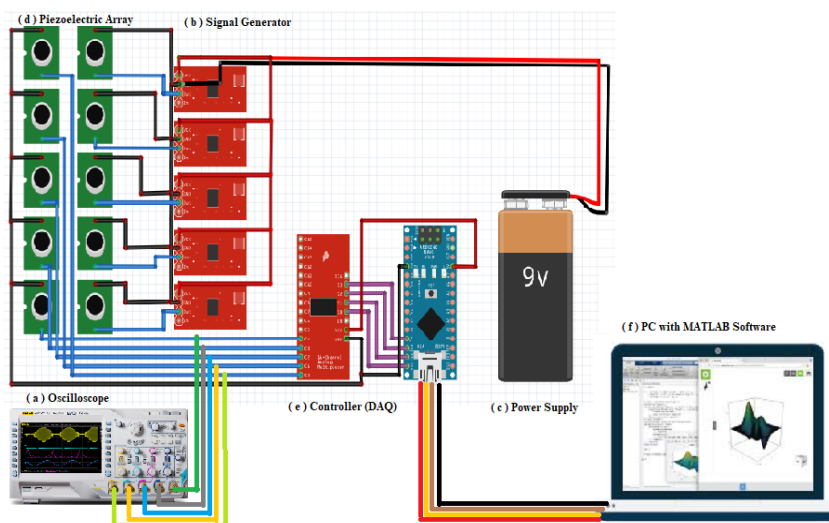
Figure 3.6   Designing of PZ-LW Drive Circuit.

3.3.4 Fabrication the Proposed Probe

The hardware designs were divided into two parts namely designing the PZ-LW full design, and the pipe support. The PZ-LW full design and pipe support included the full orientation in 3D design for pipe implementation. Each part comprised the front view, top view, and side view dimension for reference. PZ-LW probe design was combined together with control box where the all circuit was included inside the box. For pipe stand designing, it was being made as sliding until 1-meter length of pipe. All designs included the 3D dimension and 2D viewing for all dimension.

3.3.4.1 3-D PZ-LW Full Probe Design

The FPZ-LW probe design was combined together with the control box that contained system circuitry. Initially, the pipe stand was designed with the ability to slide up to a 1-meter length of pipe. Figure 3.7 shows the overall probe design with the inclusion of the PZ-LW probe shoes as well as the control box for the PZ-LW system. The dimension of PZ-LW casing for piping with 60 mm diameter was (62mm x 120mm x 90mm) and for control box is (120mm x 120mm x 80mm). Meanwhile, the middle design showed that the gap distance between Piezoelectric was applied to this system. Accordingly, it could be observed that the 2.5mm gap was set on the design based on the RSM which resulted in optimisation. The size of probe was based on the diameter gas pipe that used in industry. Other than that, it functioned to clamp the gas pipe to ensure the sensors were fix on its position in processing the data recording and analysis.
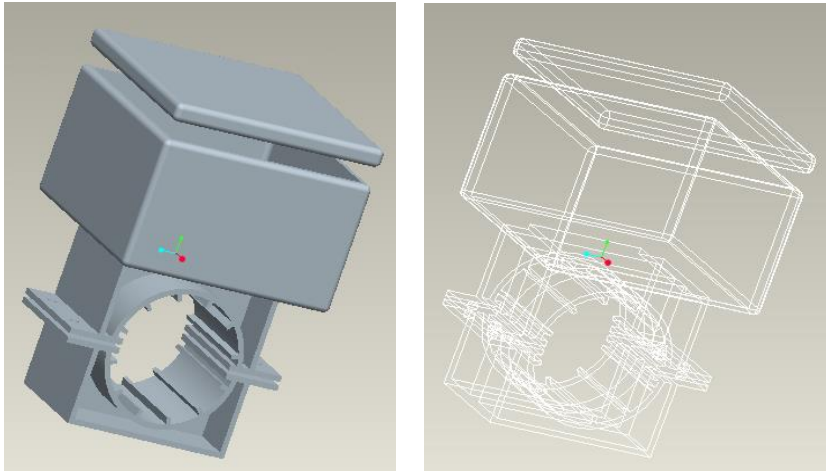
Figure 3.7   Full PZ-LW Probe Design

3.3.4.2   3-D PZ-LW Dimension View

According to the dimension of the PZ-LW probe, the direction view could be shown in four orientations; front view, top view, side view and bottom view. From here, the details of figure could be realised according to the correct surface, different diameter (inner diameter and outer diameter), and angle of the probe.

From here, the design of PZ-LW probe should be the fixed in the pipe diameter to ensure that the all pipe surface could be touched in Piezo Sensor. The probes design had the inner diameter = 62mm and the thickness for placing the Piezo and clamping the pipe was 6mm. Figure 3.8 shows the actual dimension value for front view of PZ-LW probe used. Based on front view, the high of probe was 170mm while the width was 120mm.
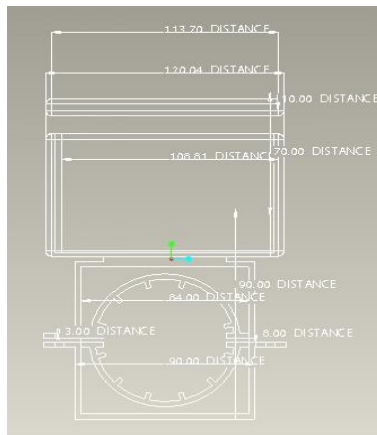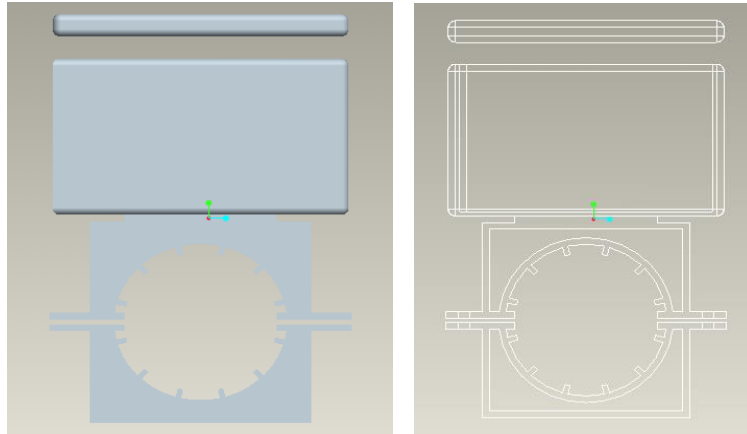
Figure 3.8   Front View Dimensioning

According to Figure 3.9, it shows the top view of PZ-LW probe. On the top view, there were the three sections: within cap (120mm x 120mm x 10mm), control box (120mm x 120mm x 80mm), and pipe clamping casing (62mm x 120mm x 90mm). This design was fixed in the size pipe 60mm outer diameter and also the control box storage was enough to store the DAQ module and multiplexer for data analysis. From here, the pipe was clamped with four-point screw to ensure the probe was tightened with the pipe for inspection.
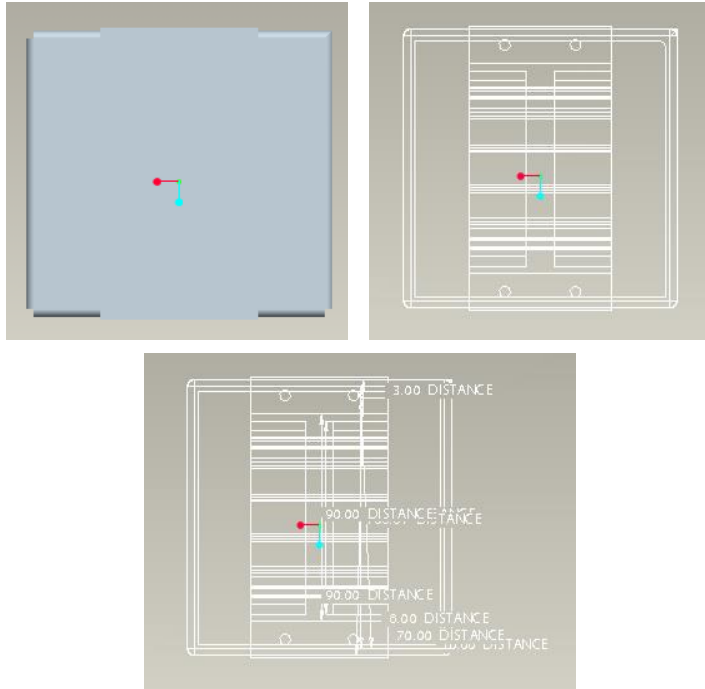
Figure 3.9   The Top View of PZ-LW Probe

The design in Figure 3.10 depicts the side view of PZ-LW probe which includes the control box. The length of this PZ-LW probe design was 170mm and width of 120mm. The thickness of control box was 5mm and enough to store all devices or modules used in this analysis. On the clamping part, there were 10 slots for Piezoelectric Sensor based on RSM optimizing design. Figure 3.10 shows the side view of PZ-LW probe.
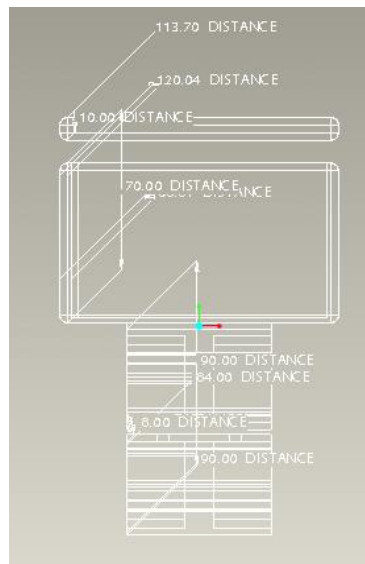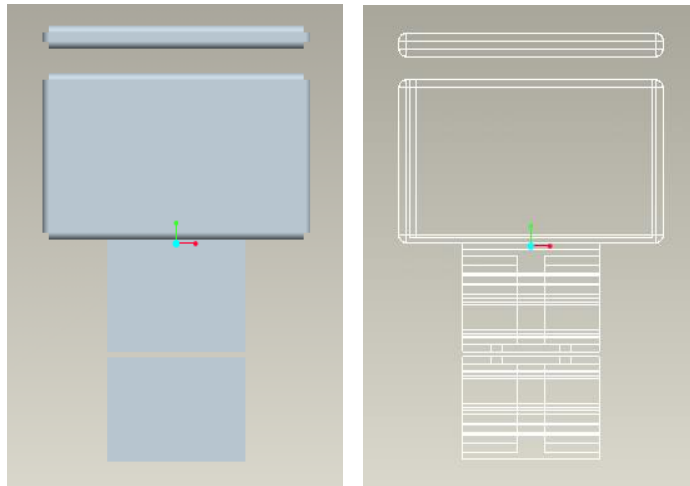
Figure 3.10   The Side View of PZ-LW Probe

3.3.4.3   Actual Probe Fabrication

Probe fabrication was made by using 3D printing with Polylactide material (PLA). The process in producing this probe was designed by using Pro-Engineering software and then the file .stl was used to convert

from 3D image to actual product. The time taken in printing process was around 82 hours. Figure 3.11 shows the probe that is separated by three parts: cap, control box and sensor, and lastly bottom clamping pipe.
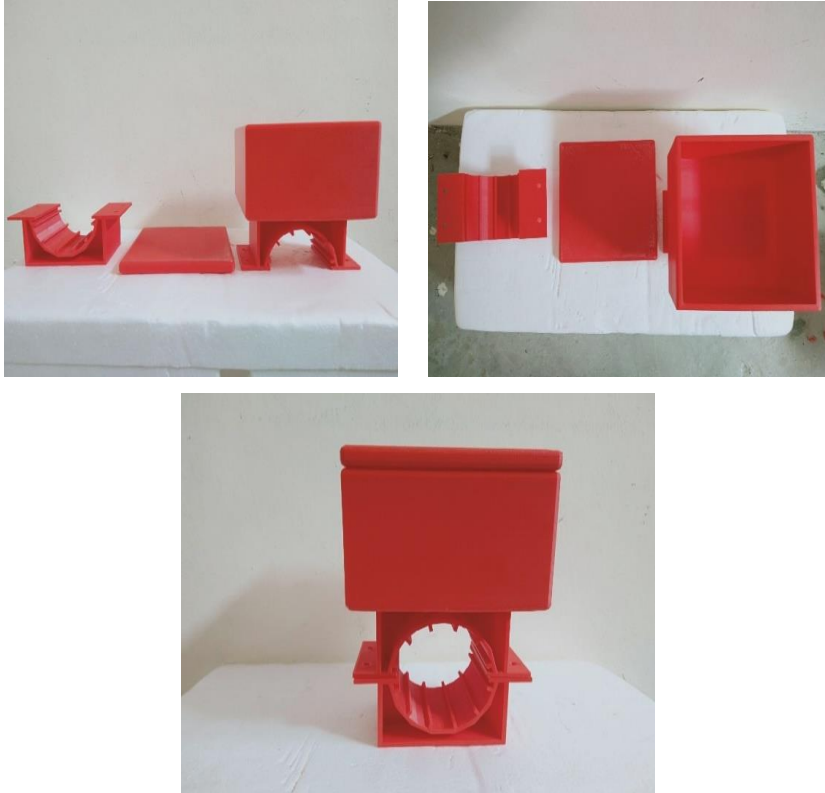
Figure 3.11   Probe Fabrication

3.3.4.4   3-D Full View Pipe Support Design

The pipe support design was designed to attach / hang the pipe before the PZ-LW probe was attached together. Based on the design in Figure 3.12, the size of pipe support was 1000mm x 500mm x 800mm. From here, the pipe was slid and at the same time, the several of diameter pipes was hung until 400mm. The limitation of pipe length was 1000mm.
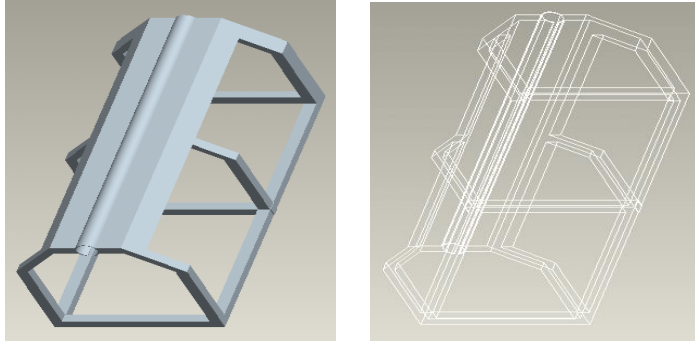
Figure 3.12   Pipe Support Design

3.3.4.5 3-D Pipe Support Dimension View

Figure 3.13 shows the front view of pipe support. The dimension size for width and high was 500mm x 800mm. From here, as for the sliding part of pipe, the pipe used was with diameter of 60mm and the thickness was 10mm. The bottom of pipe was cut with lengthwise of pipe support. The J pecans were used to hang the pipe for the both sides.
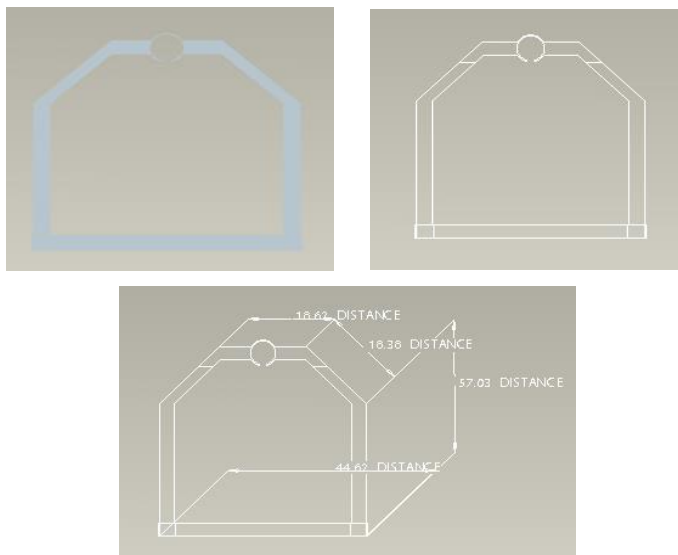
Figure 3.13   Front View for Pipe Support

The structure of pipe support was developed by using hollow steel with the size of 30mm x 30mm and the thickness was 2mm. All parts were welded together to ensure the structure was strong to support the weight of pipe. Figure 3.14 shows the side view of pipe support with the length of 1000mm.
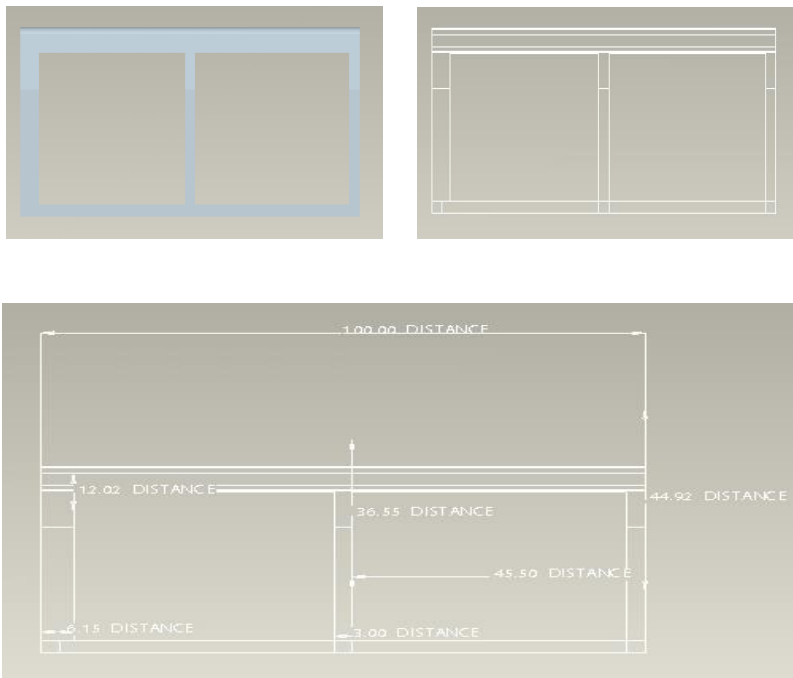
Figure 3.14   Side View For Pipe Support

3.3.4.6   Actual Pipe Support Fabrication

Figure 3.15 shows the pipe support fabrication that consisted of two J type hooks to hang the pipe. The J hook was slid to facilitate the transition of pipe based on the pipes length. The ranges of inner diameter for pipes that was hung were from 50mm until 300mm and outer

diameter until 400mm. Based on build-in structure, the load capacity was up to 70kg.

Figure 3.15   Pipe Support Fabrication

3.4   SIMNDT Simulation Procedure

The SIMNDT software was used in this experiment as an optimisation method for Piezoelectric Sensor Array and gaps between couple of Piezoelectric. This simulation was very important because the probe design was based on the result of optimisation especially in identifying the quantity of Piezoelectric in the experiment. By using this simulation, the expected result could be obtained before actual experiment was conducted. The few steps should be followed in process of optimisation

by using SIMNDT software. The first step was to set the size of pipe or plate dimensions that comprised the width, high, pixel, and label. From here, the 100mm width of plate was set with high of 100mm and the pixel was 10 (pixel is representing of clearance of pipe). From here, the pipe was labelled with value 0 (the labelling depended on the user). Figure 3.16 shows the dimension of pipe setting in SIMNDT software.
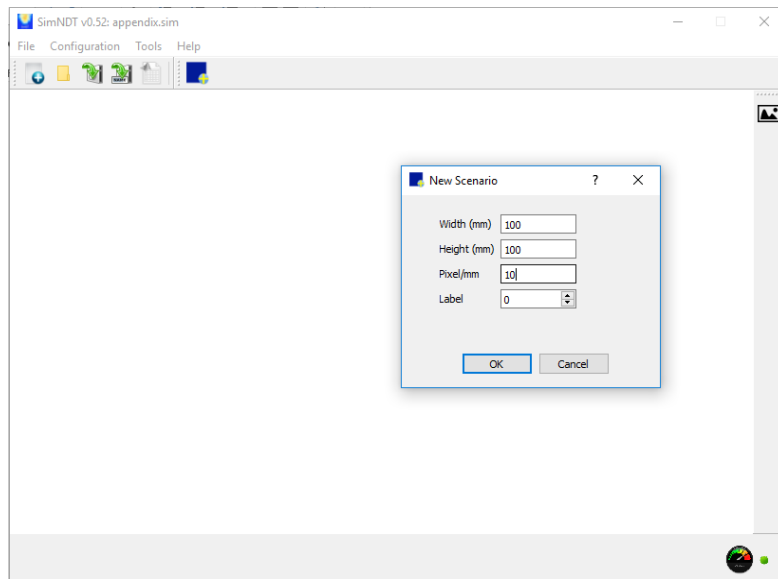
Figure 3.16   Plate Size

After dimension of pipe was completely set, the crack size / dimension was being setup. The basic of crack was based on two types which were rectangular and sphere shape. In this procedure, the rectangular crack shape was chosen where the dimension size was set according to the positioning at pipe (in x axis and y axis position coordinate), the size of crack (width and height) and angle of crack. From here, the crack labelling value should be different from the pipe labelling because of differentiation between pipe and crack. To ensure the positioning of

crack at the middle of pipe, the centre x and y was set respectively at 50mm. The width of crack was 10mm and high was 1mm. Select and set the size of defect (defect rectangular with position of 50mm x axis and 50mm y axis). The defect size of 1mm length and 10mm width. From here, the angle was 0 to ensure the crack on horizontal position and the crack size was labelled with value 40 by following the Figure 3.17 for crack setting.
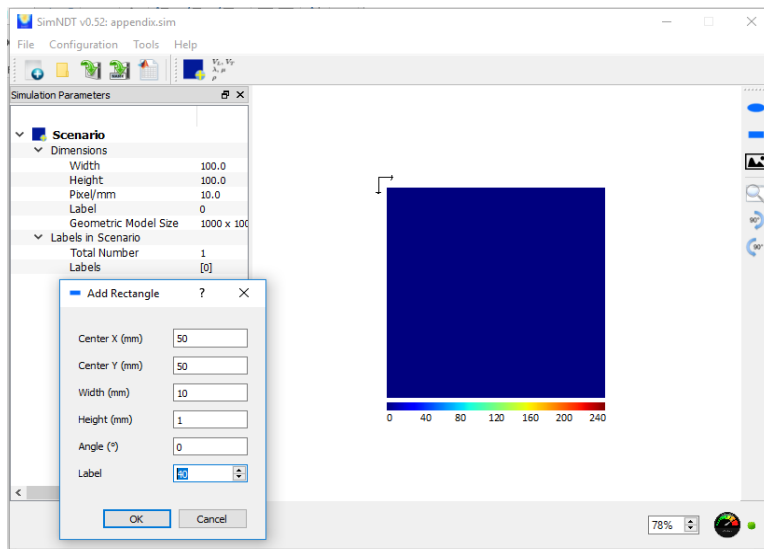
Figure 3.17   Defect Location and Dimension

When the crack size parameter was set, it showed on screen of the shape and position of crack on the pipe. From here, users could also add more crack according to the experiment that they wanted to run and also would show the different result when different shape, size, quantity, and position of crack were placed on the simulation. The dark blue represented the pipe and light blue was for crack. It also showed in colour range tone according to Figure 3.18 that shows the crack position of pipe.
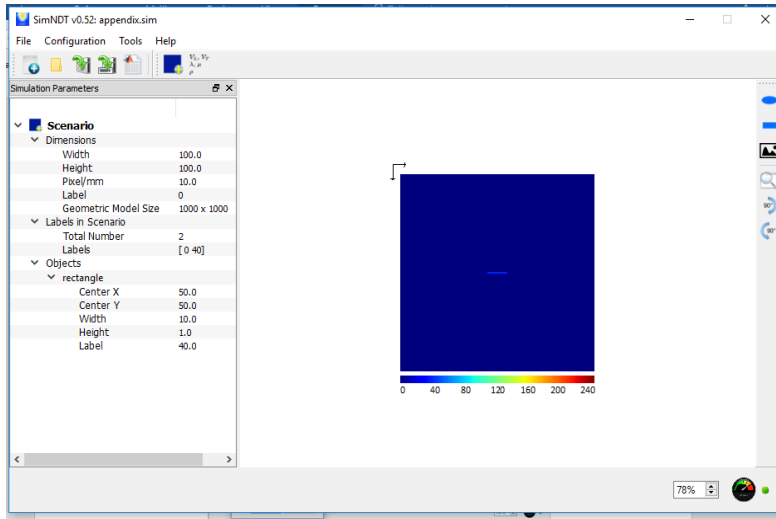
Figure 3.18   Defect Shape

The different material effected longitudinal and transverse velocity of material. From here, the characteristic of material should be the same as actual material that needed to be tested. For this simulation, the material used was steel (carbon steel S55C) with density (ρ = 7800 kg/m^3), modulus of elasticity (λ = 105.19 GPa), Tensile Strength (μ = 80.87 GPa), Longitudinal Velocity (V_L = 5850 m/s) and Transverse Velocity (V_T = 3220 m/s). Figure 3.19 shows the types of material characteristic. From here, the labelling was 0 as the pipe type. The characteristic of material could also be designed and uploaded to library through the created library template. It could also be garnered through online by loading on customised library material.
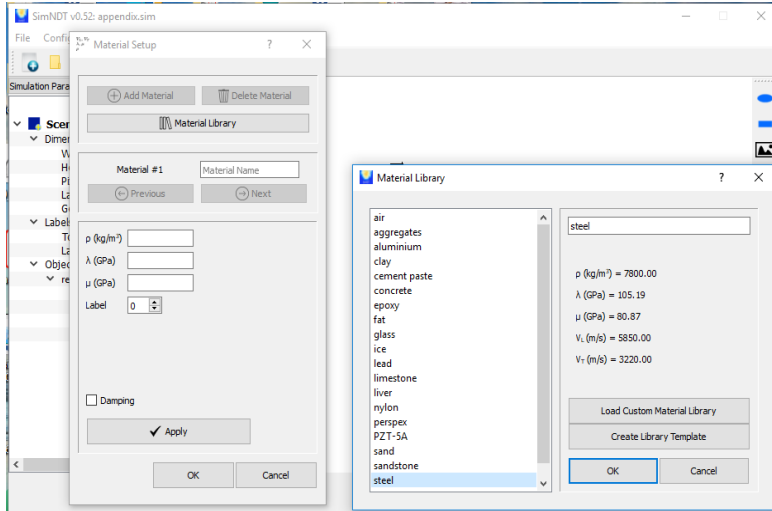
Figure 3.19   Material Properties Selecting

The setting for conditioning material did not only subject for material properties but it was also used for crack condition either in medium of air or in solution. The medium of material depended on the user to choose for simulation and experiment. Figure 3.20 shows the conditioning of air as the medium of testing with density ($\rho = 1.24$ kg/m^3), modulus of elasticity ($\lambda = 0$ GPa), Tensile Strength ($\mu = 0$ GPa), Longitudinal Velocity ($V_L = 344$ m/s) and Transverse Velocity ($V_T = 0$ m/s). In this setting, the label of this medium should be same as setting before crack within 40. This label was very important because of differentiation between pipe and crack.
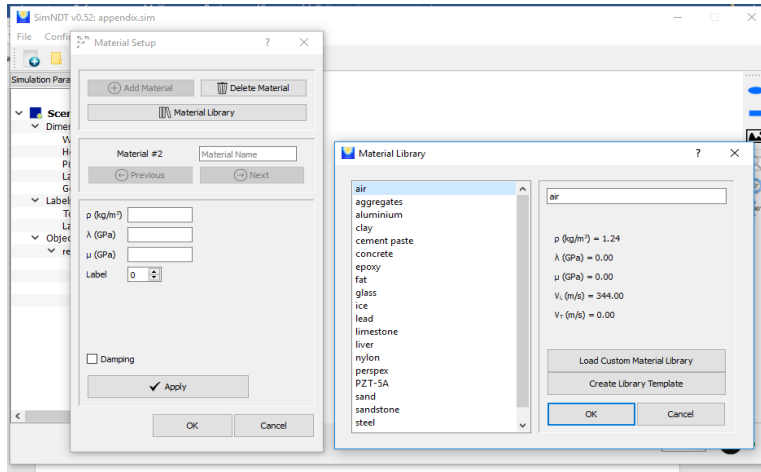
Figure 3.20   Defect Properties

In actual situation, the pipe was covered with coating in certain thickness. Normally, the coting thickness for pipe was in range between 1mm – 1.5mm. The function of coating was not only to prevent the pipe from corrosive but it was also to absorb the signal from inspection devices/tester. For simulation, the coating layer thickness was set as boundary layer for setup conditioning. In this simulation, the coating layer was assumed at 1mm for each side. Figure 3.21 show the boundary thickness setting on SIMNDT.
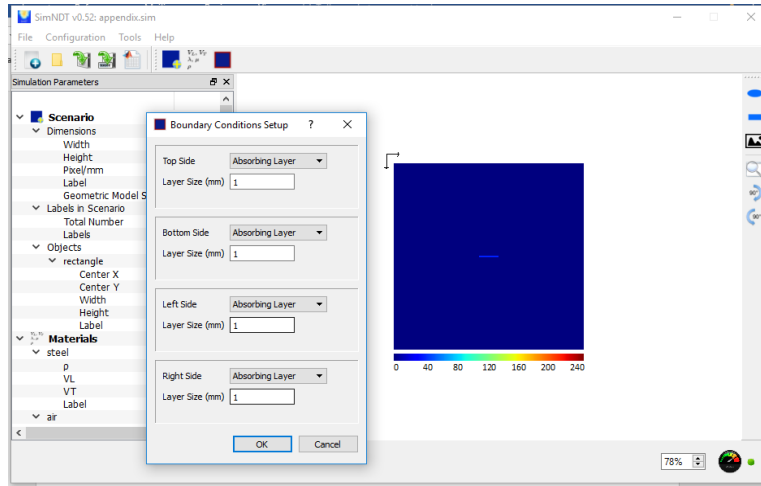
Figure 3.21   Boundary Size

In this simulation, the Piezoelectric was used for testing. There were two methods that could be chosen within Through Transmission and Pulse echo method by refer on Figure 3.22. For Through Transmission, it used two Piezoelectric with position start point of pipe (Piezo Actuator) and end point of pipe (Piezo Receiver). This method was also called as Pitch-Catch method. The focus in this research was Pulse Echo method. The concept of pulse echo method was the transmitter and receiver at the same place and point. It meant that the transmitter and receiver were being coupled together or a Piezoelectric was set as transceiver. Through this concept, the signal from transmitter / actuator received at the same time with the Piezo Receiver and the Piezo Receiver had to wait for the second signal from the pipe if the pipe had the crack (feedback signal from crack in pipe). From this setting, the size of Piezoelectric was at 10mm in the middle of horizontal point (50mm) on top side.
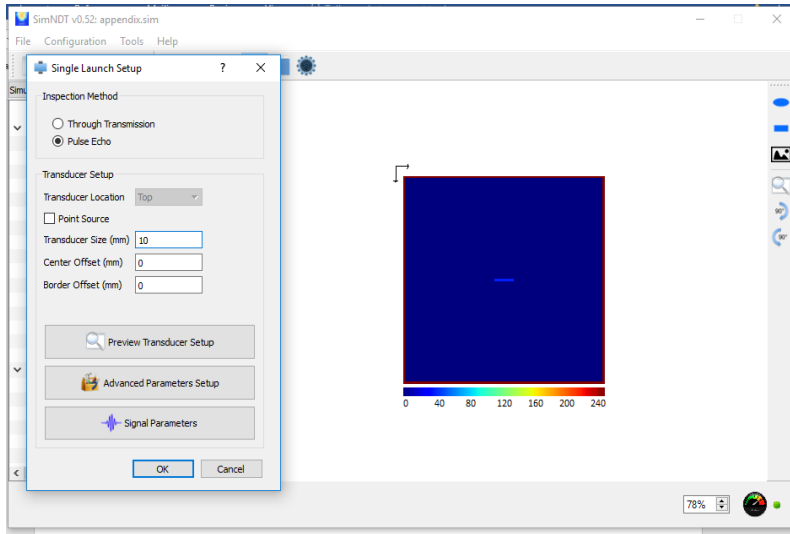
Figure 3.22   Method of Inspection

In Piezo Excitation Signal, the two types of transducer were given within PZT backing and Windowed source. This setting was setup under advanced parameters (Figure 3.23). Specifically, the advanced setup parameter for Piezoelectric Signal had three types of waves including longitudinal waves source, shear wave source, and combination longitudinal. Shear wave source consisted of three types of force including pressure, displacement and combination of pressure and displacement. In this research, the longitudinal wave was used to be experimented with displacement force.
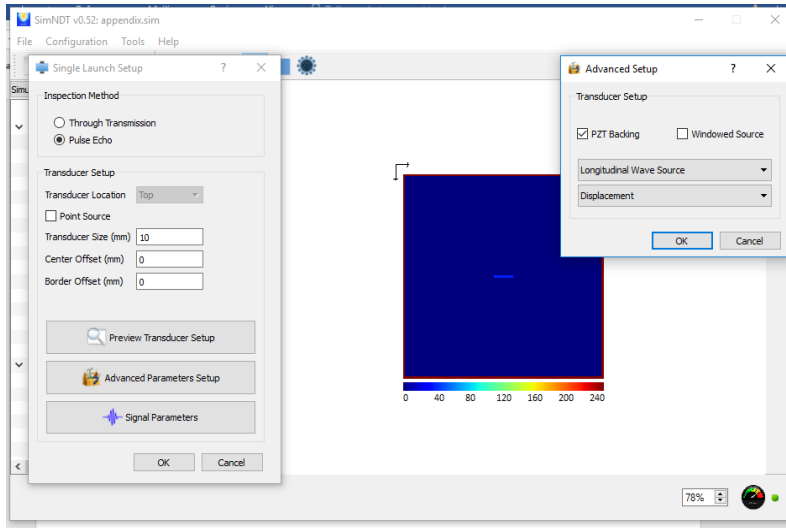
Figure 3.23   Transducer Sizing Setting

According to the experiment, the 1Mhz until 2Mhz excitation frequency was applied in Piezo Actuator / Transducer. From here, the signal parameter setting was matched between simulation and experiment. From here, the Gaussian Sine Pulse Wave was selected with 1.5Mhz frequency and five cycle waveforms. The selection of Gaussian Sine Pulse Wave was to interpret between the actual signal feedback or noise from pipe. It showed that according to the harmonically wave with different amplitudes, the feedback signal was identified from here. Five cycle was selected to avoid the draggy signal amplitude and it triggered confusion between actual signal or noise based on Figure 3.24. The length of signal also considering in this research in identifying the crack characteristic.
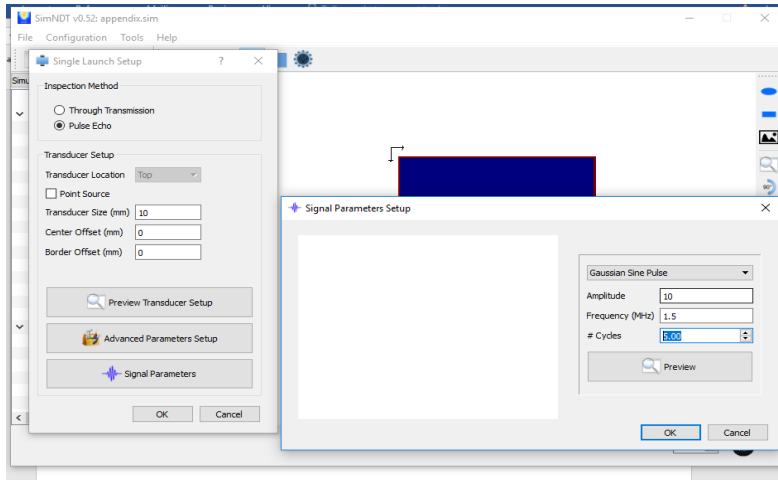
Figure 3.24   Excitation Signal Setting

To ensure the simulation functioned well, the frequency in simulation setup was matched with frequency at Piezo Actuator / Transducer. The frequency was represented in data signal transmit and receive. If the frequency setting was different, the signal transmit or receive would be lagged or leading and it contributed to data signal loses according to Figure 3.25. The simulation time was calculated according to the length of pipe and converting the frequency to time by *(t = 1/f)* and it should be multiplied by two for transmit and receive. From here, the 30us was set on simulation setup.
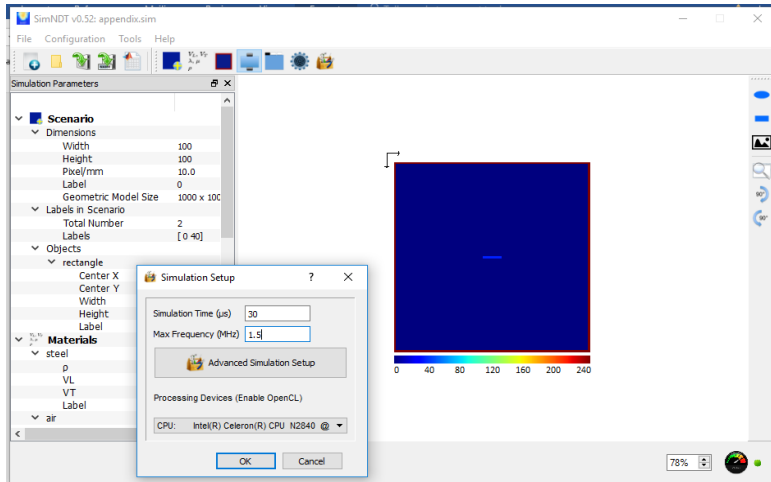
Figure 3.25   Simulation Time and Frequency Setting

After all parameter was set, the parameter was being compiled to ensure there was no parameter missing in this simulation based on Figure 3.26. This compilation will be automatically in check for simulation setup. From here, the user knew which part was problematic or it was successful without any problem. There was the area that would be compiled if there was scenario, material selection, boundaries conditions, and signal setup.
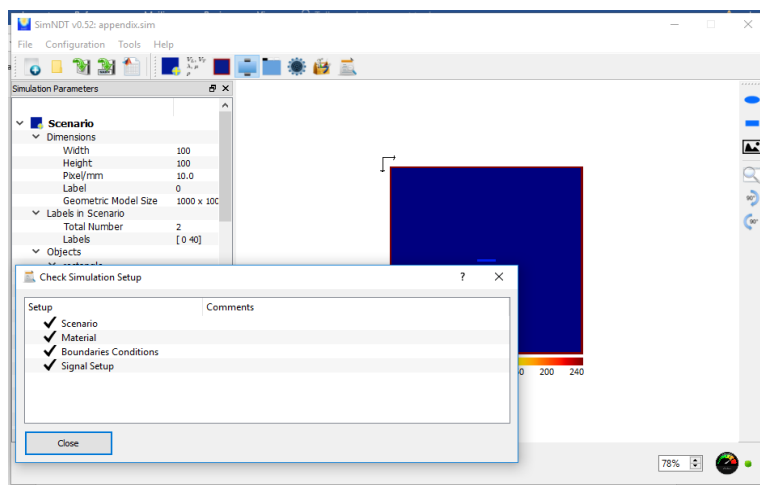
Figure 3.26   Simulation Parameter Checking

To run this simulation, the mode simulation and mode receiver signal should be enabled according to Figure 3.27. From here, the all signals were recorded according to time simulation set where the time setting was 30us. The signal was showed in PNG file for figure and also in data value in mat file format. The data in mat file could be opened through the MATLAB software and could also be analysed according to the simulation data.
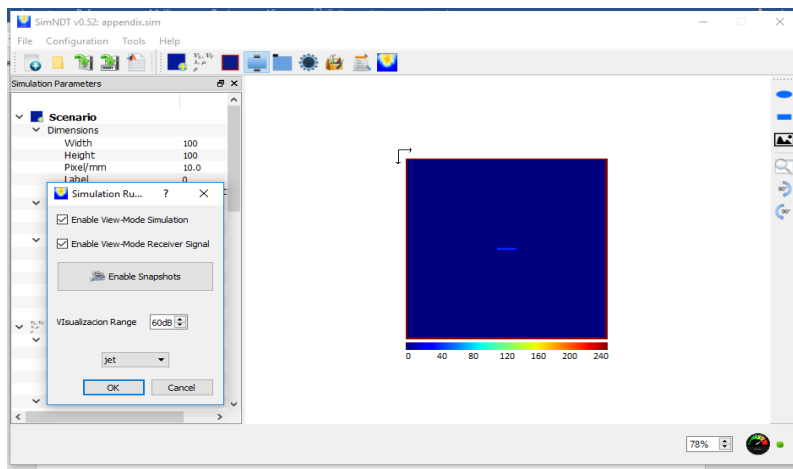
Figure 3.27   Simulation Data Display

After it was run, the signal showed in (*x and y*) graph amplitude and also in acoustic figure based on Figure 3.28. The amplitude changes were identified based on graph and also acoustic signal response. The blue colour represented as the weak signal while yellow until red for medium and high signal with high amplitude. The signals were compared between the excitation signal (transmit signal) and feedback signal (receive signal).
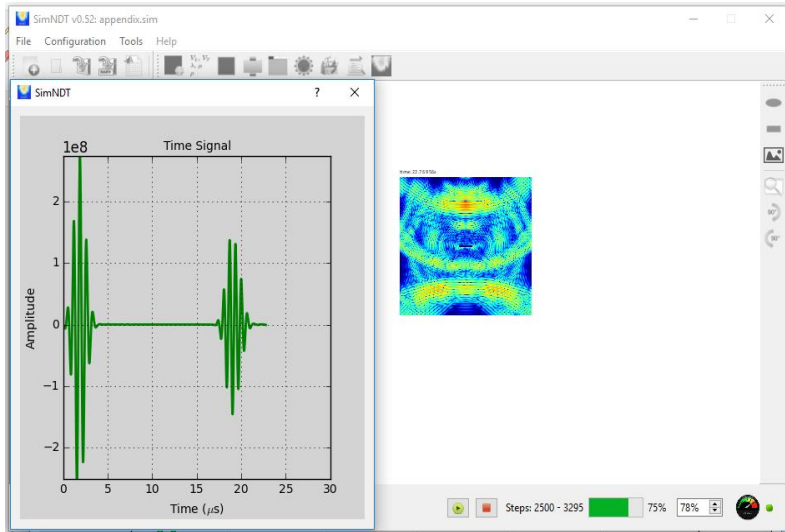
Figure 3.28   Wave form and Graph Display

From simulation, the simulating result was identified especially in probe designing based on optimisation signal. The simulation and actual result (experimental) were compared in identifying the percentage error. The simulation was very helpful in this research before the probe and frequency were designed in this (PZ-LW) system. This simulation also provided more advantages in material selection and medium testing. The correct material testing was decided without contributing to the high cost in actual material testing through simulation.

3.5   Process of Optimization Procedure

Response Surface Methodology (RSM) is a combination of statistical and mathematical technique used in engineering field for optimisation purposes. RSM is an effective tool for optimizing many factors and that their interactions influence the desired response. Generally, there are

many Designs Of Experiment (DOE) methods that can be used to optimise independent variables. These methods include: Factorial, RSM Central Composite Design (CCD), Box-Behnken Design (BBD), Mixture, and Mamdani methods. In this study, Central Composite Design (CCD) was employed to create the input parameters due to the fact that CCD provided precise prediction results compared to other methods.

The estimation procedure of this approach is shown in Figure 2.17. The desired objective was the number of the axial and hole defect detection which was determined as the response. The chosen parameters that were supposed to influence the detection of the axial and hole defect and were selected to evaluate the PZ-LW probe performance. Experiments based on the probe design for each run were performed according to the design matrix based on the Central Composite Design (CCD). RSM provided a design matrix containing 20 numbers of runs (N). In order to calculate the number of runs required for the present case of three independent variables, the following formula (Dincer, Colpan, Kizilkan, & Ezan, 2015) is shown below: where n is the number of independent variables. Replications of the test at the centre were very important as they provided an independent estimation of the experimental error. Hence, the total number of tests (N) required for the three independent variables was in Equation 3.6.

$$N = n^2 + 2 * n + n_c = 8 + 2 * 3 + 6 = 20 \qquad (3.6)$$

Where *n* was the number of independent variables. The Design-Experts software was used for the analysis responses and determining the empirical models with best fits.

The experimental results depending on different parameters design were carried out based on the design matrix in order to obtain the corresponding responses, and then the ANOVA was performed to analyse the relationship between the factors and responses.

The next step was to obtain the developed model but before doing this, the 'P-value' statistic in the analysis of variance (ANOVA) table of the model and its terms should be observed to be less than 0.05 since this value represented the significance factor, the smaller the 'P-value', the more significant the result was. Other parameters in the ANOVA were calculated as these: sum of squares divided by degree of freedom (df) gave the mean square; 'F values' which were tests of comparing models and their terms with a residual variance were calculated for a model and its terms by dividing respective mean square of the model and its terms with a residual mean square. If the variances were close to the sum, the ratio would be close to 1 and it was less likely that any of the factors had significant effect on the response. Consequently, if a 'P value' of any model and its terms were less than or equal to 0.05, the terms in the model would have significant effect on the response. The determination coefficient R^2 was utilised to test the fitting quality. A R-Squared extended from 0 to 1, where high value indicated the best fitting of the mathematical model with experimental observation.
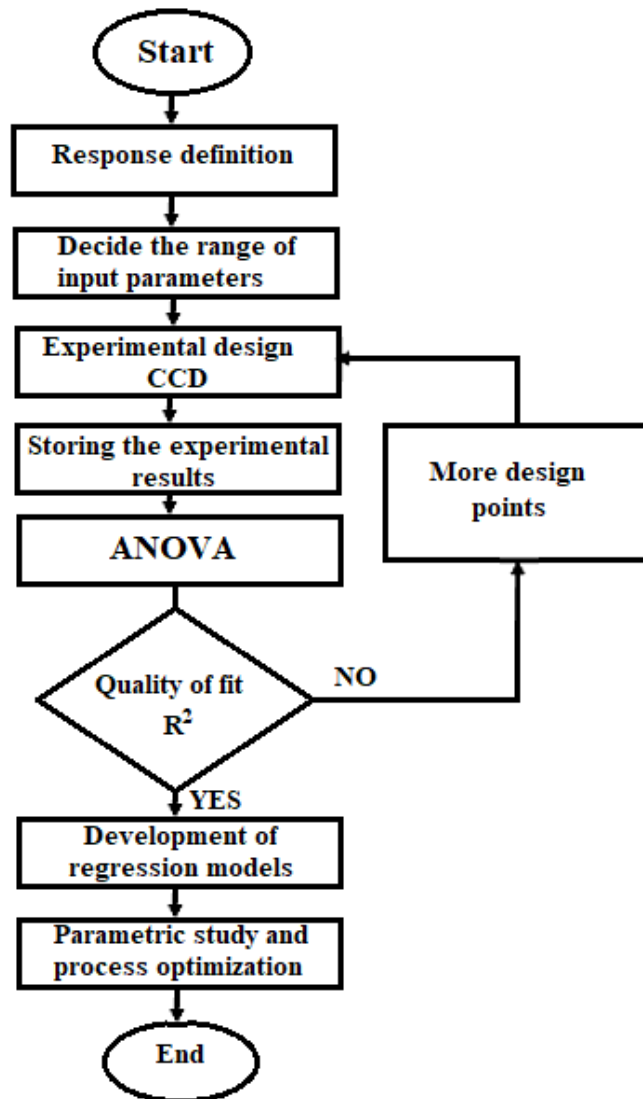
Figure 3.29   Response surface methodology (RSM) flow chart

Next, the quadratic polynomial model was obtained and utilised to predict the performance. Subsequently, optimisation was applied using the desirability profile and its functions to find out the optimum probe design parameters. The optimisation analysis was established based on

the desirability analysis in Equation 3.7 (Ghafari, Aziz, Isa, & Zinatizadeh, 2009). The optimum design variables with higher desirability were selected to be the final design for the PZ-LW probe. Finally, the optimal design of the PZ-LW probe for the inspection of 60 mm carbon steel pipe would be verified experimentally to confirm the accuracy of the inspection.

$$D = (d_1 * d_2 * \dots \dots * d_n)^{\frac{1}{n}} = (\prod_{i=1}^{n} d_i)^{\frac{1}{n}} \qquad (3.7)$$

To validate the reliability and the conclusions obtained from the statistical analysis, a comprehensive comparison between the experimental and numerical data and the results obtained from the regression analysis was done. The regression equation expressed the relationship between the dependent and independent variables. The dependent variable here was number of axial and hole defect and the independent variables were the number of sensors, gap of sensor, and frequency used. Moreover, the relative deviation between the regression model and the experimental and numerical results was measured using the following Equations 3.8.

$$Error(\%) = \left(\frac{Exp_{value} - Reg_{value}}{Exp_{value}} \right) * 100 \qquad (3.8)$$

The Design of Experiment (DOE) suggested a blueprint for the experiments and it may be identified as proposing to obtain maximum information with minimum experiments, and it may involve how to

accomplish the experiments in order to find a solution (Kleijnen, 2015). In recent years, there were many researchers focused on designing Piezoelectric probes for specified applications. The parameter design of the Piezoelectric probes were optimised to increase the resolution and sensitivity of defect detection. The parameters that affected the Piezoelectric testing probe performance that was helped to increase the capability of defect detection in the conductivity material and they are frequency, distance, and number of sensors. From the above-mentioned parameters, number of sensors, the sensor gap, and frequency were selected in this research to facilitate the study on the influence of the probe design parameters on the accuracy of defect detection in 60 mm carbon steel pipe inspection. The frequency of the Excitation Piezo Actuator for the deep penetration of Piezoelectric was fixed at 1.5MHz.

The Design-Expert software version 7.0 was applied to design the experiments based on the Central Composite Design (CCD). Table 4.5 presents the selected input parameters as well as the levels that are used to design the parameters of the PZ-LW probe. Regarding this matter, two optimisations have been analysed whereby the first refers to the effecting frequency as shown in Table 3.2, while the second is on the Piezo gap as illustrated in Table 4.6. In Table 4.5, (-1) and (+1) were respectively chosen to indicate the lowest and highest level. In addition, three PZ-LW probe design parameters were investigated and described as follows: (1) design parameter A refers to the Piezo Actuator Frequency in the array sensor, (2) design parameter B refers to the width of defect, and (3) design parameter C postulates the defect distance. Table 3.3 presents the parameter of *A* defect distance and *B* PZS gap as (-1) and (+1), respectively. Moreover, the responses in the present study managed to

detect the number of axial and hole defects. RSM was used to further investigate the influence of the probe design parameters on the accuracy of the probe defect detection in the 60 mm inspection pipe.

Table 3.2   Independent parameters considered in this study and their levels for central composite design for frequency effect

Parameter	-1	+1
Excitation frequency actuator (MHz)	1	2
Width of Defect (mm)	0.1	3
Defect Distance (mm)	10	90

Table 3.3   Independent parameters considered in this study and their levels for central composite design for sensor gap effect

Parameter	-1	+1
Distance Defect (mm)	30	80
Sensor Gap (mm)	0	5

In the current research work, optimisation was utilised with the desired profile and its function in the RSM. The highest design parameters with high desirability were chosen as the final design of the probe PZ-LW. Specifically, the goal was to maximise the number of defect detection to the defect inspection axis and the hole in the pipe. Next, another purpose is to minimise the number of Piezo Sensor (PZS) used whereby the height of the excitation signal and sensor gap distance were set within a certain range in order to achieve satisfactory results in the upper and lower limit. The solution with a high desire was deemed preferable.

Table 3.4 shows the target value as well as the value for all response parameter based on the outside pipe diameter of 60mm.

Table 3.4   The parameter range of optimize the PZ-LW probe design

Probe design parameter and respond	Target	Lower limit	Upper limit
Number of Piezo sensor	Minimize	10	12
Sensor Gap (mm)	In a range	0	3.75
Excitation Frequency (MHz)	In a range	1.5	2
Axial defect	Maximize	1	15
Hole defect	Maximize	1	15

3.6   The Error Compensation Technique

Nevertheless, it was important to note that it was still difficult to predict the size and shape of the cracks due to the complexity of cracks and unknown the crack positioning despite the numerous compensation techniques developed to compensate Piezoelectric error. In most cases, the detailed piezoelectric actuator quantity specifications were not available to the users in establishing such a relationship. Hence, the researchers resorted to advanced software computing techniques such as Fuzzy Logic and neural network which could be trained to map the relationship. Fuzzy Logic was known as an artificial intelligence tool that described complicated physical phenomena as well as able to

anticipate the linear or nonlinear results based on the collected input and output data.
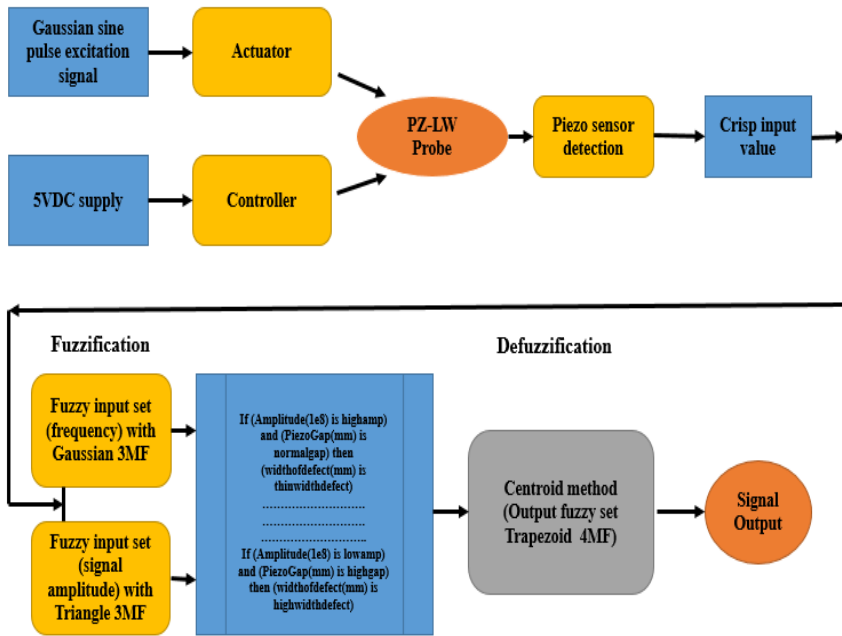
Figure 3.30   The diagram of the proposed fuzzy error compensate technique

The overall proposed Error Compensation technique is shown in Figure 3.30. Specifically, this technique utilised a single PZ-LW probe operated in two different ways stated as follows: (1) to create a set of detection channels, and (2) to create a set of gap measurement channels. Moreover, it should be noted that a simple relationship could be created between the two measurements using the Mamdani Fuzzy type. Accordingly, the discussion in the previous section suggested that the width defect parameter could be quantitatively evaluated by measuring the level of

the peak amplitude of the PZ-LW in the Piezoelectric detection. However, the PZ-LW signal could be affected by the adjustment of the gap, which then led to inaccurate PZ-LW measurement. More importantly, the effect of the gap could be reduced using the Mamdani Fuzzy type approach.

3.6.1   Fuzzy Logic Implementation

Fuzzy Logic therein analysis was applied as an administrator with the aim of providing the crack data with supported reduced features, namely amplitude, phase and width. In particular, this Fuzzy-based deciding scheme contained system input, system output, Membership Functions (MF), and IF-THEN Fuzzy rules. The inputs referred to the characteristics of crack specified amplitude, phase, and loop width, while the output of the scheme described the real crack data specified depth, width, and shape. As shown in Figure 3.31, each input is associated with one Fuzzy set with an agreeing MF. The MF reacted to the degree of each Fuzzy set as a member in the membership from the scale of 0 to 1. Furthermore, it should be noted that the Fuzzification was executed appropriately as the companion of the Fuzzy set with MFs. Fuzzy rules were declared in IF- THEN lingual condemnations whereby the relative between input and output could be described as follows: IF the amplitude (input) was high THEN the crack is the width (output). Eventually, a defuzzification action was required to convey the lingual variables into mathematical crisp values for more one Fuzzy rule which was consistently applied, including the lingual (deep) execution result.
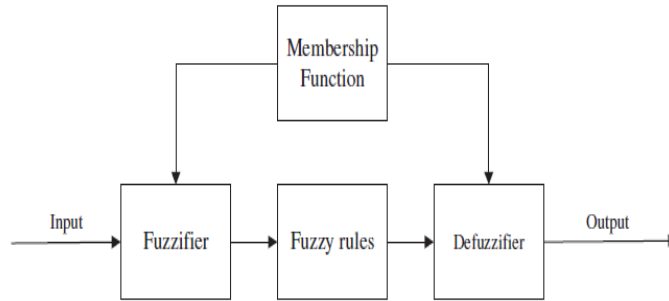
(a)
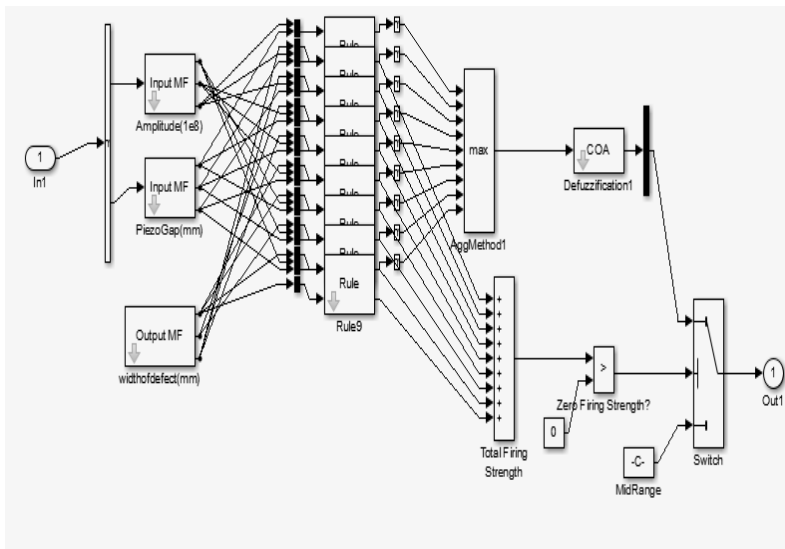
(b)

Figure 3.31   Flow chart of fuzzy logic (a) Basic block for Fuzzy
Logic, (b) Internal block function in Fuzzy Logic.

In the case of the current research, dissimilar frequencies were
implemented for the purpose of testing the crack with dissimilar width
and shapes. Moreover, the number of MFs apart from the Fuzzy rules for
each MF ought to be built severally according to the dissimilar
characteristic groups. In this work, ANFIS in MATLAB was applied as

a scheme acquiring technique in order to find a Fuzzy Logic system. Therefore, the trained Fuzzy Logic engines were implemented to predict the crack data which supported the extracted features or the combination of the characteristics.

3.6.1.1   Flow Chart

The process of signal correction can be explained according to Figure 3.32's flow chart. This process started in excitation signal transmit until signal receiving and process for correction. In this process, the Gaussian Sine Pulse wave was used as excitation signal and it was being sent to Piezo Actuator for converting from electric signal to longitudinal vibration signal and from here, the signal transmitted at pipe surface as a transmission medium. Along the pipe, if there was no crack existed in the pipe, then no signal feedback received. Otherwise, if the crack existed on the pipe, then the signal from transmission gave the feedback and received at Piezoelectric Receiver Sensor and converting from vibration signal feedback to electrical signal amplitude. From here, the signal from transmitter and receiver showed on QuickDAQ software interface and at the same time the signal sent and process at MATLAB software for correcting the signal by using Fuzzy Logic for error compensation. The signal was corrected according to the rules that were set in Fuzzy Logic through Mamdani Fuzzy Logic Rule (MFL). From here, the graph of signal amplitude for conventional signal (without Fuzzy) and actual signal (with Fuzzy) showed in scope and the percentage error was identified through this signal. The comparisons for both two signals were being showed in scope of Simulink Graphical User Interface (GUI). According to this method, the precision of width

crack was obtained and at the same time the positioning of crack was identified correctly at pipe inspection. The result after Fuzzy was compared to simulation to confirm the accuracy signal based on percentage of error. This method should have in signal analysis to ensure that the data received was correct and at the same time to avoid the misplaced in repairing pipeline where it effected on the time repairing and contributed the accident cause of pipe crack.
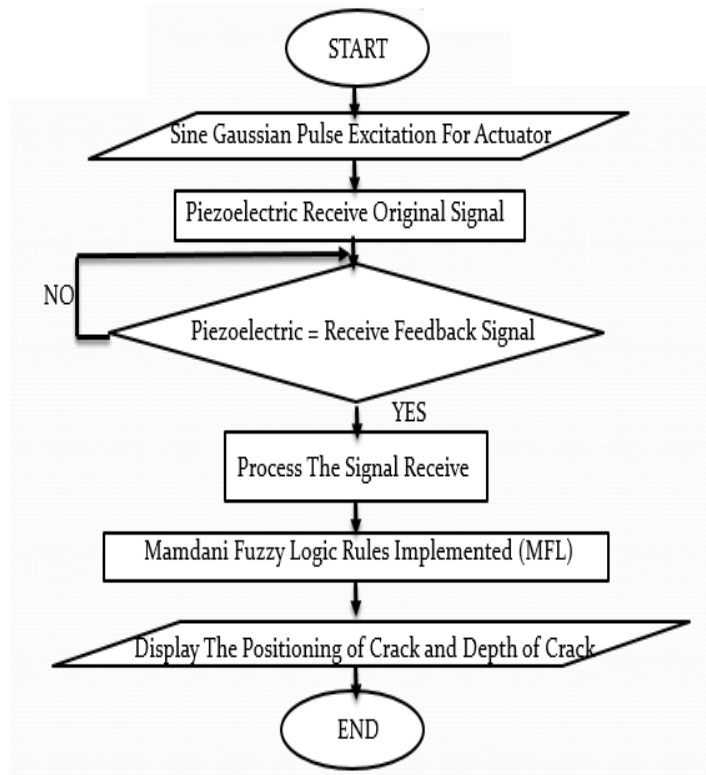
Figure 3.32   Flow Chart of Fuzzy PZ-LW Compensation Scheme

3.6.2 Rules of Fuzzy Logic

To complete the Fuzzy Logic block setting, the rule of the Fuzzy block was set according to rule editor for width of defect measuring block. From here, there were nine rules that were set.

Fuzzy rule algorithm

If (Amplitude (1e8) is high amp) and (Piezo Gap (mm) is low gap) then (width of defect (mm) is thin width defect)

If (Amplitude (1e8) is high amp) and (Piezo Gap (mm) is normal gap) then (width of defect (mm) is thin width defect)

If (Amplitude (1e8) is high amp) and (Piezo Gap (mm) is high gap) then (width of defect (mm) is normal width defect)

If (Amplitude (1e8) is medium amp) and (Piezo Gap (mm) is low gap) then (width of defect (mm) is thin width defect)

If (Amplitude (1e8) is medium amp) and (Piezo Gap (mm) is normal gap) then (width of defect (mm) is high width defect)

If (Amplitude (1e8) is medium amp) and (Piezo Gap (mm) is high gap) then (width of defect (mm) is high width defect)

If (Amplitude (1e8) is low amp) and (Piezo Gap (mm) is low gap) then (width of defect (mm) is normal width defect)

If (Amplitude (1e8) is low amp) and (Piezo Gap (mm) is normal gap) then (width of defect (mm) is high width defect)

If (Amplitude (1e8) is low amp) and (Piezo Gap (mm) is high gap) then (width of defect (mm) is high width defect)

3.6.3 Fuzzy Inference Steps

The Fuzzification method used for this project was triangular membership functions. From here, there were defined by a lower limit a, an upper limit b, and between of lower limit and upper limit value m, where a < m < b. By using the MATLAB software, the simulation and interface being made according to the step of Fuzzy setting. There were the steps of Fuzzy setting on MATLAB. The first step was to set block starting for MATLAB by typingM" Fuzzy " on the command window. Figure 3.33 shows the command window form for typing.
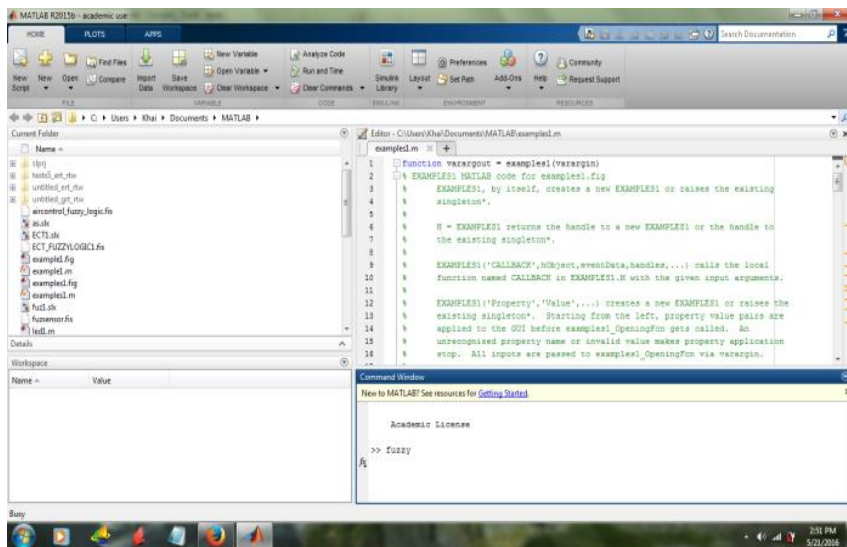
Figure 3.33   Command Window

After the Fuzzy word was typed in the command window, the second step was Fuzzy Logic design block (inference editor) setting and it appeared on the screen. From here, the users could set the value of the input and the types of membership function that they wanted to use. In

this research, the input selection was there for signal amplitude and Piezo gap and the membership functions used were Triangular and Gaussian signal. Both of input and output names were Piezo Defect Amplitude for (Amplitude) and Piezo Sensor Gap for (piezo gap) and output (width of defect).

The third step was to set the membership function for the Piezo Defect Amplitude, Piezo Sensor Gap and the output. In each input and output, they were three number of Membership Functions (MF) for input and output with the range from 0 to 6 according to the minimum and maximum width of crack and defect amplitude that could be achieved of probes. For the Piezo Defect Amplitude, the concept of the signal was inversely proportional to the width of defect.

This meant when the amplitude of receiving signal increased and the gap of Piezo sensor was low, then the width of defect was thin. When the amplitude of receiving signal was low and gap of Piezo sensor was high, then the width of defect was high on plate or pipe are inspected. The condition of pipe could be looked at the amplitude signal either it has defected or not base on higher of signal amplitude. Figure 3.34 shows the membership function of amplitude signal and sensor gap and the output for Fuzzy Logic designed.
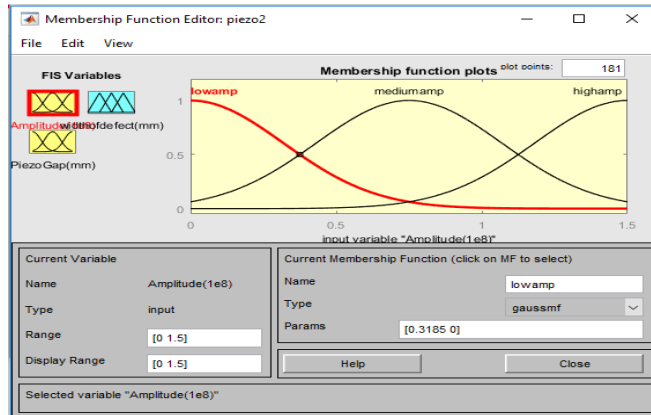
(a)
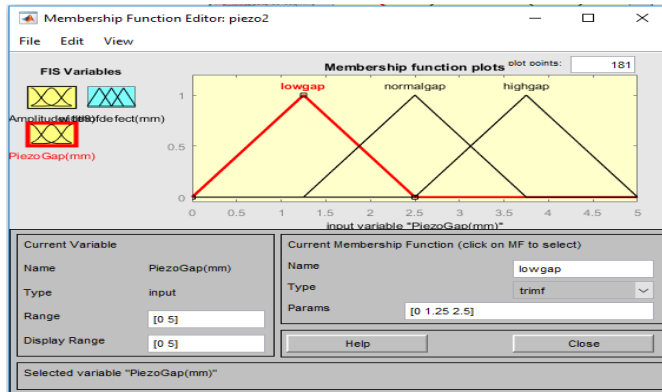
(b)
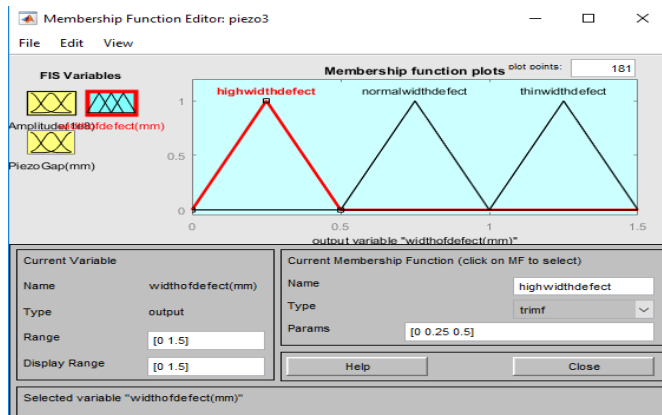
(c)

Figure 3.34   (a) Piezo amplitude signal, (b) Piezo sensor gap, (c)

Output Actual Width Defect.

3.6.4 Surface Viewer for Fuzzy Logic

The fifth step in the Fuzzy Logic setting was the result of Fuzzy setting by looking at the rule viewer and surface viewer. From here, the user could observe the input changes and effect of the output for rule viewer and for the surface viewer that showed in the 3D graph. Figure 3.35 (a) shows the rule viewer for amplitude and sensor gap and (b) is surface viewer graph.
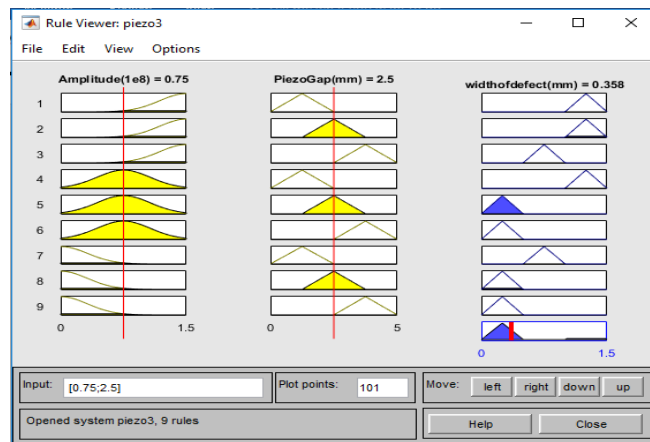
(a)
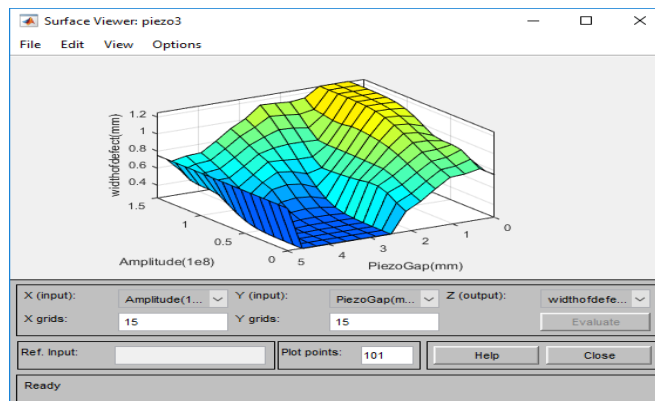
(b)

Figure 3.35   (a) Rule viewer, (b) Surface viewer

3.6.5 Graph Surface Viewer for Fuzzy Logic

In each of graph setting for amplitude and sensor gap, it was showed in the 2D graph. By referring to the Figure 3.36, the amplitude signal (1e8) and Piezo gap (mm) for the surface viewer are shown. The maximum value of amplitude signal graph was 1.5(1e8) width of defect for output at Y axis and 4.5(mm) for width of defect measuring at X axis and for Piezo Gap Signal, the maximum output for width of defect was 5mm at Y axis and for width of defect measuring was 4.5mm at X axis.
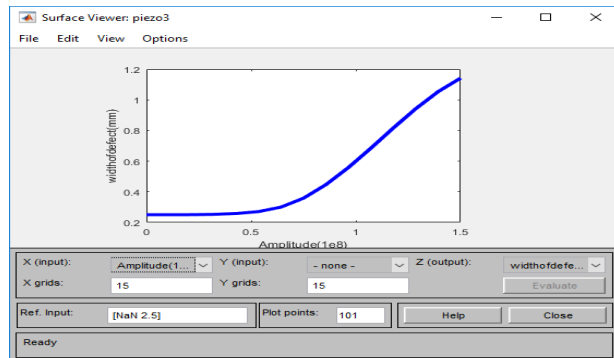
(a)
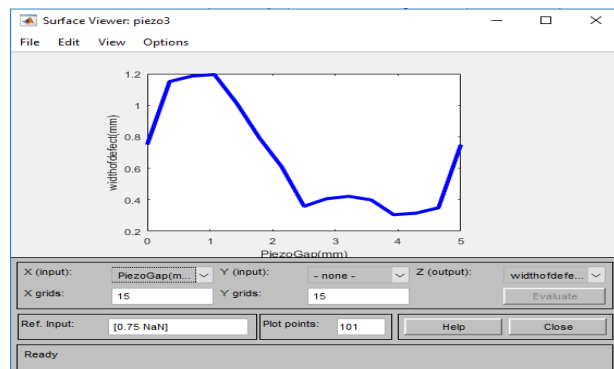
(b)

Figure 3.36   (a) Amplitude receiving signal, (b) Piezo gap for surface viewer

3.6.6 Overall of Fuzzy Logic Simulink System

In the simulation process, the MATLAB/ Simulink was utilised to simulate the input and output result signal based on the Gaussian excitation signal setting. According to Figure, 3.37, simulation block diagram model for PZ-LW contains four important parts that are utilised in the Fuzzy Logic system. The first part was the input source, followed by the conditioning process. Next, the third part referred to Fuzzy Logic process and feedback, and the final part illustrated the output display. In input source, the feedback signal from Piezoelectric Sensor was received from DAQ module and the data was sent through serial data to PC for analysis by using MATLAB software. From here, the signal received was the original signal from Piezoelectric Sensor. The input was processed in real time to ensure the continuously analysis could be done without any problems. After the signal from device was received, the signal should be gone through the conditioning part. From here, the mathematical equation was developed by knowing the sensor gap distance. This was because, the effect of sensor gap contributed to amplitude signal measurement and at the same time, it identified the actual shape of crack. The equation was developed based on simulation result for gap effect of PZ-LW inspection. In the third part, the signal was through the Fuzzy Logic process by rule. From here, the percentage of error for actual signal was identified and being corrected by using this method. The percentage error provided the feedback of Fuzzy and corrected the signal to ensure the signal in right amplitude. This part was very important in this research because of the amplitude signal contributed to width of defect on pipeline inspection. Lastly, the signal displayed in scopes as the output display. The output display showed in

graph and the comparison of signal before Fuzzy and after Fuzzy was analysed and from here, the percentage of error compensated was acquired.
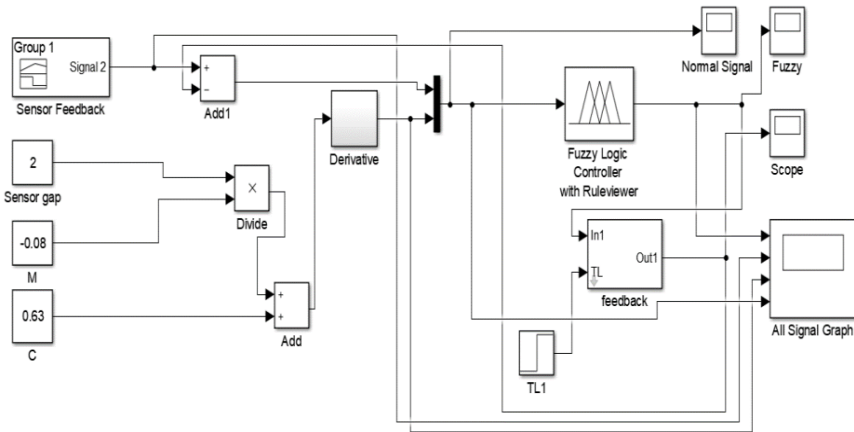
Figure 3.37   The Simulink Block Diagram Model for PZ-LW. (a) Input source, (b) Conditioning process, (c) Fuzzy logic process and feedback, (d) Output display

3.6.7   Input For Fuzzy Logic

In the simulation process, a Gaussian Sine Wave signal was used as the input and set according to the amplitude, frequency, and the phase angle of the signal. Figure 3.38 shows the input block diagram that has been set based on the input signal as well as the gap of the Piezo sensor. According to the experiment, the 10 pairs of Piezoelectric sensors used for getting the signal feedback on the pipe circumference surface with pipe diameter were 60mm. A sample of signal from Piezoelectric was

selected for Fuzzy Logic and from here, the signal was processed and analysed for signal accuracy.
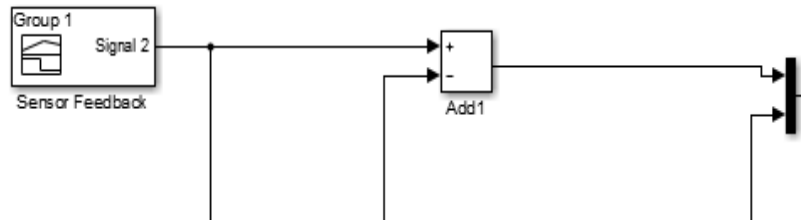
Figure 3.38   Input Block Diagram

3.6.8   Conditioning Function For Fuzzy Logic

The purpose of the conditioning function was to measure the percentage of amplitude changes based on the gap between two Piezo sensors. The gap between the two sensors tended to affect the signal amplitude; hence, the linear equation was applied to ensure the error cause of sensor gap could be avoided based on equation amplitude = -0.08 x sensor gap + 0.63. Figure 3.39 shows the conditioning block that is used in Simulink as well as the graph result from the conditional block which is displayed on the scope.
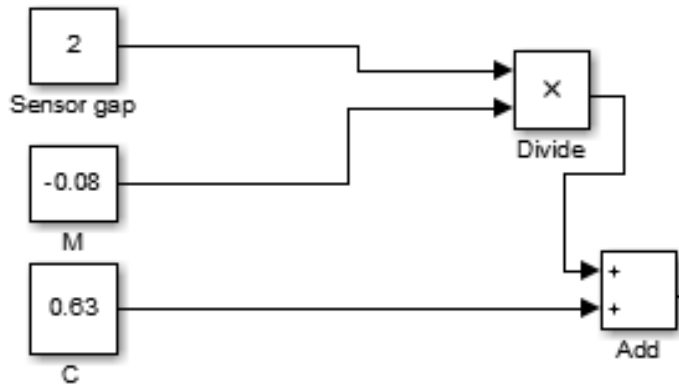
Figure 3.39   Conditioning Block Diagram

3.6.9   Fuzzy Logic Process and Feedback

The feedback and error compensation were processed according to the output signal from Fuzzy Logic. In this case, the output signal from Fuzzy went through the error compensation equation in the signal block, followed by the feedback in the error block. Figure 3.40 shows the feedback block for error compensation as well as the output produced. From here, the compensation equation was based on Fuzzy rule which was made in Fuzzy development input and output. The nine rules were developed to ensure the process of accuracy could be archived. From here, the AND conditioning for Fuzzy Logic process was used in the rules. The three parameters were considered in this rule development within signal amplitude, sensor gap, and width of crack.
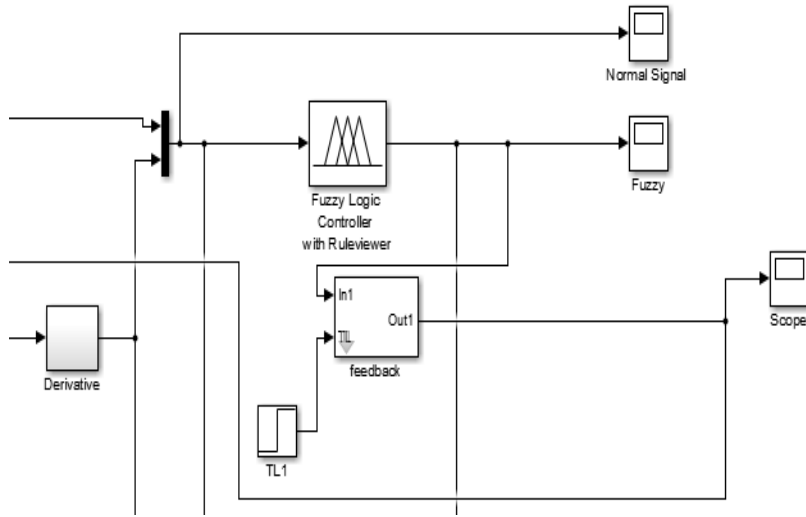
Figure 3.40   Error Compensation Feedback

3.7   Piping Sampling Preparation

The process of calibration also provided in the development of simple calibration curves that mapped signal characteristics (such as phase angle or amplitude to flaw depth). The calibration operation required the use of a Stage Wage and V2 Block, which was made of the same material as the test specimen (Mosey et al., 2014). Various defects with dimensions were introduced into the calibration standard and the calibration standard was inspected prior to the test specimen. Ultrasonic testing calibration standards were developed with different types of defects to meet any inspection needed today. The sample was made of a steel alloy of iron and carbon; the high amount of carbon gave carbon steel its familiar dark colour. The electric conductivity of this material was equal to 3.18% of the International Annealed Copper Standard. Due to its shock resistance, hardness, and strength, the non-ferromagnetic carbon steel was used in many industrial applications like power plant,

high pressure fluid transportation, water mains under roads and industrial machinery, tools and structures(Al-Sabagh, Migahed, Sadeek, & El Basiony, 2018; J.-H. Lee & Lee, 2008).

There were four sets sample artificial cracks of carbon steel pipe which were in axial, gradient axial, and hole defects. Artificial crack or man-made crack has been made by humans, not nature. On the defect size and shape, it has been made by human to show the effect of size and shape of crack at the signal receiving. The four sets sample of carbon steel pipe which were in axial, gradient axial and hole defects were made using Electrical Discharge Machining (EDM) as well as the turning machine. In the case of the present study, it was observed that both samples had a 5 mm depth intrusion inside of the pipeline wall for the defect detection testing with the proposed PZ-LW probe. Figure 3.29 presents the carbon steel pipe sample and the layout of the axial and hole defect positions. The dimension of the axial defect of 2.0 mm (width) and 40 mm (height) and the hole size 4mm was clearly illustrated in Figure 3.41(a) while the size of the hole defect shown in Figure 3.41(b) was 4 mm and 6 mm in diameter.
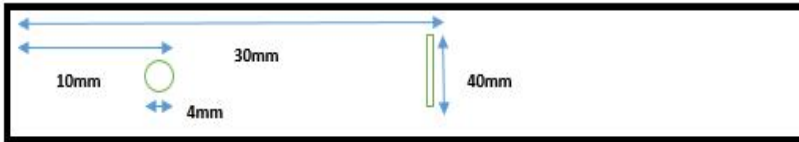
(a)
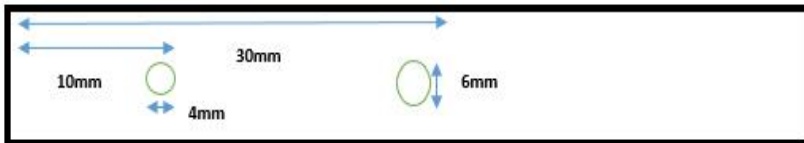
(b)

Figure 3.41   Geometrical dimension of (a) Axial defect on carbon
steel pipe (b) Hole defect on carbon steel pipe

Figure 3.42 shows the artificial cracks with the size of 40mm for the
axial defect and the width defect of 2mm. Figure 3.42(b) represents the
crack for the hole and angle defect. As could be clearly seen, the hole
defect diameter was 4mm while the angle defect of 45 degrees within

the high was 50mm and 2 mm width. The influence of time response and defect amplitude on defect measurement in Piezoelectric was tested using the proposed PZ-LW probe.

.

(a)
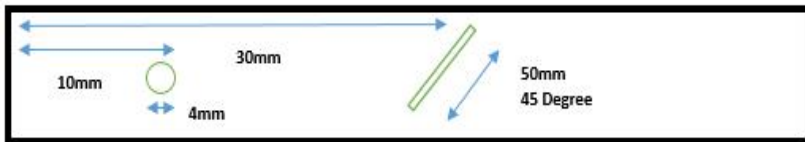
(b)

Figure 3.42   Carbon steel calibration pipe (a) The axial defect with a 2 mm width (b) The hole defect 4mm and axial defect with gradient with 6mm.

3.8   Summary

In this chapter, the research methodology was described, discussed and explained in term of main phases of experimentation. Besides, the numerical work was also being elaborated in detail. The whole process and system also provided a block diagram of the system. In addition, it informed the detail of experimental setup including overall pipeline inspection system. In this chapter, it also explained the method of experimental setting and configuration of tools. Moreover, this chapter also discussed the method of signal excitation, collecting data from reflected signal, data analysis and features extraction. Furthermore, the numerical simulation was also elaborated including finite element method and classification using Fuzzy Logic. Finally, the detailed explanation about Fuzzy Logic and rule for classifications in implementing the system was also included in this chapter.

CHAPTER 4

RESULT AND DISCUSSION

4.1   Introduction

Actual experimental and simulation results of the proposed technique are presented and compared in this section. The objective of the current research is to conduct numerical simulation and experimental study with the aim to find an effective way for detection as well as the localization of cracks (axial defect) and holes defects in the surface of the pipeline. More importantly, this takes into account on the damage from multiple cracks which may exist in the pipeline.

4.2   Simulation Result

Simulations were performed according to different transmission rates of ultrasonic waves in steel considering the fact that it was medium carbon steel as well as the presence of the inclusions. Moreover, it should be noted that pulse echo ultrasonic examination of the materials were in highly solid state such as carbon steel. Hence, complex wave propagation studies consisted of reflection, transmission, distribution, and conversion mode were deemed necessary because it could cover information related to the structural properties of the material. For the purpose of the present study, the simulation software SimNDT (Molero-armenta, Iturrarán-viveros, Aparicio, & Hernández, 2014), was adopted

in order to produce numerical simulations of two-dimensional (2D). Next, the scenario and the same material were used in the experiment. Table 4.1 shows the properties of the materials used for the numerical simulation software.

Table 4.1   Properties of materials used in the numerical simulation

Material	Density (kg/m^3)	Longitudinal Velocity (m/s)	Transversal Velocity (m/s)
Steel	7800	5850.00	3220.00
Air	1.24	344.00	0.00

The main idea of the setup was used because it only involved the Piezoelectric Transducer as a source (10 mm width) in the pulse echo technique with the aim of simulating the propagation of a plane wave. As shown at the bottom of Figure 4.1, the receiver acquired transmission simulation. In this case, the simulation of reflection was obtained by treating the source transducer as a receiver, particularly regarding changes in the thickness defect of the sample as well as the excitation frequency in the same simulation where the signal transmission was obtained. Note that this setting was based on actual laboratory experiments. Specifically, this type of excitation signal frequency was set at 1MHz, 1.5MHz and 2MHz and a thickness defect of 3mm, 1mm and 0.1mm, respectively. The size of pipe especially diameter length and thickness used for simulation and experiment was 60mm diameter, 1000mm length and 5mm thickness. However, the diameter of pipe was extended until 114 mm as the limitation with fix the length and thickness. This is because, the maximum standard size of pipe used in industrial is

114 mm. It also effected the developed capability of PZ-LW system because of I/O at DAQ was limited.

Regarding this matter, a sample with a size of 30000 mm2 and the plate size of 300mm x 100mm was utilised in order to display the reflection and transmission results. As could be seen in Figure 4.1, the size of the simulation area that was exposed to the surrounding area was 10000 mm2. According to the simulation below, the reflecting signal was higher or no reflection signal compared to the transmission signal when no defect was identified on the plate. In the case of the present study, it was observed that the harmonic reflection wave was T= 27 us until T= 35 us, while the receiving waveform managed to be recorded and presented in the graph in Figure 4.1. The amplitude showed at the simulation was in acoustic impedance (Pa.s.m^{-3}).
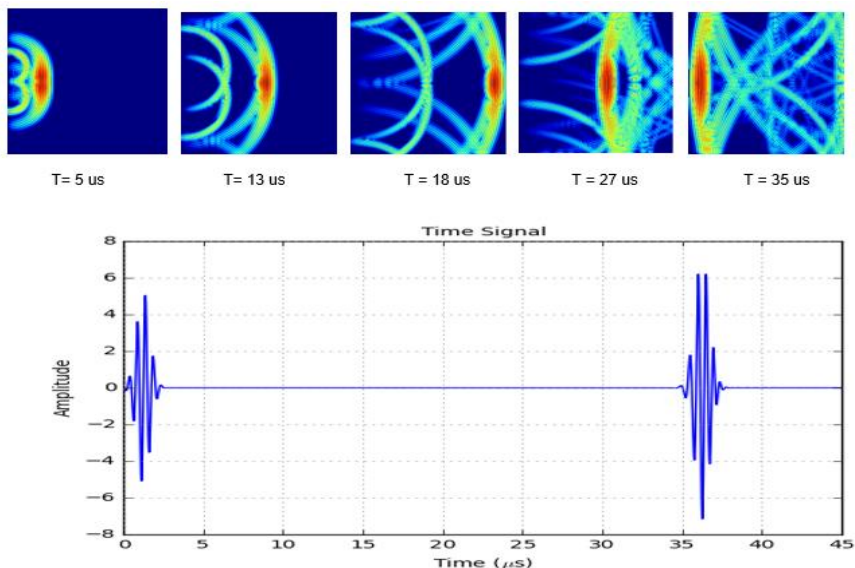
Figure 4.1   Normal condition plate without defect

4.2.1 Frequency 1MHz

The width of the defect tended to affect the aptitude of the signal. Figure 4.2 shows that the size of defect is 3mm x 5mm while the frequency setting on Gaussian Sine Pulse excitation signal is 1Mhz. According to the graph signal, it could be clearly observed that the first signal came from transmitter signal (actuator) whereas the second signal was the reflection from the defect. Moreover, in this case, the positioning of defect was 30mm from the Piezo Sensor. By using 1Mhz frequency for Piezo Actuator, the reflection signal amplitude, and shape of signal showed the difference. In this condition, the interpretation for actual reflection signal was difficult to identify because of the different harmonica shape signal. It was also hard to know the width of defect because it did not have the higher amplitude that was showed in the feedback signal. The width of defect came from the high of feedback amplitude signal. The consistencies of feedback signal could also be identified in Figure 4.2 on T=12us where the feedback signal wave was not very clear and it also distracted by signal interference that made it difficult to identify the high amplitude signal. From here, the higher excitation signal was 1.5e+08 at 2.667us and according to third amplitude on reflection signal (based on third amplitude as the high amplitude of excitation signal), it was 1.333e+07 at 13.68us. From here, the positioning of crack was identified based on equation *v=2s/t* by referring to basic velocity formula. The distance was *2s* because the signal started to travel on transmit (excitation) and would be reflected when the crack occurred in the pipe while the velocity material was based on longitudinal velocity. From here, the positioning of crack was 32.2mm and according to the distance crack setting that was 30mm

based on simulation. From here, the percentage of error was 7.33% from the actual crack setting.
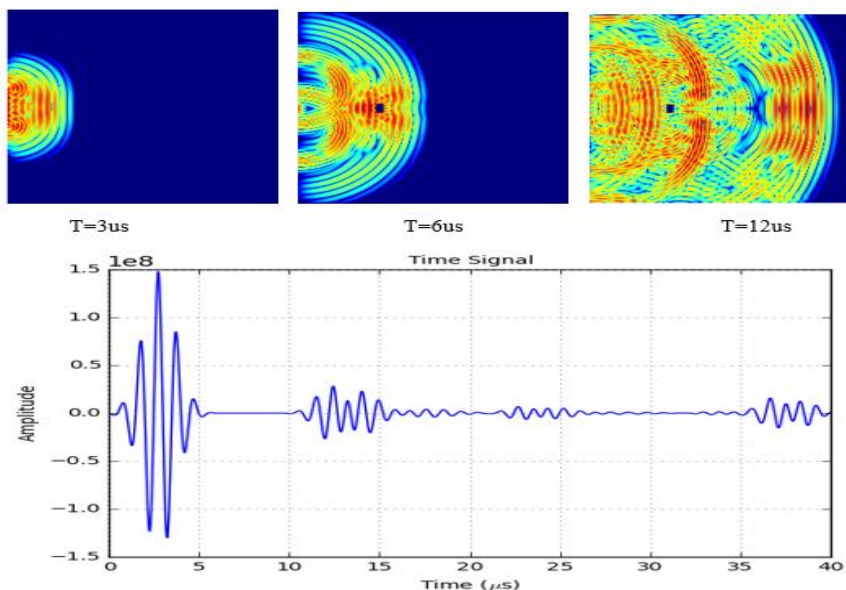
Figure 4.2   Crack position on 30mm from actuator with size 3mm x 5mm and frequency 1Mhz

In Figure 4.3, it was clearly showed that the size of the defect was 1mm x 5mm. Meanwhile, the frequency and positioning defect were the same which were 1Mhz and 30mm respectively. In addition, it could be observed that the amplitude of signal defect increased slightly compared to the signal in Figure 4.2. The reflection signal could be clearly seen at the second signal shown in the Figure 4.3 between t = 10us until 17us. According to Figure 4.3, the shape of feedback signal was also difficult to identify because harmonica shape of signal was different between excitation signal and feedback signal. However, the size of crack was different but it was also difficult to calculate the width of defect because

the amplitude shown was almost the same level within as it did not have the high amplitude that represented the width of crack. Other than that, the feedback signal was bluer that was illustrated in Figure 4.3 at T=12us. In each feedback wave, the signal did not clearly separate at T=. It also caused the signal interference that was obtained from intersection of excitation signal from actuator.
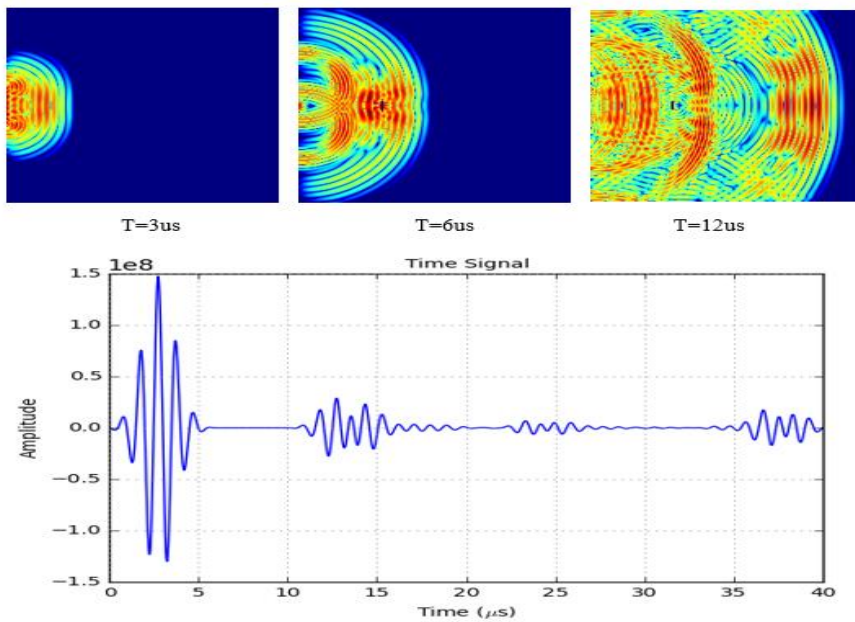
Figure 4.3   Crack position on 30mm from actuator with size 1mm x 5mm and frequency 1Mhz

Figure 4.4 illustrates the signal graph with the defect size of 0.1mm x 5mm. In this case, the amplitude of the reflection signal was high compared to the signals shown in Figure 4.2 and Figure 4.3. According to this figure, the blue colour represented the plate, followed by the stronger signal wave which started with red, orange, yellow, blue, and green colour as the weak signal. Based on Figure 4.4, it showed the

feedback signal at time range 11us until 16us. Theatrically, when the width of defect was low, the amplitude feedback signal would be high. In this case, the second amplitude and forth amplitude had similar level and it was different by comparing the excitation signal where the second and forth was on the same level but it did not represent the width of defect. The third amplitude of signal was mostly the reflection on width of defect. From here, the width of defect was not clearly shown in the third amplitude signal by using 1MHz.

| T=3us | T=6us | T=12us |
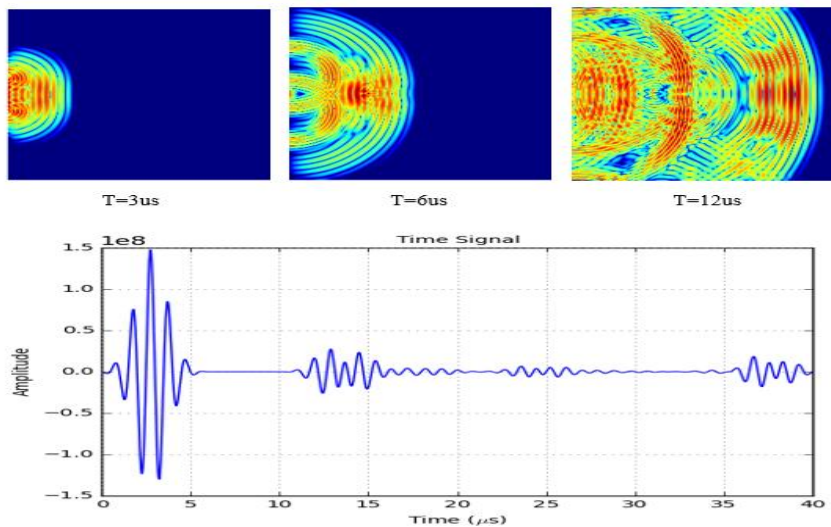
Figure 4.4   Crack position on 30mm from actuator with size 0.1mm x 5mm and frequency 1Mhz

To summarise, the 1MHz was not suitable to be used as excitation frequency because of the difficulty in identifying the width of defect based on third amplitude signal where it represented the width defect. It also showed the different shape of harmonica waveform between excitation signal and reflection signal. However, the excitation signal

amplitude and feedback signal amplitude provided the different result because of the resistance and velocity material used in inspection. Nevertheless, the shape of amplitude should be sequential and similar between excitation and feedback signal. According to the percentage of error, it showed that crack positioning was 32.2mm based on simulation by comparing the actual crack positioning of 30mm and it was accounted until 7.33% of error.

4.2.2 Frequency 1.5Mhz

The second simulation referred to the defect size of 3mm width, followed by the length of 5mm and the frequency setting of 1.5Mhz. As could be noted, the positioning of the transverse defect was on the contrary to the Piezo Actuator. Figure 4.5 shows the sample of acoustic wave simulation as well as the pulse echo response result based on the times 3us, 6us, and 12us with the positioning defect range of 30mm from actuator. Furthermore, it could be clearly observed in the Figure 4.5 that the reflecting time for defect was identified at T =10us where the amplitude of reflecting signal was 2.5 times lower than the excitation signal. According to Figure 4.5, the signal feedback on T=10us until T=14us showed the clear signal. In this condition, the second amplitude of feedback signal (second signal) represented the width of crack. From here, the amplitude of feedback signal had the same shape of excitation signal although the amplitude feedback signal was lower than excitation signal because of material resistance and material velocity. The positionig of defect was calculated by measuring the time based on higher pick signal from excitation signal until higher pick for feedback signal and was divided by 2. This was due to the positioning of

Piezoelectric receiver was at the same place of Piezo Transmiter (Piezo Actuator). In here, the Piezosensor Receiver was currently waiting for the feedback signal from excitation signal when crack occured in pipe. The higher ampitude and time for excitation signal was 1.45e+08 at 1.89us and for feedback signal was 0.633e+08 and 12.043us. From here, the distance of crack was identified at 29.7mm. According to the defect positioning result, the percentage of error was only 1%.
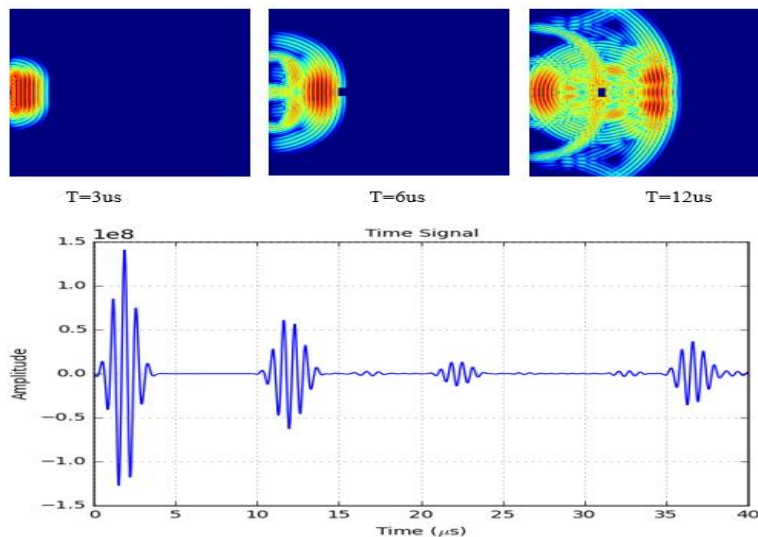
Figure 4.5   Crack position on 30mm from actuator with size 3mm x 5mm and frequency 1.5Mhz

Figure 4.6 shows that the signal from the defect size is 1mm x 5mm. In this case, the signal underwent a slight growth compared to the signal in Figure 4.2. Moreover, it could be observed that the signal graph started at t = 10us until t=14us. More importantly, the harmonic shape of the signal was consistent compared to the graph signal in Figure 4.6 which led to inconsistent frequency used. According to harmonica wave at

T=12us, the feedback signal wave clearly showed and separated in each of waveform. Although the interference signal still occurred in this simulation because of intersection from excitation signal, the reflection signal was still strong and high compared to the interferences signal. It was shown with the red colour of feedback signal at T=12us. The feedback signal was fully received with the right shape and amplitude sequences.
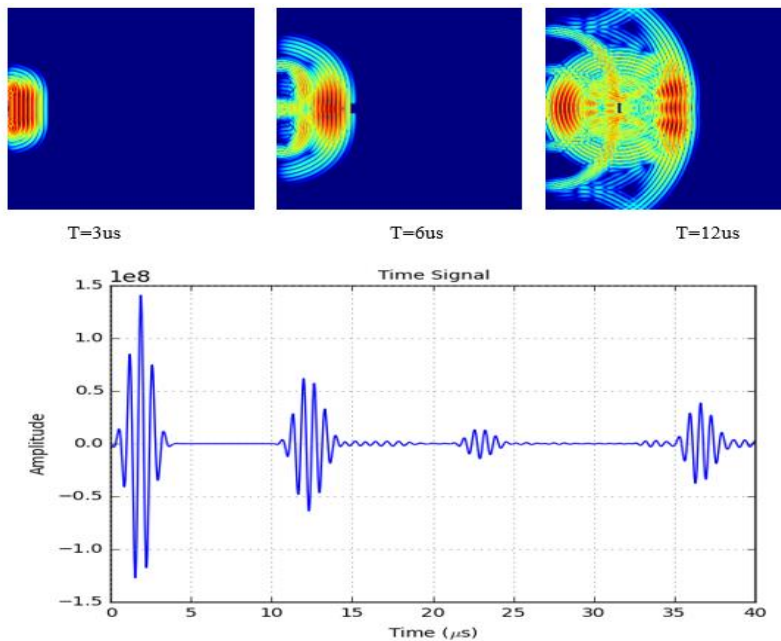
Figure 4.6   Crack position on 30mm from actuator with size 1mm x 5mm and frequency 1.5Mhz

Figure 4.7 shows the signal graph of simulation by the defect size of 0.1mm x 5mm. The gain of reflection signal could be observed to increase to 1.047 as compared to the signal graph in Figure 4.5. Moreover, the reflection signal was identified at t = 10us until t = 14us.

In this condition, the feedback signal was still in the right amplitude sequence within the third amplitude signal was high compared to first and second amplitude signal. It was filled fully with the Gausses Sine Pulse signal pattern and at the same time the pattern of excitation and feedback signal were similar according to the signal shape. By comparing the feedback signal amplitude in Figure 4.5, 4.6 and 4.7, the higher amplitude was identified in Figure 4.7 with the crack size of 0.1mm x 5mm within 9.09%. The signal amplitude was become high because of the gap between excitation signal (vibration) and reflection signal in the crack width was faster than the feedback signal as it was received at Piezoelectric Receiver that was in high amplitude.
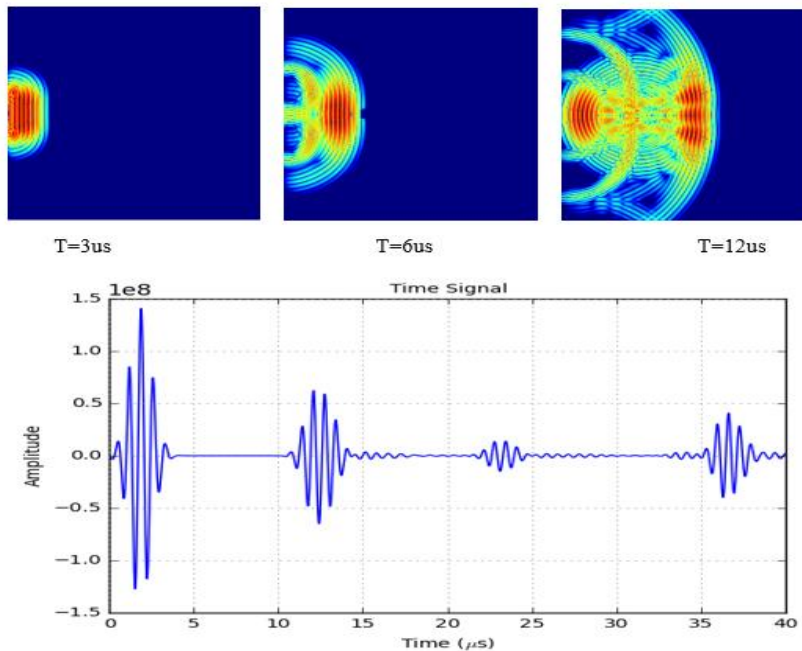
Figure 4.7   Crack position on 30mm from actuator with size 0.1mm
x 5mm and frequency 1.5Mhz

Based on three graphs in Figure 4.5, 4.6, and 4.7, the time response of the defect was mostly the same at t=10us due to the same frequency and fixed defect positioning at 30mm from the PZS. However, the difference could be identified only in the amplitude that led to different width of defect. From here, the 1.5MHz frequency exposed the good response signal with the same pattern of amplitude between excitation signal and feedback signal. It could be viewed according to the shape of signal received. According to calculation and actual setting crack in simulation, it showed the percentage of error only 1% and it was more accurate compared to 1MHz frequency used as excitation signal. Lastly, the feedback signal received showed the clear amplitude. However, the interference occurred in the simulation.

4.2.3 Frequency 2.0MHz

The third frequency used in this simulation was 2Mhz. In this case, the frequency was inversely proportional with the time when the frequency was high compared to the time with low period full-wave signal. Figure 4.8 shows the simulation test based on the defect size of 3mm x 5mm at the 30mm positioning defect from the Piezo Sensor. Moreover, the reflecting signal could be identified at the time of 10us. According to the harmonic wave graph at t =12us, it could be clearly seen that the high wave response was represented in the red colour. The response of the signal took around 3us as shown in the signal graph in Figure 4.8. According to Figure 4.8, the second amplitude of excitation signal was higher compared to the first, third, fourth, and fifth but in reflection signal, it showed higher amplitude at the third wave. It was totally different in both signals based on positioning waveform in high

amplitude. The amplitude showed in the simulation was in acoustic impedance (Pa.s.m^{-3}). From here, the higher amplitude for excitation signal was 0.83e+08 with 0.77us on time axial and for feedback signal, it was 0.47e+08 at 11.48us. The reason was the total time between high amplitude on excitation signal and high amplitude of feedback signal was 10.71us. Therefore, the different of crack distance was 31.3mm compared to the defect setting that was 30mm. Thus, the frequency 2MHz contributed to 3.67% error from actual crack position.
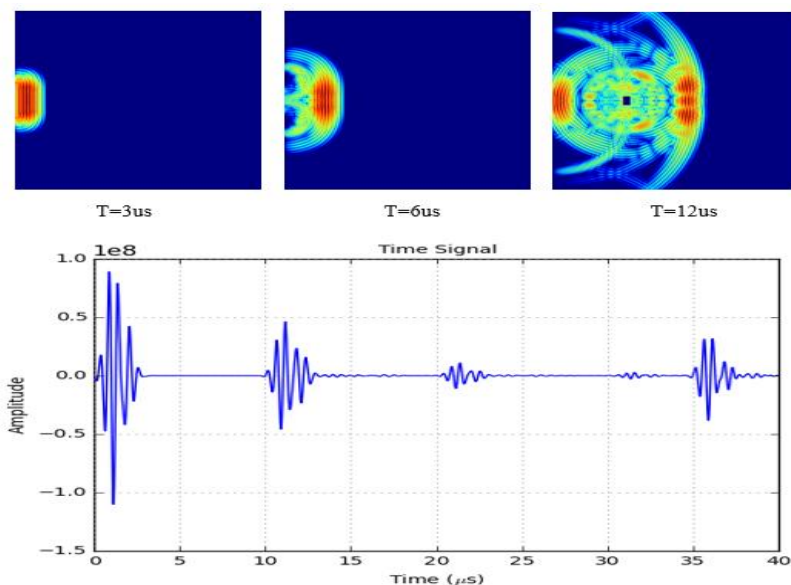
Figure 4.8   Crack position on 30mm from actuator with size 3mm x 5mm and frequency 2.0Mhz

The defect size of 1mm x 5mm was used to identify the difference of signal amplitude shown in Figure 4.9. As could be clearly observed, the defect point could be identified at t =12us in the middle of harmonica

wave with a rectangular shape of crack. Meanwhile, the width of the reflecting signal was high compared to the signal presented in the previous figure (Figure 4.8). Besides, the feedback signal was identified at T=12us with the clear signal. However, the interference did occur because of coating thickness. The feedback signal was strongly received at Piezoelectric Receiver that represented with orange colour at T=12us. The amplitude for reflection signal was increased compared to Figure 4.8 within 0.483e+08. The reason was the width of crack was thick (1mm width) compared to previous (Figure 4.8). From here, the width of crack affected on the amplitude of feedback signal.
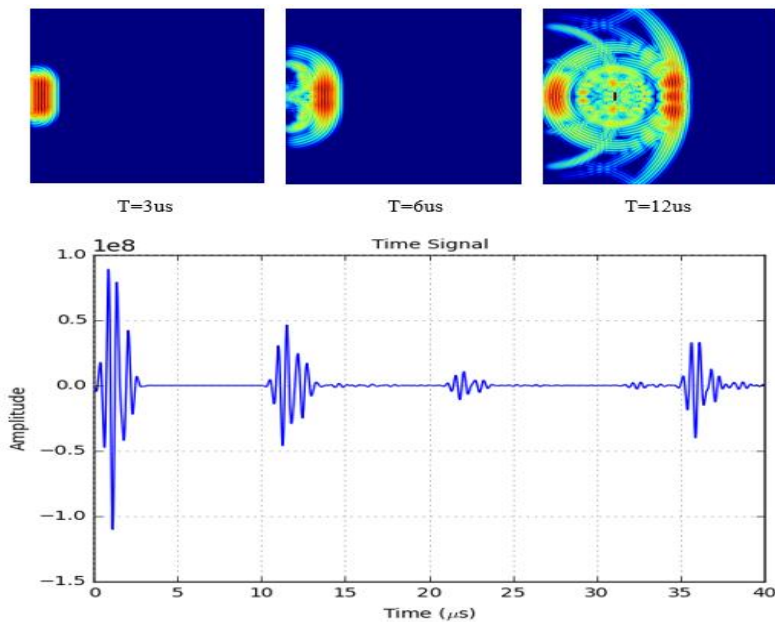
Figure 4.9   Crack position on 30mm from actuator with size 1mm x 5mm and frequency 2.0Mhz

Finally, the simulation was made at the defect size of 0.1mm x 5mm with the same frequency. However, the size of the defect did not clearly

appear in this simulation due to the low thickness shown in Figure 4.10. The defect could be identified through signal graph at the t = 10us. As could be observed in this graph, the time taken for signal to receive was at T=12us. From here, the amplitude for feedback signal was little bit increased to 0.488e+08 because the gap of crack was different between Figure 4.9 and 4.10 in term of the disparity gap that was not so wide. However, the width of defect would change the amplitude of signal either high or low based on the size of width crack.
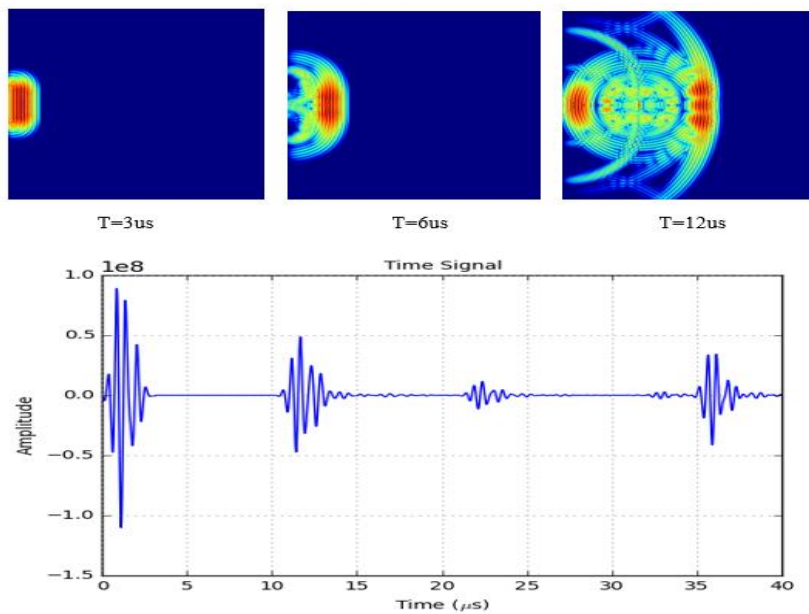
Figure 4.10   Crack position on 30mm from actuator with size 0.1mm
x 5mm and frequency 2.0Mhz

According to the graphs shown in Figure 4.8, 4.9, and 4.10, it could be concluded that the width of the defect was directly affected by the width of signal. Overall, the width of defect was directly proportional to the width of signal based on the signal graph above in Figure 4.10.

From here, the result of simulation (4.2) could be summarised that the best excitation frequency in this simulation was 1.5MHz with 1% error compared to 1MHz with 7.33% error while 2MHz was 3.67%. Besides, the 1.5MHz provided the good result of feedback signal where the sequences of feedback harmonica were same in the excitation signal shape. It was important to identify or interpret the actual signal or noise. Lastly, the clear waveform could be identified although there were interferences caused by the absorbed layer from coating thickness and excitation signal.

4.3 SIMNDT Simulation Based on Sensor Gap

The gap between sensors provided a high impact in the result especially in regard to the shape of the defect. According to the PZ-LW sensor array, a few gaps should be analysed to obtain the optimum gap, followed by higher signal feedback that could be gained from gap optimisation. In the case of the present study, the three distance of defect was tested with six different gaps between the sensor arrays. The distance defects were 30mm, 50mm, and 80mm whereby each distance defect could arrange the sensors starting from 0mm gap until 5mm gap.

4.3.1 SIMNDT 30mm Defect

Table 4.2 presents the positioning defect at 30mm from the Piezo Sensor. The gap between two Piezo Sensors was arranged to start from zero-gap until 5mm gap. The effect of gap could be identified based on the amplitude signal. According to the simulation, the maximum amplitude

was high at 0.63e+08 with zero-gap positioning, thus it was further reduced when the gap was increased until 5mm with the amplitude signal of 0.36e+08. The colouring bar on the defect figure represented the stronger signal where the red colour indicated very high signal, whereas the dark blue implied very lower signal. According to 30mm and 0 gap, (perpendicularly) the defect/crack for feedback signal provided the high amplitude with 100% reflection signal receive. It was different compared to 30mm with 1mm gap where the angle of reflection signal was 1.91°. The amplitude of signal receive was 0.576e+08 and the reducing was around 8.3% from 0 gap. It continued with 30mm and 2mm gap with 0.522e+08 high amplitudes. From here, the angle of reflection signal was 3.81° and deduction of signal amplitude increased to 16.67%. The third test was 30mm and 3mm gap with reflection signal amplitude of 0.468e+08. From here, the angle of reflection signal was 5.71° with 25% signal reducing. In the forth test within 30mm and 4mm gap, the signal amplitude received was 0.414e+08 and with 33.33% signal decrease and the angle of signal feedback was 7.59°. Lastly, the 30mm and 5mm sensor gap was tested with the amplitude result was 0.36e+08 with 41.67% signal amplitude reducing and with angle 9.46°. From here, the different amplitude in each 1mm gap changes was 0.054e+08 and the sensor gap contributed to the high effect on the accuracy signal measuring especially in sensor array for PZ-LW system.

Table 4.2   Crack Positioning 30mm with Different Gap

Positioning	Gap	Defect	Harmonic Wave
30mm	0mm		
30mm	1mm		
30mm	2mm		
30mm	3mm		
30mm	4mm		
30mm	5mm		
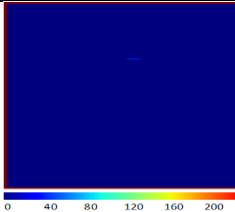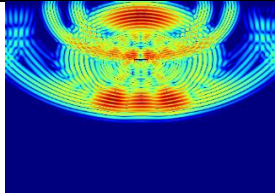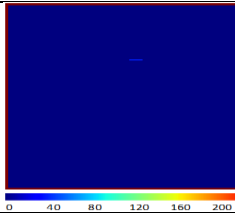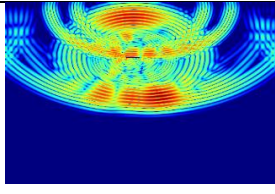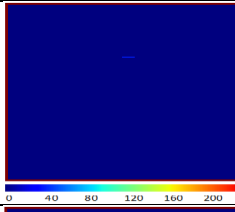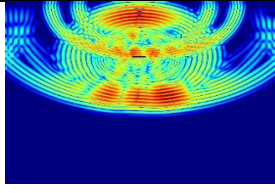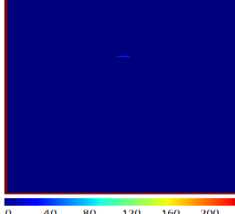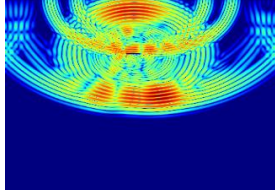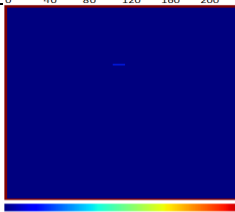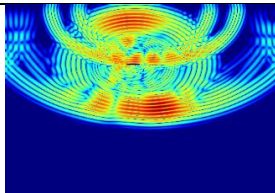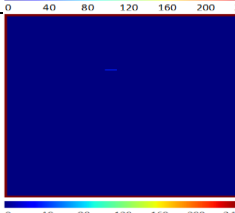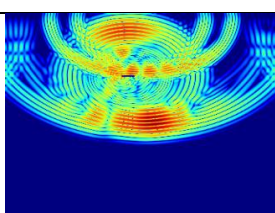
4.3.2 SIMNDT 50mm Defect

The amplitude of signal decreased when the gap of two Piezo Sensors or the positioning of defect increased. From here, the gap was inversely proportional with signal amplitude. Based on Table 4.3, it showed the effect of defect positioning was increased. From here, the higher amplitude on 0 gap was 0.41e+08 and the lower 0.32e+08 on 5mm gap. Based on 50mm and 0 gap, (90°) the defect/crack for feedback signal provided the high amplitude with 100% reflection signal receive. It was different compared to 50mm with 1mm gap where the angle of reflection signal was 1.15°. Besides, the amplitude of signal receive was 0.392e+08 and the reducing was around 4.34% from 0 gap. It continued with 50mm and 2mm gap with giving the 0.374e+08 high amplitudes. From here, the angle of reflection signal was 2.29° and deduction of signal amplitude increased to 8.70%. The third test on 50mm and 3mm gap with reflection signal amplitude was 0.356e+08 and from here, the angle of reflection signal was 3.43° with 13.04% signal reducing. In the forth test within 50mm and 4mm gap, the signal amplitude received was 0.338e+08 and with 17.40% of signal decreased while the angle of signal feedback was 4.57°. Lastly, the 50mm and 5mm sensor gap was tested with the amplitude result of 0.32e+08 with 21.74% signal amplitude reduced and with angle of 5.71°. According to sensor gap changes, the value of amplitude signal decreased as much as 0.018e+08 with 4.35% reduction from zero gap sensor.

Table 4.3   Crack Positioning 50mm with Different Gap
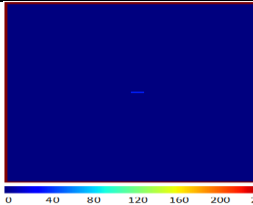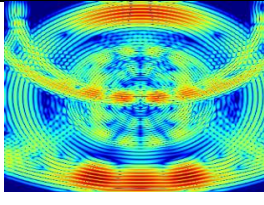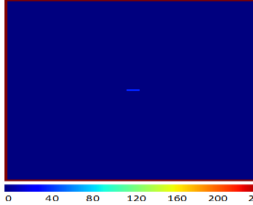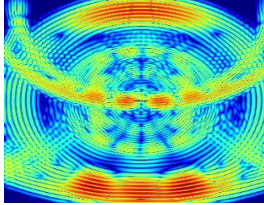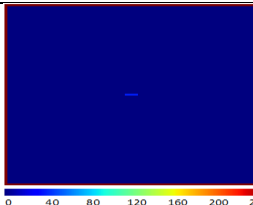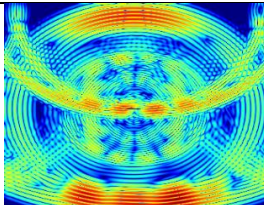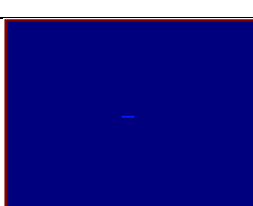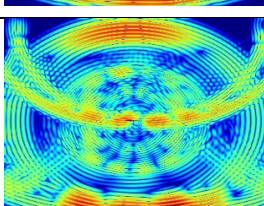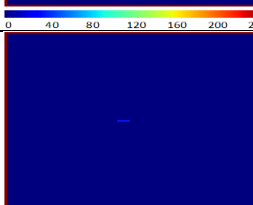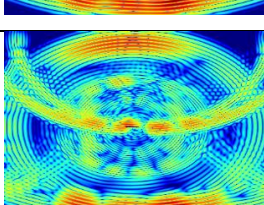
Positioning	Gap	Defect	Harmonic Wave
50mm	0mm		
50mm	1mm		
50mm	2mm		
50mm	3mm		
50mm	4mm		
50mm	5mm		
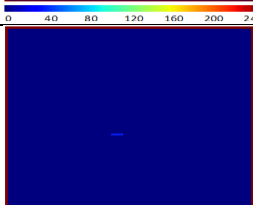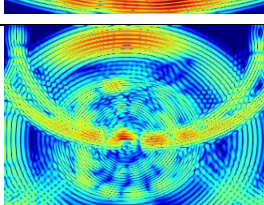
4.3.3 SIMNDT 80mm Defect

The last gap test was for positioning 80mm. From here, when the positioning of defect increased, then the time response also increased too. It showed that the positioning was directly proportional with the time response. In this simulation depicted in Table 4.4, the effect of gap and positioning defect was at 80mm. The amplitude of defect was two times decreased compared to the defect positioning of 30mm in Table 4.2. According to the Table 4.4, the higher amplitude signal on 0 gap was 0.27e+0 and the lower was 0.23e+08. According to 80mm and 0 gap, (perpendicularly) the defect/crack for feedback signal provided the high amplitude with 100% reflection signal received. It was different compared to 80mm with 1mm gap where the angle of reflection signal was 0.72°. The amplitude of signal received was 0.262e+08 and the reducing was around 2.94% from 0 gap. It continued with 80mm and 2mm gap with giving the 0.254e+08 high amplitudes. From here, the angle of reflection signal was 1.42° and deduction of signal amplitude increased to 5.88%. The third test on 80mm and 3mm gap with reflection signal amplitude was 0.246e+08 and from here, the angle of reflection signal was 2.15° with 8.82% signal reducing. In the forth test within 80mm and 4mm gap, the signal amplitude received was 0.238e+08 and with 11.76% of signal decreased and the angle of signal feedback was 2.86°. Lastly, the 80mm and 5mm sensor gap was tested with the amplitude result of 0.23e+08 with 14.71% signal amplitude reducing and with angle of 3.58°. According to the Table 4.4, the rate of changes (reduction) for signal amplitude in each 1mm gap increased was 0.008e+08 where contributed to 2.94% of signal deduction.

From here, it could be summarised that the effect of sensor gap increased contributed to decreasing feedback of signal amplitude. Besides, the angle and amplitude reflection signal decreased when the positioning of crack increased. Therefore, the function of sensor array was very important in this research to ensure the value of reflection signal received was correct with lower percentage of error.

Table 4.4   Crack Positioning 80mm with Different Gap
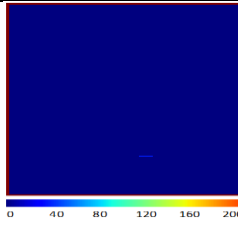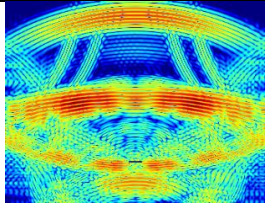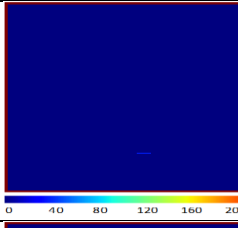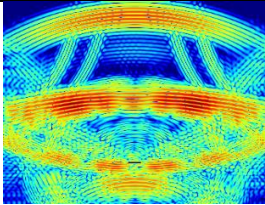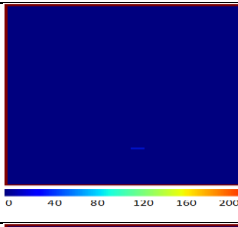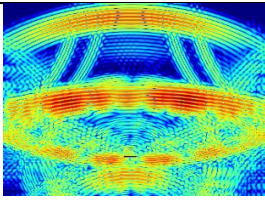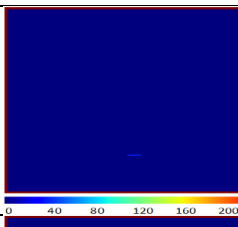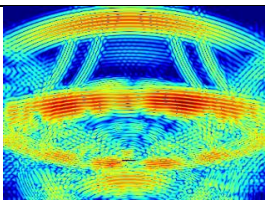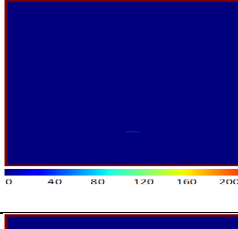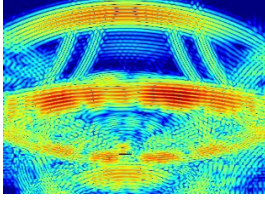
Positioning	Gap	Defect	Harmonic Wave
50mm	0mm		
50mm	1mm		
50mm	2mm		
50mm	3mm		
50mm	4mm		
50mm	5mm		
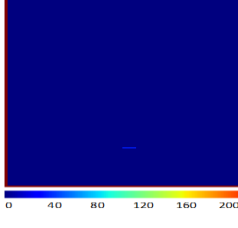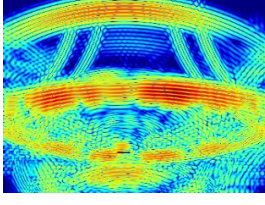
4.4 The Design of PZ-LW Probe based on RSM Optimization

The main objective of the PZ-LW probe was to optimise the steel pipeline inspection system. More importantly, this could be achieved using the Response Surface Methodology (RSM) which included Piezoelectric Sensor, signal generator, measurement instrumentation, and multiple samples of the artificial crack pipeline of a 60 mm carbon steel pipe (S55C) through the optimisation of independent parameters of the PZ-LW probe design parameters. In the case of 3-dimensional modelling of the PZ-LW probe, ProEngineering software was utilised to model the probe design that was constructed based on the optimised parameters attained from the Design Of Experiment (DOE) for Response Surface Method (RSM) as well as SIMNDT software for optimisation purposes based on the frequency and gap between two Piezoelectrics. Finally, the optimal design of the PZ-LW probe could be experimentally verified in order to confirm the accuracy of the inspection.

As part of the rule, RSM was employed to solve problems regarding a few parameters with restricted ranges which were similar to the ones investigated in the PZ-LW probe design. The system response over the entire area of interest could be solved by RSM because it is able to provide more accurate solutions compared to others (Z. Su et al., 2006). Moreover, in the current research, RSM was adopted to optimise two of the parameters that influenced the PZ-LW probe design, particularly in creating a highly efficient PZ-LW probe to inspect the defects in the surface diameter of 60 mm carbon steel pipe. Specifically, RSM comprised of three stages described as follows: (1) a succession of experiments such as the Designs Of Experiments (DOE) with the aim of

ensuring that the results were sufficient with dependable measurements of the response, (2) a mathematical model which characterised the closest match to the accumulated data that was determined from the execution of DOE, and (3) the values of the experimental parameters which were established for the purpose of producing the optimal detection of a defect in the inner carbon steel pipe.

In the case of PZ-LW probe design, the sensitivity, and efficiency of defect detection were essentially determined based on a number of factors which included the height of frequency (higher signal travelling), the number of Piezo Sensors in the array sensor and the gap between two Piezo Sensors of the probe design which tended to affect the time response for defect location. More importantly, the design parameter has an influence on the level of accuracy of the detection of a defect during the inspection of a pipe (Zagrai et al., 2010).

The effectiveness of the PZ-LW probe was primarily conditioned by its operation mode as well as the basic design. The excitation frequency, the width of the defect, sensor gap and defect distance were adopted in the present study in order to further investigate the influence of the probe design parameter on the accuracy of the probe defect detection. Meanwhile, the responses referred to the axial defects and hole defects that were detected in the 60 mm carbon steel inspection pipe. However, one of them had multiple axial defects while the second sample had two holes with different diameter defects of 100% depth out of the nine samples of carbon steel pipe. Overall, the defects in the nine samples were randomly located on the surface circumferential direction of the pipe.

The numbers of the width of the defect, excitation frequency and defect distance were changed based on the Central Composite Design (CCD). The responses in the present study referred to the number of axial defects and hole defects that were detected in the 60 mm carbon steel inspection pipes. The tabulation of the arrangement of the central composite design was clearly shown in Figure 4.11. As could be observed, six replicas at the centre of CCD were employed to determine pure error sum of squares. Furthermore, all of the experiments were performed in randomised order to minimise the influence of the extraneous parameters.

C:\Program Files (x86)\DX7Trial\relation frequency width defect and distance with time responce amplitude and width signal.dx7 - Design-Expert 7.0.0

File   Edit   View   Display Options   Design Tools   Help

Std	Run	Block	Factor 1 A:Excitation Fr Mhz	Factor 2 B:Width of Def mm	Factor 3 C:Diffect Dista mm	Response 1 Time Response us	Response 2 Amplitude x1e8	Response 3 Width of Signal us
16	2	Block 1	1.00	1.00	10.00	0.45	0.21	4.58
15	3	Block 1	1.00	3.00	10.00	0.45	0.33	4.06
1	4	Block 1	1.00	0.10	50.00	12.27	0.25	4.17
14	5	Block 1	1.00	1.00	50.00	11.67	0.29	4.58
7	6	Block 1	1.00	3.00	50.00	11.36	0.29	4.54
6	7	Block 1	1.00	0.10	90.00	25.91	0.21	4.58
10	8	Block 1	1.00	1.00	90.00	25.91	0.29	4.58
11	9	Block 1	1.00	3.00	90.00	25.45	0.21	4.17
19	10	Block 1	1.50	0.10	10.00	0.45	0.46	3.75
3	11	Block 1	1.50	1.00	10.00	0.45	0.42	3.33
4	12	Block 1	1.50	3.00	10.00	0.45	0.42	3.64
9	13	Block 1	1.50	0.10	50.00	13.75	0.63	3.75
13	14	Block 1	1.50	1.00	50.00	13.64	0.63	4.17
18	15	Block 1	1.50	3.00	50.00	13.13	0.65	3.44
17	16	Block 1	1.50	0.10	90.00	27.5	0.46	3.33
5	17	Block 1	1.50	1.00	90.00	27.22	0.42	3.33
27	18	Block 1	1.50	3.00	90.00	27.27	0.46	4.55
12	19	Block 1	2.00	0.10	10.00	0.9	0.36	3.18
20	20	Block 1	2.00	1.00	10.00	0.9	0.3	3.2
21	21	Block 1	2.00	3.00	10.00	0.45	0.32	2.665
22	22	Block 1	2.00	0.10	50.00	14.09	0.64	3.64
23	23	Block 1	2.00	1.00	50.00	12.27	0.61	3.2
24	24	Block 1	2.00	3.00	50.00	14.17	0.64	2.5
25	25	Block 1	2.00	0.10	90.00	28.64	0.5	3.64
26	26	Block 1	2.00	1.00	90.00	28.18	0.46	3.18
8	27	Block 1	2.00	3.00	90.00	27.73	0.5	2.5

Notes for relation frequenc
Design (Actual)
Summary
Graph Columns
Evaluation
Analysis
Time Response (An
Amplitude (Analyze
Width of Signal (Ana
Optimization
Numerical
Graphical
Point Prediction

For Help, press F1

Figure 4.11   Design Parameter Considering in Frequency Optimization

The arrangement of the central composite design, responses and values obtained from the experimental results of different PZ-LW probe design parameters were tabulated by the Piezoelectric System as shown in

Section 3.5. A total number of twenty-seven inspections were conducted. Then, the responses are listed in Table 4.5. As a result, Table 4.5 showed that the excitation frequency contributed to the effect on the amplitude of receiving signal for Piezo Sensor where the excitation frequency 1Mhz provided low amplitude receiving signal compared to 1.5Mhz and 2Mhz. In the increasing of receiving amplitude signal, it could be reached up to 80% based on the increasing of excitation frequency. In this case, the amplitude signal was maintained for 1.5Mhz and 2Mhz. Regarding this matter, the attenuation was high when the defect location/position increased. It showed that the pattern of attenuation growth was up until 12.12% in each of 40mm increasing of defect location. Meanwhile, the width of signal was closely related to width of defect. From here, the width of signal was inversely proportional with width of defect.

Table 4.5   Parameter Considering in Frequency Optimization

Excitation Frequency(MHz)	Width of Defect(mm)	Defect Distance(mm)	Time Response(us)	Amplitude(1e8)	Width of Signal(us)
1	0.1	10	0.45	0.25	5
1	1	10	0.45	0.21	4.58
1	3	10	0.45	0.33	4.06
1	0.1	50	12.27	0.25	4.17
1	1	50	11.67	0.29	4.58
1	3	50	11.36	0.29	4.54
1	0.1	90	25.91	0.21	4.58
1	1	90	25.91	0.29	4.58
1	3	90	25.45	0.21	4.17
1.5	0.1	10	0.45	0.46	3.75
1.5	1	10	0.45	0.42	3.33
1.5	3	10	0.45	0.42	3.64
1.5	0.1	50	13.75	0.63	3.75
1.5	1	50	13.64	0.63	4.17
1.5	3	50	13.13	0.65	3.44
1.5	0.1	90	27.5	0.46	3.33
1.5	1	90	27.22	0.42	3.33
1.5	3	90	27.27	0.46	4.55
2	0.1	10	0.9	0.36	3.18
2	1	10	0.9	0.3	3.2
2	3	10	0.45	0.32	2.665
2	0.1	50	14.09	0.64	3.64
2	1	50	12.27	0.61	3.2
2	3	50	14.17	0.64	2.5
2	0.1	90	28.64	0.5	3.64
2	1	90	28.18	0.46	3.18
2	3	90	27.73	0.5	2.5

The gap between a pair of PZS was another factor that affected the accuracy reflection signal. Figure 4.12 presents the tabulation of the

arrangement of the central composite design. In this case, the two factors which were sensor gap and the distance of defect affected the amplitude of defect in measurement. Table 4.9 shows the eighteen testing's conducted with different gap of sensor that started from zero-gap until 5mm gap. The result showed that the gap of sensor was inversely proportional to the amplitude of defect.

Figure 4.12   Design Parameter Considering in Sensor Gap Optimization

Table 4.6 shows the defect detection of the axial and hole defects are 100 % at a run inspection of 18 with the axial types of defect selected in this test. In the case of the present study, the test ran according to different defect positions of 30mm, 50mm, and 80mm with the defect size of 2mm x5mm. ANOVA analysis was executed to validate the accuracy of empirical models in predicting the defect. In particular, the value of

Probe-F must be less than 0.05 for a significant model term. Accordingly, the purpose was to ensure that the empirical model reflected the system and fitted for the purpose of predicting the response. On the other hand, the model term was deemed insignificant in the case of the Probe-F greater than 0.05. Furthermore, regression analysis and normality were carried out to verify the model accuracy in predicting the defect in the inspection pipe according to different PZ-LW probe parameter designs. The significance of the model was ascertained through a mathematical model equation derivation that demonstrated the relationship between the defect detection rate in the inspected pipe as well as the PZ-LW probe design variables after successfully carrying out the tests. The mathematical model equations obtained from the ANOVA analyses of the axial and hole detection defects response were used to optimise the proposed probe parameters design in accordance to the desirability.

Table 4.6   Parameter Considering in Sensor Gap Optimization

30mm (Gap)	Amplitude e+08
0	0.63
1	0.59
2	0.55
3	0.50
4	0.41
5	0.36
50mm (Gap)	**Amplitude e+08**
0	0.41
1	0.41
2	0.39
3	0.36
4	0.34
5	0.32
80mm (Gap)	**Amplitude e+08**
0	0.27
1	0.27
2	0.25
3	0.25
4	0.25
5	0.23

4.4.1 Analysis of Amplitude of Signal and Mathematical Modelling

The Analysis of Variance (ANOVA) was employed in the current research for the purpose of investigating the effect of independent parameters in the responses. The experimental results reflected that the number of axial and hole defect detection varied in the range of 1 to 8 as shown in Table 4.7. Meanwhile, the Analysis of Variance (ANOVA) of axial defect presented in Table 4.7 shows that all of the independent variables, the number of excitation frequency, and the defect distance were significant ($p < 0.05$). Additionally, the interaction impact of the excitation frequency and defect distance were found to be insignificant because the p-value was equal to <0.0001 and <0.0408. Hence, this led to the removal of any insignificant term, followed by the repetition of the optimisation process until all of the terms became significant. The p-value served as a tool to inspect the significance of each coefficient. In this case, the values of ''Prob > F'' were less than 0.05 which indicated that the model terms were significant. Meanwhile, A, C, AC, A2, and C2 were significant factors included in the mathematical model.

Table 4.7   Signal Amplitude Defect Detection Response in Surface

Quadratic Model

Analysis of variance table [Partial sum of squares - Type III]

Source	Sum of Squares	df	Mean Square	F Value	p-value Prob > F	
Model	0.5023703 7	5	0.1004740 74	31.443205 65	< 0.0001	significant
A-Excitation Frequency	0.2222222 22	1	0.2222222 22	69.544099 79	< 0.0001	
C-Diffect Distance	0.0107555 56	1	0.0107555 56	3.3659344 3	<0.0408	
AC	0.0261333 33	1	0.0261333 33	8.1783861 35	<0.0094	
A^2	0.1102518 52	1	0.1102518 52	34.503146 04	< 0.0001	
C^2	0.1330074 07	1	0.1330074 07	41.624461 86	< 0.0001	
Residual	0.0671037 04	21	0.0031954 14			
Cor Total	0.5694740 74	26				

The significance of each variable was evaluated ($p < 0.05$) using the p-value. The estimated yield regression coefficients for axial defect detection for the quadratic equation with ''Pred. R- Squared'' of 0.8039 was found to be in a good relationship with the ''Adj. R-Squared'' of 0.8541 with a difference of <0.05. More importantly, the implementation of RSM produced the following regression equation which described the empirical relationship between the amplitude of defect and the independent parameters as shown in Equations 4.1 and 4.2.

Amplitude =(+0.60)+(0.11 * A)+(0.024 * C)+(0.047 * A * C) –(0.14 * A^2)-(0.15 * C^2)   (4.1)

Amplitude = (-1.03671)+(1.73222 * Excitation Frequency)+(6.41667E-003

* Defect Distance)+(2.33333E-003 * Excitation Frequency * Defect Distance) -(0.54222 * Excitation Frequency^2) –(9.30556E-005 * Defect Distance^2) (4.2)

The mathematical modelling in Equations 4.1 and 4.2 was used to optimise the probe parameters design as well as predict the axial defect detection. In the case of probe design validation, the excremental result under the optimum probe parameter design was compared to the value of the predicted axial defect detection. The residual plots for the number of axial defect detection were deemed essential in evaluating the validity of a model. Figure 4.13 displays the normal probability plot for the residual distributions which acted as additional validation for the response surface methodology model. The results from the figure clearly showed that the normal probability diagram for amplitude defect detection was very close to a straight-line with no evidence of an outlier. Therefore, this indicated that the errors were normally distributed while the full quadratic regression equation exceedingly fitted the observed data.
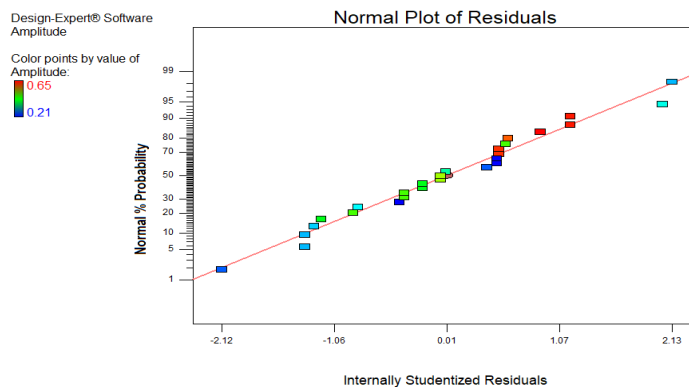
Figure 4.13   Normal probability plot for amplitude defect detection

Figure 4.14 presents the interaction relationship parameter between the defect distance and the excitation frequency in the sensor array to the effect of amplitude defect detection in the inspection pipe. As illustrated in the graph in Figure 4.14, the implementation of a maximum excitation frequency in the array sensor increased the amplitude defect which was detected by the PZ-LW probe. The increasing of amplitude signal remained significant until the number of excitation frequency signal reached 2.00. The amplitude of defect signal decreased for PZ-LW probe with > 5 mm sensor gap, thus making it difficult to identify the condition of defect on pipeline. In this case, it was crucial to note that the quantity of Piezo Sensor was dependent on the size pipe and the size of Piezo Sensor.
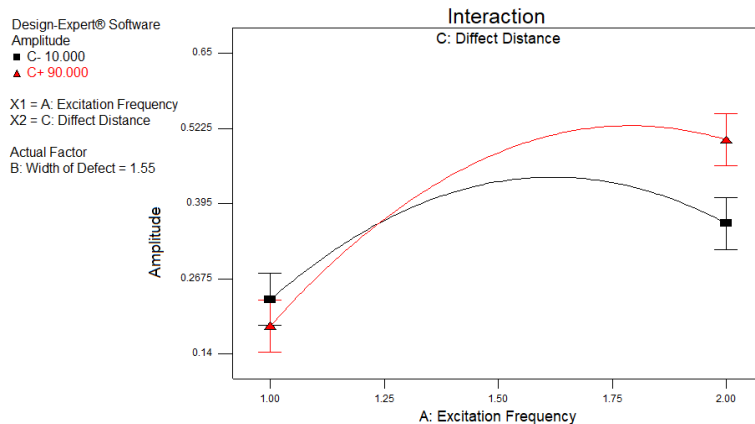
Figure 4.14   Interaction of probe design factors between excitation frequency and the defect distance detection

Figure 4.15 illustrates a 3-D surface which explains the effect of the defect distance and excitation frequency in the array sensor related to the detection effectiveness for the amplitude defect in an inspection of the

carbon steel pipe. The defect distance of 50mm provided a high amplitude of defect with the excitation frequency of 1.5Mhz. Figure 4.15 also demonstrated that low amplitude signal caused by frequency was lower than 1Mhz. Overall, the excitation frequency was directly proportional to the amplitude of signal defect.
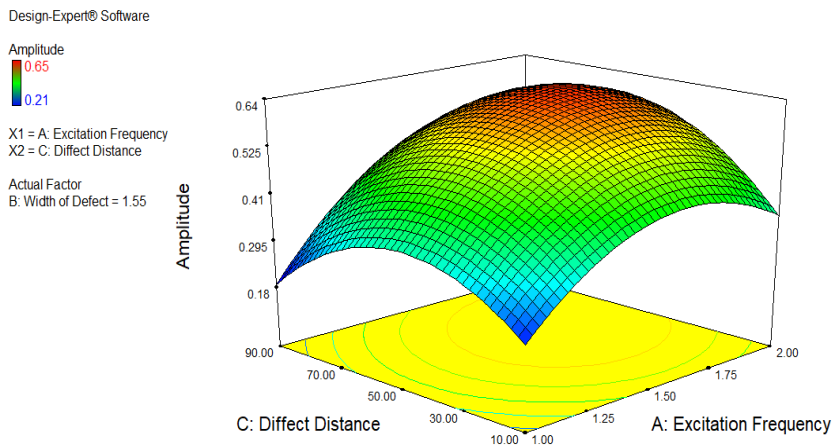
Figure 4.15   The 3-D Surface plot for influence of excitation frequency and defect distance in amplitude defect detection

4.4.2   Analysis of Gap Sensor Signal and Mathematical Modelling

Table 4.8 shows that all of the independent variables, the number of distances, and the sensor gap were significant ($p < 0.05$). The model for F-value was equal to 170.48 which implied the significance of the model. In this case, there was only a 0.01% chance that the "Model F-Value" obtained because of noise. The values of "Prob > F" which were less than 0.0500 produced a significant term of the model. Meanwhile, the values of A, B, AB, and A2 indicated significant model terms, whereas insignificant model terms were indicated if the values were

greater than 0.1000. Therefore, model reduction might be able to improve the model if there were many insignificant model terms (not counting those required to support hierarchy).

Table 4.8   Amplitude Defect Detection Response in Surface Quadratic Model

Analysis of variance table [Partial sum of squares - Type III]

Source	Sum of Squares	df	Mean Square	F Value	p-value Prob > F	
Model	118.442396	4	29.61059899	170.484984	< 0.0001	significant
A-Distance	90.75	1	90.75	522.4991329	< 0.0001	
B-Gap	16.62651793	1	16.62651793	95.72827772	< 0.0001	
AB	8.798132945	1	8.798132945	50.65583289	< 0.0001	
A^2	2.11316886	1	2.11316886	12.16670961	0.0040	
Residual	2.257898484	13	0.173684499			
Cor Total	120.7002944	17				

Based on the ANOVA in Table 4.8, ANOVA analysis showed that R-Squared was 0.9813. Other than that, the Pred. R- Squared" of 0.9600 was in a good relationship with the ''Adj. R-Squared" of 0.9755 with a difference of < 0.01. In this case, it could also be observed that the Std. Dev was 0.42 which indicated that the analysis data was significant. The implementation of RSM led to the following regression equation which was considered as an empirical relationship between the amplitude of defect as well as the independent parameters as described in Equations 4.3 and 4.4 as their actual values. The following equations described the mathematical modelling for probe optimising based on the probe parameters design as well as to predict the amplitude of defect detection.

According to Equation 4.3, the A variable represented Distance and B was sensor gap. This equation was automatically generated from ANOVA statistical analysis based on the raw data included in this software (DOE). Both of 2 Equations (4.3) and (4.4) were different based on the fix value but the answer of amplitude was similar. This was the option used to prove the theatrical value and experimental value based on equation below (Equation 4.3 and 4.4).

$$\text{Amplitude} = (+7.50) - (2.75 * A) - (1.41 * B) + (1.25 * A * B) + (0.76 * A^2) \quad (4.3)$$

$$\text{Amplitude} = (+21.38753) - (0.29395 * \text{Distance}) - (1.66035 * \text{Gap}) + (0.019923 * \text{Distance} * \text{Gap}) + (1.21944E\text{-}003 * \text{Distance}^2) \quad (4.4)$$
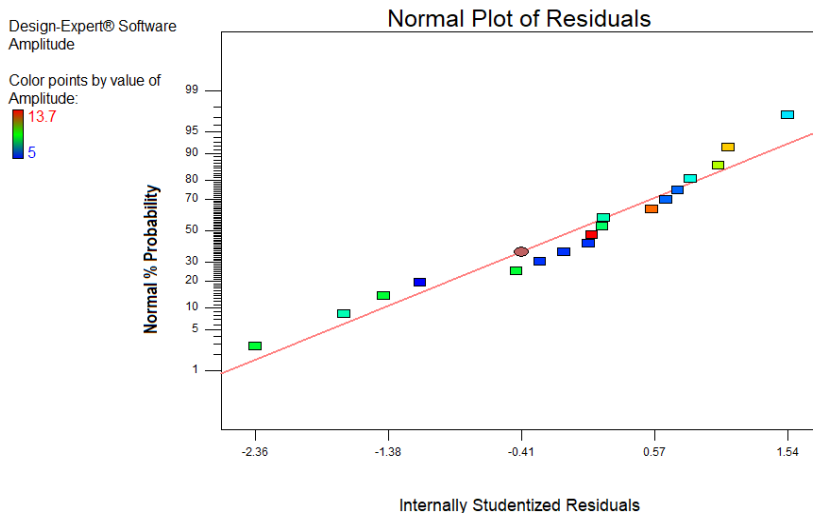
Figure 4.16   Normal Probability Plot for Amplitude Defect Detection

Based on Figure 4.17, it clearly illustrates the interaction graph between the distance and gap of the sensor for amplitude measurement. As could be observed in the graph, the value of sensor gap B decreased when the

distance of defect position increased. Accordingly, this posed an effect that might reduce the amplitude. In addition, it could be clearly seen that the minimum and maximum distance defects were only tested from 30mm until 80mm.
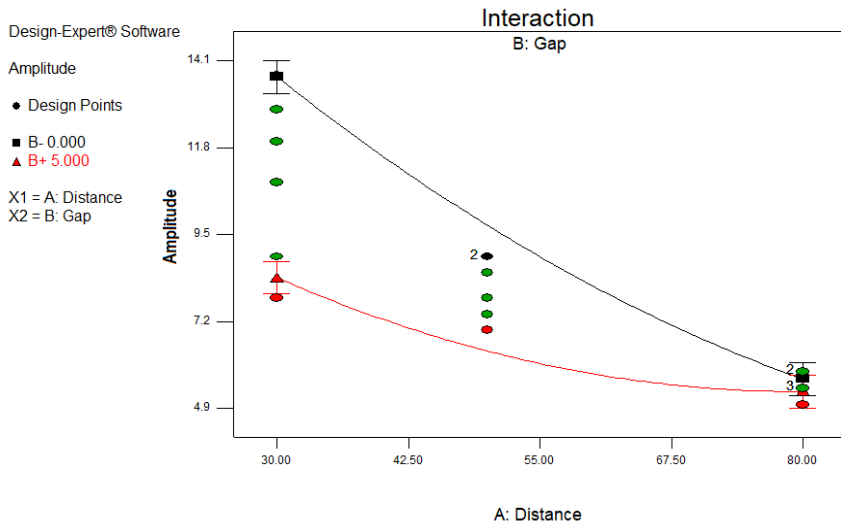
Figure 4.17   Interaction of Probe Design Factors Between Distance and the Sensor Gap

Finally, Figure 4.18 presents the 3-D surface that explains the effects of the defect distance and sensor gap in the array sensor which are related to the detection effectiveness for the amplitude defect in the inspection of the carbon steel pipe. In this case, the sensor gap started from 2.50mm with a defect distance of 42.50mm, which led to high amplitude of defect. Moreover, the amplitude of the signal became low when the sensor gap increased. Therefore, it should be understood that the sensor gap was inversely proportional to the amplitude of signal defect.
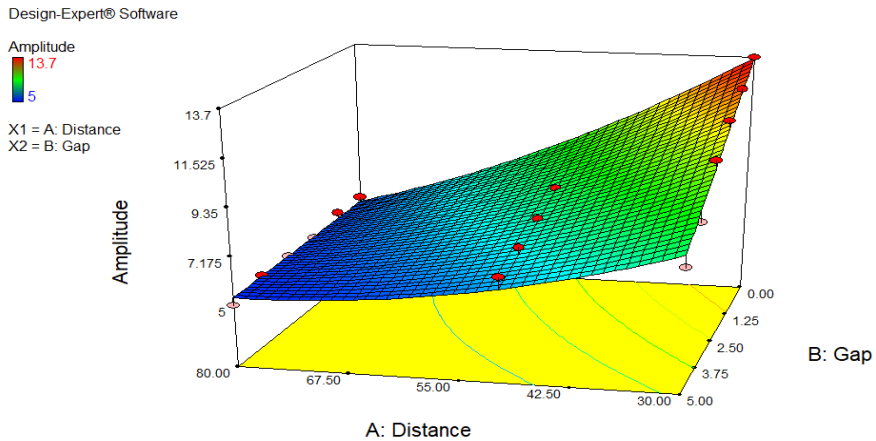
Figure 4.18   The 3-D Surface plot for influence of excitation frequency and defect distance in amplitude defect detection

4.5   Experimental Results

The experiments described in this section were tested based on three types of defect which were hole defect, axial defect, and gradient axial defect. According to the experiment setup, the size of pipes was fixed to 500mm and excitation frequency was set at 1.5Mhz with amplitude +10 to -10 (Vpp). The sizes of defect included were hole defect (4mm diameter), axial defect (2mm x 40mm), and gradient axial defect (2mm x 60mm with angle 45 degree).

4.5.1   The Experimental Result of Hole Defect Detection

The conventional inspection was done by using DAQ (DT9816) Data Translation, Oscilloscope and PC interface using MATLAB. Figure 4.19(a) shows the signal based on DAQ module reading continually.

According to signal received, there were only 3 signals that provided the feedback respond which were A2 (violet), A3 (light blue) and A4 (orange). The measurement of five pare PZ-LW sensors were shown where the one of the signals (Ain3) triggered the high amplitude where the positioning of PZ-LW sensor was against the defect. The size of hole defect was 4mm diameter with 5mm depth of defect. From here, the positioning signal feedback had the same place but different amplitude. From here, the PZ-LW sensor received the signal from the same crack positioning. Based on pattern signal received, it showed that only one point of sensor contributed to high amplitude and it meant the defect was in hole shape. By following the signal feedback colour, the A2 = 0.0110Vp, A3 = 0.0130Vp, and lastly A4=0.0113Vp. The signals amplitude data were taken at t=0.00004314s. From here, the positioning of defect was being calculated at 12.61cm based on dynamical velocity equation *(v=s/t)*. The amplitude of crack could clearly be obtained in Figure 4.19(b) on oscilloscope. From here, the orange colour represented the signal from signal generator and the blue was signal from PZ-LW sensor feedback. The maximum feedback amplitude was 20mVrms and it was equal to.14.14mVp. By referring to Figure 4.19(c), the crack positioning could be identified based on the time response at 32.53us. In this situation, the hole defect position is at the 10.23cm from PZ-LW sensor. By comparing the actual amplitude and time response based on DAQ, Oscilloscope, and Simulation showed that the feedback amplitude for DAQ was 0.0130Vp and oscilloscope was 0.01414Vp. The percentage of error was 8.06% because of % error tolerance from oscilloscope. It also followed by the crack positioning based on DAQ and simulation. From here, the DAQ time value for higher amplitude was taken at t=0.00004314s and the higher amplitude for simulation was

at t=0.00003419s. From here, the different crack positioning was 0.23cm within 2.24%. By following the simulation on defect positioning, it showed that the distance of crack was at 10.00cm in pipe line test. It referred to the longitudinal velocity 5850 m/s^2. It showed the percentage of error was lower based on comparison between actual and simulation result of crack positioning.
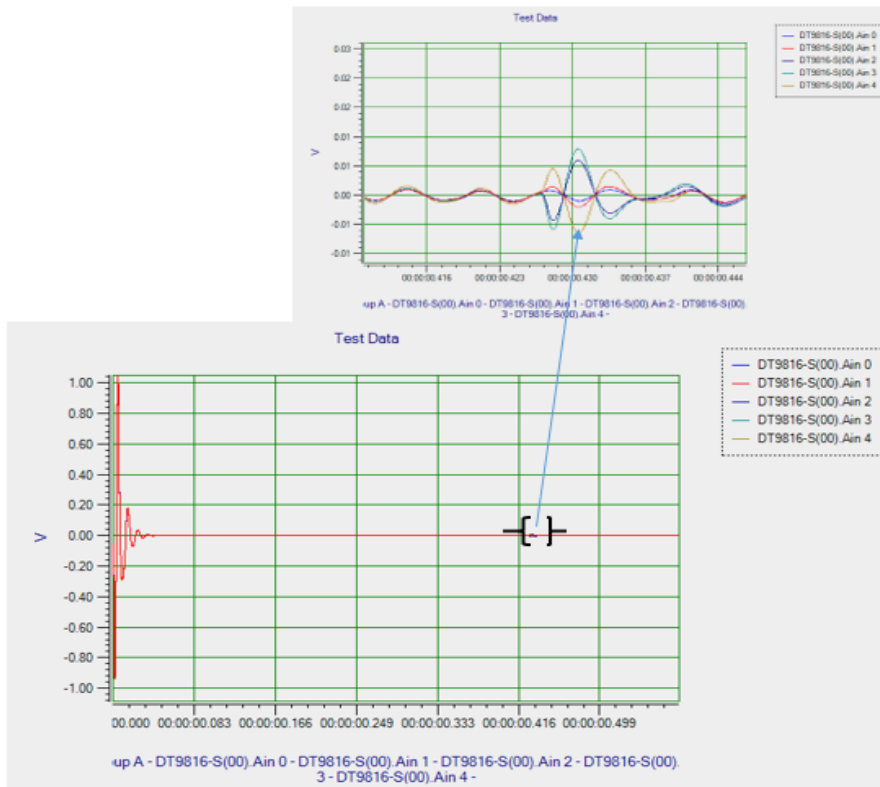
(a)

Figure 4.19   Hole defect diameter 4mm and distance position on 100mm from piezoelectric (a) From DAQ module continuously, (b) Signal from Oscilloscope, (c) The actual signal from experimental.
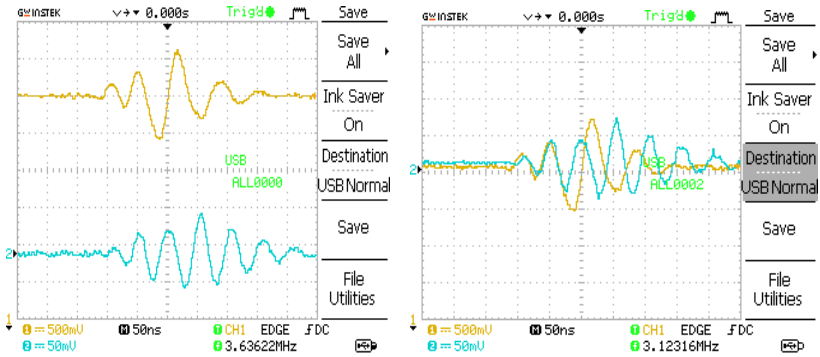
(b)
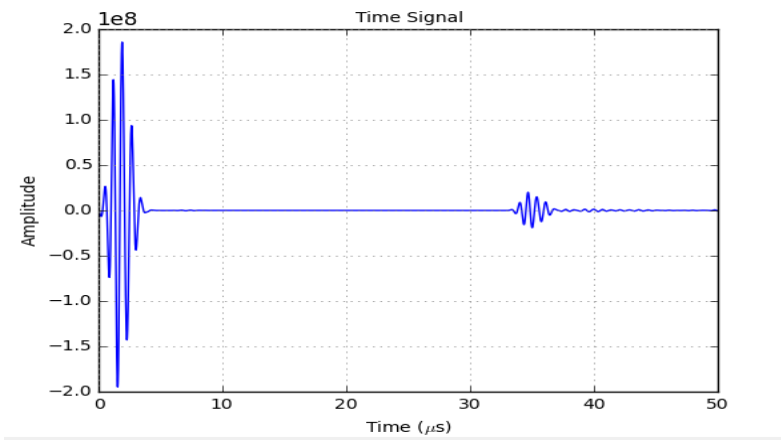
(c)

Figure 4.19　　Continued.

4.5.2　The Experimental Result of Axial Defect Detection

The second experiment was based on axial defect. From Figure 4.20(a), it showed the result of all five signals were close to each other but the higher was from Ain3. According to the experiment and simulation, the crack size was 2mm x 40mm.The crack signal was based on defect conditioning within the shape and positioning of crack on pipeline and the material velocity was based on longitudinal defect velocity properties. The positioning of defect could be identified by following the

Figure 4.20(a) where the time response started from 37.62us and the high amplitude was at 37.95us. From here, the amplitude signals were A4=7.5mV, A0=12.50mV and A3=15.00mV. By following the higher amplitude time for reflection signal, it showed that the crack positioning was 11.10cm from PZ-LW receiver sensor. Based on Figure 4.20(b), it showed the maximum amplitude of feedback signal on crack identification which was 25mVrms or 17.67mVp by representing the blue colour and it was 30 times gain reducing to compare the signal from signal generator. Figure 4.20(c) shows the excitation and reflection signal from simulation. Based on the signal graph, it showed the reflection occurred at 38.06us and the higher amplitude was at 39.35us. From here, the total range time from high amplitude of excitation signal and reflection signal was 37. 63us.The comparison was made between Figure 4.20(a) and 4.20(b) based on amplitude. From here, the percentage of error was calculated within 15.11%. It continued with comparison between Figure 4.20(a) and 4.20(c) based on time respond signal for crack distance in pipeline. According to the result, it showed the difference between experimental and simulation time respond which was only at 0.32us. From here, the percentage of error for crack location was 0.84%. It showed that the percentage of error was less than 1% for axial crack defect.
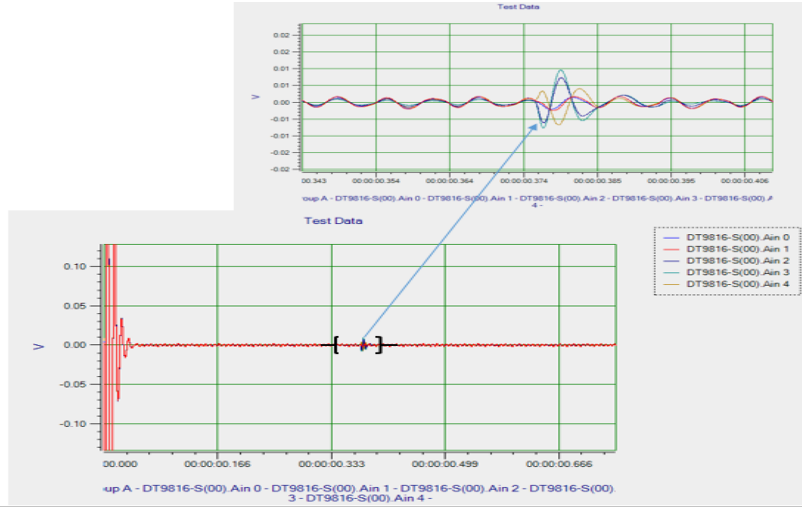
(a)
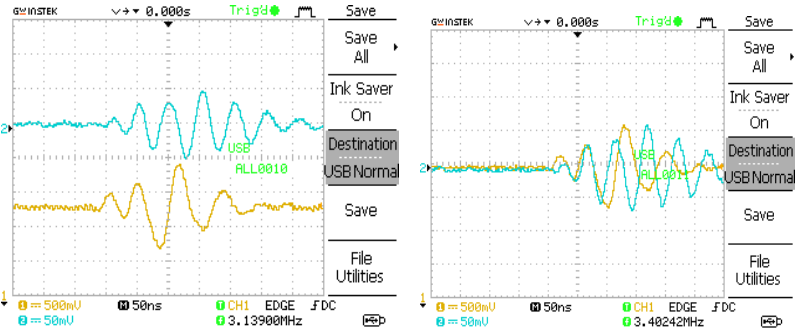
(b)
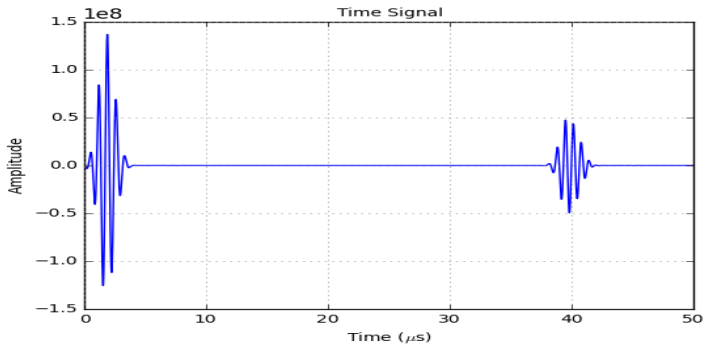
(c)

Figure 4.20   Axial defect diameter 2mm width defect and distance
position on 100mm from piezoelectric (a) From DAQ module continuously,
(b) Signal from Oscilloscope, (c) The actual signal from experimental.

4.5.3 The Experimental Result of Gradient Axial Defect Detection

The third experiment and simulation was made at gradient axial crack (angle defect). According to Figure 4.21, it shows the result of gradient defect signal by using DAQ, Oscilloscope and PC with MATLAB. The size of gradient axial crack (angle defect) which applied on the pipe was 2mm width, 6mm high, and angle 45 degree. By following the Figure 4.21(a), the for DAQ data result indicated that the three of sensors showed the amplitude signal changes within A0, A3, and A4 where A0 (blue signal) exposed 5mV signal amplitude, A3 (light blue) 8mV and A4 (orange) was 6mV. Based on the time response for signal feedback, the higher amplitude was shown at 0.00002295s and the crack location at pipeline being calculated was 6.17cm. The comparison was made between experimental result and oscilloscope measuring in Figure 4.21(b) where the amplitude from oscilloscope was 8mVrms or 5.66mVp. Figure 4.21(c) highlights the simulation result ~~by~~ based on angle defect. From here, the higher amplitude of feedback signal was defined at 0.00002176s. Based on the result comparison, it showed the percentage of error between DAQ and oscilloscope for amplitude of signal feedback was 6% error. This comparison was taken from orange signal (A4) pin from DAQ and oscilloscope. The oscilloscope measurement was taken from A4 pin from DAQ. It followed by the comparison between DAQ and simulation where the comparison was based on feedback time response for crack positioning in pipeline. From here, the crack positioning was calculated between experiment and simulation. The result showed that the crack positioning from experiment was 6.17cm and simulation was 6.36cm where the % of error

was 2.99%. By following three types of defect (hole, axial and angle defects), the higher of error was contributed at angle defect according to the defect location.
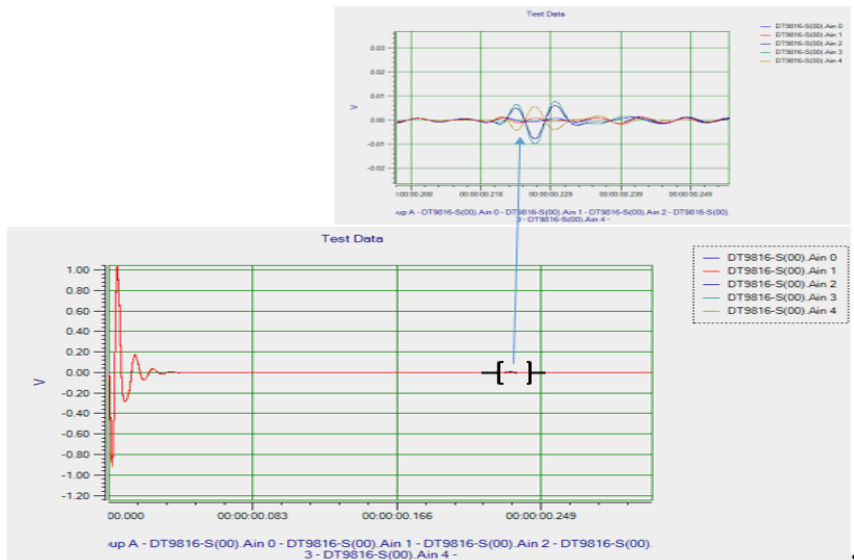
(a)
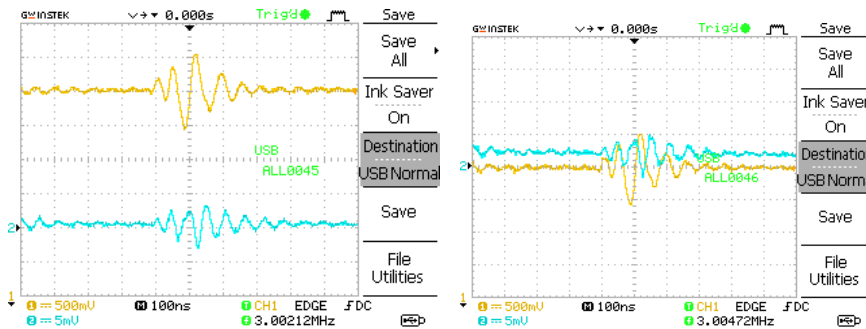
(b)

Figure 4.21   Gradient Axial defect diameter 2mm width defect and distance position on 100mm from piezoelectric, (a) From DAQ module continuously, (b) Signal from Oscilloscope, (c) The actual signal from experimental
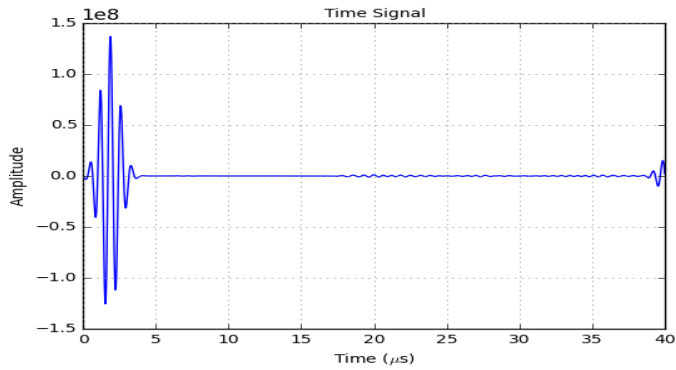
(c)

Figure 4.21   Continued.

4.5.4   The Experimental Result of Multi Defect Detection

To ensure the PZ-LW system could measure for multiple defect, the three cracks were combined at one pipe. From here, the all three types of defects were applied on the pipe with including hole, axial and gradient axial defect. All five PZ-LW sensors provided the responses based on signal feedback in Figure 4.22(a) where A0 (blue signal), A1 (red signal), A2 (violet signal), A3 (light blue signal) , and A4 (orange signal). Each pin showed the different voltage amplitude and time response for feedback signal with the respective of 0.019V (0.0000441s), 0.0005V (0.00004452s), 0.029V (0.0000443s), 0.004V (0.00004435s) and 0.002V (0.0000441s).   From here, it proved the sensors were measured at different sizes of defect and the position of defect as well. Based on the signal in Figure 4.22(b), the lower signal shown was 5mV and the higher was 150mV where the lower amplitude signal came from angle defect and higher was from axial defect by following the previous data and graph. According to Figure 4.22(c), there were three positioning of defect where the first crack identified on

time response at 43.35us, the second at 44.00us and lastly at 42.70us. By following the signal amplitude, the higher one was 44.00us (crack position 12.87cm) where it came from axial defect. It followed by second higher amplitude at 43.35us (crack position 12.68cm) which came from hole defect and lastly for low amplitude signal, it was 42.70us (crack position 12.49us) from angle defect. From here, it could be concluded that the higher signal feedback on time response was 44.00us while the lower error was within 0.68% and it came from axial defect. The second lower error was from hole defect within 1.85% and lastly angle defect 3.28%. It showed that the angle defect contributed to high error on feedback signal amplitude compared to the other two defects.
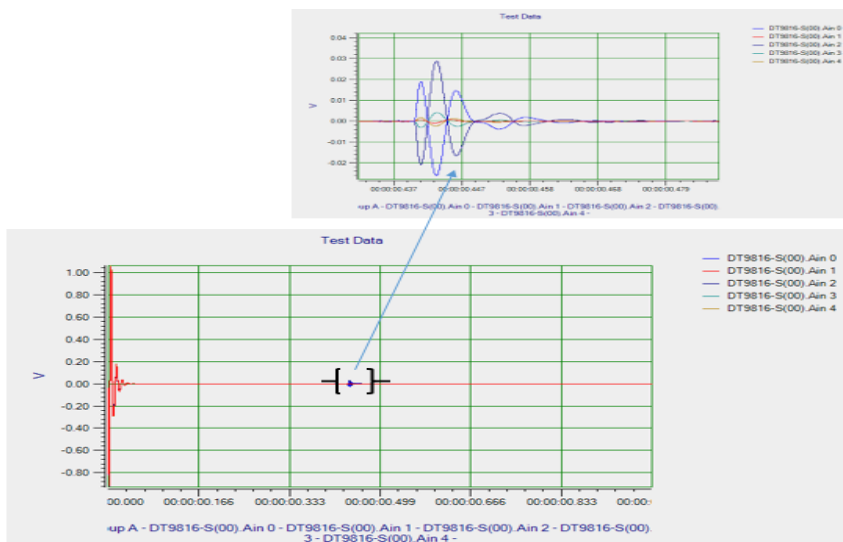
(a)

Figure 4.22   Multiple Defect for PZ-LW system, (a) From DAQ module continuously, (b) Signal from Oscilloscope, (c) The actual signal from experimental
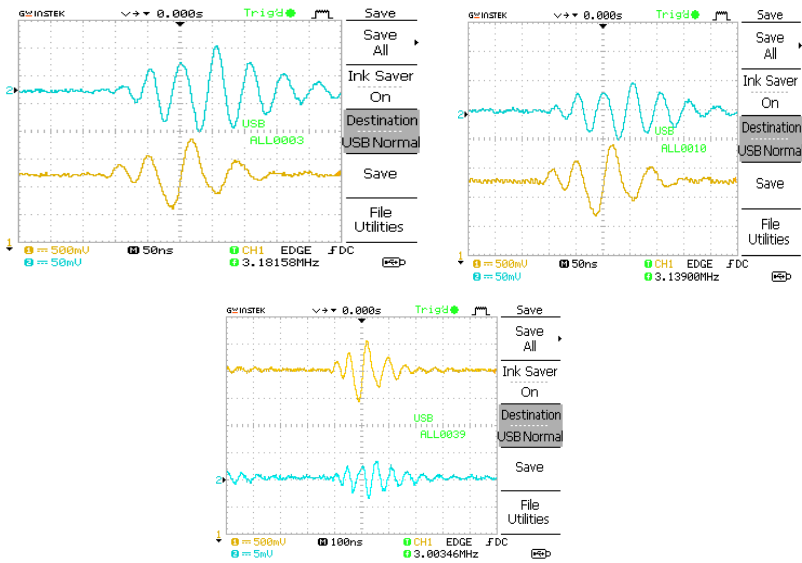
(b)
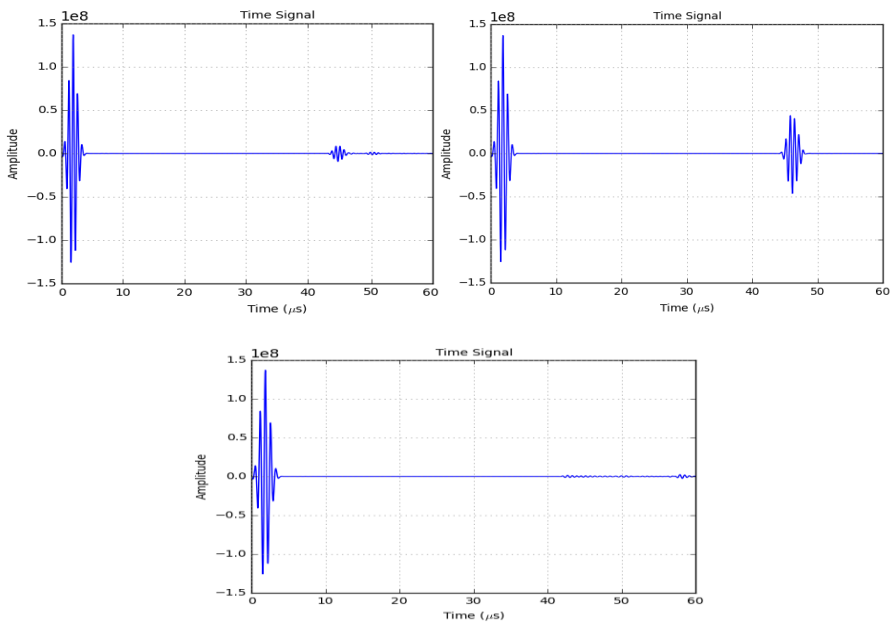
(c)

Figure 4.22   Continued.

4.6 Sensor Array Detection Result

The experiment for sensor array result was carried out based on the arrangement of six pairs of sensors in the circumference of pipeline with different types of artificial defect which included hole, axial, gradient axial, and multi defect. The size of pipe was 500mm in length, followed by the pipe thickness of 5mm, and the inner and outer diameter of 55mm and 60mm respectively. Meanwhile, the excitation amplitude for Piezo Actuator was set at 10Vpp.

In the hole defect, the higher signal could be obtained if the positioning of PZ-LW sensor was against the defect. In this case, the amplitude of defect was reduced because the PZ-LW sensor was not in line with the defect position. As could be observed in Figure 4.23, the amplitude received was 2.0Vpp when the positioning of PZ-LW sensor was against the defect, whereas the signal reflecting was reduced to 0.05Vpp if the PZ-LW was not in line with the gap of 22mm. As shown in the Figure 4.23, the amplitude obtained was 0.1Vpp when the gap of PZ-LW sensor was 12mm.

The second experiment was tested on the pipe with the axial defect of 2mm x 40mm. In this case, the result showed that the defect was against PZ-LW sensor which was given a high amplitude of 1.73Vpp. As presented in Figure 4.24, the three PZ-LW sensors that were against the defect tended to have the same signal amplitude while only two signals with gap 22 for both sides were given lower signal amplitude of 0.63Vpp. According to the time response, the entire defect signal had the

same time feedback. Hence, it could be concluded that the positioning of defect was 90 degree or vertically with PZ-LW sensor.

According to the third experiment with gradient axial defect presented in Figure 4.25, the signal of defect amplitude was very low. In this case, the maximum of feedback signal achieved was 0.85Vpp, whereas the lower signal was around 0.05Vpp. Based on the time response for signal feedback, it could be observed that the value of time response consistently increased which further implied that there was an angle in the types of defect.

Finally, the test was made for multiple defects with three types of defect namely hole defect, axial defect, and gradient axial defect on the pipeline inspection. The results presented in Figure 4.26 showed two signals where the highest was 0.5Vpp and the lowest was 0.08Vpp, particularly when the positioning of PZ-LW sensor on the gap of 22mm with the right side. Moreover, this signal came from the hole and axial defect with different position based on the time response. Furthermore, two high signal amplitudes could be observed when the positioning of PZ-LW sensor of 12mm was at the right side, in which the first signal was 0.32Vpp and the second signal was 0.64Vpp. Specifically, this signal came from the hole and axial defect at different positions, whereas the PZ-LW sensor was more against the axial defect position. The higher signal in this experiment was 1.73Vpp while the signal came from axial defect whereby the PZ-LW sensor was completely against it.
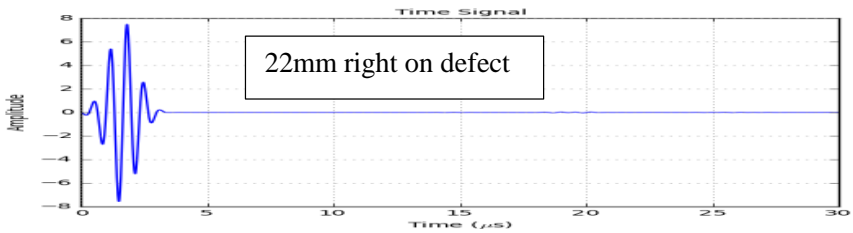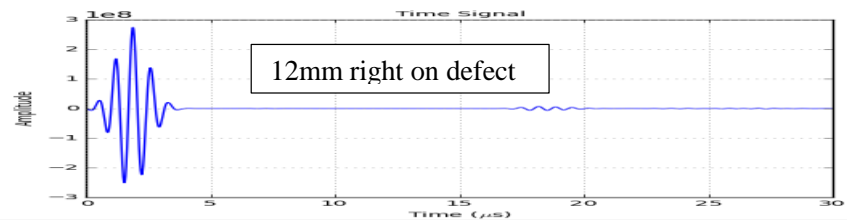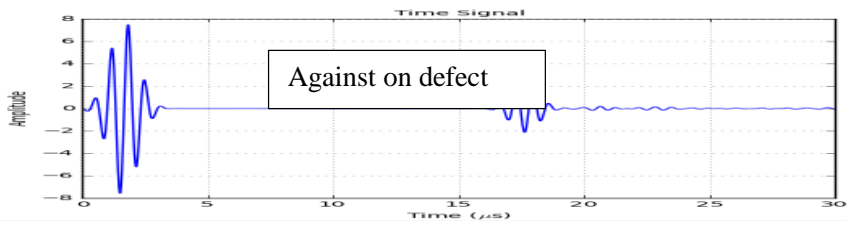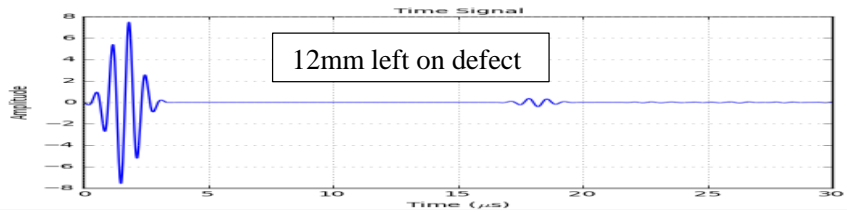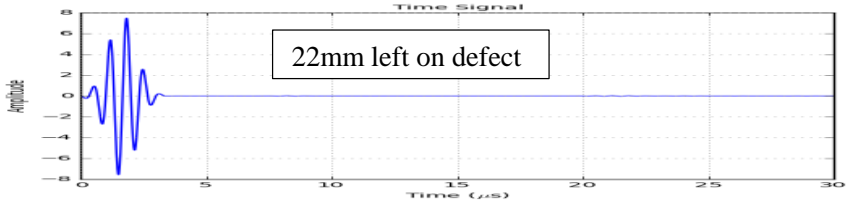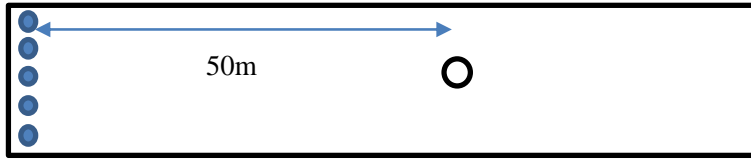
Figure 4.23   Result of Sensor Array with Hole Defect
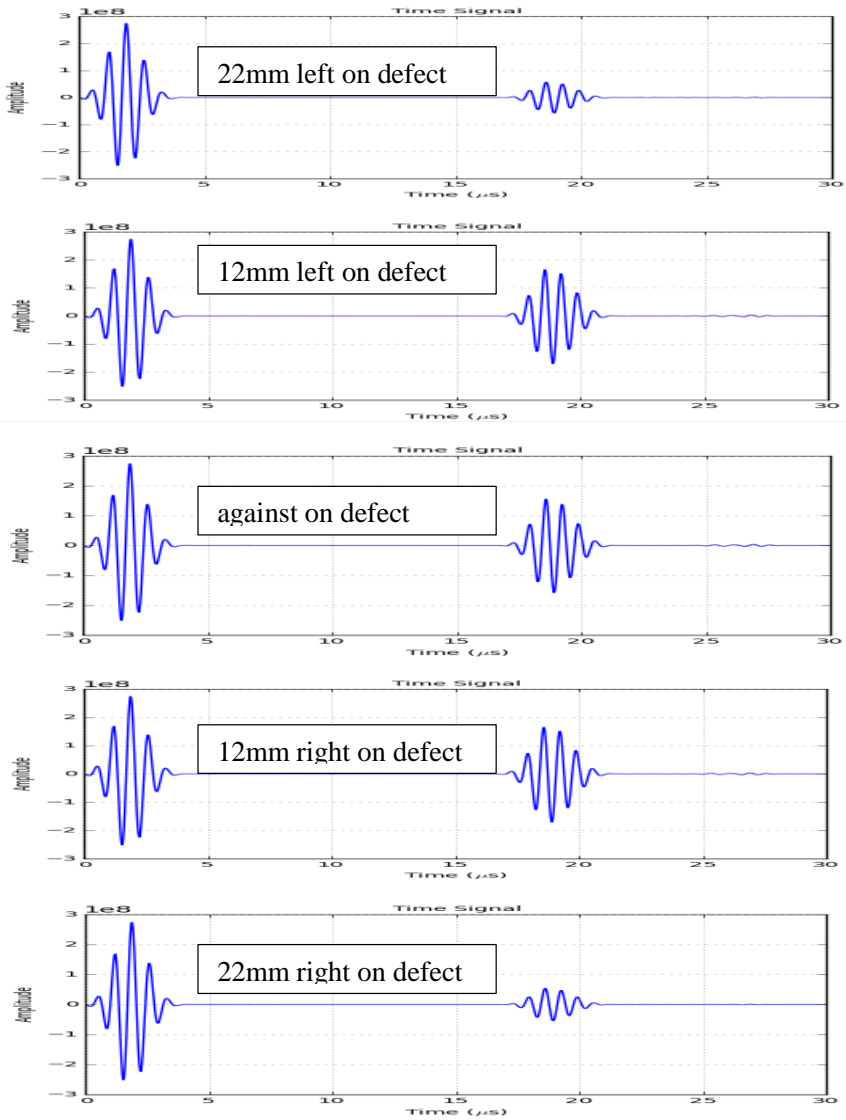
Figure 4.24   Result of Sensor Array with Axial Defect
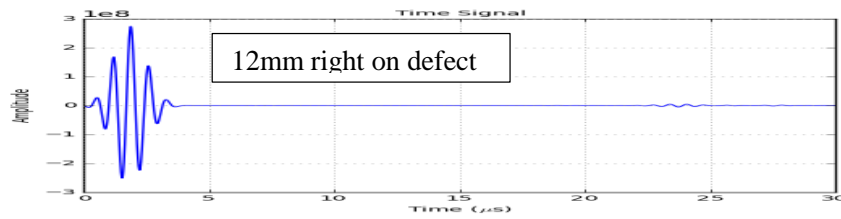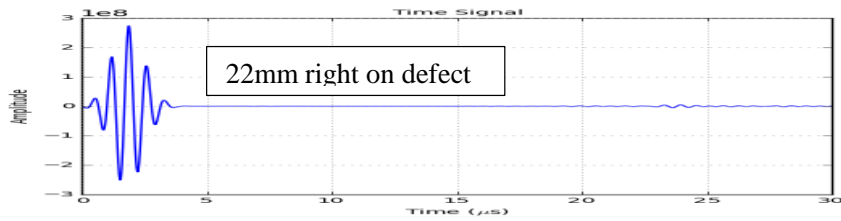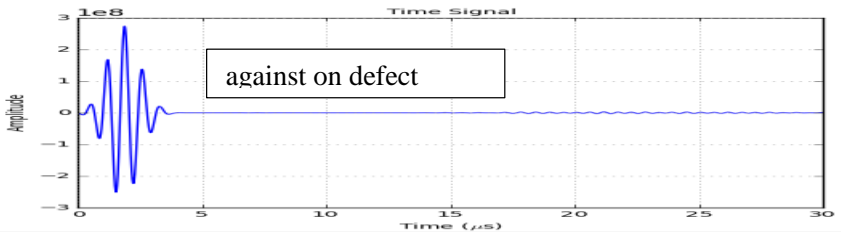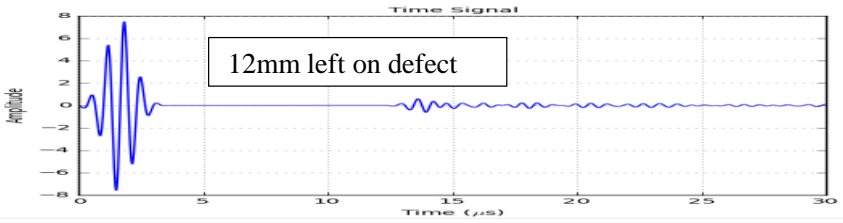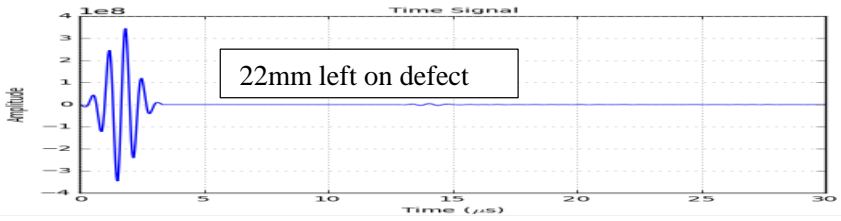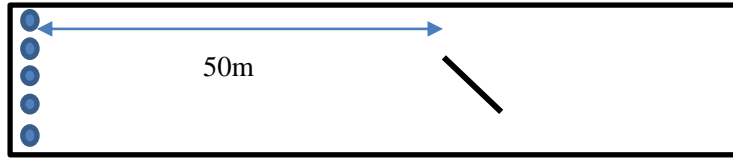
Figure 4.25   Result of Sensor Array with Gradient Axial Defect
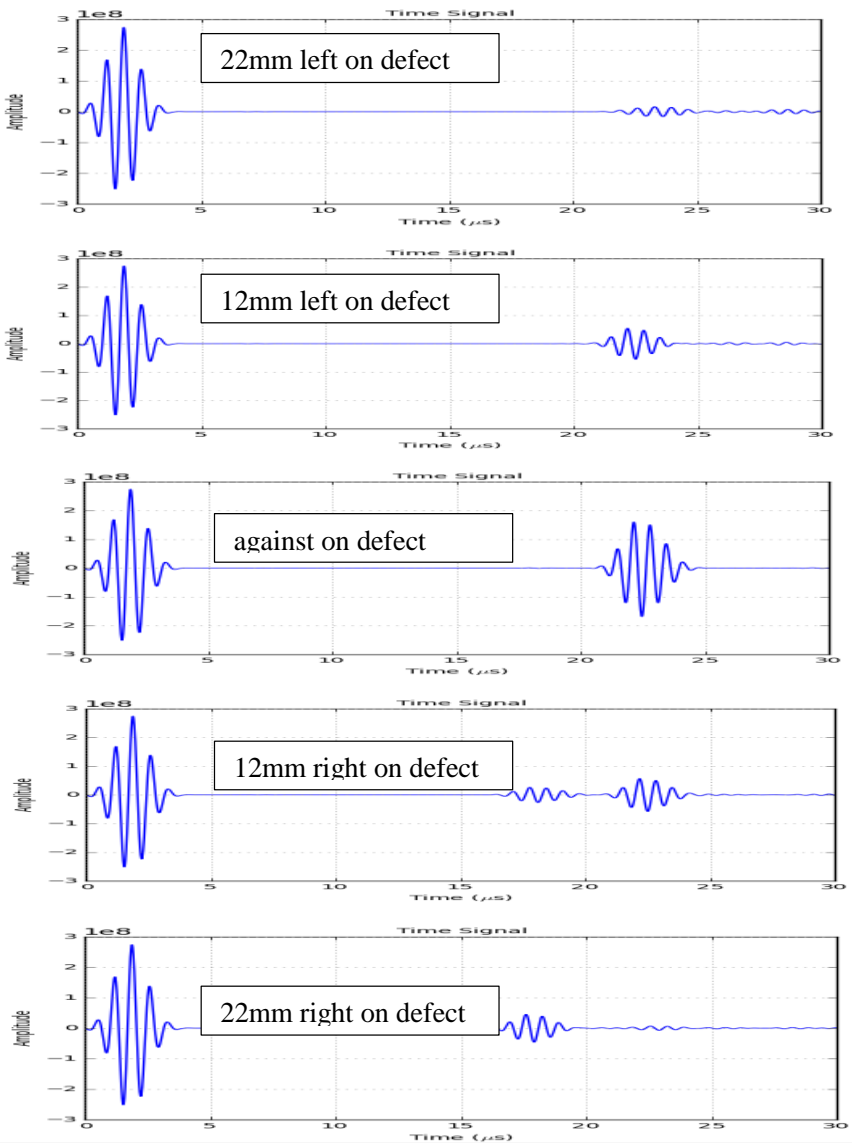
Figure 4.26   Result of Sensor Array with Multiple Defect

4.7   Error Compensation by Using Mamdani Fuzzy Logic

In this test, the PZ-LW signal with Fuzzy was compared to the conventional Piezoelectric receiver without Fuzzy. The measurement was made based on the defect sample within the hole defect (diameter 4mm), axial defect (2mm width and 40mm length), gradient axial defect (2mm width, 60mm length, and 45 degrees) and finally, the multiple defects which included a hole and axial defect. The percentage of error compensated was compared between two data or graphs. In this test, the fixed frequency (1.5Mhz) was set for both methods (with Fuzzy and without Fuzzy).

4.7.1   Validation of the Proposed Compensation Technique for Hole Defect

The first test for compensation technique was applied in the hole defect with a diameter of 4mm while the positioning defect was located 10cm from the Piezo Sensor Receiver. The result presented in Figure 4.27 showed that the signal of defect at the time of 35us until 40us. The orange colour of the signal represented the Fuzzy Signal, while the violet colour described the conventional Piezo Receiver Signal. The Actuator Signal was shown at the first signal where the higher was +1.8 to -1.8. Meanwhile, the second signal indicated that the maximum amplitude for defect within the amplitude signal was +0.25 to -0.25. The Fuzzy method was very significant in this research to ensure the % of error could be identified and at the same time, it reduced the error course of types of defect and crack positioning in the pipeline. From here, the MATLAB Simulink was used for Fuzzy development and the accuracy of signal

increased to 98.55% with 1.25% of error after Fuzzy, where the experiment for Conventional Signal Amplitude was 0.23V and after Fuzzy, it increased to 0.245V.
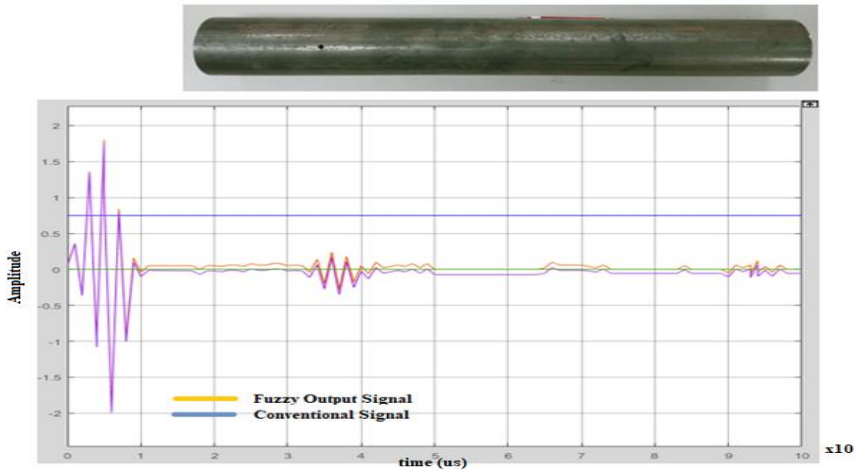
Figure 4.27   Comparing the Fuzzy signal and Conventional Signal for Hole Defect

4.7.2   Validation of the Proposed Compensation Technique for Axial Defect

Figure 4.28 shows the axial defect with the position located 10cm from the Piezo Sensor Receiver, while the size of the defect is 2mm x 40mm. The graph in Figure 4.28 showed that the Fuzzy Logic signal was slightly increased (orange colour) which led to the cause of effect of sensor gap between the actuator and Piezo Receiver. The conventional signal of Piezoelectric was represented with the violet colour. As it could be observed, the feedback signal was displayed at the time of 32us until 40us. The effect of axial and the thin width of defect led to the increase of the amplitude signal. According to the graph in Figure 4.28 below,

the maximum amplitude of feedback signal for axial defect was +1.0 to -1.0. Based on the experimental result, it showed that the Conventional Amplitude Signal (0.75V) from Piezo was lower compared to after Fuzzy (0.90V) and it increased until 13.53%. The increasing of the percentage rates of amplitude signal was based on the crack positioning. When the positioning of crack was high from PZ-LW sensor, the percentage of signal amplitude increased more. From this signal, accuracy increased until 96.05% with 3.95% of error. It showed the Fuzzy Logic could improve the accuracy of signal received and at the same time, it reduced the % error in signal feedback.
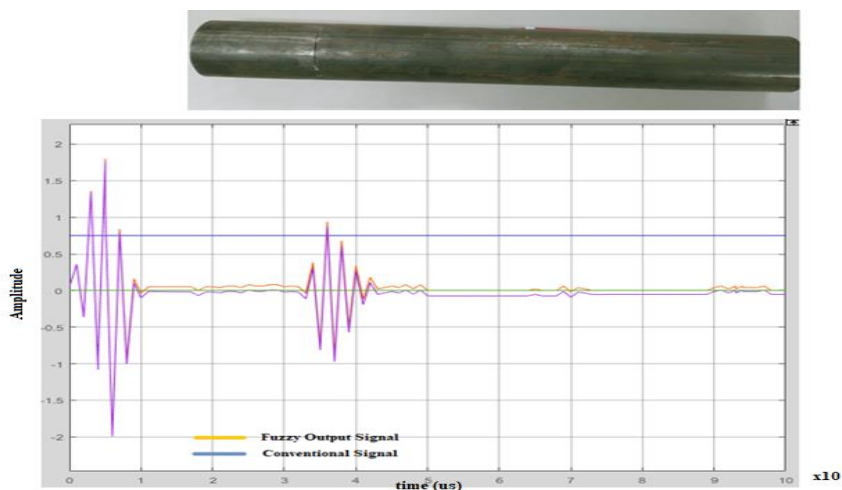
Figure 4.28   Comparing the Fuzzy signal and Conventional Signal for Axial Defect

4.7.3   Validation of the Proposed Compensation Technique for Gradient Axial Defect

According to Figure 4.29, it presents the gradient of the axial defect with the size of 2mm x 60mm with an angle of 45 degrees. The result showed

194

that the signal was low compared to the signal from hole and axial defect (Figures 4.19 and 4.20) based on the signal produced from the reflection of defect signal. The reflection amplitude signal was identified at time 25us to 30us with +0.3V to -0.3V of amplitude signal. The Fuzzy Logic signals were found to be slightly increased compared to the original signal while the length of pipe for testing was 500mm. From here, the conventional test (without Fuzzy) showed the higher amplitude for feedback signal which was 0.15V and after Fuzzy, it increased to 0.23V within 34.78% of increment. In the actual inspection of the gradient defect (angle crack), it was really challenging compared to the axial and hole crack. This was due to the vibration wave that moved 90 degrees against of crack. The crack in gradient positioning reduced the signal reflection because of the divergence to other angle according to the angle / gradient of crack.
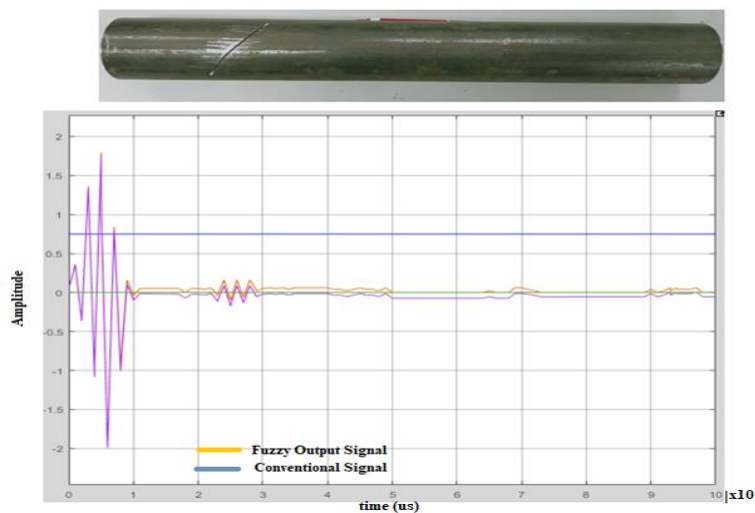
Figure 4.29   Comparing the Fuzzy signal and Conventional Signal for Gradient Axial Defect

4.7.4   Validation of the Proposed Compensation Technique for Multi Defect (Hole and Axial Defect)

Lastly, Figure 4.30 shows the two-response signal obtained from the inspection using PZ-LW testing technique. The orange colour of the signal represented the Fuzzy Signal while the violet colour described the conventional inspection. In this case, the accuracy of the signal could be considered based on the Fuzzy Logic development compared to the conventional signal (without Fuzzy) and PZ-LW system development (with Fuzzy). The maximum for first signal amplitude was 0.332 with Fuzzy while the conventional was 0.30. Next, the maximum amplitude was 0.566 with Fuzzy and the conventional was 0.55 based on the second signal.
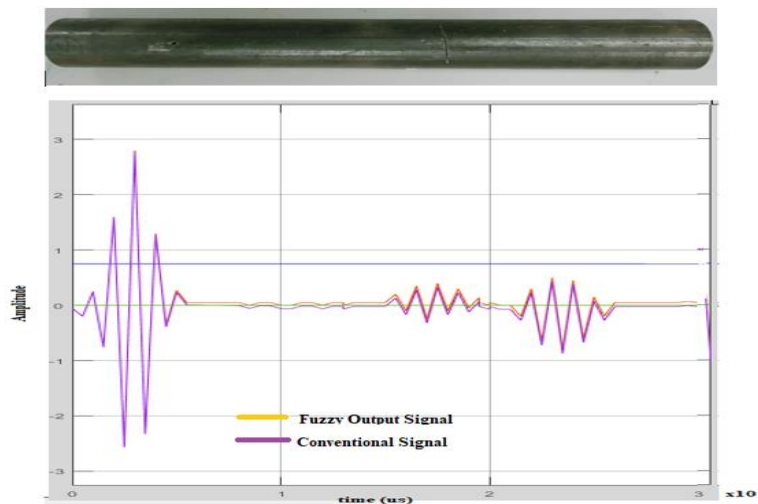
Figure 4.30   Comparing the Fuzzy signal and Conventional Signal for Multiple Defect

4.7.5 Validation of the Actual and Simulation

According to the comparison of the displacement-time curves of the simulated signal and the experiment one that has been presented in the previous sections, it could be clearly understood that the numerical simulation method was feasible and accurate. However, the time (sec) of the maximum peak of the excitation signal for both numerical simulation and experimental work were recorded to accurately validate the numerical and experimental work. Apart from that, the maximum displacement (v) for simulation and experimental work was also taken into account. Table 4.12 illustrates the obtained results of the four cases while Figure 4.31 and Figure 4.32 show the maximum peak of free damage and circumference damage.
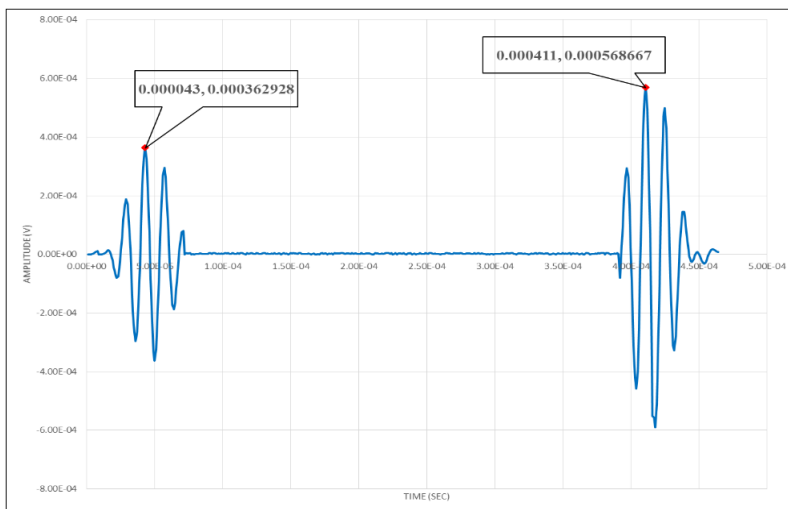
Figure 4.31 Maximum peak of the excitation signal and maximum peak of the reflected signal from end pipe versus time for perfect pipe
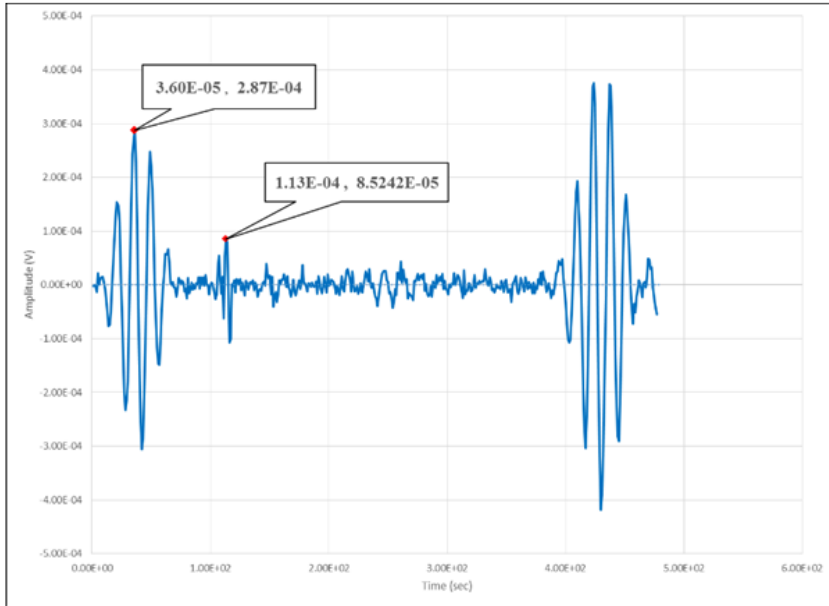
Figure 4.32   Maximum peak of the excitation signal and maximum
peak of the reflected signal from circumference damage versus time

According on Table 4.9, it shows the maximum peak voltage result and
the comparison is made between experiment (Fuzzy Logic) and
simulation. Based on the free damage pipe, the percentage of error was
1.80% by following the reflection signal amplitude result. It followed by
axial damage pipe with 0.93% and lastly hole damage pipe within
1.54%. It showed that the percentage of error was reduced after Fuzzy
Logic implemented for error compensation. The error % changers
depended on the types of crack and also the position of crack on pipeline.
Overall, the percentage of error was less than 2% or in other word, it was
98% of accuracy for amplitude signal feedback of measurement by using
Fuzzy Logic method.

Table 4.9   Maximum peak of the excitation signal and maximum
                 peak of the reflected signal versus time for all samples

Free Damaged Pipe				
Description	**Experimental**		**Simulation**	
	Time(s)	**Max disp(V)**	**Time(s)**	**Max disp(V)**
Excitation signal	0.00043	2.78E-04	0.000035	2.93E-04
Reflection signal	0.000411	4.43E-04	0.000404	4.35E-04
Axial Damaged Pipe				
Description	**Experimental**		**Simulation**	
	Time(s)	**Max disp(V)**	**Time(s)**	**Time(s)**
Excitation signal	0.000036	2.87E-04	0.000035	2.91E-04
Reflection signal	0.000113	5.32E-05	0.000109	5.27E-05
Hole Damaged Pipe				
Description	**Experimental**		**Simulation**	
	Time(s)	**Max disp(V)**	**Time(s)**	**Time(s)**
Excitation signal	0.000035	2.85E-04	0.000035	2.91E-04
Reflection signal	0.000108	5.19E-05	0.000109	5.27E-05

The results presented in Table 4.10 showed that the length of the pipe
could be measured when there was no damage or based on the damage
location. Specifically, this could be achieved by calculating the Time of
Flight (ToF) with the subtraction time at the maximum peak of the
excitation signal as well as the time at the maximum peak of the reflected
signal. In this case, ToF was taken and then multiplied by the group
speed (5400 m/s) based on the dispersion curve at the specified input
frequency of 1.5MHz.

For instance, the ToF obtained in circumference cracked pipe was 0.000077 second. Accordingly, this value was multiplied in the group of speed (5400m/sec) which made it possible to obtain the location of the crack after the result was divided by two. Therefore, the location of the crack in the mentioned case was (0.000077*5400)/2=0.2079 m. Table 4.13 illustrates the obtained results of ToF, distance calculated, actual distance, and relative error after the four cases are tested.

This table (4.10) also showed the maximum distance pipe that could be inspected for crack identification based on 5Vpp excitation signal with Gausses sine wave signal. From here, the maximum distance pipe for inspection could be reached until 311399 mm based on free damaged pipe. It refers to the Table 4.12 and Table 4.13 in free damage pipe. The 0 signal amplitude is occurring when there is no crack on pipeline. In the experiment, the amplitude 1.66667E-06 was assumed as 0 signal. Based on the calculation of the free damage pipe, the experimental result showed the maximum signal amplitude was 5.19E-05 and the zero signal was assumed as 1.66667E-07. Thus, the gain of amplitude was achieved by dividing the experimental result of amplitude with 1.66667E-07 and the result indicated the gain of 311. From here, the distance was measured with 5.19E-05 of 1000mm. After it was multiplied to 311 gain, the maximum distance of pipe for inspection could be reached until 311399mm or equal to 311m. For axial damage pipe defect, the maximum pipe that could be achieved for inspection was 64.377m and lastly for hole defect, the maximum distance could be reached was 61.267m. From here, it showed that the distance of defect depended on the types and width of crack.

Table 4.10   Comparison experimental and simulation distance with actual distance.

Free Damaged Pipe		
Description	**Experimental**	**Simulation**
Time of Flight (ToF) (sec)	0.000368	0.000369
Distance Calculation (mm)	993.6	996.3
Actual Distance (mm)	1000	1000
Relative error (%)	0.64	0.37
Axial Damaged Pipe		
Description	**Experimental**	**Simulation**
Time of Flight (ToF) (sec)	0.000077	0.000075
Distance Calculation (mm)	207.9	202.5
Actual Distance (mm)	200	200
Relative error (%)	3.95	1.25
Hole Damaged Pipe		
Description	**Experimental**	**Simulation**
Time of Flight (ToF) (sec)	0.000073	0.000074
Distance Calculation (mm)	197.1	199.8
Actual Distance (mm)	200	200
Relative error (%)	1.45	0.1

Overall, it could be concluded that the results of displacement-time curves in both numerical and experimental work were almost similar. In addition, the TOF, distance calculated, actual distance, and relative error summarised in Table 4.13 proved that the numerical simulation and experimental work led to almost very close and similar results. Furthermore, it could be understood that the numerical simulation method was feasible and accurate which made the relative error acceptable. Consequently, other experiments were also performed using numerical simulation.

4.7.6   Comparison with Ultrasonic Technique

In this section, the simulation and hardware measuring for the PZ-LW Compensation Scheme has been done by using Matlab/Simulink to validate and compared the effectiveness of the proposed scheme. From here the comparison being make with (Her & Lin, 2014) where the percentage of error as show in Table 4.1. The errors are consistently in range crack 1mm until 3mm. Based on Her & Lin the percentage of error can identify in range 4.7% until 5.0% and proposed methods respectively.

Table 4.11   Comparison the Proposed Scheme PZ-LW System

	1mm	1.5mm	2mm	2.5mm	3mm
% error from (Her & Lin)	5.0	4.7	5.0	5.0	5.0
% error from simulation	0.1	0.1	0.1	0.1	0.1
% error from conventional system UT	12	31	50	31	12
% error from PZ-LW Fuzzy Logic System	0.93	1.54	1.71	1.80	1.80

4.8   Summary

In this work, the results and findings of the experimental work in terms of Time-of-Flight Diffraction, ToFD, time, distance and error compensation are presented and discussed. Then, the data were presented and discussed following the results of numerical simulation work using the same parameters. After that, the comparison between the results of experimental and simulation (SIMNDT) are presented, in which it showed the validation of the PZ-LW system with regards to its compatibility and accuracy through the integration of Fuzzy Logic for error compensation.

Within this chapter, the results of RSM were also showed in which they identified the number of samples needed for each type of crack damage. At the same time. the optimisation of Piezoelectric sensor gap result can be identified and analysed for the sensor array. Finally, the results of Fuzzy Logic were discussed in order to show the accuracy of PZ-LW measurement for signal amplitude and crack positioning based on the error compensated through Fuzzy rules implementation on Simulink MATLAB.

In summary, the novelties of this work are as follows:

1. The design of the probe for pipeline crack measurement based on the Piezoelectric sensor array optimisation.

2. The implementation of the Fuzzy Logic Rules for crack accuracy detection based on signal amplitude and time response for PZ-LW system.

CHAPTER 5

CONCLUSION AND RECOMMENDATIONS FOR FUTURE WORK

5.1 Introduction

In this research, a PZ-LW has been developed for solving the measurement error of width of defect and time response caused by sensor gap and frequency variations. An extensive literature review has been conducted in the early stage to reveal the time response of error compensation method of Piezoelectric probe. From there, it is found that the sensor gap for error compensation method has received great attention due to its ability to improve the measurement accuracy of the sensor. The sensor gap compensation method is divided into two types of compensation which are the hardware compensation and the software compensation. In this research, both compensation methods were used.

In order to demonstrate the measurement error of the sensor under study which was caused by the sensor gap variations, an experimental setup for data collection had been conducted. The inaccuracy and error analysis have been done and a sensor gap for error compensation method has been proposed by using Mamdani-Type Fuzzy Inference System. The input MF was chosen according to the simplicity of the coding algorithm for hardware based real-time implementation. Rules have been developed based on experts' knowledge.

The input for the defuzzification process was a fuzzy set, which was the combined output of each rule, and the output is the weighted average of all rule outputs single number which is a non-fuzzy crisp value. Upon determining the effectiveness of the Fuzzy Gap Compensation Scheme, the simulation studies had been done using Matlab/Simulink Toolbox. In order to compare the performance and validity of PZ-LW testing, the other hardware for Ultrasonic Tester had also been proposed using the Ultrasonic Tester for Gap Compensation Scheme. The simulation and hardware results obtained were encouraging and they confirmed the performance of PZ-LW compared with Ultrasonic Tester Compensation Scheme in the following areas:

The PZ-LW gives optimal correction for the gap in which the reducing percentage error is only within 0.1% of its full-scale value. The PZ-LW is appropriate for measurement of gap in around 0mm until 5mm.

Based on the simulation result, the PZ-LW has implemented in hardware based real-time implementation by being embedded in Atmega328 microcontroller with C Programming Language and DAQ module (DT9816). The Atmega328 is used due to its small size and it also has larger RAM and higher speed of instruction execution as compared to PIC. The PZ-LW performance validation has been done by using real-time measurement and the output value after compensation that was displayed using LCD and Simulink Scope confirmed the performance of PZ-LW for Piezoelectric sensor in real time. According to the simulation and real-time implementation result, the PZ-LW have been successfully implemented.

5.2   Conclusion

The current work has provided a clear presentation and discussion on the effectiveness and the generality of the data-driven SHM-LRUT framework in detecting and localising different damages which include circumference, hole, and sloping in pipes. In the case of the present study, a data-driven framework based on pattern recognition and machine learning was developed in order to differentiate various types of damages.

The current research also investigated the spread of missile Lamb Wave to pipelines as well as their interaction with defects. Accordingly, a Piezoelectric sensor network (array) was organised and surface-mounted on the pipeline for the purpose of exciting and acquiring PZ-LWs. Apart from that, several simulation trials were also performed using SIMNDT software to validate the feasibility and applicability of the modified model. On a more important note, three types of defects with different sizes and locations along the pipeline were analysed under the simulation effort.

The results of the present study revealed that the model can accurately estimate the extent and location of the flaw based on the changes of the flaw size. Proceeding further with this effort, a comparative analysis was performed for various damages sizes located at different distances along the pipeline.

Overall, it can be concluded that the results of sensor gap and displacement-time curves in both numerical and experimental work were almost similar. In addition, the ToF, distance calculated, actual distance, and relative error summarised in Table 4.12 and 4.13 proved that the numerical simulation and experimental work led to almost very close and similar results.

Based on the results of the comparison, the accuracy of time response between simulation and experimental shown are dependent on the defect's types in which the hole defect of high accuracy within 99.074% and axial defect by 96.46%. From here, the frequency will be affecting the signal amplitude response wherein the amplitude represents the width of the defect. Otherwise, the attenuation is directly proportional with the defect localisation. Regarding this matter, the attenuation coefficient of signal is increased until 12.12% in each 40mm of defect positioning changes. The new discovery of this research includes the attenuation changes which are also closely related to the types of defect and excitation frequency which is applied in the PZ-LW inspection. In this optimisation, the 1.5Mhz for excitation frequency has the best frequency for PZ-LW inspection system due to the high amplitude of signal received during the inspection.

Accordingly, the optimisation for Piezo sensor gap with optimum distance can be set on 2.50mm with the high accuracy amplitude signal which is received from PZ-LW system. Specifically, the pattern of defect can be identified based on the reflection signal from Piezo sensor array on PZ-LW system which shows that until 98% precise match of shape defect can identified. Regarding this matter, the efficiency of defect

positioning can be proved by comparing between simulation and experiment whereby the hole defect positioning giving high accuracy as compared to the axial defect within 98.55% and 96.05%.

Therefore, this clearly indicates the crucial role of the model in the Structural Health Monitoring System (SHM) industrial structures such as the pipelines. In addition, this model will be able to help future works to investigate the interaction of Ultrasonic Waves with different defect sizes located at different positions along the pipe prior to carrying out any work trial.

5.3   Contribution

The contributions of this research are presented as follows:

(1) Provide a new experiment setup for steel pipeline SHM based on PZ-LW system which is usable for pipe monitoring.

(2) Provide a new SIMNDT model for simulating multi-damage in steel pipeline with detailed setting which can be used for simulation.

(3) Conducting DOE based on RSM for precisely identifying the required number of samples which shall reduce the efforts needed.

(4) Fuzzy illustrated a promising solution for classifying damages into targeted classes with high accuracy rate

5.4   Recommendations

This study has improved the SHM based on PZ-LW techniques for pipe monitoring with the focus on specific damages which include circumference, hole and sloping. However, there are several further enhancements which could be made in the future works. The following are the recommendations for future study in this field:

1- Performing similar experimental work on different pipes made of different metals other than steel as well as geometric.

2- Extend our work to other types of damages such as corrosion, or axial notch.

3- This study focused on the outer damage, thud it is recommended to study inner damage including the manufacturing damage such as internal deposit.

4- Expand the work achieved under this research to include an integrated wireless monitoring system using the suggested model under this research and determine how the signal will behave as it travels from solid media to free space and then from free space to solid media

REFERENCES

Abbas, M., & Shafiee, M. (2018). Structural Health Monitoring (SHM) and Determination of Surface Defects in Large Metallic Structures using Ultrasonic Guided Waves. *Sensors (Basel, Switzerland)*, *18*(3958), 1–26. https://doi.org/10.3390/s18113958

Al-Sabagh, A. M., Migahed, M. A., Sadeek, S. A., & El Basiony, N. M. (2018). Inhibition of Mild Steel Corrosion and Calcium Sulfate Formation in Highly Saline Synthetic Water by A Newly Synthesized Anionic Carboxylated Surfactant. *Egyptian Journal of Petroleum*, *27*(4), 811–821. https://doi.org/10.1016/j.ejpe.2017.12.003

Aranguren, G., Monje, P. M., Cokonaj, V., Barrera, E., & Ruiz, M. (2013). Ultrasonic Wave-Based Structural Health Monitoring Embedded Instrument. *Review of Scientific Instruments*, *125106*(12), 1–7. https://doi.org/10.1063/1.4834175

Aryan, P., Sampath, S., & Sohn, H. (2018). An Overview of Non-Destructive Testing Methods for Integrated Circuit Packaging Inspection. *Sensors (Switzerland)*, *18*(7), 1–27. https://doi.org/10.3390/s18071981

Ayres, J. W., & Rogers, C. A. (1996). Qualitative Health Monitoring of a Steel Bridge Joint via Piezoelectric Actuator/Sensor Patches BT - Nondestructive Evaluation of Bridges and Highways. *Photo-Optical Instrumentation Engineers (SPIE)*, *2719*(123), 211–218. https://doi.org/10.1117/12.259139

Baid, H., Banerjee, S., Joshi, S., & Mal, A. (2008). Detection of Disbonds in a Honeycomb Composite Structure Using Guided Waves. *Health Monitoring of Structural and Biological Systems*, *6935*(693504), 1–5. https://doi.org/10.1117/12.776349

Baiyang Ren, H. C. and C. J. L. (2017). A GuidedWave Sensor Enabling Simultaneous Wavenumber-Frequency Analysis for Both Lamb and Shear-HorizontalWaves. *Sensors (Switzerland)*, *17*(488), 1–15. https://doi.org/10.3390/s17030488

Bernieri, A., Ferrigno, L., Laracca, M., Rasile, A., & Ricci, M. (2017). Ultrasonic Non Destructive Testing On Aluminium Forged Bars. *IEEE International Workshop on Metrology for AeroSpace (MetroAeroSpace)*, 223–227. Padua, Italy: IEEE.

Bourdais, F. Le, Baqué, F., Baronian, V., & Reverdy, F. (2013). Design of Ultrasonic Inspection Methods for Sodium Cooled Reactors by CIVA Simulation. *3rd International Conference on Advancements in Nuclear Instrumentation, Measurement Methods and Their Applications (ANIMMA)*, 1–8. https://doi.org/10.1109/ANIMMA.2013.6727955

Braconnier, E. C. ; G. L. ; D. (2016). Fast Total Focusing Method by a Migration Approach. *IEEE Far East NDT New Technology and Application Forum, FENDT 2015*, *978*(399), 129–132. https://doi.org/10.1109/FENDT.2015.7398325

Caporale, S., Callegari, S., Riccit, M., & Burrascanot, P. (2013). Constant Envelope Pseudo Orthogonal Excitations for Ultrasound Testing. *International Conference on Digital Signal Processing (DSP)*, *5*(978), 1–8. https://doi.org/10.1109/ICDSP.2013.6622751

Carino, N. (2001). The Impact-Echo Method: An Overview. *Structures Congress & Exposition*, 1–18. https://doi.org/10.1061/40558(2001)15

Charutz, D. M., Mor, E., Harput, S., Cowell, D. M. J., Smith, P. R., & Freear, S. (2013). Guided Wave Enhancement Phased Array Beamforming Scheme using Recursive Feedback. *IEEE International Ultrasonics Symposium (IUS)*, *978*(5686), 166–169. IEEE.

Cr, S., Joseph, N., Samson, N., Jose, P., & Subramanian, M. E. P. (2013). Advanced 4S Image Correlation for Real-Time Quality Inspection of Ceramic Products Using Ultrasonic ToFD Images. *Computer Communication and Informatics, ICCCI 2013*, 1–7. https://doi.org/10.1109/ICCCI.2013.6466132

Cristina, I., Blanco, P., Alvarez, J. H. P., & Dobmann, G. (2014). Simulation for Magnetic Flux Leakage Signal Interpretation A FE-Approach to Support In-Line Magnetic Pipeline Pigging. *IEEE Far East Forum on Nondestructive Evaluation/Testing*, *978*(3296), 1–4. IEEE.

Cruza, J. F., Medina-valdes, L., & Fritsch, C. (2015). Real Time Autofocusing Hardware for Ultrasonic Imaging with Interfaces. *IEEE International Ultrasonics Symposium (IUS)*, *978*(8182), 1–4. https://doi.org/10.1109/ULTSYM.2015.0544

Cui, L., Zhou, S., Sun, H., Lei, Q., Ma, S., Tian, X., & Zhang, P. (2016). Research On Algorithms of Various Defects Detection of Thick-Wall Pipes. *Proceedings of 2015 IEEE Far East NDT New Technology and Application Forum, FENDT 2015*, 192–196. https://doi.org/10.1109/FENDT.2015.7398338

Dincer, I., Colpan, C. O., Kizilkan, O., & Ezan, M. A. (2015). Response Surface Modeling and Optimization of Chromium (VI) Removal from Aqueous Solution Using Date Stones Activated Carbon in Batch Process. *Progress in Clean Energy*, *1*(Vi), 1–9. https://doi.org/10.1007/978-3-319-16709-1

Doebling, S. W., Farrar, C. R., & Prime, M. B. (1998). A Summary Review of Vibration-Based Damage Identification Methods. *Shock and Vibration Digest*, *30*(2), 91–105. https://doi.org/10.1177/058310249803000201

Du, G., Huo, L., Kong, Q., & Song, G. (2016). Damage Detection of Pipeline Multiple Cracks Using Piezoceramic Transducers. *Journal of Vibroengineering*, *18*(5), 2828–2838. https://doi.org/doi.org/10.21595/jve.2016.17040

Elamvazhudi, B., & Gopalakannan, S. (2018). Stress Intensity Factor Calculations for Semi-Elliptical Cracked Joints Using Finite Element AnalysisIn 3D. *Materials Today: Proceedings*, *5*(5), 11808–11818. https://doi.org/10.1016/j.matpr.2018.02.151

Farinas, M. D., Alvarez-Arenas, T. E. G., Aguado, E. C., & Merino, M. G. (2013). Non-Contact Ultrasonic Inspection of CFRP Prepregs for Aeronautical Applications During Lay-Up Fabrication. *IEEE International Ultrasonics Symposium, IUS*, *978*(4412), 1590–1593. https://doi.org/10.1109/ULTSYM.2013.0405

Fendt, K. T., Mooshofer, H., Rupitsch, S. J., Lerch, R., & Ermert, H. (2013). Investigation of the Synthetic Aperture Focusing Technique Resolution for Heavy Rotor Forging Ultrasonic Inspection. *IEEE International Ultrasonics Symposium (IUS)*, *978*(4673), 1869–1872. IEEE.

Foudazi, A., Member, S., Ghasr, M. T., Member, S., & Donnell, K. M. (2014). Application of Active Microwave Thermography to Inspection of Carbon Fiber Reinforced Composites. *IEEE AUTOTEST*, *978*(3005), 1–5. https://doi.org/10.1109/AUTEST.2014.6935164

Fu, J. Q., Zhou, S. Y., Li, Z., Xu, C. G., & Pan, Q. X. (2016). Research on Guided Wave Excitation Mode Control Method of Comb Transducer. *Proceedings of 2015 IEEE Far East NDT New Technology and Application Forum, FENDT 2015*, 124–128. https://doi.org/10.1109/FENDT.2015.7398324

Gao, H., Lopez, B., Minguez, X., & Chen, J. (2015). Ultrasonic Inspection of Partially Completed Welds Using EMAT-Generated Surface Wave Technology. *IEEE Far East NDT New Technology & Application Forum (FENDT)*, *978*(7001), 2–5. https://doi.org/10.1109/FENDT.2015.7398351

Gao, X., Peng, C., Wang, Z., & Li, X. (2016). Rail Inspection Research Based on High Speed Phased Array Ultrasonic Technology. *IEEE Far East NDT New Technology & Application Forum (FENDT)*, *978*(5090), 181–184. https://doi.org/10.1109/FENDT.2016.7992020

Gao, X., Peng, J., Zhang, Y., Peng, C., & Tan, Y. (2013). Wheel and Axle Defect Detecting Technique Using Phased Array Ultrasonic. *Far East Forum on Nondestructive Evaluation/Testing: New Technology and Application*, *978*(6020), 40–45. https://doi.org/10.1109/FENDT.2013.6635525

Gaunaurd, G. C. (1989). Elastic and Acoustic Resonance Wave Scattering. *Applied Mechanics Reviews*, *42*(6), 143–193. https://doi.org/10.1115/1.3152427

Ghafari, S., Aziz, H. A., Isa, M. H., & Zinatizadeh, A. A. (2009). Application of Response Surface Methodology (RSM) to Optimize Coagulation-Flocculation Treatment of Leachate Using Poly-Aluminum Chloride (PAC) and Alum. *Journal of Hazardous Materials*, *163*(2–3), 650–656. https://doi.org/10.1016/j.jhazmat.2008.07.090

Ghavamian, A., Mustapha, F., Baharudin, B. T. H. T., & Yidris, N. (2018). Detection, Localisation and Assessment of Defects in Pipes Using Guided Wave Techniques: A Review. *Sensors (Switzerland)*, *18*(12), 1–48. https://doi.org/10.3390/s18124470

Her, S. C., & Lin, S. T. (2014). Non-Destructive Evaluation of Depth of Surface Cracks Using Ultrasonic Frequency Analysis. *Sensors (Switzerland)*, *14*(9), 17146–17158. https://doi.org/10.3390/s140917146

Hickman, G. A., Gerardi, J. J., & Feng, Y. (1991). Application of Smart Structures to Aircraft Health Monitoring. *Journal of Intelligent Material Systems and Structures*, *2*(3), 411–430. https://doi.org/10.1177/1045389X9100200308

Ihn, J.-B., & Chang, F.-K. (2004). Detection and Monitoring of Hidden Fatigue Crack Growth Using a Built-In Piezoelectric Sensor/Actuator Network: I. Diagnostics. *Smart Materials and Structures*, *13*(3), 1–5. https://doi.org/10.1088/0964-1726/13/3/02

Iriarte, J. M., Cosarinsky, G., & Brizuela, J. (2016). Synthetic Aperture Ultrasound Imaging Using GPUs (Generación De Imágenes De Ultrasonido Por Apertura Sintética Utilizando GPUs). *IEEE Conference on Computer Sciences*, *978*(1), 1–5. IEEE.

Ji, C., & Wang, Q. (2017). Corrosion Evaluation of Additive Manufacture Metal Alloy by Nondestructive Line-focused Transducer. *IEEE International Ultrasonics Symposium (IUS)*, *978*(5386), 1–4. https://doi.org/10.1109/ULTSYM.2017.8091633

José, J., España, G., William, J., & Bedoya, B. (2013). Peniel Method for the Automation of the Ultrasonic Monitoring Based on the Acoustic Impedance. *IEEE 8th Conference on Industrial Electronics and Applications (ICIEA)*, *978*(6322), 1850–1856. https://doi.org/10.1109/ICIEA.2013.6566669

Kamal, A., & Giurgiutiu, V. (2014). Shear Horizontal Wave Excitation and Reception with Shear Horizontal Piezoelectric Wafer Active Sensor (SH-PWAS). *Smart Materials and Structures*, *23*(8), 1–18. https://doi.org/10.1088/0964-1726/23/8/085019

Kamas, T., Giurgiutiu, V., & Lin, B. (2015). E / M impedance Modeling and Experimentation for the Piezoelectric Wafer Active Sensor. *Smart Materials and Structures*, *24*(11), 1–13. https://doi.org/10.1088/0964-1726/24/11/115040

Kazys, R. J., Vilpisauskas, A., & Sestoke, J. (2018). Application of Air-Coupled Ultrasonic Arrays for Excitation of a Slow Antisymmetric Lamb Wave. *Sensors (Switzerland)*, *18*(8), 1–22. https://doi.org/10.3390/s18082636

Kessler, S. S., Spearing, S. M., & Soutis, C. (2002). Damage Detection in Composite Materials Using Lamb Wave Methods. *Smart Materials and Structures*, *11*(2), 1–7.

Khan, S., Taube, W., Yogeswaran, N., Heidari, H., & Dahiya, R. (2015). Spice Model of a Piezo-Electric Transducer for Pulse-Echo System. *2015 11th Conference on Ph.D. Research in Microelectronics and Electronics, PRIME 2015*, 334–337. https://doi.org/10.1109/PRIME.2015.7251403

Kibe, T., Kimoto, K., & Kobayashi, M. (2016). Continuous Monitoring at 600 ºC by CaBi 4 Ti 4 O 15 / Pb (Zr , Ti) O 3 Sol-gel Composite Ultrasonic Transducer. *IEEE International Ultrasonics Symposium (IUS)*, *978*(5970), 16–19. https://doi.org/10.1109/ULTSYM.2016.7728726

Kim, J. S., Lee, B. Y., Hwang, W. G., & Kang, S. S. (2015). The Effect of Welding Residual Stress for Making Artificial Stress Corrosion Crack in the STS 304 Pipe. *Advances in Materials Science and Engineering*, *2015*, 1–8. https://doi.org/10.1155/2015/932512

Kirchhof, J., Krieg, F., Florian, R., Ihlow, A., Osman, A., & Galdo, G. Del. (2017). Sparse Signal Recovery For Ultrasonic Detection And Reconstruction Of Shadowed Flaws. *IEEE International Conference on Acoustics, Speech and Signal Processing (ICASSP)*, (2), 816–820. New Orleans, LA, USA: IEEE.

Kirchhof, J., Krieg, F., Romer, F., Ihlow, A., Osman, A., & Del Galdo, G. (2016). Speeding Up 3D SAFT for Ultrasonic NDT by Sparse Deconvolution. *IEEE International Ultrasonics Symposium, IUS*, *2016–Novem*, 3–6. https://doi.org/10.1109/ULTSYM.2016.7728434

Kleijnen, J. P. C. (2015). Response Surface Methodology. *International Series in Operations Research and Management Science*, *216*, 81–104. https://doi.org/10.1007/978-1-4939-1384-8_4

Kleiman, J., & Kudryavtsev, Y. (2015). Measurement of Residual Stresses in Materials and Welded Elements Using Ultrasonic Method. *IEEE Far East NDT New Technology & Application Forum (FENDT)*, *978*(4290), 143–148. https://doi.org/10.1109/FENDT.2015.7398328

Kwak, D. R., Cho, S. B., & Park, I. K. (2016). Analysis of Dynamic Characteristic for Ultra-Thin Coating Layer with Ultrasonic Atomic Force Microscopy. *Proceedings of 2015 IEEE Far East NDT New Technology and Application Forum, FENDT 2015*, (3), 3–6. https://doi.org/10.1109/FENDT.2015.7398336

Lad, P., & Pawar, M. (2017). Evolution of Railway Track Crack Detection System. *2016 2nd IEEE International Symposium on Robotics and Manufacturing Automation, ROMA 2016*, *3*(56), 1–12. https://doi.org/10.1109/ROMA.2016.7847816

Lamb, H. (1917). On Waves in an Elastic Plate. *Proceedings of the Royal Society A: Mathematical, Physical and Engineering Sciences*, *93*(648), 114–128. https://doi.org/10.1098/rspa.1917.0008

Lanza, F., Sternini, S., & Nguyen, T. V. (2017). Ultrasonic Imaging in Solids Using Wave Mode Beamforming. *IEEE Transactions on Ultrasonics, Ferroelectrics, and Frequency Control*, *64*(3), 602–616.

Lanza, F., Sternini, S., & Nguyen, T. V. (2016). *Ultrasonic Imaging in Solids Using Wave Mode Beamforming*. *3010*(c). https://doi.org/10.1109/TUFFC.2016.2637299

Lee, J.-H., & Lee, S.-J. (2008). Application of Laser-Generated Guided Wave for Evaluation of Corrosion in Carbon Steel Pipe. *NDT & E International*, *42*(3), 222–227. https://doi.org/10.1016/j.ndteint.2008.09.011

Lee, J. J., Lee, J. W., Yi, J. H., Yun, C. B., & Jung, H. Y. (2005). Neural Networks-Based Damage Detection for Bridges Considering Errors in Baseline Finite Element Models. *Journal of Sound and Vibration*, *280*(3–5), 555–578. https://doi.org/10.1016/j.jsv.2004.01.003

Li, J., & Hao, H. (2016). Health Monitoring of Joint Conditions in Steel Truss Bridges with Relative Displacement Sensors. *Measurement: Journal of the International Measurement Confederation*, *88*, 360–371. https://doi.org/10.1016/j.measurement.2015.12.009

Li, X., Zhao, X., Hao, J., Lu, Z., & Huang, Y. (2014). Kinematic Analysis and Simulation of Ultrasonic Testing Manipulator. *IEEE Far East Forum on Nondestructive Evaluation/Testing*, 1–5. https://doi.org/10.1109/FENDT.2014.6928251

Lin, Q., Xu, C., Yan, H., Zhou, S., & Yang, L. (2014). Thickness of Coating Tested Nondestructively Based on Welch Frequency. *IEEE Far East Forum on Nondestructive Evaluation/Testing*, 34–38. https://doi.org/10.1109/FENDT.2014.6928245

Lippold, J. C., Varol, I., & Baeslack, W. . (1989). Characterization of Weld Solidification Cracking in a Duplex Stainless Steel. *Metallography*, *23*(655), 1–19. https://doi.org/10.1016/0026-0800(89)90037-2

Liu, F., Xu, C., He, Y., Xiao, D., Meng, F., Xiao, Z., & Pan, Q. (2016). Research on the Ultrasonic Test System for the Complex Curved Surface Based on Robot. *Proceedings of 2015 IEEE Far East NDT New Technology and Application Forum, FENDT 2015*, 173–176. https://doi.org/10.1109/FENDT.2015.7398334

Liu, Q., Piwakowski, B., Lafhaj, Z., & Agred, K. (2014). Automated Non-Contact NDT by Ultrasonic Surface Waves. *IEEE Far East Forum on Nondestructive Evaluation/Testing*, (5), 3–7. https://doi.org/10.1109/FENDT.2014.6928237

Liu, S., Hao, J., Lu, Z., Zhang, M., & Zhao, J. (2016). A Calibration Method of Workpiece Frames for Ultrasonic Testing Using Twin-robot. *IEEE Far East NDT New Technology & Application Forum (FENDT)*, 1–5. https://doi.org/10.1109/FENDT.2016.7991997

Lopez Villaverde, E., Robert, S., & Prada, C. (2017). Ultrasonic Imaging in Highly Attenuating Materials with Hadamard Codes and the Decomposition of the Time Reversal Operator. *IEEE Transactions on Ultrasonics, Ferroelectrics, and Frequency Control*, *64*(9), 1336–1344. https://doi.org/10.1109/TUFFC.2017.2690499

Lowe, M. J. S., Alleyne, D. N., & Cawley, P. (1998). Defect Detection in Pipes Using Guided Waves. *Ultrasonics*, *36*(1–5), 147–154. https://doi.org/10.1016/S0041-624X(97)00038-3

Lu, Z. (2014). Estimating Time-Of-Flight of Multi-Superimposed Ultrasonic Echo Signal Through Envelope. *Proceedings - 2014 6th International Conference on Computational Intelligence and Communication Networks, CICN 2014*, *0*, 300–303. https://doi.org/10.1109/CICN.2014.74

Luo, Y., Lu, X., Wang, K., & Wang, L. (2014). The Application in Detection of Defects in Compound Material with Ultrasonic Phased Array Technology. *The 26th Chinese Control and Decision Conference (2014 CCDC)*, 2100–2103. https://doi.org/10.1109/CCDC.2014.6852513

Madhumitha, P., Ramkishore, S., Srikanth, K., & Palanichamy, P. (2014). Application of Decision Trees for the Identification of Weld Central Line in Austenitic Stainless Steel Weld Joints. *2014 International Conference on Computation of Power, Energy, Information and Communication (ICCPEIC)*, 400–406. https://doi.org/10.1109/ICCPEIC.2014.6915397

Mahmod, M. F., Pauzi, M. Z. M., & Bakar, E. A. (2013). Flatbed Scanner Image and Single Ultrasonic Rangefinder Technique for Composite Laminates Defect Detection. *2013 IEEE International Conference on Smart Instrumentation, Measurement and Applications, ICSIMA 2013*, (November), 26–30. https://doi.org/10.1109/ICSIMA.2013.6717929

Maia, O. M. de A., Schneider, F. K., Maia, J. M., Neves, L. C., & Penteado, S. do R. C. (2014). Wood characterization using the power spectral density and phase velocity of ultrasonic signals. *2014 IEEE International Ultrasonics Symposium*, 1416–1419. https://doi.org/10.1109/ULTSYM.2014.0350

Malik, M. S. (2016). Model Assisted POD of Laser-Ultrasonics NDT for Train Axles: A Review. *International Conference on Electrical, Electronics, and Optimization Techniques (ICEEOT)*, 4645–4648. https://doi.org/10.1109/ICEEOT.2016.7755600

Malo, S., Fateri, S., Livadas, M., Mares, C., & Gan, T. H. (2017). Wave Mode Discrimination of Coded Ultrasonic Guided Waves Using Two-Dimensional Compressed Pulse Analysis. *IEEE Transactions on Ultrasonics, Ferroelectrics, and Frequency Control*, *64*(7), 1092–1101. https://doi.org/10.1109/TUFFC.2017.2693319

Merabet, L., Robert, S., Prada, C., & Langevin, I. (2016). Development and Evaluation of f-k Migration Methods for Fast Ultrasonic Imaging in Solids. *IEEE International Ultrasonics Symposium (IUS)*, 16–19. https://doi.org/10.1109/ULTSYM.2016.7728685

Mineo, C., MacLeod, C., Morozov, M., & Pierce, S. G. (2016). Fast Ultrasonic Phased Array Inspection of Complex Geometries Delivered Through Robotic Manipulators and High Speed Data Acquisition Instrumentation. *IEEE International Ultrasonics Symposium, IUS*, *2016–Novem*, 16–19. https://doi.org/10.1109/ULTSYM.2016.7728746

Mineo, C., Summan, R., Riise, J., Macleod, C. N., & Pierce, S. G. (2017). Introducing a New Method for Efficient Visualization of Complex Shape 3D Ultrasonic Phased-Array C-Scans. *IEEE International Ultrasonics Symposium (IUS)*, *978*(3383), 2–5. https://doi.org/10.1109/ULTSYM.2017.8092990

Moallemi, N., Member, S., Shahbazpanahi, S., & Member, S. (2014). A Distributed Reflector Localization Approach to Ultrasonic Array Imaging in Non-Destructive Testing Applications. *IEEE Transactions on Signal Processing*, *62*(15), 3863–3873. https://doi.org/10.1109/TSP.2014.2329276

Moallemi, N., & Shahbazpanahi, S. (2014). Ultrasonic Array Imaging for Immersion Non-Destructive Testing. *Proceedings of the IEEE Sensor Array and Multichannel Signal Processing Workshop*, (6), 185–188. https://doi.org/10.1109/SAM.2014.6882371

Molero-armenta, M., Iturrarán-viveros, U., Aparicio, S., & Hernández, M. G. (2014). Optimized OpenCL Implementation of the Elastodynamic Finite Integration Technique for Viscoelastic Media. *Computer Physics Communications*, *10*(4655), 1–14. https://doi.org/10.1016/j.cpc.2014.05.016

Mosey, S., Sutcliffe, M., Weston, M., Knight-gregson, B., Liaptsis, D., & Talbot. (2014). Development and Implementation of Calibration Process for Full Matrix Capture. *53rd Annual Conference of the British Institute for Non-Destructive Testing*, (September), 1–10. Manchester: NDT.

Nazarchuk, Z. (2017). Propagation of Elastic Waves in Solids. *Acoustic Emission*, *2*(3), 29–73. https://doi.org/10.1007/978-3-319-49350-3

Noufid, A., & Belattar, S. (2016). Diagnosis on Concrete Structures In-Situ with Non-Destructive Testing: Sonic Auscultation & Rebond Hammer. *International Conference on Electrical Sciences and Technologies in Maghreb (CISTEM)*, *978*(17258969), 7–10. https://doi.org/10.1109/CISTEM.2016.8066793

Omar, M. (2012). Nondestructive Testing Methods and New Applications. In *Nondestructive Testing Methods and New Applications*. https://doi.org/10.5772/2227

Parfomak, P. W. (2015). Keeping America's Pipelines Safe and Secure: Key Issues for Congress. *Oil and Gas Transportation: Pipeline and Rail Infrastructure Issues*, 93–140. https://doi.org/10.1002/9781634638852.ch3

Park, H. J., Kang, M. J., & Rhee, S. (2009). Study on the Welding Technology of a Pleated Type Metallic Filter using Micropulse Gas Tungsten Arc Welding. *International Journal of Advanced Manufacturing Technology*, *45*(1–2), 25–32. https://doi.org/10.1007/s00170-009-1954-6

Parthipan, T., Jackson, P., Chong, A., Legg, M., & Mohimi, A. (2014). Long Range Ultrasonic Inspection of Aircraft Wiring. *IEEE International Symposium on Industrial Electronics*, *2*(23), 1289–1294. https://doi.org/10.1109/ISIE.2014.6864800

Pei, N., & Bond, L. J. (2015). Acoustoelastic Lamb wave analysis in thin plates. *IEEE Far East NDT New Technology & Application Forum (FENDT)*, 1–7. https://doi.org/10.1109/FENDT.2015.7398329

Peng, C. Y., Gao, X. R., Yang, Y., Wang, A., Wu, D. D., & Zhao, J. Y. (2016). Research on Axle Press-Fit Defects Detection Optimizing. *Proceedings of 2015 IEEE Far East NDT New Technology and Application Forum, FENDT 2015*, 277–281. https://doi.org/10.1109/FENDT.2015.7398354

Peng, H., Sabate, J., & Wall, K. (2017). High Frequency GaN-based Ultrasound Pulse Generator for High Energy Delivery. *IEEE Applied Power Electronics Conference and Exposition (APEC)*, 1652–1658. https://doi.org/10.1109/APEC.2017.7930921

Pipa, D. R., Guarneri, G. A., & Moura, H. L. De. (2017). Adaptive Time Corrected Gain for Ultrasound Through Time-Varying Wiener Deconvolution. *25th European Signal Processing Conference (EUSIPCO)*, 2–5. https://doi.org/10.23919/EUSIPCO.2017.8081657

Ramadas, S. N., Jackson, J. C., Dziewierz, J., Leary, R. O., & Gachagan, A. (2014). Application of Conformal Map Theory for Design of 2-D Ultrasonic Array Structure for NDT Imaging Application : A Feasibility Study. *IEEE*, *61*(3), 496–504.

Ricci, M., Laureti, S., Hutchins, D., & Davis, L. (2013). A Comparison of Coded Waveforms for Air-Coupled Ultrasonic Inspection. *18th International Conference on Digital Signal Processing (DSP)*, 1–6. https://doi.org/10.1109/ICDSP.2013.6622786

Sause, M. G. R. (2016). Propagation of Elastic Waves in Solids Elasticity. In *Springer Series in Materials Science* (Vol. 242). https://doi.org/10.1007/978-3-319-30954-5_4

Savenkov, M., Turner, M., Peralta-gorisse, A., & Services, T. (2015). Innovative Robotic Technology for Monitoring the Integrity of Generator Retaining Rings . *IEEE Far East NDT New Technology & Application Forum (FENDT)*, 1–4. https://doi.org/10.1109/FENDT.2015.7398298

Scianna, A., Jiang, Z., Christenson, R., & Dewolf, J. (2012). Implementation of a Probabilistic Structural Health Monitoring Method on a Highway Bridge. *Advances in Civil Engineering*, *2012*(5), 1–9. https://doi.org/10.1155/2012/307515

Shahdin, A., Morlier, J., Gourinat, Y., Shahdin, A., Morlier, J., & Gourinat, Y. (2018). Damage Monitoring in Sandwich Beams by Modal Parameter Shifts : A Comparative Study of Burst Random and Sine Dwell Vibration Testing. *Journal of Sound and Vibration, Elsevier*, *3*(5), 566–584. https://doi.org/10.1016/j.jsv.2009.09.029

Shen, Y. (2014). Structural Health Monitoring Using Linear and Nonlinear Ultrasonic Guided Waves. In *scholarcommons*. https://doi.org/10.1007/978-3-662-05615-8_6

Shen, Y., & Giurgiutiu, V. (2014). Predictive Modeling of Nonlinear Wave Propagation for Structural Health Monitoring with Piezoelectric Wafer Active Sensors. *Journal of Intelligent Material Systems and Structures*, *25*(4), 506–520. https://doi.org/10.1080/13683500.2014.912206

Sheng, D. G., Jun, W. Y., Yuan, Y. F., & Zhao Qing, C. (1998). Axisymmetric Guided Waves in Cylindrical Composite Structures with Weak Interfaces. *ACTA PHYSICA SINICA*, *98*(47), 28–34. https://doi.org/1000-3290/98/47(1)/0027-08

Singh, A. K., Singh, G. P., & Sudheera, K. (2015). Weld Flaw Characterization Through Mathematical Modeling from Ultrasonic Signal. *2015 International Conference on Communication and Signal Processing, ICCSP 2015*, 1539–1543. https://doi.org/10.1109/ICCSP.2015.7322774

Sirohi, J., & Chopra, I. (2000). Fundamental Understanding of Piezoelectric Strain Sensors. *Journal of Intelligent Material Systems and Structures*, *11*(4), 246–257. https://doi.org/10.1106/8BFB-GC8P-XQ47-YCQ0

Song, S., Li, Y., Wang, Y., & Du, Y. (2015). Ultrasonic Signal Compressive Sampling and Its Application in Pipeline Flaw Inner Inspection. *IEEE Far East NDT New Technology & Application Forum (FENDT)*, 9–12. https://doi.org/10.1109/FENDT.2015.7398310

Strantza, M., Aggelis, D. G., de Baere, D., Guillaume, P., & van Hemelrijck, D. (2015). Evaluation of SHM System Produced by Additive Manufacturing via Acoustic Emission and Other NDT Methods. *Sensors (Switzerland)*, *15*(10), 26709–26725. https://doi.org/10.3390/s151026709

Su, H., Luo, Z., Cao, H., Zhou, B., & Lin, L. (2016). Focal Law Design for Phased Array Ultrasonic Testing of CFRP Based on Finite Element Modeling. *IEEE Far East NDT New Technology & Application Forum (FENDT)*, 2–6. https://doi.org/10.1109/FENDT.2016.7991991

Su, Z., Ã, L. Y., & Lu, Y. (2006). Guided Lamb Waves for Identification of Damage in Composite Structures : A Review. *Journal of Sound and Vibration*, *295*, 753–780. https://doi.org/10.1016/j.jsv.2006.01.020

Sudheera, K., Nandhitha, N. M., Ganesh, N. V. S. L., Nanekar, P., Venkatraman, B., & Rani, B. S. (2014). Feasibility of Stockwell Transform for Flaw Pattern Recognition in Ultra Sonic Signals. *International Conference on Communication and Signal Processing*, *978*(3358), 962–965. https://doi.org/10.1109/ICCSP.2014.6949987

Tang, D., Yao, X., Wu, G., & Peng, Y. (2017). Free and Forced Vibration Analysis of Multi-Stepped Circular Cylindrical Shells with Arbitrary Boundary Conditions by the Method of Reverberation-Ray Matrix. *Thin-Walled Structures*, *116*, 154–168. https://doi.org/10.1016/j.tws.2017.03.023

Tatarnikov, D. A., Tsapko, G. P., & Pochivalov, Y. I. (2015). Optimization of Image Synthesis for Complex Geometry Objects in the Robotic Ultrasonic System. *International Conference on Mechanical Engineering, Automation and Control Systems (MEACS)*, *978*(8114), 1–4. https://doi.org/10.1109/MEACS.2015.7414866

Thomas, G., Emadi, A., Mijares-chan, J., & Buchanan, D. A. (2014). Low Frequency Ultrasound NDT of Power Cable Insulation. *IEEE International Instrumentation and Measurement Technology Conference (I2MTC) Proceedings*, 2–5. https://doi.org/10.1109/I2MTC.2014.6860918

Tian, F., Hao, Y., Zou, Z., Zheng, Y., He, W., Yang, L., & Li, L. (2019). An Ultrasonic Pulse-Echo Method to Detect Internal Defects in Epoxy Composite Insulation. *Energies*, *12*(24), 1–17. https://doi.org/10.3390/en12244804

Tiyasri, N., & Poopat, B. (2013). Welding Procedure Development for Welding of High Strength Carbon Steel Cladded with Austenitic Stainless Steel 316L by Using Overmatching Filler Metal. *Key Engineering Materials*, *545*, 182–187. https://doi.org/10.4028/www.scientific.net/kem.545.182

Tucker, R. W., Kercel, S. W., & Varma, K. (2003). Characterization of Gas Pipeline Flaws Using Wavelet Tucker. *Journal of Optical Microsystems*, *5132*(3), 485–493. https://doi.org/10.1117/12.515157

Tzou, H. S., & Cadre, M. (1989). Theoretical Coupled for Analysis Distributed of Multi-Layered Controls Thin With Piezoelectric Vibration. *Journal of Sound and Vibration*, *132*(3), 433–450. https://doi.org/10.1016/0022-460X(89)90637-8

Uus, A., Liatsis, P., Nardoni, G., & Rahman, E. (2015). Optimisation of Transducer Positioning in Air-Coupled Ultrasound Inspection of Concrete / Asphalt Structures. *International Conference on Systems, Signals and Image Processing (IWSSIP)*, *978*(1), 309–312. https://doi.org/10.1109/IWSSIP.2015.7314237

Victor, G. (2010). Structural Health Monitoring with Piezoelectric Wafer Active Sensors: Predictive Modeling and Simulation. *Incas Bulletin*, *2*(3), 31–44. https://doi.org/10.13111/2066-8201.2010.2.3.4

Vinckier, A., & Dhooge, A. (1979). Reheat Cracking in Welded Structures During Stress Relief Heat Treatments. *Journal of Heat Treating*, *1*(1), 72–80. https://doi.org/10.1007/BF02833212

Wang, B., & Saniie, J. (2017). Ultrasonic Target Echo Detection using Neural Network. *IEEE International Conference on Electro Information Technology (EIT)*, 286–290. https://doi.org/10.1109/EIT.2017.8053371

Wei-Can, G., Shi, J. F., & Hou, D. S. (2017). Research on Phased Array Ultrasonic Technique for Testing Butt Fusion Joint in Polyethylene Pipe. *Proceedings of 2016 IEEE Far East NDT New Technology and Application Forum, FENDT 2016*, 1–5. https://doi.org/10.1109/FENDT.2016.7991983

Wu, G., Zhou, E., Wang, R., Zhang, Q., & Zheng, T. (2015). The Experimental Research of The Damage Resistance of Low-Energy Impacted Carbon Fiber Composite Materials. *IEEE Far East NDT New Technology & Application Forum (FENDT)*, 110–114. https://doi.org/10.1109/FENDT.2015.7398321

Xiaodan, X., Zhenxiang, G., Yi, R., Haitao, W., Kai, Z., & Wei, S. (2015). Research and Design of CNG Gas Well Detection System. *IEEE Far East NDT New Technology & Application Forum (FENDT)*, 3–6. https://doi.org/10.1109/FENDT.2015.7398346

Xie, F., Zhuang, C., Jiang, H., Fan, P., & Ren, Y. (2016). Damage Assessment of Real-Size T-Beam From Deficient Prestressed Concrete Bridge Using Ultrasonic Coda Waves. *IEEE Far East NDT New Technology & Application Forum (FENDT)*, 22–25. https://doi.org/10.1109/FENDT.2016.7991987

Xin, P., Yang, L., & Li, Y. (2014). Mechanism and Application of EMAT Technology Based on NDT. *China International Conference on Electricity Distribution, CICED*, *2014–Decem*(Ciced), 100–102. https://doi.org/10.1109/CICED.2014.6991672

Xu, Y., Yang, Z. F., Zhou, H. Q., & Zhang, W. Bin. (2016). Application of Acoustoelasticity in Studying Compressive Stress State in Polymer Bonded Explosive. *Proceedings of 2015 IEEE Far East NDT New Technology and Application Forum, FENDT 2015*, 95–99. https://doi.org/10.1109/FENDT.2015.7398318

Xu, Z., Yu, H., & Wang, Y. (2015). The Effect Of Joint Geometry Parameters On Ultrasonic Weld-Guided Modes In Thick Steel Plates. *Symposium on Piezoelectricity, Acoustic Waves, and Device Applications (SPAWDA)*, 329–335. https://doi.org/10.1109/SPAWDA.2015.7364501

Y. Zou, L. T. and G. P. S. (2006). Vibration-Based Model-Dependent Damage (Delamination) Identification And Health Monitoring For Composite Structures— A Review. *Journal of Sound and Vibrationibration*, *230*(2000), 357–378. https://doi.org/10.1006/jsvi.1999.2624

Ye, C., Luo, L., Gao, X., Jiang, L., & Yue, H. (2015). Cross-correlation Phase Correction Method on Ultrasonic Synthetic Focused Signal Distortion. *IEEE Far East NDT New Technology & Application Forum (FENDT)*, 1–6. https://doi.org/10.1109/FENDT.2015.7398344

Yu, L., & Giurgiutiu, V. (2008). In Situ 2-D Piezoelectric Wafer Active Sensors Arrays for Guided Wave Damage Detection. *Ultrasonics*, *48*(2), 117–134. https://doi.org/10.1016/j.ultras.2007.10.008

Yu, L., Santoni-Bottai, G., Xu, B., Liu, W., & Giurgiutiu, V. (2008). Piezoelectric Wafer Active Sensors for In-Situ Ultrasonic-Guided Wave SHM. *Fatigue and Fracture of Engineering Materials and Structures*, *31*(8), 611–628. https://doi.org/10.1111/j.1460-2695.2008.01256.x

Yücel, M. K., Fateri, S., Legg, M., Wilkinson, A., Kappatos, V., Selcuk, C., & Gan, T. H. (2015). Pulse-Compression Based Iterative Time-Of-Flight Extraction of Dispersed Ultrasonic Guided Waves. *Proceeding - 2015 IEEE International Conference on Industrial Informatics, INDIN 2015*, 809–815. https://doi.org/10.1109/INDIN.2015.7281840

Yücel, M. K., Fateri, S., Legg, M., Wilkinson, A., Kappatos, V., Selcuk, C., & Gan, T. H. (2016). Coded Waveform Excitation for High-Resolution Ultrasonic Guided Wave Response. *IEEE Transactions on Industrial Informatics*, *12*(1), 257–266. https://doi.org/10.1109/TII.2015.2501762

Yue, H., Luo, L., & Gao, X. (2014). Correction Technique of Phase Aberration in Ultrasonic Synthetic Focusing Signal. *IEEE Far East Forum on Nondestructive Evaluation/Testing*, 74–89. https://doi.org/10.1109/FENDT.2014.6928236

Zagrai, A., Doyle, D., Gigineishvili, V., Brown, J., Gardenier, H., & Arritt, B. (2010). Piezoelectric Wafer Active Sensor Structural Health Monitoring of Space Structures. *Journal of Intelligent Material Systems and Structures*, *21*(9), 921–940. https://doi.org/10.1177/1045389X10369850

Zhang, L. (2014). A Multichannel Data Acquisition System Design for Guided Waves Ultrasound Testing. *IEEE Far East Forum on Nondestructive Evaluation/Testing*, 1–5. https://doi.org/10.1109/FENDT.2014.6928240

Zhang, Y., Tan, Y., Peng, J., Peng, C., Yang, K., & Gao, X. (2016). LU Automatic Ultrasonic Inspection System for In-service Wheelset and Its Application. *18th International Wheelset Congress (IWC)*, 100–104. https://doi.org/10.1109/IWC.2016.8068376

Zhao, L., & Rudlin, J. (2014). Development of An Advanced Ultrasonic Inspection Tool for Rapid Volumetric Examination of Aluminothermic Rail Welds. *IEEE Far East Forum on Nondestructive Evaluation/Testing*, 354–358. https://doi.org/10.1109/FENDT.2014.6928295

Zhao, Y., Zhang, Z., Wang, Q., Chen, J., Song, J., Guo, R., & Liu, S. (2016). Laser-Based Ultrasonic Detection by Using All-Fiber Adaptive Fiber Bragg Grating Sensors. *IEEE Far East NDT New Technology & Application Forum (FENDT)*, 201–205. https://doi.org/10.1109/FENDT.2016.7992024

Zhong, C. H., Croxford, A. J., & Wilcox, P. D. (2013). Investigation of Inductively Coupled Ultrasonic Transducer System for NDE. *IEEE Transactions on Ultrasonics, Ferroelectrics, and Frequency Control*, *60*(6), 1115–1125. https://doi.org/10.1109/TUFFC.2013.2674

Zhong, G., Tian, G. Y., Meng, J. S., & Gao, B. (2017). Excitation Power Design Base on Series Resonant Electromagnetic Ultrasonic Sensor for Pipeline NDT. *Proceedings of 2016 IEEE Far East NDT New Technology and Application Forum, FENDT 2016*, 2–6. https://doi.org/10.1109/FENDT.2016.7992011

Zhou, W., Li, H., & Yuan, F. G. (2014). Guided Wave Generation, Sensing and Damage Detection Using In-Plane Shear Piezoelectric Wafers. *Smart Materials and Structures*, *23*(1), 1–11. https://doi.org/10.1088/0964-1726/23/1/015014

APPENDIX   A

MATLAB SIMULINK PROGRAMMING CODE

```
/-----------------------------------------------------------------------------
---------------------------------
/---------------------------matlab i/o-----------------------------------------
-----------------------------
/-----------------------------------------------------------------------------
---------------------------------
/*
* Academic License - for use in teaching, academic
research, and meeting
* course requirements at degree granting institutions
only. Not for
* government, commercial, or other organizational use.
*
* File: test2.c
*
* Code generated for Simulink model 'test2'.
*
* Model version : 1.1
* Simulink Coder version : 8.9 (R2015b) 13-Aug-2015
* C/C++ source code generated on : Tue Sep 20 00:35:21
2016
*
* Target selection: ert.tlc
* Embedded hardware selection: Atmel->AVR
* Code generation objectives: Unspecified
* Validation result: Not run
*/
#include "test2.h"
#include "test2_private.h"
#include "test2_dt.h"
/* Block signals (auto storage) */
B_test2_T test2_B;
/* Block states (auto storage) */
DW_test2_T test2_DW;
/* Real-time model */
RT_MODEL_test2_T test2_M_;
RT_MODEL_test2_T *const test2_M = &test2_M_;
static void rate_monotonic_scheduler(void);
/*
* Set which subrates need to run this base step (base
rate always runs).
* This function must be called prior to calling the model
step function
```

```
* in order to "remember" which rates need to run this
base step. The
* buffering of events allows for overlapping preemption.
*/
void test2_SetEventsForThisBaseStep(boolean_T
*eventFlags)
{
/* Task runs when its counter is zero, computed via
rtmStepTask macro */
eventFlags[1] = ((boolean_T)rtmStepTask(test2_M, 1));
}
```

```
/*
* This function updates active task flag for each subrate
* and rate transition flags for tasks that exchange data.
* The function assumes rate-monotonic multitasking
scheduler.
* The function must be called at model base rate so that
* the generated code self-manages all its subrates and
rate
* transition flags.
*/
static void rate_monotonic_scheduler(void)
{
/* Compute which subrates run during the next base time
step. Subrates
* are an integer multiple of the base rate counter.
Therefore, the subtask
* counter is reset when it reaches its limit (zero means
run).
*/
(test2_M->Timing.TaskCounters.TID[1])++;
if ((test2_M->Timing.TaskCounters.TID[1]) > 999) {/*
Sample time: [1.0s, 0.0s] */
test2_M->Timing.TaskCounters.TID[1] = 0;
}
}
/* Model step function for TID0 */
void test2_step0(void) /* Sample time: [0.001s, 0.0s] */
{
{ /* Sample time: [0.001s, 0.0s] */
rate_monotonic_scheduler();
}
/* S-Function (arduinoanaloginput_sfcn): '<Root>/Analog
Input' */
test2_B.AnalogInput =
MW_analogRead(test2_P.AnalogInput_p1);
/* External mode */
rtExtModeUploadCheckTrigger(2);
rtExtModeUpload(0, test2_M->Timing.taskTime0);
/* signal main to stop simulation */
{ /* Sample time: [0.001s, 0.0s] */
if ((rtmGetTFinal(test2_M)!=-1) &&
!((rtmGetTFinal(test2_M)-test2_M->Timing.taskTime0) >
test2_M->Timing.taskTime0 * (DBL_EPSILON))) {
rtmSetErrorStatus(test2_M, "Simulation finished");
}
if (rtmGetStopRequested(test2_M)) {
rtmSetErrorStatus(test2_M, "Simulation finished");
}
}
/* Update absolute time */
```

```
/* The "clockTick0" counts the number of times the code
of this task has
* been executed. The absolute time is the multiplication
of "clockTick0"
```

```
* and "Timing.stepSize0". Size of "clockTick0" ensures
timer will not
* overflow during the application lifespan selected.
*/
test2_M->Timing.taskTime0 =
(++test2_M->Timing.clockTick0) * test2_M-
>Timing.stepSize0;
}
/* Model step function for TID1 */
void test2_step1(void) /* Sample time: [1.0s, 0.0s] */
{
/* S-Function (arduinoanaloginput_sfcn): '<Root>/Analog
Input1' */
test2_B.AnalogInput1 =
MW_analogRead(test2_P.AnalogInput1_p1);
rtExtModeUpload(1, ((test2_M->Timing.clockTick1) ));
/* Update absolute time */
/* The "clockTick1" counts the number of times the code
of this task has
* been executed. The resolution of this integer timer is
1.0, which is the step size
* of the task. Size of "clockTick1" ensures timer will
not overflow during the
* application lifespan selected.
*/
test2_M->Timing.clockTick1++;
}
/* Model step wrapper function for compatibility with a
static main program */
void test2_step(int_T tid)
{
switch (tid) {
case 0 :
test2_step0();
break;
case 1 :
test2_step1();
break;
default :
break;
}
}
/* Model initialize function */
void test2_initialize(void)
{
/* Registration code */
/* initialize real-time model */
(void) memset((void *)test2_M, 0,
sizeof(RT_MODEL_test2_T));
rtmSetTFinal(test2_M, 100.0);
test2_M->Timing.stepSize0 = 0.001;
```

```
/* External mode info */
test2_M->Sizes.checksums[0] = (2430959298U);
test2_M->Sizes.checksums[1] = (3618791490U);
test2_M->Sizes.checksums[2] = (3634927182U);
test2_M->Sizes.checksums[3] = (1144932162U);
```

```
{
static const sysRanDType rtAlwaysEnabled =
SUBSYS_RAN_BC_ENABLE;
static RTWExtModeInfo rt_ExtModeInfo;
static const sysRanDType *systemRan[1];
test2_M->extModeInfo = (&rt_ExtModeInfo);
rteiSetSubSystemActiveVectorAddresses(&rt_ExtModeInfo,
systemRan);
systemRan[0] = &rtAlwaysEnabled;
rteiSetModelMappingInfoPtr(test2_M->extModeInfo,
&test2_M->SpecialInfo.mappingInfo);
rteiSetChecksumsPtr(test2_M->extModeInfo, test2_M-
>Sizes.checksums);
rteiSetTPtr(test2_M->extModeInfo, rtmGetTPtr(test2_M));
}
/* block I/O */
(void) memset(((void *) &test2_B), 0,
sizeof(B_test2_T));
/* states (dwork) */
(void) memset((void *)&test2_DW, 0,
sizeof(DW_test2_T));
/* data type transition information */
{
static DataTypeTransInfo dtInfo;
(void) memset((char_T *) &dtInfo, 0,
sizeof(dtInfo));
test2_M->SpecialInfo.mappingInfo = (&dtInfo);
dtInfo.numDataTypes = 14;
dtInfo.dataTypeSizes = &rtDataTypeSizes[0];
dtInfo.dataTypeNames = &rtDataTypeNames[0];
/* Block I/O transition table */
dtInfo.B = &rtBTransTable;
/* Parameters transition table */
dtInfo.P = &rtPTransTable;
}
/* Start for S-Function (arduinoanaloginput_sfcn):
'<Root>/Analog Input' */
MW_pinModeAnalogInput(test2_P.AnalogInput_p1);
/* Start for S-Function (arduinoanaloginput_sfcn):
'<Root>/Analog Input1' */
MW_pinModeAnalogInput(test2_P.AnalogInput1_p1);
}
/* Model terminate function */
void test2_terminate(void)
{
/* (no terminate code required) */
}
/*
* File trailer for generated code.
*
* [EOF]
```

```
*/
```

APPENDIX B

HARDWARE PZ-LW SYSTEM SPECIFICATION

B1   The Commercial Ultrasonic Testing Set Unit

The USM Go is a portable ultrasonic flaw detector. In addition to its
light-weight design, the USM Go includes a clean and simple user
interface and a large, easy-to-read colour WVGA (800x480) display.
When operating in Acquire Mode, the instrument provides ultrasonic
flaw detection and thickness measurements. In this mode, it is capable
of storing A-Scans, operating parameters, and reports. Prior to using the
Acquire Mode, the instrument displays and operating parameters must
be configured by using the Setup Mode.

Calibration blocks (Stage wage) is an important supplementary material in the Ultrasonic testing, used to calibrate the sensitivity of the ultrasonic flaw detector and ultrasonic probe. The stage wage are domestic standards UT blocks, European standard UT block, NDT block, hexagonal testing block, and so on. The material for stage wage fabricating including Duplex Stainless Steel, 1018 Carbon Steel, LY12/6063/7075 Aluminum,304 Stainless Steel with dimension 200mm x 20mm x 20mm.
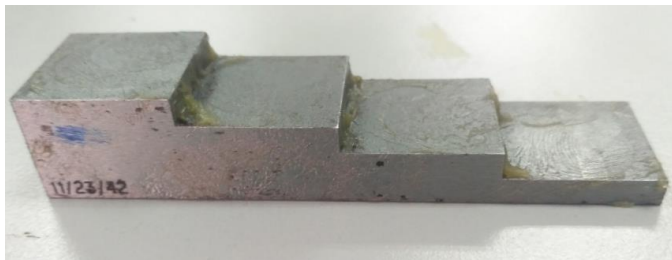
Figure B1.2 Stage Wage

V2 block have the size 12.5mm thick small calibration block for on-site checking of miniature shear wave probe index, time base, beam angle and gain. Includes a 25mm and 50 mm radius, 1.5mm hole (or 5mm), engraved reference mark scales from 35 to 75 degrees. In accordance with British Standard BS 2704 block A4, Fig. 4, and AS 2083.

• Dimensions: 75mm x 43mm x 12.5mm
• Made from titanium.

• Also available in 20mm and 25mm thicknesses for calibration of non-miniature probes.

Figure B1.3 V2 Block

Plotting card is always used to find the actual distance probe in UT inspection at welding joint inspection. From here the shape of weldment are considering in defect identification. A few calculations should be used to ensure that the actual positioning defect on the weldment could identified with comparing the actual signal on the UT inspection. From here the name of defect can be identified based on the positioning defect in the weldment.
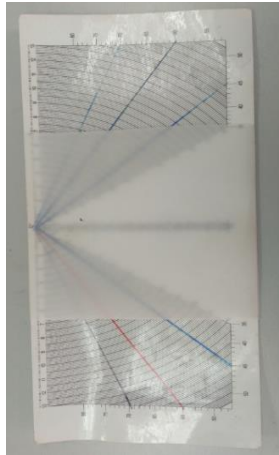
Figure B1.4 Plotting Card

C 333 dense complaint gel, special for corroded surfaces, welding, fused and forged, concave and convex surfaces. The product can also be supplied as powder to be mixed with water. It guarantees best coupling on "hard" surfaces, with more penetration and amplitude of ultrasonic signal. It dries on the surface leaving a white-blue powder, non-slippery, to be removed by washing, sanding, etc. Operating temperature range from 0 to + 90 'C.

Figure B1.5 Grease

Single Element Contact Transducers are longitudinal wave transducers designed for general purpose manual ultrasonic inspection where test materials are relatively flat and smooth. Contact transducers provide high sensitivity for better penetration and are ruggedly constructed for extended service life under the roughest testing conditions.

Figure B1.6 UT Probe

Analysis of the width of defect by Commercial Ultrasonic Probe

The commercial Ultrasonic probe (EG phase) was used to examine the influence of the types defect on Ultrasonic testing. The V2 block and Stage Wage block of the carbon steel pipe are used as shown in Figure 4. 33. Three type of artificial defects with different shape of hole, axial and gradient axial defect were used to get the relationship between the physical dimension of the machined cracks and the response of the ultrasonic testing to provide a general view of the crack shape. The types of probe used is 60-degree probe with the frequency setting is 2Mhz. The experiment setup already explains on Section 3.7 under material & methodology.

Figure B1.7 Ultrasonic Probe Measuring Pipe Defect

Based on the result from Figure 4.34 show the higher amplitude of signal is come from axial defect where the amplitude is 29.54 dB. Other than that the width of signal is 15 mm within start from 20mm until 35mm. The thereshold is only 9% where the signal gain is 55.2db.

Figure B1.8 Axial Defect Result

The second testing is make for gradient axial defect. In Figure 4.35 show the amplitude and width of signal almost 0. This means the gradient defect is very difficult to measuring either with commercial probe. The amplitude of defect is show is very near to the death zone and it can't be taken or considering on measurement.

Figure B1.9 Gradient Axial Defect Result

Lastly the UT commercial probe are tested on the hole defect Figure 4.36. From here the amplitude are obtain from inspection is 23.39. The width of signal is 10mm start from 20mm until 30mm positioning signal. The percentage of signal is 32% comparing the axial defect on Figure 4.30 is 82%.
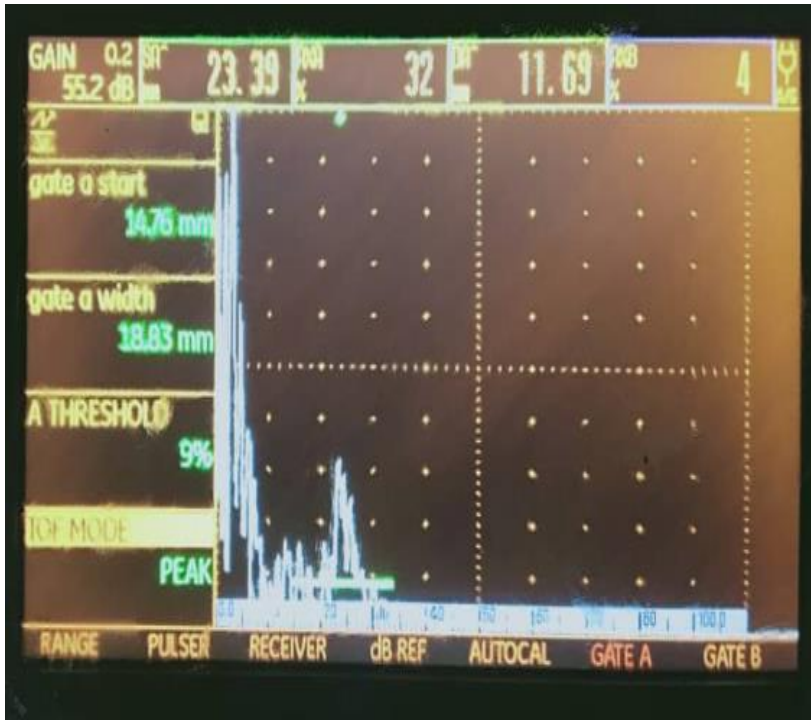
Figure B1.10 Hole Defect Result

C.1 Print Screen shot for Dispersion Curve for steel pipe (60 mm diameter, 4mm wall thickness) Crated by Matlab GUIGUW

(a)

(b)

Dispersion Curve (Group Velocity)

(c)

259

Dispersion Curve (Phase Velocity)
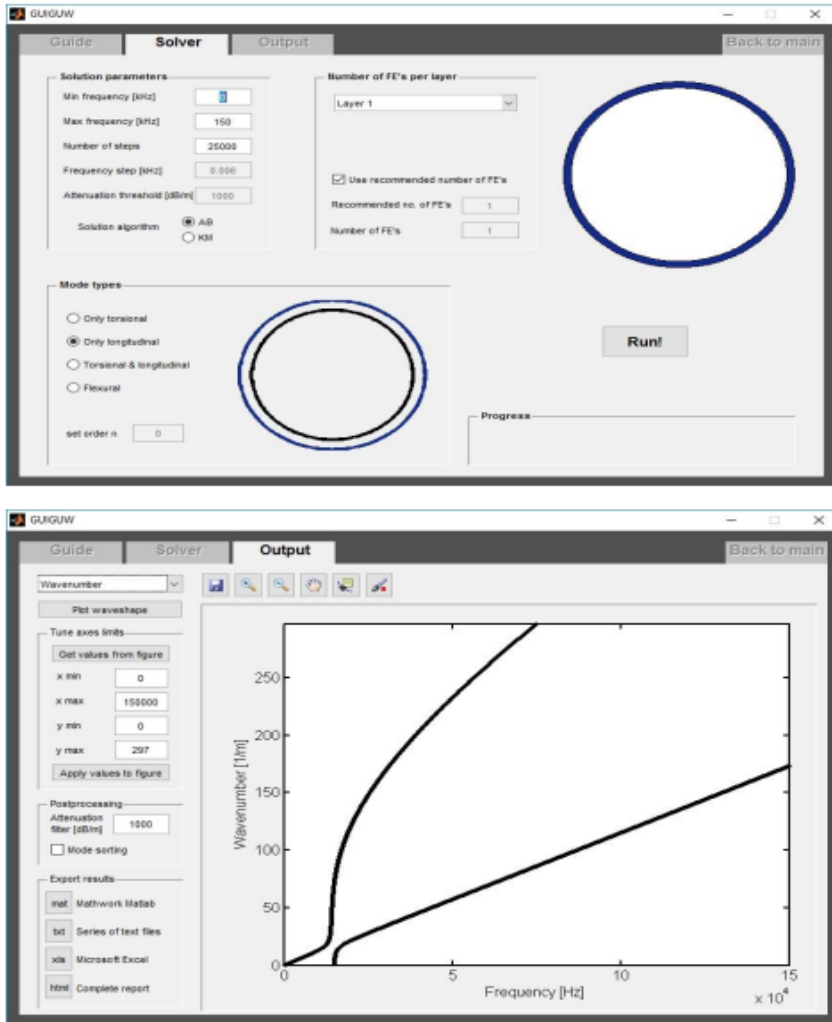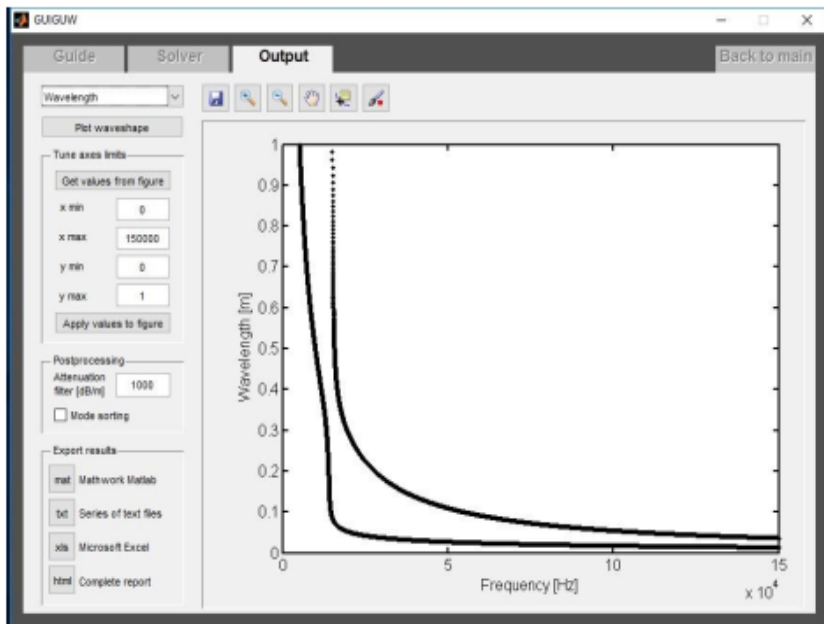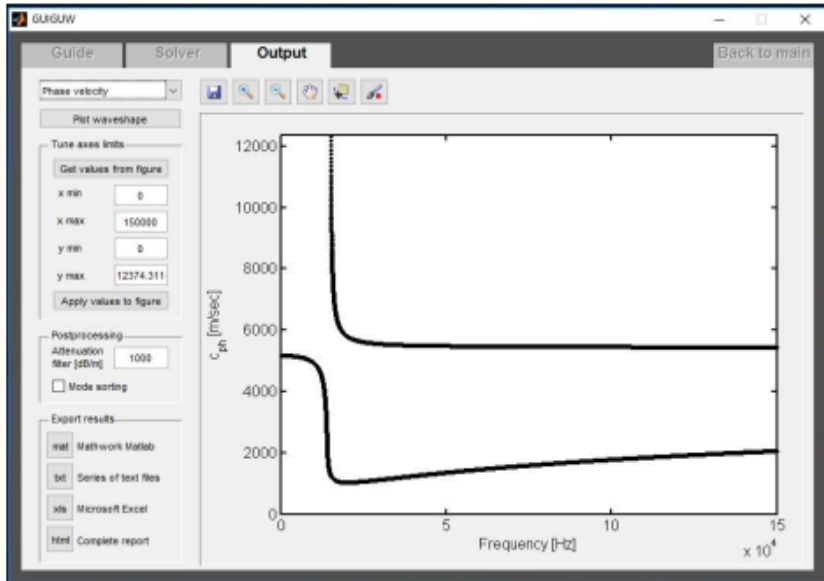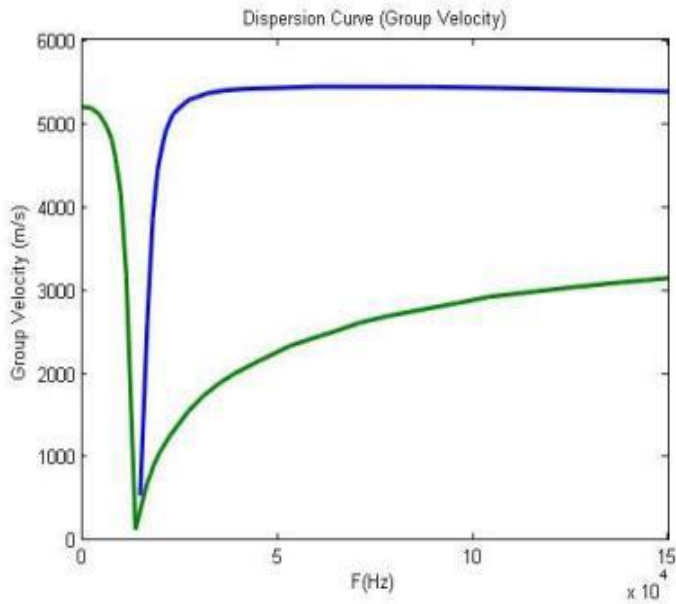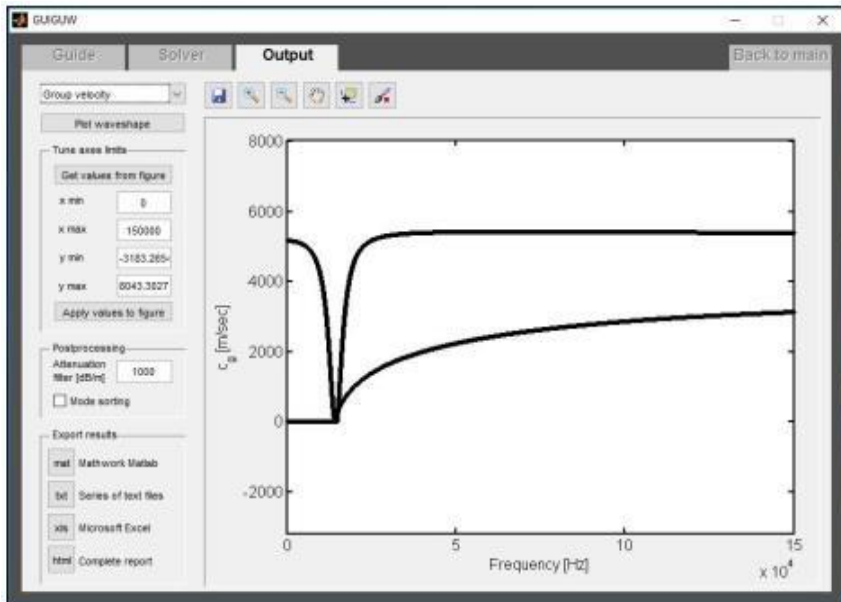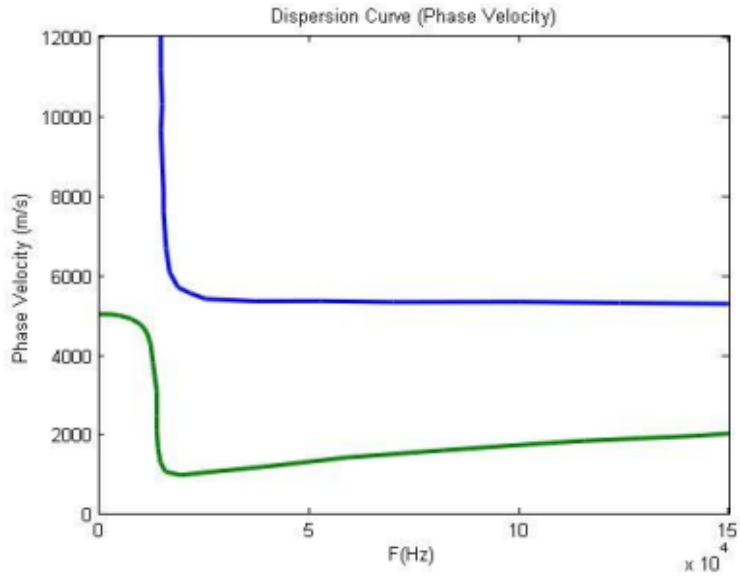
(d)

Figure C.1 Dispersion curve (a) Pipe size design for solver in longitudinal condition with maximum y value 297 and wave number (1/m), (b) Result of dispersion with wavelength (m), (c) Dispersion with group velocity (m/s), (d) Dispersion curve with phase velocity

APPENDIX D
SIGNAL DATA

Table D1.1 Table of Excitation and Reflection Hole Defect Signal

Sample Rate:	750000	Hz			
Measurement Type	Time Waveform	Time Waveform	Time Waveform	Time Waveform	Time Waveform
Channel Name	DT9816-S(00).Ain 0	DT9816-S(00).Ain 1	DT9816-S(00).Ain 2	DT9816-S(00).Ain 3	DT9816-S(00).Ain 4
X Axis Units	Sec	Sec	Sec	Sec	Sec
Y Axis Units	V	V	V	V	V
Excel Time Format	Real	Real	Real	Real	Real
43733.63938	-9.08E-04	-9.04E-04	-9.16E-04	-0.001057368	-0.00129745
43733.63938	-9.08E-04	-9.04E-04	-9.16E-04	-0.001057042	-0.001296947
43733.63938	-9.07E-04	-9.04E-04	-9.16E-04	-0.001056786	-0.001296515
43733.63938	-9.07E-04	-9.04E-04	-9.15E-04	-0.001056599	-0.001296153
43733.63938	-9.07E-04	-9.03E-04	-9.15E-04	-0.00105648	-0.001295861
43733.63938	-9.07E-04	-9.03E-04	-9.16E-04	-0.00105643	-0.00129564
43733.63938	-9.07E-04	-9.03E-04	-9.16E-04	-0.001056448	-0.001295489
43733.63938	-9.07E-04	-9.03E-04	-9.16E-04	-0.001056535	-0.001295408
43733.63938	-9.07E-04	-9.03E-04	-9.16E-04	-0.00105669	-0.001295396
43733.63938	-9.07E-04	-9.04E-04	-9.16E-04	-0.001056913	-0.001295455
43733.63938	-9.07E-04	-9.04E-04	-9.17E-04	-0.001057205	-0.001295583
43733.63938	-9.07E-04	-9.04E-04	-9.17E-04	-0.001057565	-0.001295781
43733.63938	-9.08E-04	-9.04E-04	-9.18E-04	-0.001057992	-0.001296049
43733.63938	-9.08E-04	-9.05E-04	-9.18E-04	-0.001058488	-0.001296386
43733.63938	-9.08E-04	-9.05E-04	-9.19E-04	-0.001059052	-0.001296793
43733.63938	-9.09E-04	-9.06E-04	-9.20E-04	-0.001059683	-0.001297269
43733.63938	-9.09E-04	-9.06E-04	-9.20E-04	-0.001060382	-0.001297814
43733.63938	-9.10E-04	-9.07E-04	-9.21E-04	-0.001061149	-0.001298429
43733.63938	-9.11E-04	-9.08E-04	-9.22E-04	-0.001061983	-0.001299112
43733.63938	-9.12E-04	-9.08E-04	-9.23E-04	-0.001062884	-0.001299865
43733.63938	-9.12E-04	-9.09E-04	-9.24E-04	-0.001063853	-0.001300686
43733.63938	-9.13E-04	-9.10E-04	-9.25E-04	-0.00106489	-0.001301577
43733.63938	-9.14E-04	-9.11E-04	-9.26E-04	-0.001065993	-0.001302536
43733.63938	-9.15E-04	-9.12E-04	-9.27E-04	-0.001067164	-0.001303564
43733.63938	-9.16E-04	-9.13E-04	-9.28E-04	-0.001068401	-0.00130466
43733.63938	-9.17E-04	-9.14E-04	-9.30E-04	-0.001069706	-0.001305825
43733.63938	-9.19E-04	-9.15E-04	-9.31E-04	-0.001071078	-0.001307059
43733.63938	-9.20E-04	-9.16E-04	-9.33E-04	-0.001072516	-0.00130836
43733.63938	-9.21E-04	-9.18E-04	-9.34E-04	-0.001074021	-0.00130973
43733.63938	-9.22E-04	-9.19E-04	-9.36E-04	-0.001075593	-0.001311169
43733.63938	-9.24E-04	-9.20E-04	-9.37E-04	-0.001077231	-0.001312675
43733.63938	-9.25E-04	-9.22E-04	-9.39E-04	-0.001078936	-0.001314249
43733.63938	-9.27E-04	-9.23E-04	-9.41E-04	-0.001080707	-0.001315892
43733.63938	-9.28E-04	-9.25E-04	-9.42E-04	-0.001082544	-0.001317602

43733.63938	-9.30E-04	-9.26E-04	-9.44E-04	-0.001084448	-0.00131938
43733.63938	-9.32E-04	-9.28E-04	-9.46E-04	-0.001086418	-0.001321226
43733.63938	-9.34E-04	-9.30E-04	-9.48E-04	-0.001088454	-0.001323139
43733.63938	-9.36E-04	-9.31E-04	-9.50E-04	-0.001090556	-0.00132512
43733.63938	-9.37E-04	-9.33E-04	-9.52E-04	-0.001092724	-0.001327169
43733.63938	-9.39E-04	-9.35E-04	-9.54E-04	-0.001094958	-0.001329285
43733.63938	-9.41E-04	-9.37E-04	-9.56E-04	-0.001097258	-0.001331468
43733.63938	-9.44E-04	-9.39E-04	-9.59E-04	-0.001099623	-0.001333719
43733.63938	-9.46E-04	-9.41E-04	-9.61E-04	-0.001102055	-0.001336037
43733.63938	-9.48E-04	-9.43E-04	-9.63E-04	-0.001104551	-0.001338422
43733.63938	-9.52E-04	-9.48E-04	-9.68E-04	-0.001109741	-0.001343392
43733.63938	-9.55E-04	-9.50E-04	-9.71E-04	-0.001112435	-0.001345978
43733.63938	-9.57E-04	-9.52E-04	-9.74E-04	-0.001115193	-0.001348631
43733.63938	-9.60E-04	-9.55E-04	-9.76E-04	-0.001118017	-0.001351351
43733.63938	-9.62E-04	-9.57E-04	-9.79E-04	-0.001120906	-0.001354137
43733.63938	-9.65E-04	-9.60E-04	-9.82E-04	-0.00112386	-0.00135699
43733.63938	-9.68E-04	-9.62E-04	-9.85E-04	-0.001126879	-0.001359909
43733.63938	-9.70E-04	-9.65E-04	-9.88E-04	-0.001129963	-0.001362896
43733.63938	-9.73E-04	-9.68E-04	-9.91E-04	-0.001133113	-0.001365948
43733.63938	-9.76E-04	-9.70E-04	-9.94E-04	-0.001136327	-0.001369067
43733.63938	-9.79E-04	-9.73E-04	-9.97E-04	-0.001139605	-0.001372252
43733.63938	-9.82E-04	-9.76E-04	-1.00E-03	-0.001142949	-0.001375504
43733.63938	-9.85E-04	-9.79E-04	-0.001003043	-0.001146357	-0.001378821
43733.63938	-9.88E-04	-9.82E-04	-0.001006314	-0.00114983	-0.001382205
43733.63938	-9.91E-04	-9.85E-04	-0.001009643	-0.001153368	-0.001385655
43733.63938	-9.95E-04	-9.88E-04	-0.001013031	-0.00115697	-0.001389171
43733.63938	-9.98E-04	-9.91E-04	-0.001016477	-0.001160637	-0.001392753
43733.63938	-0.001001146	-9.94E-04	-0.001019983	-0.001164368	-0.001396401
43733.63938	-0.001004542	-9.98E-04	-0.001023547	-0.001168163	-0.001400115
43733.63938	-0.001007997	-0.001000808	-0.001027169	-0.001172023	-0.001403895
43733.63938	-0.001011511	-0.001004166	-0.00103085	-0.001175947	-0.00140774
43733.63938	-0.001015084	-0.001007579	-0.00103459	-0.001179935	-0.001411651
43733.63938	-0.001018715	-0.001011048	-0.001038388	-0.001183987	-0.001415628
43733.63938	-0.001022406	-0.001014573	-0.001042244	-0.001188104	-0.00141967
43733.63938	-0.001026154	-0.001018154	-0.001046159	-0.001192284	-0.001423778
43733.63938	-0.001029962	-0.00102179	-0.001050132	-0.001196529	-0.001427952
43733.63938	-0.001033828	-0.001025482	-0.001054164	-0.001200837	-0.001432191
43733.63938	-0.001037752	-0.00102923	-0.001058254	-0.00120521	-0.001436495
43733.63938	-0.001041735	-0.001033033	-0.001062402	-0.001209646	-0.001440865
43733.63938	-0.001045777	-0.001036892	-0.001066608	-0.001214146	-0.0014453
43733.63938	-0.001049877	-0.001040807	-0.001070872	-0.00121871	-0.001449801
43733.63938	-0.001054035	-0.001044777	-0.001075195	-0.001223338	-0.001454366
43733.63938	-0.001058252	-0.001048802	-0.001079575	-0.00122803	-0.001458997
43733.63938	-0.001062528	-0.001052883	-0.001084014	-0.001232785	-0.001463694
43733.63938	-0.001066861	-0.00105702	-0.001088511	-0.001237604	-0.001468455
43733.63938	-0.001071253	-0.001061211	-0.001093066	-0.001242487	-0.001473281
43733.63938	-0.001075703	-0.001065459	-0.001097678	-0.001247433	-0.001478173
43733.63938	-0.001080211	-0.001069761	-0.001102349	-0.001252443	-0.00148313
43733.63938	-0.001084778	-0.001074119	-0.001107078	-0.001257516	-0.001488151
43733.63938	-0.001089403	-0.001078533	-0.001111865	-0.001262653	-0.001493238
43733.63938	-0.001094086	-0.001083001	-0.001116709	-0.001267853	-0.001498389

43733.63938	-0.001098827	-0.001087525	-0.001121612	-0.001273117	-0.001503606
43733.63938	-0.001103627	-0.001092105	-0.001126572	-0.001278444	-0.001508887
43733.63938	-0.001108484	-0.001096739	-0.00113159	-0.001283835	-0.001514234
43733.63938	-0.0011134	-0.001101429	-0.001136666	-0.001289289	-0.001519645
43733.63938	-0.001118373	-0.001106174	-0.0011418	-0.001294806	-0.001525121
43733.63938	-0.001123405	-0.001110975	-0.001146992	-0.001300387	-0.001530662
43733.63938	-0.001128495	-0.001115831	-0.001152241	-0.001306031	-0.001536267
43733.63938	-0.001133643	-0.001120742	-0.001157548	-0.001311738	-0.001541938
43733.63938	-0.001138849	-0.001125708	-0.001162913	-0.001317509	-0.001547673
43733.63938	-0.001144114	-0.00113073	-0.001168336	-0.001323343	-0.001553473
43733.63938	-0.001149436	-0.001135807	-0.001173817	-0.00132924	-0.001559337
43733.63938	-0.001160255	-0.001146126	-0.001184951	-0.001341224	-0.001571261
43733.63938	-0.001165751	-0.001151369	-0.001190605	-0.001347311	-0.00157732
43733.63938	-0.001171306	-0.001156667	-0.001196317	-0.001353461	-0.001583443
43733.63938	-0.001176918	-0.00116202	-0.001202086	-0.001359674	-0.001589631
43733.63938	-0.001182589	-0.001167428	-0.001207913	-0.001365951	-0.001595884
43733.63938	-0.001188317	-0.001172892	-0.001213798	-0.001372291	-0.001602202
43733.63938	-0.001194104	-0.001178411	-0.001219741	-0.001378694	-0.001608584
43733.63938	-0.001199949	-0.001183985	-0.001225742	-0.00138516	-0.001615031
43733.63938	-0.001205852	-0.001189615	-0.0012318	-0.001391689	-0.001621543
43733.63938	-0.001211813	-0.0011953	-0.001237916	-0.001398282	-0.001628119
43733.63938	-0.001217832	-0.00120104	-0.00124409	-0.001404937	-0.00163476
43733.63938	-0.001223909	-0.001206836	-0.001250322	-0.001411656	-0.001641465
43733.63938	-0.001230044	-0.001212687	-0.001256611	-0.001418439	-0.001648236
43733.63938	-0.001236238	-0.001218594	-0.001262958	-0.001425284	-0.001655071
43733.63938	-0.00124249	-0.001224556	-0.001269364	-0.001432193	-0.00166197
43733.63938	-0.001248799	-0.001230574	-0.001275827	-0.001439164	-0.001668935
43733.63938	-0.001255167	-0.001236647	-0.001282348	-0.0014462	-0.001675964
43733.63938	-0.001261594	-0.001242775	-0.001288927	-0.001453298	-0.001683058
43733.63938	-0.001268078	-0.001248959	-0.001295564	-0.00146046	-0.001690216
43733.63938	-0.001274621	-0.001255199	-0.001302258	-0.001467685	-0.00169744
43733.63938	-0.001281222	-0.001261494	-0.001309011	-0.001474973	-0.001704728
43733.63938	-0.001287881	-0.001267845	-0.001315822	-0.001482325	-0.001712081
43733.63938	-0.001294599	-0.001274251	-0.001322691	-0.001489739	-0.001719498
43733.63938	-0.001301375	-0.001280714	-0.001329618	-0.001497218	-0.001726981
43733.63938	-0.00130821	-0.001287232	-0.001336603	-0.00150476	-0.001734529
43733.63938	-0.001315103	-0.001293805	-0.001343646	-0.001512365	-0.001742141
43733.63938	-0.001322054	-0.001300435	-0.001350748	-0.001520033	-0.001749818
43733.63938	-0.001329064	-0.00130712	-0.001357907	-0.001527766	-0.00175756
43733.63938	-0.001336133	-0.001313862	-0.001365125	-0.001535561	-0.001765368
43733.63938	-0.00134326	-0.001320659	-0.001372401	-0.00154342	-0.00177324
43733.63938	-0.001350446	-0.001327512	-0.001379736	-0.001551343	-0.001781177
43733.63938	-0.00135769	-0.001334422	-0.001387129	-0.00155933	-0.00178918
43733.63938	-0.001364994	-0.001341387	-0.00139458	-0.00156738	-0.001797247
43733.63938	-0.001372355	-0.001348409	-0.00140209	-0.001575493	-0.00180538
43733.63938	-0.001379776	-0.001355486	-0.001409658	-0.001583671	-0.001813578
43733.63938	-0.001387256	-0.00136262	-0.001417285	-0.001591912	-0.001821841
43733.63938	-0.001394795	-0.001369811	-0.00142497	-0.001600217	-0.001830169
43733.63938	-0.001402392	-0.001377058	-0.001432714	-0.001608586	-0.001838563
43733.63938	-0.001410049	-0.001384361	-0.001440517	-0.001617018	-0.001847022
43733.63938	-0.001417764	-0.00139172	-0.001448379	-0.001625515	-0.001855546

43733.63938	-0.001425539	-0.001399136	-0.001456299	-0.001634076	-0.001864136
43733.63938	-0.001433373	-0.001406609	-0.001464278	-0.001642701	-0.001872792
43733.63938	-0.001441266	-0.001414139	-0.001472316	-0.001651389	-0.001881513
43733.63938	-0.001449219	-0.001421725	-0.001480413	-0.001660142	-0.001890299
43733.63938	-0.001457231	-0.001429368	-0.00148857	-0.00166896	-0.001899152
43733.63938	-0.001465302	-0.001437068	-0.001496785	-0.001677841	-0.00190807
43733.63938	-0.001473433	-0.001444825	-0.001505059	-0.001686787	-0.001917054
43733.63938	-0.001481624	-0.001452639	-0.001513393	-0.001695797	-0.001926103
43733.63938	-0.001489874	-0.00146051	-0.001521786	-0.001704872	-0.001935219
43733.63938	-0.001498184	-0.001468438	-0.001530239	-0.001714011	-0.001944401
43733.63938	-0.001506553	-0.001476423	-0.001538751	-0.001723214	-0.001953648
43733.63938	-0.001514983	-0.001484466	-0.001547322	-0.001732482	-0.001962962
43733.63938	-0.001532022	-0.001500724	-0.001564644	-0.001751213	-0.001981788
43733.63938	-0.001540631	-0.001508939	-0.001573395	-0.001760676	-0.001991301
43733.63938	-0.001549301	-0.001517212	-0.001582205	-0.001770203	-0.002000879
43733.63938	-0.001558031	-0.001525543	-0.001591076	-0.001779796	-0.002010525
43733.63938	-0.001566822	-0.001533931	-0.001600006	-0.001789453	-0.002020237
43733.63938	-0.001575672	-0.001542378	-0.001608997	-0.001799176	-0.002030015
43733.63938	-0.001584584	-0.001550883	-0.001618047	-0.001808964	-0.00203986
43733.63938	-0.001593556	-0.001559445	-0.001627158	-0.001818817	-0.002049772
43733.63938	-0.001602588	-0.001568066	-0.00163633	-0.001828736	-0.002059751
43733.63938	-0.001611682	-0.001576745	-0.001645561	-0.00183872	-0.002069797
43733.63938	-0.001620836	-0.001585483	-0.001654854	-0.001848769	-0.00207991
43733.63938	-0.001630052	-0.001594279	-0.001664207	-0.001858885	-0.00209009
43733.63938	-0.001639328	-0.001603134	-0.00167362	-0.001869066	-0.002100337
43733.63938	-0.001648666	-0.001612048	-0.001683095	-0.001879313	-0.002110652
43733.63938	-0.001658064	-0.00162102	-0.00169263	-0.001889625	-0.002121034
43733.63938	-0.001667525	-0.001630052	-0.001702227	-0.001900004	-0.002131483
43733.63938	-0.001677047	-0.001639142	-0.001711885	-0.001910449	-0.002142
43733.63938	-0.00168663	-0.001648292	-0.001721604	-0.00192096	-0.002152585
43733.63938	-0.001696275	-0.0016575	-0.001731384	-0.001931537	-0.002163237
43733.63938	-0.001705982	-0.001666769	-0.001741226	-0.001942181	-0.002173958
43733.63938	-0.001715751	-0.001676097	-0.001751129	-0.001952891	-0.002184746
43733.63938	-0.001725581	-0.001685484	-0.001761094	-0.001963668	-0.002195603
43733.63938	-0.001735474	-0.001694931	-0.001771121	-0.001974512	-0.002206527
43733.63938	-0.00174543	-0.001704438	-0.00178121	-0.001985422	-0.00221752
43733.63938	-0.001755447	-0.001714005	-0.001791361	-0.001996399	-0.002228582
43733.63938	-0.001765527	-0.001723633	-0.001801574	-0.002007444	-0.002239712
43733.63938	-0.00177567	-0.00173332	-0.001811849	-0.002018555	-0.00225091
43733.63938	-0.001785876	-0.001743068	-0.001822186	-0.002029734	-0.002262178
43733.63938	-0.001796144	-0.001752876	-0.001832586	-0.00204098	-0.002273514
43733.63938	-0.001806475	-0.001762745	-0.001843049	-0.002052294	-0.002284919
43733.63938	-0.00181687	-0.001772675	-0.001853575	-0.002063675	-0.002296394
43733.63938	-0.001827328	-0.001782665	-0.001864163	-0.002075124	-0.002307937
43733.63938	-0.001837849	-0.001792717	-0.001874815	-0.002086641	-0.00231955
43733.63938	-0.001848433	-0.00180283	-0.001885529	-0.002098225	-0.002331233
43733.63938	-0.001859082	-0.001813004	-0.001896307	-0.002109878	-0.002342985
43733.63938	-0.001869794	-0.00182324	-0.001907148	-0.0021216	-0.002354807
43733.63938	-0.00188057	-0.001833537	-0.001918053	-0.002133389	-0.002366699
43733.63938	-0.00189141	-0.001843896	-0.001929022	-0.002145247	-0.00237866
43733.63938	-0.001902314	-0.001854317	-0.001940054	-0.002157174	-0.002390692

43733.63938	-0.001913282	-0.0018648	-0.00195115	-0.002169169	-0.002402794
43733.63938	-0.001924315	-0.001875345	-0.001962311	-0.002181233	-0.002414967
43733.63938	-0.001935413	-0.001885952	-0.001973536	-0.002193367	-0.00242721
43733.63938	-0.001946575	-0.001896622	-0.001984825	-0.002205569	-0.002439524
43733.63938	-0.001957803	-0.001907355	-0.001996178	-0.002217841	-0.002451908
43733.63938	-0.001969095	-0.00191815	-0.002007597	-0.002230182	-0.002464364
43733.63938	-0.001980453	-0.001929009	-0.00201908	-0.002242593	-0.002476891
43733.63938	-0.001991876	-0.00193993	-0.002030628	-0.002255073	-0.002489489
43733.63938	-0.002003365	-0.001950915	-0.002042242	-0.002267624	-0.002502158
43733.63938	-0.002014919	-0.001961963	-0.00205392	-0.002280244	-0.002514899
43733.63938	-0.002026539	-0.001973075	-0.002065665	-0.002292935	-0.002527712
43733.63938	-0.002038225	-0.001984251	-0.002077474	-0.002305696	-0.002540596
43733.63938	-0.002049977	-0.00199549	-0.00208935	-0.002318527	-0.002553553
43733.63938	-0.002073681	-0.002018162	-0.002113299	-0.002344402	-0.002579683
43733.63938	-0.002085633	-0.002029594	-0.002125373	-0.002357446	-0.002592856
43733.63938	-0.002097652	-0.002041091	-0.002137514	-0.002370561	-0.002606102
43733.63938	-0.002109737	-0.002052653	-0.002149721	-0.002383748	-0.002619421
43733.63938	-0.00212189	-0.00206428	-0.002161995	-0.002397005	-0.002632813
43733.63938	-0.00213411	-0.002075972	-0.002174336	-0.002410335	-0.002646279
43733.63938	-0.002146398	-0.002087729	-0.002186744	-0.002423736	-0.002659817
43733.63938	-0.002158753	-0.002099552	-0.002199219	-0.002437209	-0.002673429
43733.63938	-0.002171177	-0.002111441	-0.002211762	-0.002450754	-0.002687115
43733.63938	-0.002183668	-0.002123395	-0.002224372	-0.002464371	-0.002700874
43733.63938	-0.002196228	-0.002135416	-0.002237051	-0.002478061	-0.002714708
43733.63938	-0.002208856	-0.002147503	-0.002249797	-0.002491823	-0.002728615
43733.63938	-0.002221552	-0.002159656	-0.002262611	-0.0025005659	-0.002742598
43733.63938	-0.002234318	-0.002171876	-0.002275494	-0.002519567	-0.002756654
43733.63938	-0.002247152	-0.002184163	-0.002288446	-0.002533548	-0.002770785
43733.63938	-0.002260056	-0.002196517	-0.002301466	-0.002547603	-0.002784992
43733.63938	-0.002273029	-0.002208938	-0.002314556	-0.002561731	-0.002799273
43733.63938	-0.002286071	-0.002221427	-0.002327714	-0.002575933	-0.002813629
43733.63938	-0.002299184	-0.002233983	-0.002340942	-0.002590209	-0.002828062
43733.63938	-0.002312366	-0.002246607	-0.002354239	-0.002604559	-0.002842569
43733.63938	-0.002325618	-0.0022593	-0.002367607	-0.002618983	-0.002857153
43733.63938	-0.002338941	-0.00227206	-0.002381044	-0.002633482	-0.002871812
43733.63938	-0.002352334	-0.002284889	-0.002394551	-0.002648055	-0.002886548
43733.63938	-0.002365798	-0.002297787	-0.002408128	-0.002662704	-0.00290136
43733.63938	-0.002379333	-0.002310753	-0.002421777	-0.002677427	-0.002916249
43733.63938	-0.00239294	-0.002323789	-0.002435495	-0.002692225	-0.002931215
43733.63938	-0.002406617	-0.002336893	-0.002449285	-0.002707099	-0.002946258
43733.63938	-0.002420366	-0.002350068	-0.002463146	-0.002722049	-0.002961377
43733.63938	-0.002434187	-0.002363312	-0.002477079	-0.002737074	-0.002976575
43733.63938	-0.00244808	-0.002376626	-0.002491083	-0.002752175	-0.00299185
43733.63938	-0.002462045	-0.00239001	-0.002505158	-0.002767353	-0.003007203
43733.63938	-0.002476082	-0.002403465	-0.002519306	-0.002782607	-0.003022633
43733.63938	-0.002490193	-0.00241699	-0.002533526	-0.002797938	-0.003038142
43733.63938	-0.002504376	-0.002430587	-0.002547819	-0.002813345	-0.00305373
43733.63938	-0.002518632	-0.002444254	-0.002562184	-0.00282883	-0.003069396
43733.63938	-0.002532961	-0.002457992	-0.002576622	-0.002844392	-0.003085141
43733.63938	-0.002547364	-0.002471802	-0.002591133	-0.002860031	-0.003100966
43733.63938	-0.002561841	-0.002485684	-0.002605717	-0.002875749	-0.003116869

43733.63938	-0.002576391	-0.002499638	-0.002620375	-0.002891544	-0.003132852
43733.63938	-0.002591016	-0.002513664	-0.002635107	-0.002907417	-0.003148915
43733.63938	-0.002605716	-0.002527763	-0.002649913	-0.002923369	-0.003165058
43733.63938	-0.002620489	-0.002541934	-0.002664793	-0.002939399	-0.003181281
43733.63938	-0.002635338	-0.002556178	-0.002679747	-0.002955508	-0.003197585
43733.63938	-0.002650262	-0.002570495	-0.002694777	-0.002971696	-0.003213969
43733.63938	-0.002665262	-0.002584886	-0.002709881	-0.002987963	-0.003230434
43733.63938	-0.002680337	-0.00259935	-0.00272506	-0.00300431	-0.00324698
43733.63938	-0.002695487	-0.002613889	-0.002740315	-0.003020737	-0.003263608
43733.63938	-0.002710714	-0.002628501	-0.002755645	-0.003037243	-0.003280317
43733.63938	-0.002726017	-0.002643188	-0.002771051	-0.00305383	-0.003297108
43733.63938	-0.002741397	-0.002657949	-0.002786534	-0.003070497	-0.003313981
43733.63938	-0.002756854	-0.002672786	-0.002802093	-0.003087245	-0.003330936
43733.63938	-0.002772387	-0.002687697	-0.002817728	-0.003104074	-0.003347974
43733.63938	-0.002803687	-0.002717747	-0.002849229	-0.003137975	-0.003382299
43733.63938	-0.002819453	-0.002732885	-0.002865096	-0.003155048	-0.003399586
43733.63938	-0.002835297	-0.0027481	-0.00288104	-0.003172202	-0.003416956
43733.63938	-0.00285122	-0.002763391	-0.002897063	-0.003189439	-0.00343441
43733.63938	-0.002867221	-0.002778759	-0.002913163	-0.003206758	-0.003451948
43733.63938	-0.002883301	-0.002794204	-0.002929342	-0.00322416	-0.003469571
43733.63938	-0.00289946	-0.002809726	-0.002945599	-0.003241644	-0.003487278
43733.63938	-0.002915698	-0.002825326	-0.002961935	-0.003259212	-0.00350507
43733.63938	-0.002932016	-0.002841003	-0.00297835	-0.003276863	-0.003522946
43733.63938	-0.002948414	-0.002856758	-0.002994845	-0.003294597	-0.003540908
43733.63938	-0.002964892	-0.002872592	-0.00301142	-0.003312416	-0.003558956
43733.63938	-0.00298145	-0.002888504	-0.003028074	-0.003330318	-0.003577089
43733.63938	-0.002998089	-0.002904495	-0.003044808	-0.003348305	-0.003595309
43733.63938	-0.003014809	-0.002920565	-0.003061623	-0.003366377	-0.003613614
43733.63938	-0.00303161	-0.002936714	-0.003078519	-0.003384533	-0.003632006
43733.63938	-0.003048493	-0.002952944	-0.003095496	-0.003402775	-0.003650486
43733.63938	-0.003065457	-0.002969253	-0.003112554	-0.003421102	-0.003669052
43733.63938	-0.003082504	-0.002985642	-0.003129694	-0.003439514	-0.003687705
43733.63938	-0.003099632	-0.003002112	-0.003146915	-0.003458013	-0.003706446
43733.63938	-0.003116843	-0.003018663	-0.003164218	-0.003476598	-0.003725275
43733.63938	-0.003134137	-0.003035294	-0.003181604	-0.003495269	-0.003744193
43733.63938	-0.003151514	-0.003052007	-0.003199073	-0.003514027	-0.003763198
43733.63938	-0.003168975	-0.003068802	-0.003216624	-0.003532872	-0.003782293
43733.63938	-0.003186519	-0.003085679	-0.003234259	-0.003551804	-0.003801476
43733.63938	-0.003204147	-0.003102638	-0.003251977	-0.003570824	-0.003820749
43733.63938	-0.00322186	-0.003119679	-0.003269779	-0.003589932	-0.003840111
43733.63938	-0.003239657	-0.003136803	-0.003287665	-0.003609127	-0.003859563
43733.63938	-0.003257538	-0.00315401	-0.003305635	-0.003628411	-0.003879105
43733.63938	-0.003275505	-0.003171301	-0.00332369	-0.003647784	-0.003898738
43733.63938	-0.003293557	-0.003188676	-0.00334183	-0.003667246	-0.003918461
43733.63938	-0.003311695	-0.003206134	-0.003360055	-0.003686797	-0.003938275
43733.63938	-0.003329919	-0.003223677	-0.003378366	-0.003706438	-0.00395818
43733.63938	-0.003348229	-0.003241304	-0.003396762	-0.003726168	-0.003978177
43733.63938	-0.003366626	-0.003259016	-0.003415245	-0.003745988	-0.003998266
43733.63938	-0.00338511	-0.003276813	-0.003433814	-0.003765899	-0.004018447
43733.63938	-0.003403681	-0.003294696	-0.00345247	-0.003785901	-0.00403872
43733.63938	-0.003422339	-0.003312665	-0.003471212	-0.003805993	-0.004059086

266

43733.63938	-0.003441085	-0.00333072	-0.003490042	-0.003826177	-0.004079545
43733.63938	-0.003459919	-0.003348861	-0.00350896	-0.003846452	-0.004100097
43733.63938	-0.003478842	-0.003367089	-0.003527965	-0.003866819	-0.004120743
43733.63938	-0.003497853	-0.003385404	-0.003547059	-0.003887278	-0.004141483
43733.63938	-0.003516953	-0.003403806	-0.003566241	-0.00390783	-0.004162317
43733.63938	-0.003536143	-0.003422297	-0.003585512	-0.003928474	-0.004183246
43733.63938	-0.003555422	-0.003440875	-0.003604872	-0.003949212	-0.004204269
43733.63938	-0.003574791	-0.003459541	-0.003624321	-0.003970042	-0.004225387
43733.63938	-0.00359425	-0.003478296	-0.003643861	-0.003990967	-0.004246601
43733.63938	-0.0036138	-0.00349714	-0.00366349	-0.004011985	-0.00426791
43733.63938	-0.003633441	-0.003516073	-0.00368321	-0.004033097	-0.004289316
43733.63938	-0.003653172	-0.003535096	-0.00370302	-0.004054304	-0.004310818
43733.63938	-0.003672996	-0.003554209	-0.003722921	-0.004075606	-0.004332416
43733.63938	-0.003692911	-0.003573412	-0.003742914	-0.004097003	-0.004354111
43733.63938	-0.003712918	-0.003592705	-0.003762998	-0.004118496	-0.004375904
43733.63938	-0.00375321	-0.003631566	-0.003803443	-0.004161769	-0.004419782
43733.63938	-0.003773496	-0.003651133	-0.003823804	-0.004183549	-0.004441869
43733.63938	-0.003793875	-0.003670792	-0.003844258	-0.004205427	-0.004464054
43733.63938	-0.003814348	-0.003690543	-0.003864805	-0.004227402	-0.004486337
43733.63938	-0.003834915	-0.003710387	-0.003885446	-0.004249474	-0.00450872
43733.63938	-0.003855576	-0.003730324	-0.003906181	-0.004271643	-0.004531202
43733.63938	-0.003876332	-0.003750354	-0.00392701	-0.004293911	-0.004553784
43733.63938	-0.003897183	-0.003770478	-0.003947933	-0.004316277	-0.004576467
43733.63938	-0.003918129	-0.003790695	-0.003968952	-0.004338741	-0.004599249
43733.63938	-0.003939172	-0.003811007	-0.003990066	-0.004361305	-0.004622133
43733.63938	-0.00396031	-0.003831413	-0.004011275	-0.004383968	-0.004645118
43733.63938	-0.003981545	-0.003851914	-0.00403258	-0.00440673	-0.004668204
43733.63938	-0.004002876	-0.003872511	-0.004053981	-0.004429592	-0.004691391
43733.63938	-0.004024304	-0.003893203	-0.004075479	-0.004452555	-0.004714681
43733.63938	-0.00404583	-0.003913991	-0.004097074	-0.004475618	-0.004738074
43733.63938	-0.004067454	-0.003934875	-0.004118766	-0.004498782	-0.004761569
43733.63938	-0.004089175	-0.003955856	-0.004140555	-0.004522048	-0.004785167
43733.63938	-0.004110996	-0.003976934	-0.004162443	-0.004545415	-0.004808869
43733.63938	-0.004132915	-0.003998109	-0.004184428	-0.004568883	-0.004832674
43733.63938	-0.004154933	-0.004019382	-0.004206513	-0.004592455	-0.004856584
43733.63938	-0.00417705	-0.004040753	-0.004228696	-0.004616128	-0.004880598
43733.63938	-0.004199267	-0.004062223	-0.004250979	-0.004639905	-0.004904717
43733.63938	-0.004221585	-0.004083791	-0.004273361	-0.004663785	-0.004928941
43733.63938	-0.004244003	-0.004105458	-0.004295843	-0.004687769	-0.00495327
43733.63938	-0.004266522	-0.004127225	-0.004318425	-0.004711856	-0.004977705
43733.63938	-0.004289142	-0.004149092	-0.004341109	-0.004736048	-0.005002247
43733.63938	-0.004311864	-0.004171058	-0.004363893	-0.004760344	-0.005026894
43733.63938	-0.004334687	-0.004193126	-0.004386779	-0.004784746	-0.005051649
43733.63938	-0.004357613	-0.004215294	-0.004409766	-0.004809252	-0.005076511
43733.63938	-0.004380642	-0.004237564	-0.004432856	-0.004833865	-0.005101481
43733.63938	-0.004403773	-0.004259935	-0.004456047	-0.004858583	-0.005126558
43733.63938	-0.004427008	-0.004282408	-0.004479342	-0.004883408	-0.005151744
43733.63938	-0.004450346	-0.004304984	-0.00450274	-0.004908339	-0.005177038
43733.63938	-0.004473789	-0.004327662	-0.004526242	-0.004933378	-0.005202441
43733.63938	-0.004497336	-0.004350443	-0.004549847	-0.004958524	-0.005227954
43733.63938	-0.004520988	-0.004373328	-0.004573557	-0.004983778	-0.005253576

43733.63938	-0.004544745	-0.004396317	-0.004597371	-0.005009139	-0.005279308
43733.63938	-0.004568608	-0.00441941	-0.00462129	-0.00503461	-0.005305151
43733.63938	-0.004592576	-0.004442607	-0.004645315	-0.005060189	-0.005331104
43733.63938	-0.004616651	-0.00446591	-0.004669445	-0.005085877	-0.005357169
43733.63938	-0.004640832	-0.004489317	-0.004693681	-0.005111675	-0.005383345
43733.63938	-0.00466512	-0.004512831	-0.004718024	-0.005137583	-0.005409633
43733.63938	-0.004689516	-0.004536451	-0.004742474	-0.005163601	-0.005436033
43733.63938	-0.004714019	-0.004560177	-0.004767031	-0.00518973	-0.005462545
43733.63938	-0.004738631	-0.004584009	-0.004791695	-0.005215969	-0.005489171
43733.63938	-0.004763351	-0.00460795	-0.004816467	-0.00524232	-0.005515909
43733.63938	-0.004788179	-0.004631997	-0.004841348	-0.005268783	-0.005542762
43733.63938	-0.004813117	-0.004656153	-0.004866337	-0.005295358	-0.005569728
43733.63938	-0.004838165	-0.004680417	-0.004891435	-0.005322045	-0.005596809
43733.63938	-0.004863323	-0.00470479	-0.004916643	-0.005348845	-0.005624005
43733.63938	-0.004888591	-0.004729272	-0.004941961	-0.005375758	-0.005651315
43733.63938	-0.004913969	-0.004753863	-0.004967388	-0.005402785	-0.005678742
43733.63938	-0.00496506	-0.004803376	-0.005018576	-0.00545718	-0.005733942
43733.63938	-0.004990774	-0.004828298	-0.005044336	-0.00548455	-0.005761717
43733.63938	-0.005016599	-0.004853331	-0.005070208	-0.005512034	-0.005789609
43733.63938	-0.005042537	-0.004878476	-0.005096192	-0.005539634	-0.005817618
43733.63938	-0.005068588	-0.004903733	-0.005122289	-0.00556735	-0.005845745
43733.63938	-0.005094753	-0.004929102	-0.005148499	-0.005595182	-0.00587399
43733.63938	-0.005121031	-0.004954583	-0.005174821	-0.00562313	-0.005902354
43733.63938	-0.005147423	-0.004980178	-0.005201258	-0.005651196	-0.005930837
43733.63938	-0.00517393	-0.005005886	-0.005227808	-0.005679378	-0.005959438
43733.63938	-0.005200552	-0.005031707	-0.005254473	-0.005707678	-0.00598816
43733.63938	-0.00522729	-0.005057643	-0.005281253	-0.005736097	-0.006017001
43733.63938	-0.005254143	-0.005083694	-0.005308147	-0.005764633	-0.006045963
43733.63938	-0.005281112	-0.005109859	-0.005335158	-0.005793289	-0.006075046
43733.63938	-0.005308198	-0.00513614	-0.005362284	-0.005822063	-0.00610425
43733.63938	-0.0053354	-0.005162537	-0.005389526	-0.005850957	-0.006133575
43733.63938	-0.00536272	-0.00518905	-0.005416886	-0.005879972	-0.006163023
43733.63938	-0.005390158	-0.00521568	-0.005444362	-0.005909106	-0.006192593
43733.63938	-0.005417713	-0.005242426	-0.005471956	-0.005938361	-0.006222285
43733.63938	-0.005445388	-0.00526929	-0.005499668	-0.005967737	-0.006252101
43733.63938	-0.005473181	-0.005296272	-0.005527498	-0.005997235	-0.00628204
43733.63938	-0.005501093	-0.005323372	-0.005555447	-0.006026855	-0.006312103
43733.63938	-0.005529125	-0.00535059	-0.005583515	-0.006056596	-0.00634229
43733.63938	-0.005557277	-0.005377928	-0.005611702	-0.006086461	-0.006372602
43733.63938	-0.00558555	-0.005405385	-0.005640009	-0.006116448	-0.006403039
43733.63938	-0.005613944	-0.005432962	-0.005668437	-0.006146559	-0.006433602
43733.63938	-0.005642458	-0.005460659	-0.005696986	-0.006176794	-0.00646429
43733.63938	-0.005671095	-0.005488477	-0.005725655	-0.006207153	-0.006495105
43733.63938	-0.005699854	-0.005516415	-0.005754446	-0.006237636	-0.006526046
43733.63938	-0.005728735	-0.005544476	-0.005783359	-0.006268245	-0.006557115
43733.63938	-0.005757739	-0.005572658	-0.005812394	-0.006298979	-0.006588311
43733.63938	-0.005786866	-0.005600962	-0.005841552	-0.006329839	-0.006619634
43733.63938	-0.005816117	-0.00562939	-0.005870833	-0.006360824	-0.006651086
43733.63938	-0.005845492	-0.00565794	-0.005900238	-0.006391937	-0.006682667
43733.63938	-0.005874992	-0.005686614	-0.005929766	-0.006423176	-0.006714377
43733.63938	-0.005904617	-0.005715412	-0.005959419	-0.006454543	-0.006746216

43733.63938	-0.005934367	-0.005744334	-0.005989197	-0.006486038	-0.006778185
43733.63938	-0.005964242	-0.005773381	-0.006019099	-0.00651766	-0.006810284
43733.63938	-0.005994244	-0.005802553	-0.006049128	-0.006549412	-0.006842514
43733.63938	-0.006024373	-0.005831851	-0.006079282	-0.006581292	-0.006874875
43733.63938	-0.006054628	-0.005861275	-0.006109563	-0.006613301	-0.006907367
43733.63938	-0.006085011	-0.005890825	-0.00613997	-0.006645441	-0.006939991
43733.63938	-0.006115522	-0.005920502	-0.006170505	-0.00667771	-0.006972748
43733.63938	-0.006146161	-0.005950307	-0.006201168	-0.006710111	-0.007005637
43733.63938	-0.006176928	-0.005980239	-0.006231958	-0.006742642	-0.00703866
43733.63938	-0.006207825	-0.006010299	-0.006262877	-0.006775304	-0.007071816
43733.63938	-0.006238851	-0.006040488	-0.006293925	-0.006808098	-0.007105105
43733.63938	-0.006270007	-0.006070806	-0.006325102	-0.006841025	-0.007138529
43733.63938	-0.006301294	-0.006101254	-0.006356409	-0.006874084	-0.007172088
43733.63938	-0.006332711	-0.006131831	-0.006387845	-0.006907276	-0.007205782
43733.63938	-0.006364259	-0.006162538	-0.006419413	-0.006940602	-0.007239612
43733.63938	-0.006395939	-0.006193376	-0.006451111	-0.006974061	-0.007273577
43733.63938	-0.006427751	-0.006224346	-0.006482941	-0.007007655	-0.007307679
43733.63938	-0.006491772	-0.006286679	-0.006546996	-0.007075246	-0.007376294
43733.63938	-0.006523982	-0.006318044	-0.006579223	-0.007109245	-0.007410807
43733.63938	-0.006556326	-0.006349542	-0.006611582	-0.00714338	-0.007445459
43733.63938	-0.006588805	-0.006381174	-0.006644075	-0.007177651	-0.007480249
43733.63938	-0.006621417	-0.006412938	-0.006676702	-0.007212058	-0.007515178
43733.63938	-0.006654165	-0.006444838	-0.006709464	-0.007246603	-0.007550246
43733.63938	-0.006687048	-0.006476871	-0.00674236	-0.007281285	-0.007585454
43733.63938	-0.006720066	-0.00650904	-0.006775391	-0.007316105	-0.007620802
43733.63938	-0.006753221	-0.006541344	-0.006808558	-0.007351064	-0.00765629
43733.63938	-0.006786513	-0.006573784	-0.00684186	-0.007386161	-0.00769192
43733.63938	-0.006819942	-0.00660636	-0.0068753	-0.007421398	-0.007727691
43733.63938	-0.006853508	-0.006639073	-0.006908876	-0.007456774	-0.007763603
43733.63938	-0.006887212	-0.006671923	-0.006942589	-0.00749229	-0.007799658
43733.63938	-0.006921055	-0.00670491	-0.00697644	-0.007527947	-0.007835856
43733.63938	-0.006955036	-0.006738036	-0.00701043	-0.007563744	-0.007872196
43733.63938	-0.006989156	-0.0067713	-0.007044558	-0.007599683	-0.00790868
43733.63938	-0.007023417	-0.006804703	-0.007078825	-0.007635764	-0.007945308
43733.63938	-0.007057817	-0.006838245	-0.007113231	-0.007671986	-0.00798208
43733.63938	-0.007092358	-0.006871927	-0.007147777	-0.007708351	-0.008018997
43733.63938	-0.007127039	-0.006905749	-0.007182464	-0.007744859	-0.00805606
43733.63938	-0.007161862	-0.006939712	-0.007217291	-0.007781511	-0.008093267
43733.63938	-0.007196827	-0.006973816	-0.0072526	-0.007818306	-0.008130621
43733.63938	-0.007231934	-0.007008061	-0.00728737	-0.007855245	-0.008168121
43733.63938	-0.007267184	-0.007042449	-0.007322622	-0.007892329	-0.008205768
43733.63938	-0.007302577	-0.007076979	-0.007358017	-0.007929558	-0.008243563
43733.63938	-0.007338113	-0.007111651	-0.007393554	-0.007966933	-0.008281505
43733.63938	-0.007373794	-0.007146467	-0.007429235	-0.008004453	-0.008319595
43733.63938	-0.007409618	-0.007181427	-0.00746506	-0.00804212	-0.008357834
43733.63938	-0.007445588	-0.00721653	-0.007501029	-0.008079934	-0.008396222
43733.63938	-0.007481703	-0.007251779	-0.007537142	-0.008117895	-0.008434759
43733.63938	-0.007517964	-0.007287172	-0.007573401	-0.008156003	-0.008473446
43733.63938	-0.00755437	-0.007322711	-0.007609805	-0.008194259	-0.008512284
43733.63938	-0.007590924	-0.007358396	-0.007646355	-0.008232664	-0.008551272
43733.63938	-0.007627624	-0.007394227	-0.007683051	-0.008271218	-0.008590411

43733.63938	-0.007664472	-0.007430205	-0.007719894	-0.008309921	-0.008629702
43733.63938	-0.007701468	-0.00746633	-0.007756885	-0.008348774	-0.008669145
43733.63938	-0.007738612	-0.007502603	-0.007794023	-0.008387777	-0.00870874
43733.63938	-0.007775904	-0.007539024	-0.007831309	-0.00842693	-0.008748488
43733.63938	-0.007813346	-0.007575594	-0.007868744	-0.008466235	-0.008788389
43733.63938	-0.007850938	-0.007612313	-0.007906328	-0.008505691	-0.008828445
43733.63938	-0.00788868	-0.007649181	-0.007944061	-0.008545298	-0.008868654
43733.63938	-0.007926572	-0.007686199	-0.007981944	-0.008585058	-0.008909018
43733.63938	-0.007964616	-0.007723368	-0.008019978	-0.008624971	-0.008949537
43733.63938	-0.00800281	-0.007760687	-0.008058162	-0.008665037	-0.008990211
43733.63938	-0.008041157	-0.007798158	-0.008096497	-0.008705257	-0.009031041
43733.63938	-0.008079656	-0.00783578	-0.008134984	-0.00874563	-0.009072028
43733.63938	-0.008118307	-0.007873555	-0.008173624	-0.008786158	-0.009113171
43733.63938	-0.008157112	-0.007911482	-0.008212415	-0.008826841	-0.009154472
43733.63938	-0.00819607	-0.007949562	-0.00825136	-0.008867679	-0.00919593
43733.63938	-0.008235183	-0.007987796	-0.008290458	-0.008908673	-0.009237546
43733.63938	-0.00827445	-0.008026183	-0.00832971	-0.008949823	-0.009279321
43733.63938	-0.008313872	-0.008064725	-0.008369116	-0.00899113	-0.009321254
43733.63938	-0.008393182	-0.008142274	-0.008448393	-0.009074215	-0.0094056
43733.63938	-0.008433071	-0.008181282	-0.008488265	-0.009115994	-0.009448013
43733.63938	-0.008473117	-0.008220447	-0.008528293	-0.009157931	-0.009490587
43733.63938	-0.008513321	-0.008259767	-0.008568477	-0.009200027	-0.009533321
43733.63938	-0.008553682	-0.008299245	-0.008608818	-0.009242283	-0.009576218
43733.63938	-0.0085942	-0.008338881	-0.008649317	-0.009284698	-0.009619276
43733.63938	-0.008634878	-0.008378674	-0.008689973	-0.009327273	-0.009662497
43733.63938	-0.008675714	-0.008418626	-0.008730788	-0.009370008	-0.00970588
43733.63938	-0.00871671	-0.008458737	-0.008771761	-0.009412905	-0.009749427
43733.63938	-0.008757865	-0.008499007	-0.008812894	-0.009455962	-0.009793137
43733.63938	-0.008799181	-0.008539437	-0.008854186	-0.009499182	-0.009837012
43733.63938	-0.008840658	-0.008580027	-0.008895638	-0.009542563	-0.009881051
43733.63938	-0.008882295	-0.008620778	-0.008937251	-0.009586108	-0.009925256
43733.63938	-0.008924095	-0.008661691	-0.008979025	-0.009629815	-0.009969625
43733.63938	-0.008966056	-0.008702764	-0.00902096	-0.009673686	-0.010014161
43733.63938	-0.00900818	-0.008744	-0.009063057	-0.009717721	-0.010058863
43733.63938	-0.009050467	-0.008785398	-0.009105316	-0.00976192	-0.010103732
43733.63938	-0.009092917	-0.00882696	-0.009147738	-0.009806285	-0.010148768
43733.63938	-0.009135531	-0.008868684	-0.009190323	-0.009850814	-0.010193971
43733.63938	-0.009178309	-0.008910573	-0.009233072	-0.009895509	-0.010239343
43733.63938	-0.009221252	-0.008952626	-0.009275984	-0.00994037	-0.010284883
43733.63938	-0.00926436	-0.008994844	-0.009319062	-0.009985398	-0.010330592
43733.63938	-0.009307634	-0.009037227	-0.009362304	-0.010030593	-0.010376471
43733.63938	-0.009351074	-0.009079775	-0.009405711	-0.010075955	-0.010422519
43733.63938	-0.00939468	-0.00912249	-0.009449285	-0.010121485	-0.010468738
43733.63938	-0.009438454	-0.009165371	-0.009493024	-0.010167183	-0.010515127
43733.63938	-0.009482394	-0.00920842	-0.009536931	-0.01021305	-0.010561688
43733.63938	-0.009526503	-0.009251636	-0.009581005	-0.010259087	-0.01060842
43733.63938	-0.00957078	-0.009295019	-0.009625246	-0.010305293	-0.010655324
43733.63938	-0.009615226	-0.009338572	-0.009669655	-0.010351668	-0.010702401
43733.63938	-0.009659841	-0.009382293	-0.009714233	-0.010398215	-0.01074965
43733.63938	-0.009704625	-0.009426183	-0.00975898	-0.010444932	-0.010797073
43733.63938	-0.00974958	-0.009470243	-0.009803896	-0.010491821	-0.01084467

43733.63938	-0.009794705	-0.009514474	-0.009848982	-0.010538881	-0.010892441
43733.63938	-0.009840001	-0.009558875	-0.009894238	-0.010586114	-0.010940386
43733.63938	-0.009885468	-0.009603447	-0.009939665	-0.010633519	-0.010988507
43733.63938	-0.009931108	-0.009648191	-0.009985264	-0.010681097	-0.011036803
43733.63938	-0.009976919	-0.009693106	-0.010031034	-0.010728849	-0.011085276
43733.63938	-0.010022904	-0.009738194	-0.010076976	-0.010776775	-0.011133924
43733.63938	-0.010069062	-0.009783456	-0.01012309	-0.010824875	-0.01118275
43733.63938	-0.010115393	-0.00982889	-0.010169378	-0.01087315	-0.011231752
43733.63938	-0.010161898	-0.009874498	-0.010215839	-0.0109216	-0.011280933
43733.63938	-0.010208578	-0.009920281	-0.010262474	-0.010970226	-0.011330291
43733.63938	-0.010255434	-0.009966239	-0.010309283	-0.011019028	-0.011379829
43733.63938	-0.010302464	-0.010012371	-0.010356267	-0.011068007	-0.011429545
43733.63938	-0.01034967	-0.010058679	-0.010403426	-0.011117162	-0.011479441
43733.63938	-0.010397053	-0.010105164	-0.01045076	-0.011166495	-0.011529516
43733.63938	-0.010444613	-0.010151825	-0.010498271	-0.011216006	-0.011579772
43733.63938	-0.010492349	-0.010198662	-0.010545959	-0.011265696	-0.011630209
43733.63938	-0.010540264	-0.010245678	-0.010593823	-0.011315564	-0.011680827
43733.63938	-0.010588356	-0.010292871	-0.010641865	-0.011365611	-0.011731627
43733.63938	-0.010636627	-0.010340243	-0.010690085	-0.011415837	-0.011782609
43733.63938	-0.010733707	-0.010435523	-0.01078706	-0.011516831	-0.01188512
43733.63938	-0.010782516	-0.010483432	-0.010835816	-0.011567599	-0.011936651
43733.63938	-0.010831506	-0.010531521	-0.010884751	-0.011618549	-0.011988366
43733.63938	-0.010880677	-0.010579792	-0.010933867	-0.01166968	-0.012040265
43733.63938	-0.010930029	-0.010628243	-0.010983163	-0.011720994	-0.012092348
43733.63938	-0.010979562	-0.010676876	-0.011032641	-0.01177249	-0.012144617
43733.63938	-0.011029278	-0.01072569	-0.011082299	-0.011824169	-0.012197071
43733.63938	-0.011079176	-0.010774687	-0.01113214	-0.011876031	-0.012249712
43733.63938	-0.011129257	-0.010823867	-0.011182163	-0.011928078	-0.012302538
43733.63938	-0.011179522	-0.010873231	-0.011232369	-0.011980309	-0.012355552
43733.63938	-0.011229971	-0.010922778	-0.011282758	-0.012032724	-0.012408753
43733.63938	-0.011280604	-0.010972509	-0.01133333	-0.012085325	-0.012462142
43733.63938	-0.011331422	-0.011022425	-0.011384087	-0.012138112	-0.012515719
43733.63938	-0.011382425	-0.011072526	-0.011435028	-0.012191085	-0.012569485
43733.63938	-0.011433613	-0.011122812	-0.011486155	-0.012244244	-0.012623439
43733.63938	-0.011484988	-0.011173285	-0.011537466	-0.01229759	-0.012677584
43733.63938	-0.011536549	-0.011223944	-0.011588964	-0.012351123	-0.012731918
43733.63938	-0.011588298	-0.01127479	-0.011640648	-0.012404845	-0.012786442
43733.63938	-0.011640234	-0.011325823	-0.011692518	-0.012458754	-0.012841158
43733.63938	-0.011692357	-0.011377045	-0.011744576	-0.012512852	-0.012896064
43733.63938	-0.011744669	-0.011428454	-0.011796821	-0.01256714	-0.012951162
43733.63938	-0.01179717	-0.011480052	-0.011849255	-0.012621617	-0.013006453
43733.63938	-0.01184986	-0.011531839	-0.011901877	-0.012676283	-0.013061936
43733.63938	-0.01190274	-0.011583816	-0.011954688	-0.012731141	-0.013117611
43733.63938	-0.01195581	-0.011635983	-0.012007688	-0.012786189	-0.013173481
43733.63938	-0.01200907	-0.01168834	-0.012060878	-0.012841428	-0.013229544
43733.63938	-0.012062521	-0.011740889	-0.012114259	-0.012896859	-0.013285801
43733.63938	-0.012116164	-0.011793628	-0.01216783	-0.012952482	-0.013342253
43733.63938	-0.012169999	-0.01184656	-0.012221592	-0.013008297	-0.0133989
43733.63938	-0.012224025	-0.011899683	-0.012275546	-0.013064306	-0.013455742
43733.63938	-0.012278245	-0.011953	-0.012329692	-0.013120508	-0.013512781
43733.63938	-0.012332658	-0.012006509	-0.01238403	-0.013176903	-0.013570016

43733.63938	-0.012387264	-0.012060212	-0.012438562	-0.013233493	-0.013627448
43733.63938	-0.012442064	-0.01211411	-0.012493286	-0.013290278	-0.013685077
43733.63938	-0.012497059	-0.012168201	-0.012548205	-0.013347257	-0.013742904
43733.63938	-0.012552249	-0.012222488	-0.012603317	-0.013404432	-0.013800928
43733.63938	-0.012607634	-0.01227697	-0.012658625	-0.013461803	-0.013859152
43733.63938	-0.012663215	-0.012331648	-0.012714127	-0.013519371	-0.013917574
43733.63938	-0.012718992	-0.012386522	-0.012769825	-0.013577135	-0.013976196
43733.63938	-0.012774966	-0.012441592	-0.012825718	-0.013635096	-0.014035017
43733.63938	-0.012831137	-0.01249686	-0.012881809	-0.013693255	-0.014094039
43733.63938	-0.012887505	-0.012552325	-0.012938096	-0.013751612	-0.014153262
43733.63938	-0.012944072	-0.012607989	-0.01299458	-0.013810167	-0.014212685
43733.63938	-0.013000836	-0.012663851	-0.013051262	-0.013868922	-0.01427231
43733.63938	-0.0130578	-0.012719911	-0.013108142	-0.013927875	-0.014332137
43733.63938	-0.013114963	-0.012776171	-0.013165221	-0.013987029	-0.014392167
43733.63938	-0.013172325	-0.012832631	-0.013222498	-0.014046382	-0.014452399
43733.63938	-0.013229888	-0.012889291	-0.013279975	-0.014105936	-0.014512834
43733.63938	-0.013287651	-0.012946152	-0.013337652	-0.014165691	-0.014573473
43733.63938	-0.013345615	-0.013003213	-0.013395529	-0.014225647	-0.014634316
43733.63938	-0.013403781	-0.013060477	-0.013453607	-0.014285806	-0.014695363
43733.63938	-0.013462148	-0.013117942	-0.013511886	-0.014346166	-0.014756616
43733.63938	-0.01357949	-0.01323348	-0.013629049	-0.014467495	-0.014879737
43733.63938	-0.013638466	-0.013291553	-0.013687934	-0.014528465	-0.014941606
43733.63938	-0.013697645	-0.01334983	-0.013747022	-0.014589639	-0.015003682
43733.63938	-0.013757028	-0.013408312	-0.013806313	-0.014651016	-0.015065965
43733.63938	-0.013816615	-0.013466998	-0.013865807	-0.014712599	-0.015128456
43733.63938	-0.013876408	-0.013525889	-0.013925506	-0.014774387	-0.015191154
43733.63938	-0.013936405	-0.013584985	-0.01398541	-0.01483638	-0.015254061
43733.63938	-0.013996608	-0.013644287	-0.014045518	-0.014898579	-0.015317176
43733.63938	-0.014057018	-0.013703795	-0.014105832	-0.014960985	-0.0153805
43733.63938	-0.014117634	-0.01376351	-0.014166352	-0.015023597	-0.015444034
43733.63938	-0.014178456	-0.013823433	-0.014227077	-0.015086417	-0.015507777
43733.63938	-0.014239487	-0.013883562	-0.01428801	-0.015149444	-0.015571731
43733.63938	-0.014300725	-0.0139439	-0.01434915	-0.015212679	-0.015635896
43733.63938	-0.014362171	-0.014004446	-0.014410497	-0.015276123	-0.015700271
43733.63938	-0.014423826	-0.014065201	-0.014472052	-0.015339776	-0.015764859
43733.63938	-0.01448569	-0.014126165	-0.014533815	-0.015403637	-0.015829658
43733.63938	-0.014547763	-0.014187339	-0.014595787	-0.015467709	-0.015894669
43733.63938	-0.014610047	-0.014248723	-0.014657969	-0.01553199	-0.015959894
43733.63938	-0.01467254	-0.014310318	-0.01472036	-0.015596482	-0.016025331
43733.63938	-0.014735245	-0.014372123	-0.014782961	-0.015661185	-0.016090982
43733.63938	-0.01479816	-0.01443414	-0.014845773	-0.015726099	-0.016156847
43733.63938	-0.014861288	-0.014496369	-0.014908795	-0.015791225	-0.016222926
43733.63938	-0.014924627	-0.01455881	-0.014972029	-0.015856563	-0.016289221
43733.63938	-0.014988178	-0.014621464	-0.015035474	-0.015922113	-0.01635573
43733.63938	-0.015051943	-0.01468433	-0.015099131	-0.015987877	-0.016422455
43733.63938	-0.01511592	-0.01474741	-0.015163001	-0.016053853	-0.016489396
43733.63938	-0.015180112	-0.014810705	-0.015227084	-0.016120044	-0.016556554
43733.63938	-0.015244517	-0.014874213	-0.015291381	-0.016186448	-0.016623928
43733.63938	-0.015309137	-0.014937936	-0.015355891	-0.016253067	-0.01669152
43733.63938	-0.015373972	-0.015001874	-0.015420615	-0.016319901	-0.016759329
43733.63938	-0.015439022	-0.015066028	-0.015485554	-0.01638695	-0.016827356

43733.63938	-0.015504287	-0.015130398	-0.015550707	-0.016454215	-0.016895601
43733.63938	-0.015569769	-0.015194984	-0.015616077	-0.016521696	-0.016964066
43733.63938	-0.015635467	-0.015259788	-0.015681662	-0.016589393	-0.01703275
43733.63938	-0.015701383	-0.015324808	-0.015747463	-0.016657307	-0.017101653
43733.63938	-0.015767515	-0.015390046	-0.015813481	-0.016725439	-0.017170776
43733.63938	-0.015833866	-0.015455502	-0.015879716	-0.016793788	-0.01724012
43733.63938	-0.015900434	-0.015521176	-0.015946168	-0.016862355	-0.017309684
43733.63938	-0.015967222	-0.01558707	-0.016012838	-0.016931141	-0.01737947
43733.63938	-0.016034228	-0.015653183	-0.016079727	-0.017000146	-0.017449478
43733.63938	-0.016101453	-0.015719515	-0.016146834	-0.017069369	-0.017519707
43733.63938	-0.016168898	-0.015786068	-0.01621416	-0.017138813	-0.017590159
43733.63938	-0.016236564	-0.015852841	-0.016281706	-0.017208476	-0.017660833
43733.63938	-0.01630445	-0.015919835	-0.016349471	-0.01727836	-0.017731731
43733.63938	-0.016372557	-0.01598705	-0.016417457	-0.017348465	-0.017802852
43733.63938	-0.016440885	-0.016054487	-0.016485664	-0.017418791	-0.017874197
43733.63938	-0.016509435	-0.016122146	-0.016554091	-0.017489338	-0.017945767
43733.63938	-0.016578208	-0.016190028	-0.01662274	-0.017560108	-0.018017561
43733.63938	-0.016647202	-0.016258133	-0.016691611	-0.0176311	-0.01808958
43733.63938	-0.01671642	-0.016326461	-0.016760704	-0.017702314	-0.018161825
43733.63938	-0.016785861	-0.016395012	-0.01683002	-0.017773752	-0.018234296
43733.63938	-0.016855526	-0.016463788	-0.016899559	-0.017845413	-0.018306993
43733.63938	-0.016995529	-0.016602014	-0.017039307	-0.017989407	-0.018453068
43733.63938	-0.017065868	-0.016671465	-0.017109517	-0.018061741	-0.018526446
43733.63938	-0.017136432	-0.016741142	-0.017179952	-0.0181343	-0.018600052
43733.63938	-0.017207222	-0.016811044	-0.017250612	-0.018207085	-0.018673886
43733.63938	-0.017278237	-0.016881174	-0.017321497	-0.018280095	-0.018747949
43733.63938	-0.01734948	-0.01695153	-0.017392608	-0.018353331	-0.01882224
43733.63938	-0.017420949	-0.017022113	-0.017463946	-0.018426794	-0.018896761
43733.63938	-0.017492645	-0.017092924	-0.01753551	-0.018500484	-0.018971512
43733.63938	-0.017564569	-0.017163964	-0.017607301	-0.018574401	-0.019046493
43733.63938	-0.017636722	-0.017235232	-0.017679319	-0.018648546	-0.019121704
43733.63938	-0.017709102	-0.017306728	-0.017751565	-0.018722918	-0.019197146
43733.63938	-0.017781712	-0.017378454	-0.017824039	-0.018797519	-0.019272819
43733.63938	-0.01785455	-0.01745041	-0.017896741	-0.018872349	-0.019348724
43733.63938	-0.017927619	-0.017522596	-0.017969672	-0.018947408	-0.019424861
43733.63938	-0.018000917	-0.017595012	-0.018042833	-0.019022697	-0.01950123
43733.63938	-0.018074445	-0.017667659	-0.018116223	-0.019098215	-0.019577831
43733.63938	-0.018148205	-0.017740537	-0.018189844	-0.019173964	-0.019654666
43733.63938	-0.018222195	-0.017813647	-0.018263694	-0.019249943	-0.019731734
43733.63938	-0.018296417	-0.017886989	-0.018337776	-0.019326153	-0.019809036
43733.63938	-0.018370871	-0.017960563	-0.018412088	-0.019402595	-0.019886572
43733.63938	-0.018445556	-0.01803437	-0.018486632	-0.019479268	-0.019964343
43733.63938	-0.018520475	-0.01810841	-0.018561409	-0.019556174	-0.020042348
43733.63938	-0.018595627	-0.018182683	-0.018636417	-0.019633311	-0.020120589
43733.63938	-0.018671011	-0.018257191	-0.018711658	-0.019710682	-0.020199065
43733.63938	-0.01874663	-0.018331932	-0.018787132	-0.019788286	-0.020277778
43733.63938	-0.018822483	-0.018406909	-0.018862839	-0.019866123	-0.020356726
43733.63938	-0.01889857	-0.01848212	-0.01893878	-0.019944194	-0.020435911
43733.63938	-0.018974892	-0.018557567	-0.019014955	-0.020022499	-0.020515334
43733.63938	-0.019051449	-0.018633249	-0.019091365	-0.020101039	-0.020594993
43733.63938	-0.019128242	-0.018709168	-0.01916801	-0.020179814	-0.020674891

43733.63938	-0.019205271	-0.018785323	-0.01924489	-0.020258824	-0.020755026
43733.63938	-0.019282536	-0.018861715	-0.019322005	-0.020338069	-0.0208354
43733.63938	-0.019360038	-0.018938344	-0.019399356	-0.020417551	-0.020916013

Table D1.2 Table of Excitation and Reflection Axial Defect Signal

Sample Rate:	750000	Hz			
Measurement Type	Time Waveform	Time Waveform	Time Waveform	Time Waveform	Time Waveform
Channel Name	DT9816-S(00).Ain 0	DT9816-S(00).Ain 1	DT9816-S(00).Ain 2	DT9816-S(00).Ain 3	DT9816-S(00).Ain 4
X Axis Units	Sec	Sec	Sec	Sec	Sec
Y Axis Units	V	V	V	V	V
Excel Time Format	Real	Real	Real	Real	Real
43733.59201	0.00111623	0.00125489	7.36E-04	4.82E-04	9.37E-04
43733.59201	0.001114085	0.001252219	7.34E-04	4.82E-04	9.35E-04
43733.59201	0.001111962	0.001249581	7.33E-04	4.81E-04	9.34E-04
43733.59201	0.001109863	0.001246975	7.31E-04	4.80E-04	9.33E-04
43733.59201	0.001107787	0.001244402	7.30E-04	4.80E-04	9.31E-04
43733.59201	0.001105734	0.001241862	7.28E-04	4.79E-04	9.30E-04
43733.59201	0.001103704	0.001239354	7.27E-04	4.78E-04	9.28E-04
43733.59201	0.001101697	0.001236879	7.25E-04	4.78E-04	9.27E-04
43733.59201	0.001099713	0.001234436	7.23E-04	4.77E-04	9.26E-04
43733.59201	0.001097751	0.001232026	7.22E-04	4.76E-04	9.24E-04
43733.59201	0.001095813	0.001229648	7.20E-04	4.76E-04	9.23E-04
43733.59201	0.001093898	0.001227303	7.19E-04	4.75E-04	9.22E-04
43733.59201	0.001092005	0.00122499	7.17E-04	4.74E-04	9.20E-04
43733.59201	0.001090135	0.00122271	7.16E-04	4.74E-04	9.19E-04
43733.59201	0.001088288	0.001220462	7.14E-04	4.73E-04	9.18E-04
43733.59201	0.001086464	0.001218246	7.13E-04	4.72E-04	9.17E-04
43733.59201	0.001084663	0.001216062	7.11E-04	4.72E-04	9.16E-04
43733.59201	0.001082884	0.001213911	7.10E-04	4.71E-04	9.14E-04
43733.59201	0.001081129	0.001211792	7.08E-04	4.70E-04	9.13E-04
43733.59201	0.001079395	0.001209705	7.07E-04	4.69E-04	9.12E-04
43733.59201	0.001077685	0.00120765	7.06E-04	4.69E-04	9.11E-04
43733.59201	0.001075997	0.001205627	7.04E-04	4.68E-04	9.10E-04
43733.59201	0.001074332	0.001203637	7.03E-04	4.67E-04	9.09E-04
43733.59201	0.001072689	0.001201678	7.01E-04	4.66E-04	9.08E-04
43733.59201	0.001071069	0.001199751	7.00E-04	4.66E-04	9.07E-04

43733.59201	0.001069472	0.001197856	6.98E-04	4.65E-04	9.06E-04
43733.59201	0.001067897	0.001195994	6.97E-04	4.64E-04	9.05E-04
43733.59201	0.001066344	0.001194163	6.96E-04	4.64E-04	9.04E-04
43733.59201	0.001064814	0.001192364	6.94E-04	4.63E-04	9.03E-04
43733.59201	0.001063306	0.001190596	6.93E-04	4.62E-04	9.02E-04
43733.59201	0.001061821	0.001188861	6.92E-04	4.61E-04	9.01E-04
43733.59201	0.001060358	0.001187157	6.90E-04	4.60E-04	9.00E-04
43733.59201	0.001058918	0.001185484	6.89E-04	4.60E-04	8.99E-04
43733.59201	0.001057499	0.001183844	6.88E-04	4.59E-04	8.98E-04
43733.59201	0.001056103	0.001182235	6.86E-04	4.58E-04	8.97E-04
43733.59201	0.001054729	0.001180657	6.85E-04	4.57E-04	8.96E-04
43733.59201	0.001053378	0.001179111	6.84E-04	4.57E-04	8.95E-04
43733.59201	0.001050741	0.001176113	6.81E-04	4.55E-04	8.94E-04
43733.59201	0.001049456	0.001174661	6.80E-04	4.54E-04	8.93E-04
43733.59201	0.001048192	0.00117324	6.78E-04	4.53E-04	8.92E-04
43733.59201	0.001046951	0.001171851	6.77E-04	4.53E-04	8.91E-04
43733.59201	0.001045732	0.001170493	6.76E-04	4.52E-04	8.91E-04
43733.59201	0.001044534	0.001169166	6.75E-04	4.51E-04	8.90E-04
43733.59201	0.001043359	0.00116787	6.73E-04	4.50E-04	8.89E-04
43733.59201	0.001042205	0.001166605	6.72E-04	4.49E-04	8.88E-04
43733.59201	0.001041073	0.001165371	6.71E-04	4.48E-04	8.88E-04
43733.59201	0.001039963	0.001164168	6.70E-04	4.48E-04	8.87E-04
43733.59201	0.001038874	0.001162996	6.68E-04	4.47E-04	8.86E-04
43733.59201	0.001037808	0.001161854	6.67E-04	4.46E-04	8.86E-04
43733.59201	0.001036762	0.001160744	6.66E-04	4.45E-04	8.85E-04
43733.59201	0.001035739	0.001159664	6.65E-04	4.44E-04	8.85E-04
43733.59201	0.001034737	0.001158615	6.64E-04	4.43E-04	8.84E-04
43733.59201	0.001033756	0.001157596	6.63E-04	4.42E-04	8.83E-04
43733.59201	0.001032797	0.001156608	6.61E-04	4.42E-04	8.83E-04
43733.59201	0.001031859	0.00115565	6.60E-04	4.41E-04	8.82E-04
43733.59201	0.001030942	0.001154723	6.59E-04	4.40E-04	8.82E-04
43733.59201	0.001030046	0.001153826	6.58E-04	4.39E-04	8.81E-04
43733.59201	0.001029172	0.001152959	6.57E-04	4.38E-04	8.81E-04
43733.59201	0.001028319	0.001152122	6.56E-04	4.37E-04	8.80E-04
43733.59201	0.001027487	0.001151316	6.55E-04	4.36E-04	8.80E-04
43733.59201	0.001026676	0.00115054	6.53E-04	4.35E-04	8.80E-04
43733.59201	0.001025886	0.001149793	6.52E-04	4.35E-04	8.79E-04
43733.59201	0.001025117	0.001149077	6.51E-04	4.34E-04	8.79E-04

43733.59201	0.001024368	0.00114839	6.50E-04	4.33E-04	8.78E-04
43733.59201	0.001023641	0.001147733	6.49E-04	4.32E-04	8.78E-04
43733.59201	0.001022934	0.001147106	6.48E-04	4.31E-04	8.78E-04
43733.59201	0.001022248	0.001146508	6.47E-04	4.30E-04	8.77E-04
43733.59201	0.001021582	0.00114594	6.46E-04	4.29E-04	8.77E-04
43733.59201	0.001020937	0.001145401	6.45E-04	4.28E-04	8.77E-04
43733.59201	0.001020312	0.001144892	6.44E-04	4.27E-04	8.76E-04
43733.59201	0.001019707	0.001144412	6.43E-04	4.26E-04	8.76E-04
43733.59201	0.001019123	0.001143961	6.42E-04	4.25E-04	8.76E-04
43733.59201	0.001018559	0.00114354	6.41E-04	4.24E-04	8.76E-04
43733.59201	0.001018015	0.001143147	6.40E-04	4.23E-04	8.75E-04
43733.59201	0.001014013	0.001140905	6.31E-04	4.14E-04	8.74E-04
43733.59201	0.001013666	0.001140798	6.30E-04	4.13E-04	8.74E-04
43733.59201	0.001013338	0.001140719	6.29E-04	4.12E-04	8.74E-04
43733.59201	0.001013029	0.001140667	6.28E-04	4.11E-04	8.74E-04
43733.59201	0.001012739	0.001140644	6.27E-04	4.10E-04	8.74E-04
43733.59201	0.001012468	0.001140648	6.26E-04	4.09E-04	8.74E-04
43733.59201	0.001012216	0.001140679	6.25E-04	4.08E-04	8.74E-04
43733.59201	0.001011983	0.001140738	6.24E-04	4.07E-04	8.74E-04
43733.59201	0.001011768	0.001140825	6.23E-04	4.06E-04	8.74E-04
43733.59201	0.001011572	0.001140939	6.22E-04	4.05E-04	8.74E-04
43733.59201	0.001011395	0.001141079	6.21E-04	4.04E-04	8.74E-04
43733.59201	0.001011235	0.001141247	6.21E-04	4.03E-04	8.74E-04
43733.59201	0.001011094	0.001141442	6.20E-04	4.02E-04	8.74E-04
43733.59201	0.001010971	0.001141664	6.19E-04	4.01E-04	8.74E-04
43733.59201	0.001010866	0.001141912	6.18E-04	4.00E-04	8.74E-04
43733.59201	0.001010779	0.001142187	6.17E-04	3.98E-04	8.74E-04
43733.59201	0.001010709	0.001142488	6.16E-04	3.97E-04	8.75E-04
43733.59201	0.001010658	0.001142815	6.15E-04	3.96E-04	8.75E-04
43733.59201	0.001010623	0.001143169	6.14E-04	3.95E-04	8.75E-04
43733.59201	0.001010607	0.001143549	6.14E-04	3.94E-04	8.75E-04
43733.59201	0.001010607	0.001143954	6.13E-04	3.93E-04	8.75E-04
43733.59201	0.001010625	0.001144386	6.12E-04	3.92E-04	8.75E-04
43733.59201	0.00101066	0.001144843	6.11E-04	3.91E-04	8.76E-04
43733.59201	0.001010711	0.001145326	6.10E-04	3.89E-04	8.76E-04
43733.59201	0.00101078	0.001145834	6.09E-04	3.88E-04	8.76E-04
43733.59201	0.001010865	0.001146367	6.09E-04	3.87E-04	8.76E-04
43733.59201	0.001010967	0.001146925	6.08E-04	3.86E-04	8.77E-04

43733.59201	0.001011085	0.001147508	6.07E-04	3.85E-04	8.77E-04
43733.59201	0.00101122	0.001148117	6.06E-04	3.83E-04	8.77E-04
43733.59201	0.001011371	0.001148749	6.05E-04	3.82E-04	8.77E-04
43733.59201	0.001011537	0.001149407	6.04E-04	3.81E-04	8.78E-04
43733.59201	0.00101172	0.001150089	6.04E-04	3.80E-04	8.78E-04
43733.59201	0.001011918	0.001150795	6.03E-04	3.79E-04	8.78E-04
43733.59201	0.001012133	0.001151525	6.02E-04	3.77E-04	8.79E-04
43733.59201	0.001012362	0.001152279	6.01E-04	3.76E-04	8.79E-04
43733.59201	0.001012607	0.001153056	6.00E-04	3.75E-04	8.79E-04
43733.59201	0.001012867	0.001153858	6.00E-04	3.73E-04	8.80E-04
43733.59201	0.001015867	0.001162108	5.93E-04	3.62E-04	8.84E-04
43733.59201	0.001016271	0.001163136	5.92E-04	3.60E-04	8.84E-04
43733.59201	0.001016688	0.001164187	5.91E-04	3.59E-04	8.84E-04
43733.59201	0.001017118	0.001165259	5.90E-04	3.58E-04	8.85E-04
43733.59201	0.001017562	0.001166353	5.89E-04	3.56E-04	8.85E-04
43733.59201	0.001018019	0.001167468	5.89E-04	3.55E-04	8.86E-04
43733.59201	0.001018488	0.001168604	5.88E-04	3.53E-04	8.86E-04
43733.59201	0.00101897	0.001169761	5.87E-04	3.52E-04	8.87E-04
43733.59201	0.001019465	0.001170938	5.86E-04	3.50E-04	8.87E-04
43733.59201	0.001019972	0.001172137	5.86E-04	3.49E-04	8.88E-04
43733.59201	0.001020491	0.001173355	5.85E-04	3.48E-04	8.89E-04
43733.59201	0.001021022	0.001174594	5.84E-04	3.46E-04	8.89E-04
43733.59201	0.001021565	0.001175852	5.83E-04	3.45E-04	8.90E-04
43733.59201	0.001022119	0.001177131	5.83E-04	3.43E-04	8.90E-04
43733.59201	0.001022685	0.001178429	5.82E-04	3.42E-04	8.91E-04
43733.59201	0.001023262	0.001179746	5.81E-04	3.40E-04	8.91E-04
43733.59201	0.001023849	0.001181083	5.80E-04	3.38E-04	8.92E-04
43733.59201	0.001024448	0.001182438	5.79E-04	3.37E-04	8.93E-04
43733.59201	0.001025058	0.001183812	5.79E-04	3.35E-04	8.93E-04
43733.59201	0.001025677	0.001185205	5.78E-04	3.34E-04	8.94E-04
43733.59201	0.001026307	0.001186616	5.77E-04	3.32E-04	8.94E-04
43733.59201	0.001026947	0.001188045	5.76E-04	3.31E-04	8.95E-04
43733.59201	0.001027597	0.001189493	5.76E-04	3.29E-04	8.96E-04
43733.59201	0.001028257	0.001190958	5.75E-04	3.27E-04	8.96E-04
43733.59201	0.001028926	0.00119244	5.74E-04	3.26E-04	8.97E-04
43733.59201	0.001029604	0.00119394	5.73E-04	3.24E-04	8.97E-04
43733.59201	0.001030292	0.001195457	5.72E-04	3.22E-04	8.98E-04
43733.59201	0.001030988	0.00119699	5.72E-04	3.21E-04	8.99E-04

43733.59201	0.001031692	0.00119854	5.71E-04	3.19E-04	8.99E-04
43733.59201	0.001032405	0.001200107	5.70E-04	3.17E-04	9.00E-04
43733.59201	0.001033127	0.00120169	5.69E-04	3.16E-04	9.01E-04
43733.59201	0.001033856	0.001203289	5.68E-04	3.14E-04	9.01E-04
43733.59201	0.001034593	0.001204903	5.68E-04	3.12E-04	9.02E-04
43733.59201	0.001035338	0.001206533	5.67E-04	3.10E-04	9.03E-04
43733.59201	0.001036089	0.001208179	5.66E-04	3.09E-04	9.03E-04
43733.59201	0.001036848	0.001209839	5.65E-04	3.07E-04	9.04E-04
43733.59201	0.001037614	0.001211514	5.64E-04	3.05E-04	9.04E-04
43733.59201	0.001044777	0.001227215	5.57E-04	2.88E-04	9.11E-04
43733.59201	0.001045599	0.001229024	5.56E-04	2.86E-04	9.11E-04
43733.59201	0.001046425	0.001230846	5.55E-04	2.84E-04	9.12E-04
43733.59201	0.001047255	0.001232679	5.54E-04	2.82E-04	9.13E-04
43733.59201	0.001048088	0.001234524	5.53E-04	2.80E-04	9.13E-04
43733.59201	0.001048926	0.00123638	5.52E-04	2.78E-04	9.14E-04
43733.59201	0.001049766	0.001238247	5.51E-04	2.76E-04	9.15E-04
43733.59201	0.00105061	0.001240125	5.50E-04	2.74E-04	9.15E-04
43733.59201	0.001051456	0.001242013	5.49E-04	2.72E-04	9.16E-04
43733.59201	0.001052305	0.001243912	5.48E-04	2.69E-04	9.17E-04
43733.59201	0.001053156	0.001245821	5.47E-04	2.67E-04	9.17E-04
43733.59201	0.001054009	0.001247739	5.46E-04	2.65E-04	9.18E-04
43733.59201	0.001054863	0.001249666	5.45E-04	2.63E-04	9.18E-04
43733.59201	0.00105572	0.001251603	5.44E-04	2.61E-04	9.19E-04
43733.59201	0.001056577	0.001253548	5.43E-04	2.58E-04	9.20E-04
43733.59201	0.001057435	0.001255502	5.42E-04	2.56E-04	9.20E-04
43733.59201	0.001058294	0.001257465	5.41E-04	2.54E-04	9.21E-04
43733.59201	0.001059153	0.001259435	5.40E-04	2.52E-04	9.22E-04
43733.59201	0.001060013	0.001261413	5.39E-04	2.49E-04	9.22E-04
43733.59201	0.001060872	0.001263398	5.38E-04	2.47E-04	9.23E-04
43733.59201	0.00106173	0.001265391	5.37E-04	2.45E-04	9.24E-04
43733.59201	0.001062588	0.00126739	5.36E-04	2.42E-04	9.24E-04
43733.59201	0.001063445	0.001269396	5.35E-04	2.40E-04	9.25E-04
43733.59201	0.001064301	0.001271408	5.34E-04	2.37E-04	9.25E-04
43733.59201	0.001065155	0.001273425	5.33E-04	2.35E-04	9.26E-04
43733.59201	0.001066007	0.001275449	5.32E-04	2.32E-04	9.27E-04
43733.59201	0.001066857	0.001277478	5.30E-04	2.30E-04	9.27E-04
43733.59201	0.001067704	0.001279512	5.29E-04	2.27E-04	9.28E-04
43733.59201	0.001068549	0.00128155	5.28E-04	2.25E-04	9.28E-04

43733.59201	0.001069391	0.001283593	5.27E-04	2.22E-04	9.29E-04
43733.59201	0.001070229	0.00128564	5.26E-04	2.20E-04	9.29E-04
43733.59201	0.001071064	0.001287691	5.25E-04	2.17E-04	9.30E-04
43733.59201	0.001071895	0.001289746	5.23E-04	2.14E-04	9.30E-04
43733.59201	0.001072721	0.001291803	5.22E-04	2.12E-04	9.31E-04
43733.59201	0.001073543	0.001293864	5.21E-04	2.09E-04	9.32E-04
43733.59201	0.00107436	0.001295926	5.20E-04	2.06E-04	9.32E-04
43733.59201	0.001075172	0.001297991	5.18E-04	2.04E-04	9.33E-04
43733.59201	0.001082196	0.001316623	5.06E-04	1.78E-04	9.37E-04
43733.59201	0.001082939	0.001318692	5.04E-04	1.75E-04	9.37E-04
43733.59201	0.001083673	0.001320759	5.03E-04	1.71E-04	9.37E-04
43733.59201	0.001084399	0.001322825	5.01E-04	1.68E-04	9.38E-04
43733.59201	0.001085115	0.001324889	5.00E-04	1.65E-04	9.38E-04
43733.59201	0.001085821	0.00132695	4.98E-04	1.62E-04	9.38E-04
43733.59201	0.001086517	0.001329008	4.97E-04	1.59E-04	9.39E-04
43733.59201	0.001087203	0.001331064	4.95E-04	1.56E-04	9.39E-04
43733.59201	0.001087879	0.001333115	4.94E-04	1.53E-04	9.39E-04
43733.59201	0.001088543	0.001335163	4.92E-04	1.49E-04	9.39E-04
43733.59201	0.001089196	0.001337207	4.90E-04	1.46E-04	9.40E-04
43733.59201	0.001089837	0.001339246	4.89E-04	1.43E-04	9.40E-04
43733.59201	0.001090467	0.00134128	4.87E-04	1.39E-04	9.40E-04
43733.59201	0.001091084	0.001343309	4.85E-04	1.36E-04	9.40E-04
43733.59201	0.001091688	0.001345332	4.84E-04	1.32E-04	9.41E-04
43733.59201	0.001092279	0.001347349	4.82E-04	1.29E-04	9.41E-04
43733.59201	0.001092857	0.00134936	4.80E-04	1.25E-04	9.41E-04
43733.59201	0.001093421	0.001351364	4.78E-04	1.22E-04	9.41E-04
43733.59201	0.00109397	0.00135336	4.76E-04	1.18E-04	9.41E-04
43733.59201	0.001094506	0.00135535	4.75E-04	1.15E-04	9.41E-04
43733.59201	0.001095026	0.001357331	4.73E-04	1.11E-04	9.41E-04
43733.59201	0.001095531	0.001359304	4.71E-04	1.07E-04	9.41E-04
43733.59201	0.001096021	0.001361269	4.69E-04	1.04E-04	9.41E-04
43733.59201	0.001096494	0.001363224	4.67E-04	9.99E-05	9.41E-04
43733.59201	0.001096952	0.00136517	4.65E-04	9.61E-05	9.41E-04
43733.59201	0.001097392	0.001367107	4.63E-04	9.23E-05	9.41E-04
43733.59201	0.001097816	0.001369033	4.61E-04	8.85E-05	9.41E-04
43733.59201	0.001098222	0.001370949	4.59E-04	8.46E-05	9.41E-04
43733.59201	0.00109861	0.001372854	4.57E-04	8.06E-05	9.41E-04
43733.59201	0.001098981	0.001374747	4.55E-04	7.67E-05	9.41E-04

43733.59201	0.001099332	0.001376629	4.53E-04	7.27E-05	9.41E-04
43733.59201	0.001099665	0.001378499	4.50E-04	6.86E-05	9.41E-04
43733.59201	0.001099979	0.001380356	4.48E-04	6.45E-05	9.40E-04
43733.59201	0.001100272	0.0013822	4.46E-04	6.04E-05	9.40E-04
43733.59201	0.001100546	0.001384031	4.44E-04	5.62E-05	9.40E-04
43733.59201	0.001100799	0.001385849	4.41E-04	5.20E-05	9.40E-04
43733.59201	0.001101032	0.001387652	4.39E-04	4.78E-05	9.39E-04
43733.59201	0.001102122	0.001403182	4.17E-04	7.70E-06	9.36E-04
43733.59201	0.001102124	0.001404822	4.14E-04	3.03E-06	9.35E-04
43733.59201	0.001102102	0.001406444	4.11E-04	-1.68E-06	9.34E-04
43733.59201	0.001102053	0.001408046	4.09E-04	-6.44E-06	9.34E-04
43733.59201	0.001101979	0.00140963	4.06E-04	-1.12E-05	9.33E-04
43733.59201	0.001101878	0.001411193	4.03E-04	-1.61E-05	9.32E-04
43733.59201	0.001101751	0.001412736	4.00E-04	-2.10E-05	9.32E-04
43733.59201	0.001101596	0.001414259	3.97E-04	-2.59E-05	9.31E-04
43733.59201	0.001101414	0.00141576	3.95E-04	-3.09E-05	9.30E-04
43733.59201	0.001101203	0.00141724	3.92E-04	-3.59E-05	9.29E-04
43733.59201	0.001100964	0.001418697	3.89E-04	-4.10E-05	9.29E-04
43733.59201	0.001100696	0.001420133	3.86E-04	-4.61E-05	9.28E-04
43733.59201	0.001100399	0.001421545	3.83E-04	-5.13E-05	9.27E-04
43733.59201	0.001100072	0.001422935	3.80E-04	-5.65E-05	9.26E-04
43733.59201	0.001099715	0.0014243	3.76E-04	-6.18E-05	9.25E-04
43733.59201	0.001099328	0.001425641	3.73E-04	-6.71E-05	9.24E-04
43733.59201	0.001098909	0.001426958	3.70E-04	-7.25E-05	9.23E-04
43733.59201	0.001098459	0.00142825	3.67E-04	-7.79E-05	9.22E-04
43733.59201	0.001097977	0.001429516	3.63E-04	-8.34E-05	9.20E-04
43733.59201	0.001097463	0.001430756	3.60E-04	-8.89E-05	9.19E-04
43733.59201	0.001096916	0.00143197	3.57E-04	-9.45E-05	9.18E-04
43733.59201	0.001096336	0.001433157	3.53E-04	-1.00E-04	9.17E-04
43733.59201	0.001095722	0.001434317	3.50E-04	-1.06E-04	9.16E-04
43733.59201	0.001095074	0.001435449	3.46E-04	-1.12E-04	9.14E-04
43733.59201	0.001094392	0.001436552	3.43E-04	-1.17E-04	9.13E-04
43733.59201	0.001093674	0.001437628	3.39E-04	-1.23E-04	9.11E-04
43733.59201	0.001092922	0.001438674	3.36E-04	-1.29E-04	9.10E-04
43733.59201	0.001092133	0.00143969	3.32E-04	-1.35E-04	9.09E-04
43733.59201	0.001091309	0.001440677	3.28E-04	-1.41E-04	9.07E-04
43733.59201	0.001090447	0.001441633	3.25E-04	-1.47E-04	9.05E-04
43733.59201	0.001089549	0.001442558	3.21E-04	-1.53E-04	9.04E-04

43733.59201	0.001088613	0.001443451	3.17E-04	-1.59E-04	9.02E-04
43733.59201	0.001087639	0.001444313	3.13E-04	-1.66E-04	9.00E-04
43733.59201	0.001086626	0.001445142	3.09E-04	-1.72E-04	8.99E-04
43733.59201	0.001085574	0.001445939	3.05E-04	-1.78E-04	8.97E-04
43733.59201	0.001084483	0.001446702	3.01E-04	-1.84E-04	8.95E-04
43733.59201	0.001083353	0.001447432	2.97E-04	-1.91E-04	8.93E-04
43733.59201	0.001071305	0.001452401	2.58E-04	-2.52E-04	8.74E-04
43733.59201	0.00106975	0.001452767	2.53E-04	-2.59E-04	8.72E-04
43733.59201	0.001068151	0.001453094	2.49E-04	-2.66E-04	8.70E-04
43733.59201	0.001066505	0.001453382	2.44E-04	-2.73E-04	8.67E-04
43733.59201	0.001064814	0.001453629	2.39E-04	-2.80E-04	8.65E-04
43733.59201	0.001063077	0.001453836	2.34E-04	-2.87E-04	8.62E-04
43733.59201	0.001061292	0.001454002	2.29E-04	-2.95E-04	8.60E-04
43733.59201	0.00105946	0.001454126	2.24E-04	-3.02E-04	8.57E-04
43733.59201	0.001057581	0.001454208	2.19E-04	-3.10E-04	8.54E-04
43733.59201	0.001055653	0.001454248	2.14E-04	-3.17E-04	8.52E-04
43733.59201	0.001053676	0.001454245	2.09E-04	-3.25E-04	8.49E-04
43733.59201	0.00105165	0.001454199	2.04E-04	-3.33E-04	8.46E-04
43733.59201	0.001049574	0.001454108	1.99E-04	-3.40E-04	8.43E-04
43733.59201	0.001047448	0.001453973	1.94E-04	-3.48E-04	8.40E-04
43733.59201	0.001045271	0.001453794	1.88E-04	-3.56E-04	8.37E-04
43733.59201	0.001043043	0.001453568	1.83E-04	-3.64E-04	8.34E-04
43733.59201	0.001040763	0.001453297	1.78E-04	-3.72E-04	8.31E-04
43733.59201	0.001038431	0.001452979	1.72E-04	-3.80E-04	8.28E-04
43733.59201	0.001036046	0.001452614	1.66E-04	-3.88E-04	8.24E-04
43733.59201	0.001033608	0.001452202	1.61E-04	-3.97E-04	8.21E-04
43733.59201	0.001031117	0.001451741	1.55E-04	-4.05E-04	8.18E-04
43733.59201	0.001028571	0.001451232	1.49E-04	-4.13E-04	8.14E-04
43733.59201	0.001025971	0.001450674	1.44E-04	-4.22E-04	8.11E-04
43733.59201	0.001023315	0.001450066	1.38E-04	-4.30E-04	8.07E-04
43733.59201	0.001020603	0.001449409	1.32E-04	-4.39E-04	8.04E-04
43733.59201	0.001017836	0.001448701	1.26E-04	-4.47E-04	8.00E-04
43733.59201	0.001015012	0.001447941	1.20E-04	-4.56E-04	7.96E-04
43733.59201	0.00101213	0.00144713	1.14E-04	-4.65E-04	7.92E-04
43733.59201	0.001009191	0.001446267	1.07E-04	-4.74E-04	7.89E-04
43733.59201	0.001006194	0.001445351	1.01E-04	-4.83E-04	7.85E-04
43733.59201	0.001003137	0.001444382	9.47E-05	-4.92E-04	7.81E-04
43733.59201	0.001000022	0.001443359	8.83E-05	-5.01E-04	7.77E-04

43733.59201	9.97E-04	0.001442282	8.19E-05	-5.10E-04	7.73E-04
43733.59201	9.94E-04	0.00144115	7.53E-05	-5.19E-04	7.68E-04
43733.59201	9.90E-04	0.001439963	6.87E-05	-5.29E-04	7.64E-04
43733.59201	9.87E-04	0.00143872	6.21E-05	-5.38E-04	7.60E-04
43733.59201	9.84E-04	0.001437421	5.53E-05	-5.48E-04	7.55E-04
43733.59201	9.50E-04	0.001423101	-8.50E-06	-6.37E-04	7.13E-04
43733.59201	9.46E-04	0.001421208	-1.60E-05	-6.47E-04	7.08E-04
43733.59201	9.42E-04	0.001419253	-2.35E-05	-6.57E-04	7.03E-04
43733.59201	9.37E-04	0.001417235	-3.11E-05	-6.68E-04	6.98E-04
43733.59201	9.33E-04	0.001415154	-3.88E-05	-6.78E-04	6.92E-04
43733.59201	9.29E-04	0.001413009	-4.65E-05	-6.89E-04	6.87E-04
43733.59201	9.24E-04	0.0014108	-5.44E-05	-7.00E-04	6.82E-04
43733.59201	9.20E-04	0.001408525	-6.23E-05	-7.10E-04	6.76E-04
43733.59201	9.15E-04	0.001406185	-7.03E-05	-7.21E-04	6.71E-04
43733.59201	9.11E-04	0.001403779	-7.83E-05	-7.32E-04	6.65E-04
43733.59201	9.06E-04	0.001401306	-8.65E-05	-7.43E-04	6.59E-04
43733.59201	9.01E-04	0.001398765	-9.47E-05	-7.54E-04	6.53E-04
43733.59201	8.97E-04	0.001396157	-1.03E-04	-7.66E-04	6.47E-04
43733.59201	8.92E-04	0.001393481	-1.11E-04	-7.77E-04	6.41E-04
43733.59201	8.87E-04	0.001390736	-1.20E-04	-7.88E-04	6.35E-04
43733.59201	8.82E-04	0.001387921	-1.28E-04	-8.00E-04	6.29E-04
43733.59201	8.76E-04	0.001385036	-1.37E-04	-8.12E-04	6.23E-04
43733.59201	8.71E-04	0.001382081	-1.46E-04	-8.23E-04	6.17E-04
43733.59201	8.66E-04	0.001379054	-1.55E-04	-8.35E-04	6.10E-04
43733.59201	8.61E-04	0.001375956	-1.63E-04	-8.47E-04	6.04E-04
43733.59201	8.55E-04	0.001372786	-1.72E-04	-8.59E-04	5.97E-04
43733.59201	8.50E-04	0.001369542	-1.81E-04	-8.71E-04	5.91E-04
43733.59201	8.44E-04	0.001366226	-1.91E-04	-8.83E-04	5.84E-04
43733.59201	8.38E-04	0.001362835	-2.00E-04	-8.95E-04	5.77E-04
43733.59201	8.33E-04	0.00135937	-2.09E-04	-9.07E-04	5.71E-04
43733.59201	8.27E-04	0.00135583	-2.18E-04	-9.20E-04	5.64E-04
43733.59201	8.21E-04	0.001352214	-2.28E-04	-9.32E-04	5.57E-04
43733.59201	8.15E-04	0.001348522	-2.38E-04	-9.45E-04	5.49E-04
43733.59201	8.09E-04	0.001344753	-2.47E-04	-9.58E-04	5.42E-04
43733.59201	8.03E-04	0.001340906	-2.57E-04	-9.71E-04	5.35E-04
43733.59201	7.96E-04	0.001336982	-2.67E-04	-9.83E-04	5.28E-04
43733.59201	7.90E-04	0.001332979	-2.77E-04	-9.96E-04	5.20E-04
43733.59201	7.84E-04	0.001328898	-2.87E-04	-0.001009526	5.13E-04

43733.59201	7.77E-04	0.001324736	-2.97E-04	-0.001022717	5.05E-04
43733.59201	7.71E-04	0.001320494	-3.07E-04	-0.001036007	4.97E-04
43733.59201	7.64E-04	0.001316172	-3.17E-04	-0.001049396	4.89E-04
43733.59201	7.57E-04	0.001311768	-3.28E-04	-0.001062885	4.81E-04
43733.59201	6.92E-04	0.001268373	-4.25E-04	-0.00118887	4.06E-04
43733.59201	6.85E-04	0.001263124	-4.37E-04	-0.001203387	3.97E-04
43733.59201	6.77E-04	0.001257786	-4.48E-04	-0.00121801	3.88E-04
43733.59201	6.69E-04	0.00125236	-4.60E-04	-0.001232738	3.79E-04
43733.59201	6.61E-04	0.001246845	-4.71E-04	-0.001247574	3.70E-04
43733.59201	6.53E-04	0.00124124	-4.83E-04	-0.001262517	3.61E-04
43733.59201	6.45E-04	0.001235545	-4.95E-04	-0.001277567	3.51E-04
43733.59201	6.37E-04	0.00122976	-5.07E-04	-0.001292726	3.42E-04
43733.59201	6.29E-04	0.001223883	-5.19E-04	-0.001307993	3.32E-04
43733.59201	6.20E-04	0.001217914	-5.31E-04	-0.00132337	3.23E-04
43733.59201	6.12E-04	0.001211853	-5.43E-04	-0.001338857	3.13E-04
43733.59201	6.03E-04	0.001205698	-5.55E-04	-0.001354454	3.03E-04
43733.59201	5.94E-04	0.00119945	-5.68E-04	-0.001370162	2.93E-04
43733.59201	5.86E-04	0.001193108	-5.80E-04	-0.001385981	2.83E-04
43733.59201	5.77E-04	0.00118667	-5.93E-04	-0.001401913	2.73E-04
43733.59201	5.68E-04	0.001180138	-6.06E-04	-0.001417957	2.63E-04
43733.59201	5.59E-04	0.001173509	-6.19E-04	-0.001434114	2.52E-04
43733.59201	5.50E-04	0.001166783	-6.32E-04	-0.001450384	2.42E-04
43733.59201	5.40E-04	0.00115996	-6.45E-04	-0.001466769	2.31E-04
43733.59201	5.31E-04	0.001153039	-6.58E-04	-0.001483268	2.21E-04
43733.59201	5.21E-04	0.00114602	-6.71E-04	-0.001499883	2.10E-04
43733.59201	5.12E-04	0.001138901	-6.84E-04	-0.001516613	1.99E-04
43733.59201	5.02E-04	0.001131683	-6.98E-04	-0.001533459	1.88E-04
43733.59201	4.92E-04	0.001124365	-7.12E-04	-0.001550423	1.77E-04
43733.59201	4.82E-04	0.001116946	-7.25E-04	-0.001567503	1.66E-04
43733.59201	4.72E-04	0.001109425	-7.39E-04	-0.001584702	1.54E-04
43733.59201	4.62E-04	0.001101802	-7.53E-04	-0.001602018	1.43E-04
43733.59201	4.52E-04	0.001094076	-7.67E-04	-0.001619454	1.31E-04
43733.59201	4.42E-04	0.001086247	-7.81E-04	-0.001637009	1.20E-04
43733.59201	4.31E-04	0.001078315	-7.96E-04	-0.001654685	1.08E-04
43733.59201	4.21E-04	0.001070277	-8.10E-04	-0.001672481	9.59E-05
43733.59201	4.10E-04	0.001062135	-8.24E-04	-0.001690398	8.38E-05
43733.59201	3.99E-04	0.001053887	-8.39E-04	-0.001708436	7.17E-05
43733.59201	3.88E-04	0.001045532	-8.54E-04	-0.001726597	5.95E-05

283

43733.59201	3.77E-04	0.001037071	-8.69E-04	-0.00174488	4.71E-05
43733.59201	3.66E-04	0.001028502	-8.84E-04	-0.001763287	3.46E-05
43733.59201	3.55E-04	0.001019824	-8.99E-04	-0.001781818	2.20E-05
43733.59201	2.49E-04	9.37E-04	-0.001039926	-0.001954254	-9.67E-05
43733.59201	2.37E-04	9.27E-04	-0.001056218	-0.001974053	-1.10E-04
43733.59201	2.24E-04	9.17E-04	-0.001072633	-0.001993982	-1.24E-04
43733.59201	2.11E-04	9.07E-04	-0.001089172	-0.00201404	-1.38E-04
43733.59201	1.99E-04	8.97E-04	-0.001105835	-0.00203423	-1.53E-04
43733.59201	1.86E-04	8.87E-04	-0.001122623	-0.002054552	-1.67E-04
43733.59201	1.73E-04	8.76E-04	-0.001139537	-0.002075005	-1.81E-04
43733.59201	1.60E-04	8.66E-04	-0.001156577	-0.002095591	-1.96E-04
43733.59201	1.47E-04	8.55E-04	-0.001173743	-0.00211631	-2.11E-04
43733.59201	1.33E-04	8.44E-04	-0.001191037	-0.002137162	-2.25E-04
43733.59201	1.20E-04	8.34E-04	-0.001208458	-0.002158149	-2.40E-04
43733.59201	1.06E-04	8.23E-04	-0.001226009	-0.002179271	-2.55E-04
43733.59201	9.24E-05	8.12E-04	-0.001243687	-0.002200528	-2.70E-04
43733.59201	7.86E-05	8.00E-04	-0.001261496	-0.002221921	-2.86E-04
43733.59201	6.47E-05	7.89E-04	-0.001279435	-0.00224345	-3.01E-04
43733.59201	5.06E-05	7.78E-04	-0.001297504	-0.002265116	-3.17E-04
43733.59201	3.64E-05	7.66E-04	-0.001315705	-0.00228692	-3.33E-04
43733.59201	2.20E-05	7.54E-04	-0.001334037	-0.002308862	-3.48E-04
43733.59201	7.54E-06	7.42E-04	-0.001352502	-0.002330943	-3.64E-04
43733.59201	-7.06E-06	7.30E-04	-0.0013711	-0.002353162	-3.80E-04
43733.59201	-2.18E-05	7.18E-04	-0.001389831	-0.002375522	-3.97E-04
43733.59201	-3.67E-05	7.06E-04	-0.001408697	-0.002398022	-4.13E-04
43733.59201	-5.16E-05	6.94E-04	-0.001427697	-0.002420662	-4.30E-04
43733.59201	-6.68E-05	6.81E-04	-0.001446833	-0.002443445	-4.46E-04
43733.59201	-8.20E-05	6.69E-04	-0.001466104	-0.002466369	-4.63E-04
43733.59201	-9.74E-05	6.56E-04	-0.001485512	-0.002489435	-4.80E-04
43733.59201	-1.13E-04	6.43E-04	-0.001505057	-0.002512645	-4.97E-04
43733.59201	-1.29E-04	6.30E-04	-0.00152474	-0.002535998	-5.14E-04
43733.59201	-1.44E-04	6.17E-04	-0.001544561	-0.002559496	-5.32E-04
43733.59201	-1.60E-04	6.04E-04	-0.00156452	-0.002583138	-5.49E-04
43733.59201	-1.76E-04	5.90E-04	-0.001584619	-0.002606925	-5.67E-04
43733.59201	-1.93E-04	5.77E-04	-0.001604858	-0.002630859	-5.84E-04
43733.59201	-2.09E-04	5.63E-04	-0.001625237	-0.002654939	-6.02E-04
43733.59201	-2.25E-04	5.50E-04	-0.001645758	-0.002679166	-6.20E-04
43733.59201	-2.42E-04	5.36E-04	-0.00166642	-0.00270354	-6.39E-04

43733.59201	-2.59E-04	5.22E-04	-0.001687224	-0.002728062	-6.57E-04
43733.59201	-2.76E-04	5.07E-04	-0.001708171	-0.002752733	-6.75E-04
43733.59201	-4.34E-04	3.74E-04	-0.001903218	-0.002981554	-8.48E-04
43733.59201	-4.52E-04	3.58E-04	-0.001925625	-0.003007743	-8.68E-04
43733.59201	-4.71E-04	3.42E-04	-0.001948182	-0.003034086	-8.88E-04
43733.59201	-4.89E-04	3.26E-04	-0.001970888	-0.003060584	-9.08E-04
43733.59201	-5.08E-04	3.10E-04	-0.001993745	-0.003087238	-9.29E-04
43733.59201	-5.27E-04	2.94E-04	-0.002016752	-0.003114049	-9.49E-04
43733.59201	-5.46E-04	2.78E-04	-0.002039911	-0.003141017	-9.70E-04
43733.59201	-5.65E-04	2.61E-04	-0.002063222	-0.003168142	-9.91E-04
43733.59201	-5.84E-04	2.45E-04	-0.002086686	-0.003195426	-0.001011905
43733.59201	-6.04E-04	2.28E-04	-0.002110303	-0.003222868	-0.001033068
43733.59201	-6.24E-04	2.11E-04	-0.002134074	-0.003250469	-0.001054387
43733.59201	-6.43E-04	1.94E-04	-0.002158	-0.003278231	-0.001075861
43733.59201	-6.63E-04	1.77E-04	-0.00218208	-0.003306152	-0.001097492
43733.59201	-6.83E-04	1.60E-04	-0.002206316	-0.003334235	-0.001119281
43733.59201	-7.04E-04	1.42E-04	-0.002230709	-0.003362479	-0.001141227
43733.59201	-7.24E-04	1.25E-04	-0.002255258	-0.003390885	-0.001163331
43733.59201	-7.45E-04	1.07E-04	-0.002279964	-0.003419454	-0.001185595
43733.59201	-7.65E-04	8.89E-05	-0.002304828	-0.003448186	-0.001208018
43733.59201	-7.86E-04	7.08E-05	-0.002329851	-0.003477081	-0.001230602
43733.59201	-8.07E-04	5.25E-05	-0.002355033	-0.003506141	-0.001253346
43733.59201	-8.28E-04	3.41E-05	-0.002380374	-0.003535366	-0.001276252
43733.59201	-8.50E-04	1.56E-05	-0.002405876	-0.003564756	-0.001299319
43733.59201	-8.71E-04	-3.12E-06	-0.002431539	-0.003594312	-0.00132255
43733.59201	-8.93E-04	-2.20E-05	-0.002457363	-0.003624035	-0.001345943
43733.59201	-9.15E-04	-4.10E-05	-0.002483349	-0.003653925	-0.001369501
43733.59201	-9.37E-04	-6.02E-05	-0.002509498	-0.003683982	-0.001393223
43733.59201	-9.59E-04	-7.95E-05	-0.00253581	-0.003714208	-0.00141711
43733.59201	-9.81E-04	-9.90E-05	-0.002562285	-0.003744602	-0.001441163
43733.59201	-0.001003624	-1.19E-04	-0.002588925	-0.003775166	-0.001465382
43733.59201	-0.001026247	-1.38E-04	-0.00261573	-0.003805899	-0.001489768
43733.59201	-0.001049033	-1.58E-04	-0.0026427	-0.003836803	-0.001514321
43733.59201	-0.001071982	-1.79E-04	-0.002669836	-0.003867878	-0.001539043
43733.59201	-0.001095096	-1.99E-04	-0.002697139	-0.003899124	-0.001563933
43733.59201	-0.001118374	-2.19E-04	-0.00272461	-0.003930543	-0.001588993
43733.59201	-0.001141818	-2.40E-04	-0.002752248	-0.003962134	-0.001614223
43733.59201	-0.001165427	-2.61E-04	-0.002780054	-0.003993898	-0.001639623

43733.59201	-0.001189204	-2.82E-04	-0.002808029	-0.004025837	-0.001665194
43733.59201	-0.001410787	-4.78E-04	-0.003067507	-0.004321191	-0.001903137
43733.59201	-0.001436263	-5.00E-04	-0.003097204	-0.004354897	-0.001930453
43733.59201	-0.001461912	-5.23E-04	-0.003127076	-0.004388784	-0.001957947
43733.59201	-0.001487735	-5.46E-04	-0.003157124	-0.00442285	-0.001985619
43733.59201	-0.001513732	-5.69E-04	-0.003187349	-0.004457098	-0.002013471
43733.59201	-0.001539905	-5.93E-04	-0.003217751	-0.004491527	-0.002041502
43733.59201	-0.001566253	-6.16E-04	-0.00324833	-0.004526138	-0.002069713
43733.59201	-0.001592777	-6.40E-04	-0.003279088	-0.004560932	-0.002098104
43733.59201	-0.001619479	-6.64E-04	-0.003310024	-0.004595909	-0.002126678
43733.59201	-0.001646358	-6.88E-04	-0.00334114	-0.00463107	-0.002155433
43733.59201	-0.001673415	-7.12E-04	-0.003372436	-0.004666415	-0.002184371
43733.59201	-0.001700651	-7.36E-04	-0.003403912	-0.004701945	-0.002213492
43733.59201	-0.001728066	-7.61E-04	-0.003435569	-0.00473766	-0.002242797
43733.59201	-0.001755661	-7.86E-04	-0.003467408	-0.004773562	-0.002272286
43733.59201	-0.001783436	-8.10E-04	-0.00349943	-0.004809649	-0.002301961
43733.59201	-0.001811393	-8.36E-04	-0.003531634	-0.004845924	-0.002331821
43733.59201	-0.001839532	-8.61E-04	-0.003564021	-0.004882387	-0.002361867
43733.59201	-0.001867852	-8.86E-04	-0.003596593	-0.004919037	-0.0023921
43733.59201	-0.001896356	-9.12E-04	-0.003629349	-0.004955876	-0.00242252
43733.59201	-0.001925044	-9.38E-04	-0.00366229	-0.004992905	-0.002453129
43733.59201	-0.001953915	-9.64E-04	-0.003695417	-0.005030123	-0.002483925
43733.59201	-0.001982971	-9.90E-04	-0.00372873	-0.005067532	-0.002514912
43733.59201	-0.002012213	-0.001016152	-0.00376223	-0.005105131	-0.002546088
43733.59201	-0.00204164	-0.00104269	-0.003795917	-0.005142922	-0.002577454
43733.59201	-0.002071255	-0.001069413	-0.003829792	-0.005180905	-0.002609011
43733.59201	-0.002101056	-0.001096322	-0.003863856	-0.005219081	-0.00264076
43733.59201	-0.002131045	-0.001123416	-0.003898109	-0.005257449	-0.002672701
43733.59201	-0.002161222	-0.001150698	-0.003932552	-0.005296011	-0.002704835
43733.59201	-0.002191588	-0.001178166	-0.003967185	-0.005334767	-0.002737162
43733.59201	-0.002222144	-0.001205823	-0.004002009	-0.005373718	-0.002769684
43733.59201	-0.00225289	-0.001233668	-0.004037024	-0.005412865	-0.002802399
43733.59201	-0.002283827	-0.001261702	-0.004072231	-0.005452207	-0.00283531
43733.59201	-0.002314955	-0.001289926	-0.004107631	-0.005491745	-0.002868417
43733.59201	-0.002346275	-0.00131834	-0.004143223	-0.00553148	-0.00290172
43733.59201	-0.002377787	-0.001346945	-0.00417901	-0.005571413	-0.00293522
43733.59201	-0.002409493	-0.001375742	-0.00421499	-0.005611543	-0.002968917
43733.59201	-0.002441392	-0.001404731	-0.004251166	-0.005651872	-0.003002812

286

43733.59201	-0.002737301	-0.001674379	-0.004585603	-0.006023855	-0.003316883
43733.59201	-0.00277117	-0.001705324	-0.004623758	-0.006066199	-0.003352791
43733.59201	-0.002805239	-0.001736467	-0.004662113	-0.006108747	-0.003388905
43733.59201	-0.002839509	-0.001767809	-0.00470067	-0.0061515	-0.003425223
43733.59201	-0.002873981	-0.001799352	-0.004739429	-0.006194458	-0.003461747
43733.59201	-0.002908654	-0.001831096	-0.004778391	-0.006237623	-0.003498478
43733.59201	-0.00294353	-0.00186304	-0.004817556	-0.006280994	-0.003535415
43733.59201	-0.002978609	-0.001895187	-0.004856924	-0.006324572	-0.00357256
43733.59201	-0.003013892	-0.001927536	-0.004896497	-0.006368358	-0.003609912
43733.59201	-0.003049379	-0.001960088	-0.004936275	-0.006412351	-0.003647474
43733.59201	-0.003085071	-0.001992844	-0.004976258	-0.006456554	-0.003685244
43733.59201	-0.003120969	-0.002025805	-0.005016448	-0.006500966	-0.003723225
43733.59201	-0.003157072	-0.00205897	-0.005056844	-0.006545587	-0.003761416
43733.59201	-0.003193383	-0.00209234	-0.005097447	-0.006590419	-0.003799817
43733.59201	-0.0032299	-0.002125917	-0.005138257	-0.006635461	-0.00383843
43733.59201	-0.003266625	-0.002159701	-0.005179276	-0.006680715	-0.003877256
43733.59201	-0.003303559	-0.002193692	-0.005220504	-0.00672618	-0.003916294
43733.59201	-0.003340702	-0.00222789	-0.005261941	-0.006771858	-0.003955545
43733.59201	-0.003378054	-0.002262298	-0.005303587	-0.006817749	-0.00399501
43733.59201	-0.003415616	-0.002296914	-0.005345444	-0.006863853	-0.004034689
43733.59201	-0.003453389	-0.00233174	-0.005387513	-0.006910171	-0.004074583
43733.59201	-0.003491373	-0.002366776	-0.005429792	-0.006956704	-0.004114693
43733.59201	-0.00352957	-0.002402024	-0.005472284	-0.007003451	-0.004155019
43733.59201	-0.003567978	-0.002437482	-0.005514988	-0.007050414	-0.004195561
43733.59201	-0.0036066	-0.002473153	-0.005557906	-0.007097593	-0.004236321
43733.59201	-0.003645435	-0.002509037	-0.005601037	-0.007144989	-0.004277299
43733.59201	-0.003684484	-0.002545133	-0.005644382	-0.007192602	-0.004318495
43733.59201	-0.003723748	-0.002581444	-0.005687942	-0.007240432	-0.004359909
43733.59201	-0.003763227	-0.002617969	-0.005731718	-0.00728848	-0.004401544
43733.59201	-0.003802923	-0.002654709	-0.005775709	-0.007336747	-0.004443398
43733.59201	-0.003842834	-0.002691665	-0.005819917	-0.007385233	-0.004485473
43733.59201	-0.003882963	-0.002728836	-0.005864342	-0.007433938	-0.004527769
43733.59201	-0.003923309	-0.002766225	-0.005908984	-0.007482864	-0.004570287
43733.59201	-0.003963873	-0.002803831	-0.005953844	-0.007532011	-0.004613028
43733.59201	-0.004004656	-0.002841655	-0.005998923	-0.007581378	-0.004655991
43733.59201	-0.004045658	-0.002879697	-0.006044221	-0.007630967	-0.004699177
43733.59201	-0.00408688	-0.002917959	-0.006089738	-0.007680779	-0.004742588
43733.59201	-0.004128323	-0.00295644	-0.006135476	-0.007730813	-0.004786223

43733.59201	-0.004467864	-0.003272269	-0.006509368	-0.008139164	-0.005143455
43733.59201	-0.004511316	-0.003312754	-0.006557111	-0.008191225	-0.005189136
43733.59201	-0.004554993	-0.003353464	-0.00660508	-0.008243514	-0.005235048
43733.59201	-0.004598897	-0.003394401	-0.006653275	-0.008296032	-0.005281189
43733.59201	-0.004643028	-0.003435563	-0.006701696	-0.008348778	-0.005327562
43733.59201	-0.004687386	-0.003476953	-0.006750344	-0.008401753	-0.005374167
43733.59201	-0.004731973	-0.003518571	-0.00679922	-0.008454958	-0.005421004
43733.59201	-0.004776789	-0.003560417	-0.006848324	-0.008508393	-0.005468074
43733.59201	-0.004821834	-0.003602492	-0.006897657	-0.008562059	-0.005515378
43733.59201	-0.004867108	-0.003644797	-0.006947219	-0.008615956	-0.005562915
43733.59201	-0.004912614	-0.003687332	-0.006997011	-0.008670085	-0.005610686
43733.59201	-0.00495835	-0.003730097	-0.007047032	-0.008724447	-0.005658693
43733.59201	-0.005004317	-0.003773093	-0.007097285	-0.008779041	-0.005706935
43733.59201	-0.005050517	-0.003816321	-0.007147769	-0.008833868	-0.005755414
43733.59201	-0.005096949	-0.003859782	-0.007198484	-0.008888929	-0.005804129
43733.59201	-0.005143614	-0.003903475	-0.007249432	-0.008944224	-0.005853081
43733.59201	-0.005190513	-0.003947402	-0.007300612	-0.008999753	-0.00590227
43733.59201	-0.005237647	-0.003991562	-0.007352026	-0.009055518	-0.005951698
43733.59201	-0.005285015	-0.004035958	-0.007403674	-0.009111519	-0.006001365
43733.59201	-0.005332618	-0.004080588	-0.007455556	-0.009167755	-0.006051271
43733.59201	-0.005380457	-0.004125454	-0.007507673	-0.009224229	-0.006101417
43733.59201	-0.005428533	-0.004170556	-0.007560025	-0.009280939	-0.006151803
43733.59201	-0.005476845	-0.004215895	-0.007612613	-0.009337887	-0.006202431
43733.59201	-0.005525395	-0.004261471	-0.007665437	-0.009395073	-0.006253299
43733.59201	-0.005574183	-0.004307285	-0.007718498	-0.009452498	-0.00630441
43733.59201	-0.005623209	-0.004353338	-0.007771797	-0.009510161	-0.006355763
43733.59201	-0.005672475	-0.004399629	-0.007825333	-0.009568064	-0.006407359
43733.59201	-0.00572198	-0.00444616	-0.007879108	-0.009626207	-0.006459198
43733.59201	-0.005771725	-0.004492932	-0.007933122	-0.009684591	-0.006511282
43733.59201	-0.005821711	-0.004539943	-0.007987375	-0.009743215	-0.00656361
43733.59201	-0.005871938	-0.004587196	-0.008041868	-0.009802081	-0.006616183
43733.59201	-0.005922406	-0.004634691	-0.008096601	-0.009861189	-0.006669002
43733.59201	-0.005973117	-0.004682428	-0.008151576	-0.009920539	-0.006722067
43733.59201	-0.006024071	-0.004730408	-0.008206791	-0.009980132	-0.006775379
43733.59201	-0.006075268	-0.004778631	-0.008262249	-0.010039968	-0.006828938
43733.59201	-0.006126708	-0.004827097	-0.008317949	-0.010100048	-0.006882744
43733.59201	-0.006178393	-0.004875809	-0.008373892	-0.010160372	-0.006936799
43733.59201	-0.006230323	-0.004924765	-0.008430078	-0.010220941	-0.006991102

43733.59201	-0.006387587	-0.005073109	-0.008600101	-0.010404121	-0.00715551
43733.59201	-0.006440501	-0.005123051	-0.008657266	-0.010465673	-0.007210814
43733.59201	-0.006493663	-0.00517324	-0.008714676	-0.010527473	-0.007266368
43733.59201	-0.006547073	-0.005223677	-0.008772333	-0.010589519	-0.007322175
43733.59201	-0.006600731	-0.005274363	-0.008830236	-0.010651814	-0.007378234
43733.59201	-0.006654638	-0.005325299	-0.008888387	-0.010714357	-0.007434545

Table D1.3 Table of Excitation and Reflection Angle / Gradient Axial Defect Signal

Sample Rate:	750000	Hz			
Measurement Type	Time Waveform	Time Waveform	Time Waveform	Time Waveform	Time Waveform
Channel Name	DT9816-S(00).Ain 0	DT9816-S(00).Ain 1	DT9816-S(00).Ain 2	DT9816-S(00).Ain 3	DT9816-S(00).Ain 4
X Axis Units	Sec	Sec	Sec	Sec	Sec
Y Axis Units	V	V	V	V	V
Excel Time Format	Real	Real	Real	Real	Real
43733.74812	-7.54E-04	-6.46E-04	-8.91E-04	-5.26E-04	-4.21E-04
43733.74812	-7.54E-04	-6.46E-04	-8.91E-04	-5.26E-04	-4.21E-04
43733.74812	-7.53E-04	-6.45E-04	-8.91E-04	-5.26E-04	-4.21E-04
43733.74812	-7.53E-04	-6.45E-04	-8.90E-04	-5.26E-04	-4.21E-04
43733.74812	-7.53E-04	-6.45E-04	-8.90E-04	-5.26E-04	-4.21E-04
43733.74812	-7.52E-04	-6.45E-04	-8.90E-04	-5.26E-04	-4.21E-04
43733.74812	-7.52E-04	-6.44E-04	-8.90E-04	-5.26E-04	-4.21E-04
43733.74812	-7.52E-04	-6.44E-04	-8.90E-04	-5.26E-04	-4.21E-04
43733.74812	-7.51E-04	-6.44E-04	-8.91E-04	-5.26E-04	-4.21E-04
43733.74812	-7.51E-04	-6.44E-04	-8.91E-04	-5.26E-04	-4.21E-04
43733.74812	-7.51E-04	-6.44E-04	-8.91E-04	-5.26E-04	-4.21E-04
43733.74812	-7.50E-04	-6.44E-04	-8.91E-04	-5.26E-04	-4.22E-04
43733.74812	-7.50E-04	-6.44E-04	-8.91E-04	-5.27E-04	-4.22E-04
43733.74812	-7.50E-04	-6.44E-04	-8.91E-04	-5.27E-04	-4.22E-04
43733.74812	-7.49E-04	-6.44E-04	-8.91E-04	-5.27E-04	-4.22E-04
43733.74812	-7.49E-04	-6.44E-04	-8.92E-04	-5.28E-04	-4.23E-04
43733.74812	-7.49E-04	-6.44E-04	-8.92E-04	-5.28E-04	-4.23E-04
43733.74812	-7.49E-04	-6.44E-04	-8.92E-04	-5.28E-04	-4.23E-04
43733.74812	-7.48E-04	-6.44E-04	-8.92E-04	-5.29E-04	-4.24E-04

43733.74812	-7.48E-04	-6.44E-04	-8.93E-04	-5.29E-04	-4.24E-04
43733.74812	-7.48E-04	-6.44E-04	-8.93E-04	-5.30E-04	-4.25E-04
43733.74812	-7.47E-04	-6.44E-04	-8.94E-04	-5.30E-04	-4.25E-04
43733.74812	-7.47E-04	-6.44E-04	-8.94E-04	-5.31E-04	-4.26E-04
43733.74812	-7.47E-04	-6.45E-04	-8.94E-04	-5.32E-04	-4.26E-04
43733.74812	-7.46E-04	-6.45E-04	-8.95E-04	-5.32E-04	-4.27E-04
43733.74812	-7.46E-04	-6.45E-04	-8.95E-04	-5.33E-04	-4.28E-04
43733.74812	-7.46E-04	-6.45E-04	-8.96E-04	-5.34E-04	-4.28E-04
43733.74812	-7.46E-04	-6.46E-04	-8.96E-04	-5.34E-04	-4.29E-04
43733.74812	-7.45E-04	-6.46E-04	-8.97E-04	-5.35E-04	-4.30E-04
43733.74812	-7.45E-04	-6.47E-04	-8.97E-04	-5.36E-04	-4.31E-04
43733.74812	-7.45E-04	-6.47E-04	-8.98E-04	-5.37E-04	-4.31E-04
43733.74812	-7.44E-04	-6.47E-04	-8.99E-04	-5.38E-04	-4.32E-04
43733.74812	-7.44E-04	-6.48E-04	-8.99E-04	-5.39E-04	-4.33E-04
43733.74812	-7.44E-04	-6.48E-04	-9.00E-04	-5.40E-04	-4.34E-04
43733.74812	-7.43E-04	-6.49E-04	-9.01E-04	-5.41E-04	-4.35E-04
43733.74812	-7.43E-04	-6.49E-04	-9.01E-04	-5.42E-04	-4.36E-04
43733.74812	-7.42E-04	-6.52E-04	-9.04E-04	-5.46E-04	-4.40E-04
43733.74812	-7.42E-04	-6.52E-04	-9.05E-04	-5.47E-04	-4.41E-04
43733.74812	-7.42E-04	-6.53E-04	-9.06E-04	-5.49E-04	-4.43E-04
43733.74812	-7.41E-04	-6.54E-04	-9.07E-04	-5.50E-04	-4.44E-04
43733.74812	-7.41E-04	-6.54E-04	-9.08E-04	-5.51E-04	-4.45E-04
43733.74812	-7.41E-04	-6.55E-04	-9.09E-04	-5.52E-04	-4.46E-04
43733.74812	-7.40E-04	-6.56E-04	-9.10E-04	-5.54E-04	-4.48E-04
43733.74812	-7.40E-04	-6.57E-04	-9.11E-04	-5.55E-04	-4.49E-04
43733.74812	-7.40E-04	-6.58E-04	-9.12E-04	-5.57E-04	-4.50E-04
43733.74812	-7.40E-04	-6.59E-04	-9.13E-04	-5.58E-04	-4.52E-04
43733.74812	-7.39E-04	-6.59E-04	-9.14E-04	-5.60E-04	-4.53E-04
43733.74812	-7.39E-04	-6.60E-04	-9.15E-04	-5.61E-04	-4.54E-04
43733.74812	-7.39E-04	-6.61E-04	-9.16E-04	-5.63E-04	-4.56E-04
43733.74812	-7.39E-04	-6.62E-04	-9.17E-04	-5.64E-04	-4.57E-04
43733.74812	-7.38E-04	-6.63E-04	-9.18E-04	-5.66E-04	-4.59E-04
43733.74812	-7.38E-04	-6.64E-04	-9.19E-04	-5.67E-04	-4.61E-04
43733.74812	-7.38E-04	-6.65E-04	-9.20E-04	-5.69E-04	-4.62E-04
43733.74812	-7.38E-04	-6.66E-04	-9.22E-04	-5.71E-04	-4.64E-04
43733.74812	-7.37E-04	-6.67E-04	-9.23E-04	-5.73E-04	-4.66E-04
43733.74812	-7.37E-04	-6.69E-04	-9.24E-04	-5.74E-04	-4.67E-04
43733.74812	-7.37E-04	-6.70E-04	-9.25E-04	-5.76E-04	-4.69E-04

43733.74812	-7.37E-04	-6.71E-04	-9.27E-04	-5.78E-04	-4.71E-04
43733.74812	-7.36E-04	-6.72E-04	-9.28E-04	-5.80E-04	-4.73E-04
43733.74812	-7.36E-04	-6.73E-04	-9.29E-04	-5.82E-04	-4.74E-04
43733.74812	-7.36E-04	-6.74E-04	-9.31E-04	-5.84E-04	-4.76E-04
43733.74812	-7.36E-04	-6.76E-04	-9.32E-04	-5.86E-04	-4.78E-04
43733.74812	-7.35E-04	-6.77E-04	-9.33E-04	-5.88E-04	-4.80E-04
43733.74812	-7.35E-04	-6.78E-04	-9.35E-04	-5.90E-04	-4.82E-04
43733.74812	-7.35E-04	-6.80E-04	-9.36E-04	-5.92E-04	-4.84E-04
43733.74812	-7.35E-04	-6.81E-04	-9.38E-04	-5.94E-04	-4.86E-04
43733.74812	-7.34E-04	-6.82E-04	-9.39E-04	-5.96E-04	-4.88E-04
43733.74812	-7.34E-04	-6.84E-04	-9.41E-04	-5.98E-04	-4.90E-04
43733.74812	-7.34E-04	-6.85E-04	-9.42E-04	-6.00E-04	-4.92E-04
43733.74812	-7.34E-04	-6.87E-04	-9.44E-04	-6.03E-04	-4.95E-04
43733.74812	-7.34E-04	-6.88E-04	-9.46E-04	-6.05E-04	-4.97E-04
43733.74812	-7.33E-04	-6.90E-04	-9.47E-04	-6.07E-04	-4.99E-04
43733.74812	-7.33E-04	-6.96E-04	-9.54E-04	-6.17E-04	-5.08E-04
43733.74812	-7.32E-04	-6.98E-04	-9.56E-04	-6.19E-04	-5.11E-04
43733.74812	-7.32E-04	-6.99E-04	-9.58E-04	-6.22E-04	-5.13E-04
43733.74812	-7.32E-04	-7.01E-04	-9.59E-04	-6.24E-04	-5.15E-04
43733.74812	-7.32E-04	-7.03E-04	-9.61E-04	-6.27E-04	-5.18E-04
43733.74812	-7.32E-04	-7.04E-04	-9.63E-04	-6.29E-04	-5.20E-04
43733.74812	-7.31E-04	-7.06E-04	-9.65E-04	-6.32E-04	-5.23E-04
43733.74812	-7.31E-04	-7.08E-04	-9.67E-04	-6.35E-04	-5.25E-04
43733.74812	-7.31E-04	-7.10E-04	-9.69E-04	-6.37E-04	-5.28E-04
43733.74812	-7.31E-04	-7.12E-04	-9.71E-04	-6.40E-04	-5.31E-04
43733.74812	-7.31E-04	-7.14E-04	-9.73E-04	-6.43E-04	-5.33E-04
43733.74812	-7.31E-04	-7.15E-04	-9.75E-04	-6.46E-04	-5.36E-04
43733.74812	-7.30E-04	-7.17E-04	-9.77E-04	-6.49E-04	-5.39E-04
43733.74812	-7.30E-04	-7.19E-04	-9.79E-04	-6.51E-04	-5.42E-04
43733.74812	-7.30E-04	-7.21E-04	-9.81E-04	-6.54E-04	-5.44E-04
43733.74812	-7.30E-04	-7.23E-04	-9.83E-04	-6.57E-04	-5.47E-04
43733.74812	-7.30E-04	-7.25E-04	-9.85E-04	-6.60E-04	-5.50E-04
43733.74812	-7.30E-04	-7.27E-04	-9.87E-04	-6.63E-04	-5.53E-04
43733.74812	-7.30E-04	-7.29E-04	-9.89E-04	-6.66E-04	-5.56E-04
43733.74812	-7.29E-04	-7.32E-04	-9.91E-04	-6.69E-04	-5.59E-04
43733.74812	-7.29E-04	-7.34E-04	-9.94E-04	-6.72E-04	-5.62E-04
43733.74812	-7.29E-04	-7.36E-04	-9.96E-04	-6.76E-04	-5.65E-04
43733.74812	-7.29E-04	-7.38E-04	-9.98E-04	-6.79E-04	-5.68E-04

43733.74812	-7.29E-04	-7.40E-04	-0.001000272	-6.82E-04	-5.71E-04
43733.74812	-7.29E-04	-7.43E-04	-0.001002577	-6.85E-04	-5.74E-04
43733.74812	-7.29E-04	-7.45E-04	-0.001004906	-6.88E-04	-5.77E-04
43733.74812	-7.29E-04	-7.47E-04	-0.00100726	-6.92E-04	-5.80E-04
43733.74812	-7.28E-04	-7.49E-04	-0.001009638	-6.95E-04	-5.84E-04
43733.74812	-7.28E-04	-7.52E-04	-0.001012042	-6.98E-04	-5.87E-04
43733.74812	-7.28E-04	-7.54E-04	-0.001014471	-7.02E-04	-5.90E-04
43733.74812	-7.28E-04	-7.56E-04	-0.001016925	-7.05E-04	-5.93E-04
43733.74812	-7.28E-04	-7.59E-04	-0.001019404	-7.09E-04	-5.97E-04
43733.74812	-7.28E-04	-7.61E-04	-0.001021909	-7.12E-04	-6.00E-04
43733.74812	-7.28E-04	-7.64E-04	-0.001024438	-7.16E-04	-6.04E-04
43733.74812	-7.28E-04	-7.66E-04	-0.001026994	-7.19E-04	-6.07E-04
43733.74812	-7.28E-04	-7.69E-04	-0.001029574	-7.23E-04	-6.10E-04
43733.74812	-7.28E-04	-7.79E-04	-0.001040153	-7.38E-04	-6.25E-04
43733.74812	-7.28E-04	-7.82E-04	-0.001042862	-7.41E-04	-6.28E-04
43733.74812	-7.28E-04	-7.85E-04	-0.001045597	-7.45E-04	-6.32E-04
43733.74812	-7.28E-04	-7.87E-04	-0.001048358	-7.49E-04	-6.36E-04
43733.74812	-7.28E-04	-7.90E-04	-0.001051145	-7.53E-04	-6.39E-04
43733.74812	-7.28E-04	-7.93E-04	-0.001053959	-7.57E-04	-6.43E-04
43733.74812	-7.28E-04	-7.96E-04	-0.001056799	-7.61E-04	-6.47E-04
43733.74812	-7.28E-04	-7.99E-04	-0.001059665	-7.65E-04	-6.51E-04
43733.74812	-7.28E-04	-8.01E-04	-0.001062557	-7.69E-04	-6.55E-04
43733.74812	-7.28E-04	-8.04E-04	-0.001065476	-7.73E-04	-6.59E-04
43733.74812	-7.28E-04	-8.07E-04	-0.001068422	-7.77E-04	-6.63E-04
43733.74812	-7.28E-04	-8.10E-04	-0.001071395	-7.81E-04	-6.67E-04
43733.74812	-7.28E-04	-8.13E-04	-0.001074394	-7.85E-04	-6.71E-04
43733.74812	-7.28E-04	-8.16E-04	-0.001077421	-7.89E-04	-6.75E-04
43733.74812	-7.28E-04	-8.19E-04	-0.001080474	-7.93E-04	-6.79E-04
43733.74812	-7.28E-04	-8.22E-04	-0.001083555	-7.98E-04	-6.83E-04
43733.74812	-7.28E-04	-8.25E-04	-0.001086663	-8.02E-04	-6.87E-04
43733.74812	-7.28E-04	-8.28E-04	-0.001089798	-8.06E-04	-6.91E-04
43733.74812	-7.28E-04	-8.32E-04	-0.001092961	-8.11E-04	-6.95E-04
43733.74812	-7.28E-04	-8.35E-04	-0.001096151	-8.15E-04	-7.00E-04
43733.74812	-7.29E-04	-8.38E-04	-0.001099369	-8.19E-04	-7.04E-04
43733.74812	-7.29E-04	-8.41E-04	-0.001102615	-8.24E-04	-7.08E-04
43733.74812	-7.29E-04	-8.44E-04	-0.001105889	-8.28E-04	-7.13E-04
43733.74812	-7.29E-04	-8.48E-04	-0.001109191	-8.33E-04	-7.17E-04
43733.74812	-7.29E-04	-8.51E-04	-0.001112521	-8.38E-04	-7.22E-04

43733.74812	-7.29E-04	-8.54E-04	-0.00111588	-8.42E-04	-7.26E-04
43733.74812	-7.29E-04	-8.58E-04	-0.001119267	-8.47E-04	-7.31E-04
43733.74812	-7.30E-04	-8.61E-04	-0.001122682	-8.52E-04	-7.35E-04
43733.74812	-7.30E-04	-8.65E-04	-0.001126126	-8.56E-04	-7.40E-04
43733.74812	-7.30E-04	-8.68E-04	-0.001129599	-8.61E-04	-7.44E-04
43733.74812	-7.30E-04	-8.72E-04	-0.001133101	-8.66E-04	-7.49E-04
43733.74812	-7.30E-04	-8.75E-04	-0.001136632	-8.71E-04	-7.54E-04
43733.74812	-7.31E-04	-8.79E-04	-0.001140192	-8.76E-04	-7.58E-04
43733.74812	-7.31E-04	-8.82E-04	-0.001143781	-8.80E-04	-7.63E-04
43733.74812	-7.31E-04	-8.86E-04	-0.0011474	-8.85E-04	-7.68E-04
43733.74812	-7.31E-04	-8.90E-04	-0.001151048	-8.90E-04	-7.73E-04
43733.74812	-7.33E-04	-9.05E-04	-0.001165941	-9.11E-04	-7.93E-04
43733.74812	-7.33E-04	-9.08E-04	-0.001169739	-9.16E-04	-7.98E-04
43733.74812	-7.33E-04	-9.12E-04	-0.001173568	-9.21E-04	-8.03E-04
43733.74812	-7.34E-04	-9.16E-04	-0.001177428	-9.26E-04	-8.08E-04
43733.74812	-7.34E-04	-9.20E-04	-0.001181318	-9.32E-04	-8.13E-04
43733.74812	-7.34E-04	-9.24E-04	-0.001185239	-9.37E-04	-8.18E-04
43733.74812	-7.35E-04	-9.28E-04	-0.001189192	-9.42E-04	-8.23E-04
43733.74812	-7.35E-04	-9.32E-04	-0.001193175	-9.48E-04	-8.29E-04
43733.74812	-7.36E-04	-9.36E-04	-0.00119719	-9.53E-04	-8.34E-04
43733.74812	-7.36E-04	-9.40E-04	-0.001201236	-9.59E-04	-8.39E-04
43733.74812	-7.37E-04	-9.44E-04	-0.001205315	-9.64E-04	-8.45E-04
43733.74812	-7.37E-04	-9.48E-04	-0.001209425	-9.70E-04	-8.50E-04
43733.74812	-7.37E-04	-9.53E-04	-0.001213567	-9.75E-04	-8.55E-04
43733.74812	-7.38E-04	-9.57E-04	-0.001217741	-9.81E-04	-8.61E-04
43733.74812	-7.38E-04	-9.61E-04	-0.001221948	-9.87E-04	-8.66E-04
43733.74812	-7.39E-04	-9.65E-04	-0.001226187	-9.92E-04	-8.72E-04
43733.74812	-7.39E-04	-9.70E-04	-0.001230459	-9.98E-04	-8.78E-04
43733.74812	-7.40E-04	-9.74E-04	-0.001234763	-0.001004035	-8.83E-04
43733.74812	-7.41E-04	-9.78E-04	-0.001239101	-0.001009885	-8.89E-04
43733.74812	-7.41E-04	-9.83E-04	-0.001243472	-0.001015776	-8.95E-04
43733.74812	-7.42E-04	-9.87E-04	-0.001247876	-0.001021708	-9.00E-04
43733.74812	-7.42E-04	-9.92E-04	-0.001252314	-0.001027681	-9.06E-04
43733.74812	-7.43E-04	-9.96E-04	-0.001256786	-0.001033696	-9.12E-04
43733.74812	-7.44E-04	-0.001000765	-0.001261292	-0.001039752	-9.18E-04
43733.74812	-7.44E-04	-0.001005361	-0.001265832	-0.00104585	-9.24E-04
43733.74812	-7.45E-04	-0.001009992	-0.001270406	-0.001051991	-9.30E-04
43733.74812	-7.46E-04	-0.00101466	-0.001275015	-0.001058173	-9.36E-04

43733.74812	-7.46E-04	-0.001019363	-0.001279658	-0.001064398	-9.42E-04
43733.74812	-7.47E-04	-0.001024103	-0.001284336	-0.001070665	-9.48E-04
43733.74812	-7.48E-04	-0.00102888	-0.00128905	-0.001076975	-9.54E-04
43733.74812	-7.49E-04	-0.001033694	-0.001293799	-0.001083328	-9.60E-04
43733.74812	-7.49E-04	-0.001038545	-0.001298583	-0.001089724	-9.67E-04
43733.74812	-7.50E-04	-0.001043433	-0.001303403	-0.001096164	-9.73E-04
43733.74812	-7.51E-04	-0.001048358	-0.001308258	-0.001102646	-9.79E-04
43733.74812	-7.52E-04	-0.001053321	-0.00131315	-0.001109173	-9.86E-04
43733.74812	-7.53E-04	-0.001058322	-0.001318078	-0.001115743	-9.92E-04
43733.74812	-7.56E-04	-0.001078708	-0.001338158	-0.001142467	-0.00101805
43733.74812	-7.57E-04	-0.001083902	-0.001343271	-0.001149259	-0.001024672
43733.74812	-7.58E-04	-0.001089134	-0.001348421	-0.001156097	-0.00103134
43733.74812	-7.59E-04	-0.001094406	-0.001353609	-0.00116298	-0.001038052
43733.74812	-7.60E-04	-0.001099717	-0.001358835	-0.001169908	-0.001044809
43733.74812	-7.61E-04	-0.001105069	-0.0013641	-0.001176882	-0.001051612
43733.74812	-7.63E-04	-0.00111046	-0.001369402	-0.001183901	-0.00105846
43733.74812	-7.64E-04	-0.001115891	-0.001374744	-0.001190967	-0.001065354
43733.74812	-7.65E-04	-0.001121363	-0.001380124	-0.001198079	-0.001072293
43733.74812	-7.66E-04	-0.001126875	-0.001385543	-0.001205238	-0.001079279
43733.74812	-7.67E-04	-0.001132429	-0.001391002	-0.001212443	-0.001086311
43733.74812	-7.68E-04	-0.001138023	-0.0013965	-0.001219695	-0.00109339
43733.74812	-7.69E-04	-0.001143659	-0.001402038	-0.001226995	-0.001100516
43733.74812	-7.71E-04	-0.001149337	-0.001407616	-0.001234342	-0.001107689
43733.74812	-7.72E-04	-0.001155056	-0.001413235	-0.001241736	-0.001114909
43733.74812	-7.73E-04	-0.001160817	-0.001418894	-0.001249178	-0.001122176
43733.74812	-7.75E-04	-0.001166621	-0.001424593	-0.001256668	-0.001129492
43733.74812	-7.76E-04	-0.001172467	-0.001430334	-0.001264207	-0.001136855
43733.74812	-7.77E-04	-0.001178356	-0.001436116	-0.001271794	-0.001144267
43733.74812	-7.79E-04	-0.001184288	-0.001441939	-0.001279429	-0.001151727
43733.74812	-7.80E-04	-0.001190263	-0.001447804	-0.001287114	-0.001159235
43733.74812	-7.81E-04	-0.001196282	-0.001453711	-0.001294848	-0.001166793
43733.74812	-7.83E-04	-0.001202344	-0.00145966	-0.001302631	-0.0011744
43733.74812	-7.84E-04	-0.001208451	-0.001465652	-0.001310464	-0.001182056
43733.74812	-7.86E-04	-0.001214602	-0.001471686	-0.001318347	-0.001189762
43733.74812	-7.87E-04	-0.001220797	-0.001477763	-0.00132628	-0.001197517
43733.74812	-7.89E-04	-0.001227037	-0.001483884	-0.001334263	-0.001205323
43733.74812	-7.91E-04	-0.001233322	-0.001490048	-0.001342297	-0.00121318
43733.74812	-7.92E-04	-0.001239653	-0.001496256	-0.001350382	-0.001221087

43733.74812	-7.94E-04	-0.001246029	-0.001502507	-0.001358518	-0.001229045
43733.74812	-7.96E-04	-0.001252451	-0.001508803	-0.001366706	-0.001237054
43733.74812	-7.97E-04	-0.001258919	-0.001515144	-0.001374945	-0.001245114
43733.74812	-7.99E-04	-0.001265433	-0.001521529	-0.001383236	-0.001253227
43733.74812	-8.01E-04	-0.001271994	-0.001527959	-0.001391579	-0.001261391
43733.74812	-8.03E-04	-0.001278601	-0.001534435	-0.001399974	-0.001269607
43733.74812	-8.04E-04	-0.001285256	-0.001540956	-0.001408422	-0.001277876
43733.74812	-8.12E-04	-0.001312353	-0.001567503	-0.001442746	-0.001311482
43733.74812	-8.14E-04	-0.001319247	-0.001574256	-0.001451462	-0.001320017
43733.74812	-8.16E-04	-0.001326191	-0.001581057	-0.001460231	-0.001328607
43733.74812	-8.18E-04	-0.001333184	-0.001587905	-0.001469055	-0.00133725
43733.74812	-8.20E-04	-0.001340225	-0.001594801	-0.001477934	-0.001345949
43733.74812	-8.22E-04	-0.001347317	-0.001601745	-0.001486868	-0.001354702
43733.74812	-8.25E-04	-0.001354459	-0.001608737	-0.001495857	-0.001363511
43733.74812	-8.27E-04	-0.00136165	-0.001615779	-0.001504901	-0.001372375
43733.74812	-8.29E-04	-0.001368893	-0.001622869	-0.001514002	-0.001381295
43733.74812	-8.31E-04	-0.001376186	-0.001630008	-0.001523158	-0.001390271
43733.74812	-8.33E-04	-0.00138353	-0.001637197	-0.001532372	-0.001399303
43733.74812	-8.36E-04	-0.001390926	-0.001644436	-0.001541641	-0.001408392
43733.74812	-8.38E-04	-0.001398373	-0.001651724	-0.001550968	-0.001417538
43733.74812	-8.41E-04	-0.001405872	-0.001659064	-0.001560352	-0.001426741
43733.74812	-8.43E-04	-0.001413424	-0.001666454	-0.001569794	-0.001436002
43733.74812	-8.45E-04	-0.001421028	-0.001673895	-0.001579293	-0.00144532
43733.74812	-8.48E-04	-0.001428685	-0.001681387	-0.001588851	-0.001454696
43733.74812	-8.51E-04	-0.001436395	-0.001688931	-0.001598467	-0.001464131
43733.74812	-8.53E-04	-0.001444159	-0.001696527	-0.001608141	-0.001473625
43733.74812	-8.56E-04	-0.001451976	-0.001704176	-0.001617875	-0.001483178
43733.74812	-8.58E-04	-0.001459848	-0.001711876	-0.001627668	-0.001492789
43733.74812	-8.61E-04	-0.001467774	-0.00171963	-0.001637521	-0.001502461
43733.74812	-8.64E-04	-0.001475754	-0.001727437	-0.001647433	-0.001512192
43733.74812	-8.67E-04	-0.00148379	-0.001735297	-0.001657406	-0.001521984
43733.74812	-8.69E-04	-0.001491881	-0.001743212	-0.001667439	-0.001531836
43733.74812	-8.72E-04	-0.001500028	-0.00175118	-0.001677533	-0.001541749
43733.74812	-8.75E-04	-0.001508231	-0.001759203	-0.001687688	-0.001551724
43733.74812	-8.78E-04	-0.00151649	-0.00176728	-0.001697905	-0.001561759
43733.74812	-8.81E-04	-0.001524806	-0.001775413	-0.001708183	-0.001571857
43733.74812	-8.84E-04	-0.001533179	-0.001783601	-0.001718524	-0.001582016
43733.74812	-8.87E-04	-0.001541609	-0.001791845	-0.001728926	-0.001592238

43733.74812	-8.90E-04	-0.001550096	-0.001800145	-0.001739392	-0.001602523
43733.74812	-8.93E-04	-0.001558642	-0.001808501	-0.00174992	-0.001612871
43733.74812	-8.97E-04	-0.001567246	-0.001816914	-0.001760511	-0.001623282
43733.74812	-9.00E-04	-0.001575908	-0.001825384	-0.001771166	-0.001633757
43733.74812	-9.03E-04	-0.001584629	-0.001833911	-0.001781886	-0.001644296
43733.74812	-9.17E-04	-0.00162011	-0.001868601	-0.001825407	-0.001687098
43733.74812	-9.20E-04	-0.001629131	-0.001877421	-0.001836451	-0.001697962
43733.74812	-9.24E-04	-0.001638213	-0.001886299	-0.00184756	-0.001708892
43733.74812	-9.27E-04	-0.001647356	-0.001895238	-0.001858736	-0.001719889
43733.74812	-9.31E-04	-0.001656561	-0.001904236	-0.001869978	-0.001730952
43733.74812	-9.35E-04	-0.001665828	-0.001913295	-0.001881287	-0.001742082
43733.74812	-9.38E-04	-0.001675157	-0.001922415	-0.001892663	-0.001753279
43733.74812	-9.42E-04	-0.001684549	-0.001931596	-0.001904106	-0.001764545
43733.74812	-9.46E-04	-0.001694003	-0.001940839	-0.001915618	-0.001775878
43733.74812	-9.50E-04	-0.001703521	-0.001950143	-0.001927197	-0.00178728
43733.74812	-9.54E-04	-0.001713103	-0.001959509	-0.001938845	-0.00179875
43733.74812	-9.58E-04	-0.001722749	-0.001968938	-0.001950562	-0.00181029
43733.74812	-9.62E-04	-0.001732459	-0.00197843	-0.001962349	-0.001821899
43733.74812	-9.66E-04	-0.001742234	-0.001987985	-0.001974204	-0.001833577
43733.74812	-9.70E-04	-0.001752075	-0.001997604	-0.00198613	-0.001845326
43733.74812	-9.74E-04	-0.00176198	-0.002007286	-0.001998126	-0.001857146
43733.74812	-9.78E-04	-0.001771952	-0.002017033	-0.002010192	-0.001869036
43733.74812	-9.83E-04	-0.00178199	-0.002026845	-0.00202233	-0.001880997
43733.74812	-9.87E-04	-0.001792094	-0.002036721	-0.002034539	-0.00189303
43733.74812	-9.91E-04	-0.001802265	-0.002046664	-0.002046819	-0.001905135
43733.74812	-9.96E-04	-0.001812504	-0.002056671	-0.002059171	-0.001917313
43733.74812	-0.001000345	-0.00182281	-0.002066745	-0.002071596	-0.001929563
43733.74812	-0.001004896	-0.001833184	-0.002076886	-0.002084093	-0.001941886
43733.74812	-0.001009502	-0.001843627	-0.002087093	-0.002096664	-0.001954282
43733.74812	-0.001014163	-0.001854139	-0.002097368	-0.002109307	-0.001966752
43733.74812	-0.001018879	-0.001864719	-0.00210771	-0.002122025	-0.001979296
43733.74812	-0.00102365	-0.001875369	-0.002118121	-0.002134817	-0.001991915
43733.74812	-0.001028478	-0.001886089	-0.002128599	-0.002147683	-0.002004608
43733.74812	-0.001033363	-0.00189688	-0.002139147	-0.002160624	-0.002017377
43733.74812	-0.001038304	-0.001907741	-0.002149763	-0.00217364	-0.002030221
43733.74812	-0.001043303	-0.001918673	-0.002160449	-0.002186732	-0.002043142
43733.74812	-0.001048359	-0.001929676	-0.002171205	-0.0021999	-0.002056138
43733.74812	-0.001053474	-0.001940752	-0.002182032	-0.002213144	-0.002069212

43733.74812	-0.001058648	-0.001951899	-0.002192929	-0.002226465	-0.002082362
43733.74812	-0.00106388	-0.001963119	-0.002203897	-0.002239863	-0.00209559
43733.74812	-0.001069173	-0.001974412	-0.002214936	-0.002253338	-0.002108896
43733.74812	-0.001090945	-0.002020321	-0.002259816	-0.002308021	-0.002162905
43733.74812	-0.001096542	-0.002031985	-0.002271218	-0.002321889	-0.002176606
43733.74812	-0.0011022	-0.002043724	-0.002282694	-0.002335837	-0.002190387
43733.74812	-0.001107922	-0.002055538	-0.002294245	-0.002349865	-0.002204249
43733.74812	-0.001113706	-0.002067429	-0.00230587	-0.002363974	-0.002218191
43733.74812	-0.001119553	-0.002079396	-0.00231757	-0.002378163	-0.002232215
43733.74812	-0.001125465	-0.00209144	-0.002329345	-0.002392433	-0.002246321
43733.74812	-0.001131441	-0.002103562	-0.002341196	-0.002406785	-0.002260508
43733.74812	-0.001137482	-0.002115761	-0.002353123	-0.002421219	-0.002274779
43733.74812	-0.001143588	-0.002128038	-0.002365127	-0.002435736	-0.002289132
43733.74812	-0.001149759	-0.002140393	-0.002377208	-0.002450335	-0.002303568
43733.74812	-0.001155997	-0.002152828	-0.002389366	-0.002465017	-0.002318088
43733.74812	-0.001162302	-0.002165342	-0.002401602	-0.002479783	-0.002332693
43733.74812	-0.001168673	-0.002177935	-0.002413916	-0.002494633	-0.002347382
43733.74812	-0.001175112	-0.002190609	-0.002426309	-0.002509567	-0.002362155
43733.74812	-0.001181619	-0.002203363	-0.002438781	-0.002524586	-0.002377014
43733.74812	-0.001188195	-0.002216198	-0.002451332	-0.00253969	-0.002391959
43733.74812	-0.001194839	-0.002229114	-0.002463963	-0.00255488	-0.00240699
43733.74812	-0.001201553	-0.002242112	-0.002476674	-0.002570155	-0.002422108
43733.74812	-0.001208336	-0.002255193	-0.002489466	-0.002585517	-0.002437312
43733.74812	-0.00121519	-0.002268356	-0.002502339	-0.002600966	-0.002452604
43733.74812	-0.001222114	-0.002281602	-0.002515294	-0.002616502	-0.002467983
43733.74812	-0.00122911	-0.002294931	-0.00252833	-0.002632125	-0.002483451
43733.74812	-0.001236177	-0.002308344	-0.002541449	-0.002647836	-0.002499008
43733.74812	-0.001243317	-0.002321842	-0.002554651	-0.002663636	-0.002514653
43733.74812	-0.001250529	-0.002335424	-0.002567936	-0.002679524	-0.002530388
43733.74812	-0.001257814	-0.002349091	-0.002581304	-0.002695502	-0.002546212
43733.74812	-0.001265172	-0.002362844	-0.002594756	-0.002711569	-0.002562127
43733.74812	-0.001272605	-0.002376682	-0.002608293	-0.002727726	-0.002578133
43733.74812	-0.001280112	-0.002390607	-0.002621915	-0.002743974	-0.00259423
43733.74812	-0.001287694	-0.002404619	-0.002635622	-0.002760312	-0.002610418
43733.74812	-0.001295351	-0.002418718	-0.002649415	-0.002776742	-0.002626698
43733.74812	-0.001303084	-0.002432905	-0.002663294	-0.002793263	-0.002643071
43733.74812	-0.001310894	-0.00244718	-0.002677259	-0.002809876	-0.002659536
43733.74812	-0.00131878	-0.002461543	-0.002691312	-0.002826582	-0.002676095

43733.74812	-0.001326744	-0.002475996	-0.002705452	-0.002843381	-0.002692747
43733.74812	-0.001359381	-0.002534703	-0.002762895	-0.002911513	-0.002760301
43733.74812	-0.001367738	-0.002549607	-0.002777479	-0.002928782	-0.002777428
43733.74812	-0.001376176	-0.002564602	-0.002792153	-0.002946147	-0.002794651
43733.74812	-0.001384694	-0.002579689	-0.002806917	-0.002963608	-0.00281197
43733.74812	-0.001393293	-0.002594869	-0.002821773	-0.002981165	-0.002829387
43733.74812	-0.001401975	-0.002610141	-0.00283672	-0.002998819	-0.002846902
43733.74812	-0.001410738	-0.002625507	-0.002851758	-0.00301657	-0.002864514
43733.74812	-0.001419584	-0.002640967	-0.002866889	-0.003034418	-0.002882225
43733.74812	-0.001428513	-0.002656521	-0.002882113	-0.003052364	-0.002900035
43733.74812	-0.001437525	-0.002672169	-0.00289743	-0.003070409	-0.002917943
43733.74812	-0.001446622	-0.002687913	-0.00291284	-0.003088553	-0.002935952
43733.74812	-0.001455803	-0.002703752	-0.002928345	-0.003106796	-0.002954061
43733.74812	-0.001465069	-0.002719687	-0.002943944	-0.003125138	-0.00297227
43733.74812	-0.001474421	-0.002735718	-0.002959638	-0.003143581	-0.002990581
43733.74812	-0.001483859	-0.002751847	-0.002975427	-0.003162125	-0.003008993
43733.74812	-0.001493384	-0.002768073	-0.002991312	-0.003180769	-0.003027507
43733.74812	-0.001502996	-0.002784396	-0.003007294	-0.003199515	-0.003046123
43733.74812	-0.001512695	-0.002800818	-0.003023373	-0.003218363	-0.003064842
43733.74812	-0.001522482	-0.002817339	-0.003039548	-0.003237313	-0.003083664
43733.74812	-0.001532358	-0.002833959	-0.003055822	-0.003256366	-0.003102591
43733.74812	-0.001542323	-0.002850678	-0.003072193	-0.003275522	-0.003121621
43733.74812	-0.001552378	-0.002867497	-0.003088663	-0.003294782	-0.003140756
43733.74812	-0.001562522	-0.002884417	-0.003105232	-0.003314146	-0.003159996
43733.74812	-0.001572758	-0.002901438	-0.003121901	-0.003333614	-0.003179341
43733.74812	-0.001583084	-0.002918561	-0.00313867	-0.003353188	-0.003198793
43733.74812	-0.001593502	-0.002935785	-0.003155539	-0.003372866	-0.003218351
43733.74812	-0.001604012	-0.002953112	-0.003172509	-0.003392651	-0.003238016
43733.74812	-0.001614615	-0.002970541	-0.00318958	-0.003412542	-0.003257788
43733.74812	-0.00162531	-0.002988074	-0.003206754	-0.00343254	-0.003277668
43733.74812	-0.0016361	-0.003005711	-0.003224029	-0.003452646	-0.003297657
43733.74812	-0.001646983	-0.003023452	-0.003241408	-0.003472858	-0.003317754
43733.74812	-0.001657962	-0.003041297	-0.003258889	-0.003493179	-0.00333796
43733.74812	-0.001669035	-0.003059248	-0.003276474	-0.003513609	-0.003358276
43733.74812	-0.001680204	-0.003077304	-0.003294164	-0.003534148	-0.003378702
43733.74812	-0.001691469	-0.003095466	-0.003311958	-0.003554796	-0.003399239
43733.74812	-0.001702831	-0.003113735	-0.003329857	-0.003575554	-0.003419887
43733.74812	-0.001714291	-0.003132111	-0.003347862	-0.003596422	-0.003440646

43733.74812	-0.001749257	-0.003187886	-0.003402514	-0.003659695	-0.003503597
43733.74812	-0.00176111	-0.003206694	-0.003420945	-0.003681009	-0.003524807
43733.74812	-0.001773063	-0.003225613	-0.003439485	-0.003702436	-0.003546131
43733.74812	-0.001785117	-0.00324464	-0.003458133	-0.003723977	-0.003567569
43733.74812	-0.001797271	-0.003263779	-0.00347689	-0.003745631	-0.003589121
43733.74812	-0.001809527	-0.003283028	-0.003495756	-0.003767399	-0.003610789
43733.74812	-0.001821884	-0.003302388	-0.003514732	-0.003789282	-0.003632573
43733.74812	-0.001834344	-0.00332186	-0.003533819	-0.003811279	-0.003654473
43733.74812	-0.001846907	-0.003341445	-0.003553016	-0.003833393	-0.00367649
43733.74812	-0.001859574	-0.003361142	-0.003572325	-0.003855622	-0.003698623
43733.74812	-0.001872344	-0.003380952	-0.003591745	-0.003877967	-0.003720875
43733.74812	-0.001885219	-0.003400876	-0.003611277	-0.003900429	-0.003743244
43733.74812	-0.001898199	-0.003420914	-0.003630923	-0.003923009	-0.003765732
43733.74812	-0.001911285	-0.003441067	-0.003650681	-0.003945706	-0.003788339
43733.74812	-0.001924477	-0.003461335	-0.003670553	-0.003968522	-0.003811065
43733.74812	-0.001937775	-0.003481718	-0.003690539	-0.003991456	-0.003833912
43733.74812	-0.001951181	-0.003502218	-0.00371064	-0.00401451	-0.003856878
43733.74812	-0.001964694	-0.003522834	-0.003730856	-0.004037683	-0.003879966
43733.74812	-0.001978316	-0.003543567	-0.003751188	-0.004060976	-0.003903175
43733.74812	-0.001992046	-0.003564417	-0.003771636	-0.00408439	-0.003926506
43733.74812	-0.002005886	-0.003585386	-0.0037922	-0.004107925	-0.00394996
43733.74812	-0.002019835	-0.003606473	-0.003812882	-0.004131581	-0.003973536
43733.74812	-0.002033895	-0.003627679	-0.003833681	-0.00415536	-0.003997236
43733.74812	-0.002048065	-0.003649005	-0.003854598	-0.004179261	-0.004021059
43733.74812	-0.002062348	-0.003670451	-0.003875634	-0.004203285	-0.004045007
43733.74812	-0.002076742	-0.003692017	-0.003896788	-0.004227432	-0.00406908
43733.74812	-0.002091248	-0.003713704	-0.003918062	-0.004251703	-0.004093277
43733.74812	-0.002105868	-0.003735512	-0.003939457	-0.004276099	-0.004117601
43733.74812	-0.002120601	-0.003757443	-0.003960971	-0.004300619	-0.004142051
43733.74812	-0.002135448	-0.003779495	-0.003982607	-0.004325265	-0.004166627
43733.74812	-0.00215041	-0.003801671	-0.004004364	-0.004350037	-0.004191331
43733.74812	-0.002165488	-0.00382397	-0.004026244	-0.004374935	-0.004216162
43733.74812	-0.002180681	-0.003846393	-0.004048245	-0.004399959	-0.004241122
43733.74812	-0.00219599	-0.00386894	-0.00407037	-0.004425111	-0.00426621
43733.74812	-0.002211416	-0.003891613	-0.004092618	-0.004450391	-0.004291427
43733.74812	-0.002226959	-0.00391441	-0.00411499	-0.004475799	-0.004316774
43733.74812	-0.002290318	-0.004006864	-0.004205729	-0.004578722	-0.004419468
43733.74812	-0.002306456	-0.004030296	-0.004228728	-0.004604778	-0.004445471

43733.74812	-0.002322715	-0.004053857	-0.004251854	-0.004630965	-0.004471606
43733.74812	-0.002339095	-0.004077546	-0.004275108	-0.004657283	-0.004497874
43733.74812	-0.002355597	-0.004101364	-0.00429849	-0.004683734	-0.004524276
43733.74812	-0.002372221	-0.004125313	-0.004322	-0.004710318	-0.004550812
43733.74812	-0.002388968	-0.004149391	-0.00434564	-0.004737034	-0.004577482
43733.74812	-0.002405838	-0.004173601	-0.004369408	-0.004763884	-0.004604288
43733.74812	-0.002422833	-0.004197942	-0.004393307	-0.004790868	-0.004631229
43733.74812	-0.002439951	-0.004222414	-0.004417336	-0.004817986	-0.004658306
43733.74812	-0.002457195	-0.004247019	-0.004441496	-0.004845239	-0.004685519
43733.74812	-0.002474564	-0.004271757	-0.004465788	-0.004872628	-0.00471287
43733.74812	-0.002492059	-0.004296629	-0.004490211	-0.004900153	-0.004740358
43733.74812	-0.002509681	-0.004321634	-0.004514767	-0.004927814	-0.004767984
43733.74812	-0.002527431	-0.004346773	-0.004539456	-0.004955612	-0.004795749
43733.74812	-0.002545307	-0.004372048	-0.004564279	-0.004983547	-0.004823652
43733.74812	-0.002563313	-0.004397457	-0.004589235	-0.005011621	-0.004851695
43733.74812	-0.002581447	-0.004423003	-0.004614326	-0.005039833	-0.004879879
43733.74812	-0.00259971	-0.004448685	-0.004639552	-0.005068183	-0.004908202
43733.74812	-0.002618104	-0.004474504	-0.004664914	-0.005096673	-0.004936667
43733.74812	-0.002636628	-0.00450046	-0.004690411	-0.005125303	-0.004965273
43733.74812	-0.002655282	-0.004526554	-0.004716045	-0.005154073	-0.004994021
43733.74812	-0.002674069	-0.004552786	-0.004741817	-0.005182984	-0.005022912
43733.74812	-0.002692988	-0.004579158	-0.004767725	-0.005212037	-0.005051946
43733.74812	-0.002712039	-0.004605669	-0.004793772	-0.005241231	-0.005081123
43733.74812	-0.002731224	-0.004632319	-0.004819957	-0.005270567	-0.005110444
43733.74812	-0.002750543	-0.00465911	-0.004846281	-0.005300047	-0.00513991
43733.74812	-0.002769996	-0.004686042	-0.004872745	-0.005329669	-0.005169521
43733.74812	-0.002789583	-0.004713116	-0.004899349	-0.005359436	-0.005199277
43733.74812	-0.002809307	-0.004740331	-0.004926094	-0.005389346	-0.005229179
43733.74812	-0.002829166	-0.004767689	-0.004952979	-0.005419402	-0.005259228
43733.74812	-0.002849162	-0.00479519	-0.004980007	-0.005449602	-0.005289424
43733.74812	-0.002869296	-0.004822834	-0.005007176	-0.005479949	-0.005319768
43733.74812	-0.002889567	-0.004850623	-0.005034488	-0.005510442	-0.005350259
43733.74812	-0.002909976	-0.004878555	-0.005061943	-0.005541081	-0.005380899
43733.74812	-0.002930524	-0.004906633	-0.005089542	-0.005571868	-0.005411688
43733.74812	-0.003014116	-0.005020405	-0.005201384	-0.005696497	-0.005536344
43733.74812	-0.003035366	-0.005049215	-0.005229709	-0.005728028	-0.005567886
43733.74812	-0.003056759	-0.005078174	-0.00525818	-0.005759708	-0.00559958
43733.74812	-0.003078294	-0.005107281	-0.005286799	-0.00579154	-0.005631426

43733.74812	-0.003099973	-0.005136537	-0.005315566	-0.005823522	-0.005663425
43733.74812	-0.003121796	-0.005165942	-0.005344481	-0.005855657	-0.005695578
43733.74812	-0.003143763	-0.005195498	-0.005373544	-0.005887943	-0.005727885
43733.74812	-0.003165875	-0.005225205	-0.005402757	-0.005920382	-0.005760347
43733.74812	-0.003188133	-0.005255062	-0.00543212	-0.005952975	-0.005792964
43733.74812	-0.003210536	-0.005285072	-0.005461633	-0.005985721	-0.005825736
43733.74812	-0.003233087	-0.005315233	-0.005491297	-0.006018621	-0.005858665
43733.74812	-0.003255784	-0.005345547	-0.005521112	-0.006051676	-0.00589175
43733.74812	-0.00327863	-0.005376014	-0.005551079	-0.006084886	-0.005924992
43733.74812	-0.003301624	-0.005406635	-0.005581199	-0.006118252	-0.005958392
43733.74812	-0.003324766	-0.005437411	-0.005611471	-0.006151774	-0.00599195
43733.74812	-0.003348058	-0.005468341	-0.005641897	-0.006185453	-0.006025666
43733.74812	-0.0033715	-0.005499426	-0.005672477	-0.006219289	-0.006059542
43733.74812	-0.003395093	-0.005530667	-0.005703211	-0.006253283	-0.006093577
43733.74812	-0.003418837	-0.005562064	-0.005734101	-0.006287435	-0.006127773
43733.74812	-0.003442733	-0.005593618	-0.005765145	-0.006321745	-0.006162129
43733.74812	-0.00346678	-0.005625329	-0.005796346	-0.006356215	-0.006196647
43733.74812	-0.003490981	-0.005657198	-0.005827703	-0.006390844	-0.006231326
43733.74812	-0.003515335	-0.005689225	-0.005859218	-0.006425634	-0.006266167